The Dissertation Committee for Migdalys Beatriz Salazar Certifies that this is the approved version of the following dissertation:

The Impact of Shelf Margin Geometry and Tectonics on Shelf-To-Sink Sediment Dynamics and Resultant Basin Fill Architectures

Committee:

Lesli J. Wood, Supervisor

Lorena G. Moscardelli, Co-Supervisor

Ronald J. Steel

David Mohrig

William L. Fisher

Peter Flaig

The Impact of Shelf Margin Geometry and Tectonics on Shelf-To-Sink Sediment Dynamics and Resultant Basin Fill Architectures

by

Migdalys Beatriz Salazar, B.S.; M.S.; M.S.Geo.Sci.

Dissertation

Presented to the Faculty of the Graduate School of

The University of Texas at Austin

in Partial Fulfillment

of the Requirements

for the Degree of

Doctor of Philosophy

The University of Texas at Austin

May 2014

Acknowledgements

First at all, I wish to express my deep gratitude to my advisors, Drs. Lorena Moscardelli and Lesli Wood, who gave me their financial and technical support. I really appreciate all your support and patience.

I extend my appreciation to my Examining Committee members, Ronald Steel, David Mohrig, William Fisher, and Peter Flaig. Comments from Peter Flaig significantly improved the earliest version of this dissertation and discussions with David Mohrig were fundamental to complete the modeling section of this study.

I thank the New Zealand Ministry of Economic Development, Plains Exploration and Production Company, and Glenn Lovitz for the generous donation of data in order to pursue this research. I would also like to thank Dallas Dunlap who helped me with the difficult job of collecting and setting the data and Dr. Maria Antonieta Lorente for her support during the biostratigraphic revision.

Funding of this dissertation was made possible by several entities, including members of the Quantitative Clastics Laboratory Industrial Associates Program at the Bureau of Economic Geology, Jackson School of Geosciences, The University of Texas at Austin. I also thank AAPG, GCSSEPM and the Graduate Suppor Committee for providing external grants and scholarships during my time as a graduate student.

Thanks to my friends in the BEG for their understanding, encouragement and companionship, and thanks to my family who was always with me spiritually. Allen, thanks for your support and for having always kind words, you made it possible to continue and finish my studies.

Thanks to all.

The Impact of Shelf Margin Geometry and Tectonics on Shelf-To-Sink Sediment Dynamics and Resultant Basin Fill Architectures

Migdalys Beatriz Salazar, Ph.D.

The University of Texas at Austin, 2014

Supervisor: Lesli J. Wood

This dissertation focuses on understanding the relative importance of external (eustacy) versus local tectonic and sedimentary processes in controlling continental-margin depositional architectures and their implications for sediment distribution. The emphasis of this study is the interpretation of clinoform geometries and stratigraphic relationships observed on 3D and 2D seismic reflection data in the Taranaki Basin, which is characterized by a variety of clinoform architectures on its Pliocene-Recent margin (Giant Foresets Formation). I combined seismic stratigraphic interpretations and biostratigraphic studies using a dataset that consists of 1,700 km^2 of 3D seismic lines, 4,000 km of 2D regional seismic lines, and data from six wells. The study was divided into three sections. First, three major stages of clinoform evolution were identified based on their architectural and geomorphological characteristics. Isochron maps were generated to identify correlations between stratigraphy and paleostructures, and seismic attribute maps were elaborated to identify and characterize geological features and depositional elements. In the second phase of the study, 2D stratigraphic forward modeling techniques were applied in an effort to quantitatively determine the relative importance of the mechanisms acting in the basin (eustacy, tectonism and sediment supply). Finally, a similar approach was applied using clinoform morphologies in the

eastern Trinidad margin where the tectonic configuration of the basin was completely different to the one in the Taranaki Basin. The objective was to compare the results in a region with different a tectonic setting to validate the applicability of the methodology in other basins worldwide.

The results of this research indicate that the methodology that was developed for the quantitative analysis of clinoform architectures in the Taranaki Basin is applicable to other basins worldwide and that the work flow provides a more comprehensive understanding of the factors that influence continental margin development. Generic observations of this research showed that (1) underlying structures in the shelf and slope area can play an important role in influencing the location and morphology of the shelf edge area and controlling sediment distribution; (2) high sediment supply, along with accommodation, play a key role in the construction of high-relief clinoforms and earlier dispersal of sediments into deep water; and (3) lateral variations associated with high sediment discharge sources (e.g. paleo Orinoco shelf-edge delta) can generate important changes in continental-scale clinoform architectures alongstrike in continental margins influence sediment distribution patterns in the deep-water component of the basin.

Table of Contents

List of Tables

List of Figures

CHAPTER 1: INTRODUCTION

PROBLEM AND SIGNIFICANCE

The study of continental margins has received increasing attention in recent years because of the interest of the oil industry in the exploration of deepwater deposits. Understanding how sediment is transferred and distributed along continental margins is crucial for the development of exploration-oriented sedimentary models of continental margin evolution. The development of continental margins is the result of the complex interactions between external (e.g., eustacy and climate) and local (e.g., tectonics and sediment supply) processes that operate from the source areas to the final sink. These processes are not easy to isolate because they may occur at the same time and generate similar sedimentary responses (Galloway, 1989). Clinoform stratal architectures are commonly identified in different time and geographic scales on seismic profiles worldwide. Clinoforms are inclined depositional surfaces, associated with strata prograding into deep water, that are composed of three geometric elements (Rich, 1951): (1) a topset, the shallowest and lowst-angle area, (2) a foreset, the central and steepest area, and (3) a bottomset, the flat area farther basinward. Because of their broad distribution and sensitivity to variations in the basin conditions, continental-scale clinoforms have been studied by several workers worldwide to investigate the response of depositional systems to relative sea-level variations and to predict the accumulation of deepwater deposits (Johannessen and Steel, 2005; Carvajal and Steel, 2009; Henriksen et al., 2009). This research is concerned with the study of continental-scale clinoforms, how these systems develop, and the implications associated with sediment distribution in an outer shelf to sink configuration. Understanding how clinoforms form, evolve and degrade is critical to the understanding of the transport mechanisms affecting the shelf margin region as well as sediment partitioning of a given basin.

OBJECTIVES

The objectives of this study are:

- To develop a method that will allow for the quantification of the temporal and spatial variability within a clinoformal succession by using observations extracted from seismic and well data.
- To deduce the processes acting in the basin (from global to local scales) through the study of clinoform morphologies and their distribution, and to identify changes in basin conditions through the study of variations in clinoform morphologies and architectures through time.
- To separate out the stratigraphic signatures of tectonics versus sediment supply and relative sea level fluctuations in a structurally active shelf margin region.
- To understand the partitioning of sediments in a given basin through the study of morphological characteristics of continental-scale clinoforms.
- To examine under what conditions high relief clinoforms (height > 700m) can be developed.

These objectives are achieved by pursuing a detailed geomorphological study of clinoform architectures within the Pliocene-Pleistocene stratigraphic section of the northern Taranaki Basin of New Zealand. The study seeks to better understand the evolution of these continental margins and to deduce the relationships between clinoform development and the variables that influenced sediment movement in the shelf edge and slope regions, including sea-level fluctuations, sediment input and tectonics. The quantitative data were also used as input to forward model clinoform architectures in the Taranaki Basin so that the main controlling factors influencing the genesis of clinoforms could be identified (sediment supply, relative sea-level fluctuations, tectonics, etc). The methodology for clinoform characterization was applied to continental-scale clinoforms

documented in the eastern offshore Trinidad (Moscardelli et al., 2012) allows me to compare results in a region where tectonics and other geologic conditions vary from the Taranaki Basin.

AREA OF STUDY

The Taranaki Basin of New Zealand was selected for this study because: (1) the presence of high-quality seismic datasets; (2) well-developed clinoform architectures (Giant Foresets Formation, GFF) in the Neogene section; (3) clinoforms characterized by having high relief similar to continental-scale clinoforms deposited in the Magallanes Basin (Chile) and the North Slope of Alaska (Figure 1.1); and (4) the occurrence of different tectonic episodes that should be expressed on the basin architectures and clinoform morphologies.

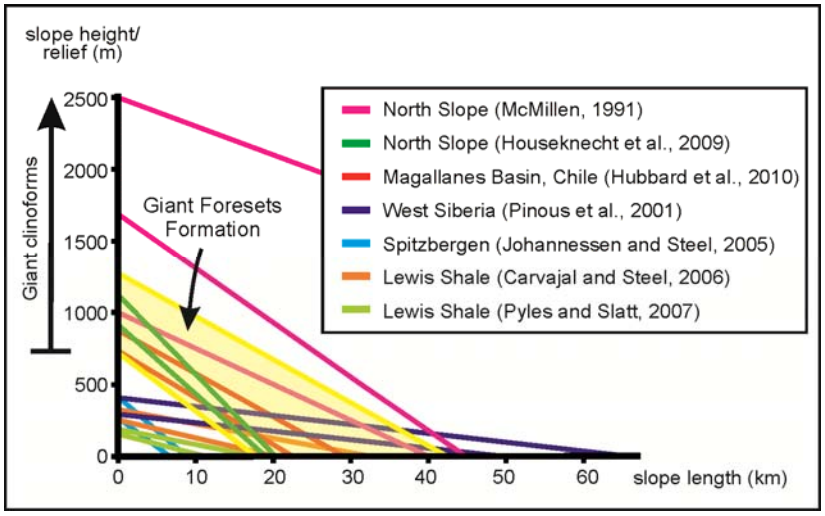

Figure 1.1: Comparison of clinoform lengths and heights from various slope systems. Of the slope systems considered, the relief and angle of the clinoforms mapped in the Taranaki Basin are most comparable to those of the North Slope, Alaska.

OVERVIEW OF SUBSEQUENT CHAPTERS

This dissertation has been structured into six main chapters. Chapters 2 to 4 are manuscripts that are either submitted, in revision or in preparation for publication.

Chapter 2

Chapter 2 documents the methodology that was followed to collect quantitative data associated with clinoform architectures (height, length, slope inclination, rollover trajectories). This chapter also describes the methodology that was followed to define seismic units and stages of clinoform evolution within the northern Taranaki Basin, and contains all the elements linked to the regional geologic setting of the basin.

Chapter 3

Chapter 3 incorporates 2D stratigraphic forward modeling techniques to define the predominant mechanisms acting in the basin. This chapter discusses in detail the methodology that was used to generate the modeling. The aim of this section is to discuss which geologic factors most likely represented the main controls influencing clinoform architectures and if they varied in space and time.

Chapter 4

Chapter 4 uses a similar procedure to that in Chapter 3 to quantify clinoform morphologies in the eastern Trinidad margin. The purpose of this chapter is to investigate to what degree our results can be extrapolated to other basins.

Chapter 5

Chapter 5 compares the clinoform systems in the northern Taranaki Basin and eastern offshore Trinidad to present a discussion surrounding the applicability of the methodologies developed in this work in other basins.

Chapter 6

Chapter 6 summarizes the major contributions of this research and explores the implications of these results for other studies and for a better understanding of the Taranaki Basin.

CHAPTER 2: UTILIZING CLINOFORM ARCHITECTURE TO UNDERSTAND THE DRIVERS OF BASIN MARGIN EVOLUTION: A CASE STUDY IN THE TARANAKI BASIN, NEW ZEALAND

ABSTRACT

The study of morphological variations within continental-margin clinoforms is critical to the understanding of sediment dispersal, composition, and transport mechanisms affecting the shelf margin region. In this study, I combine the analysis of 2D and 3D reflection data with paleontological studies to document variations in clinoform morphologies within the Pliocene-Recent Giant Foresets Formation of the northern Taranaki Basin, New Zealand. Quantitative analysis of slope geometries, shelf edge trajectories and incisional patterns allowed for the identification of three major stages of clinoform evolution. These results were combined with the analysis of isochron maps and seismic attribute extractions to determine relationships with depositional and tectonic settings. Clinoforms developed during Stage 1 (early Pliocene) have gentle and smooth architectures, low-angle foresets, and rising rollover trajectories. Seismic geomorphological analysis suggests a stable shelf-edge region, and the development of a few slope fans. Stage 2 (early–late Pliocene) clinoforms are characterized by concave profiles, increased foreset steepness, mostly flat rollover trajectories and dissected shelf-edge regions. This stage reflects an increase in canyon incision and sediment bypass toward the basin acting on a background of relative sea level fall. In addition, the activation of a back-arc rifting structure (Northern Graben) during this stage allowed local changes in basin physiography and redirection of sediment pathways through the structure, potential deep water deposits are expected in deeper parts of this structure. Stage 3 (late Pliocene-Recent) is characterized by sigmoidal, higher and steeper clinoforms, rising rollover trajectories and dissected slopes without a clear connection to

the shelf edge area. Increase in sediment supply and accommodation were necessary for molding these geometries. The progradation of the system into deeper water resulted in gradually steeper slope gradients that triggered mass-wasting processes. This work highlights the way systematic description of clinoform architectures can be coupled with process-oriented interpretations associated with paleoenvironmental and tectonic conditions at the time of deposition.

INTRODUCTION

The amount of sediment that ultimately ends up in the deep-water regions of a continental margin is influenced by the character of the source area, the nature of the fluvial systems that reach the shoreline and the accommodation regime from source to sink. However, it is the deltaic and shelf repositories that sequester sediment, where it is often acted upon by marine processes that influence the nature and distribution of these shallow marine sediments, before they are ultimately transferred to the slope and deep-water basins.

The geomorphology and efficiency of shelf-to-basin transfer zones are influenced by a variety of factors including relative sea-level fluctuations, tectonism, variations in sedimentation rates, and current-controlled processes among others (Martinsen & Helland-Hansen, 1995; Carvajal & Steel, 2009; Kertznus & Kneller, 2009; Moscardelli et al., 2012). It is widely recognized that the clinoform is the primary architecture of sediment storage in shallow marine settings prior to sediment transfer to deeper waters (Muto and Steel, 2002). A clinoform is an inclined depositional plane whose dip section is composed of three geometric elements: a topset (the most shallow and low-angle part of the depositional profile), a foreset (the central and steepest portion of the depositional profile), and a bottomset (the region of the depositional profile that is furthest basinward) (Mitchum & Vail, 1977; Figure 2.1). The break in seafloor slope between the topset and

the foreset is often called the rollover point. Several different types of clinoforms have been described (Wolinzky & Pratson, 2007; Helland-Hansen and Hampson, 2009), including: delta front clinoforms (subaerial); subaqueous delta clinoforms; and large scale continental margin clinoforms which include as part of their configuration the shelf-slope-continental rise (e.g., the Giant Foresets Formations).

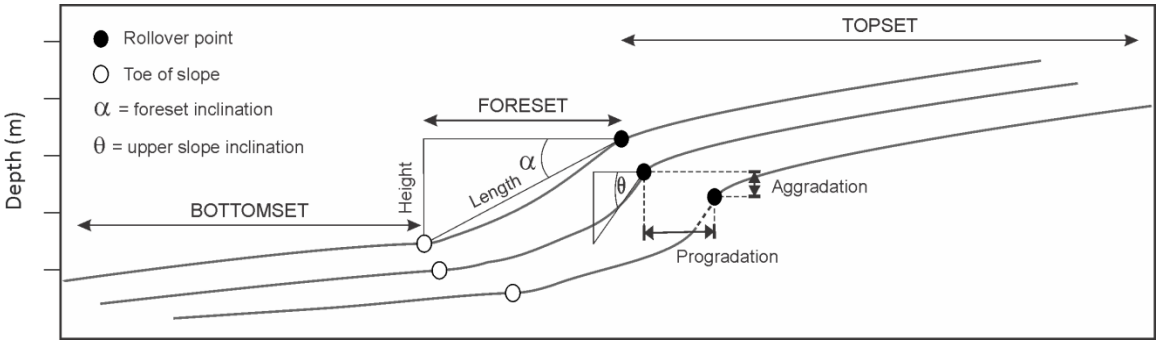

Figure 2.1: Sketch showing idealized clinoform morphologies and geometric parameters for each seismic unit.

Clinoform dimensions are often calculated by measuring clinoform height (vertical distance between the bottomset and the upper portion of a clinoform foreset) (Figure 2.1). Clinoform heights can vary from tens of meters (delta scale) to hundreds of meters (continental scale) (Wolinsky & Pratson, 2007; Helland-Hansen & Hampson, 2009). Analysis of clinoform architectures has applications for the study of continental margin evolution including the estimation of paleo-water depth (e.g., Schlager, 1981; Kominz & Pekar, 2001), lithologies (Orton & Reading, 1993), and tracking temporal changes in margin growth (Johannessen & Steel, 2005; Carvajal & Steel, 2009). Some studies suggest that the correlation between deltaic clinoform inclination (downward slope) and lithology is a relationship that can be extended to continental margin clinoforms (e.g., O'Grady et al., 2000; Adams & Schlager, 2000; Wolisky & Pratson, 2007). Finally, clinoform rollover positions can be used as a means to predict continental

margin trajectories through time (Figure 2.1) (Johannessen & Steel, 2005; Carvajal & Steel, 2009; Henriksen et al., 2009).

Although modelers looking at continental margin evolution have historically placed emphasis on the influence of relative sea-level on continental margin development, several researchers have begun to give considerable attention to the influence that tectonism and current-controlled processes may have on shaping these margins (e.g., Jordan and Flemings, 1991; Martinsen & Helland-Hansen, 1995; Boyd et al., 2008; Hubble et al., 2011; Georgiopoulou et al., 2011; Moscardelli et al., 2012). Tectonics can influence the bathymetric profile as well as the tortuosity of sedimentary pathways that bypass sediment from the shelf to the slope region.

Tectonic pulses occurring in sediment source areas can trigger variations in sediment supply that can influence depositional styles along these margins (e.g., Miall, 1986). Likewise, current-controlled processes play an increasingly evident role in redistributing sediments in both shelfal and deep-water environments (Boyd et al., 2008; Zhu et al., 2010; Georgiopoulou et al., 2011; Hubble et al., 2011; Moscardelli et al., 2012). Researchers using high quality, 3D seismic have been able to obtain a spatially-dense, three-dimensional understanding of architectures within many of the modern and ancient shelf-edge regions. When integrated with temporally detailed lithologic, faunal and floral information from well logs and core, the resulting integrated depositional framework provides the type of architectural and stratigraphic detail that can help unravel the roles of tectonics, eustasy and sediment supply in the construction of such continental margins and basin infilling (e.g., Posamentier & Kolla, 2003; Moscardelli et al., 2006; Carvajal & Steel, 2009; Kertznus & Kneller, 2009; Moscardelli et al., 2012).

The main objective of this work is to pursue a detailed seismic architecture and geomorphological study of shelf-edge architectures of the Giant Foresets Formation

within the Taranaki Basin of New Zealand (Figure 2.2) in order to better understand the evolution of this continental margin from the Pliocene to Recent times. In addition, I deduce the relationships between clinoform development and controlling variables (e.g., ocean processes, sea-level fluctuations, sediment input and tectonics) that influenced sediment movement in the shelf edge and slope region during the Pliocene–recent.

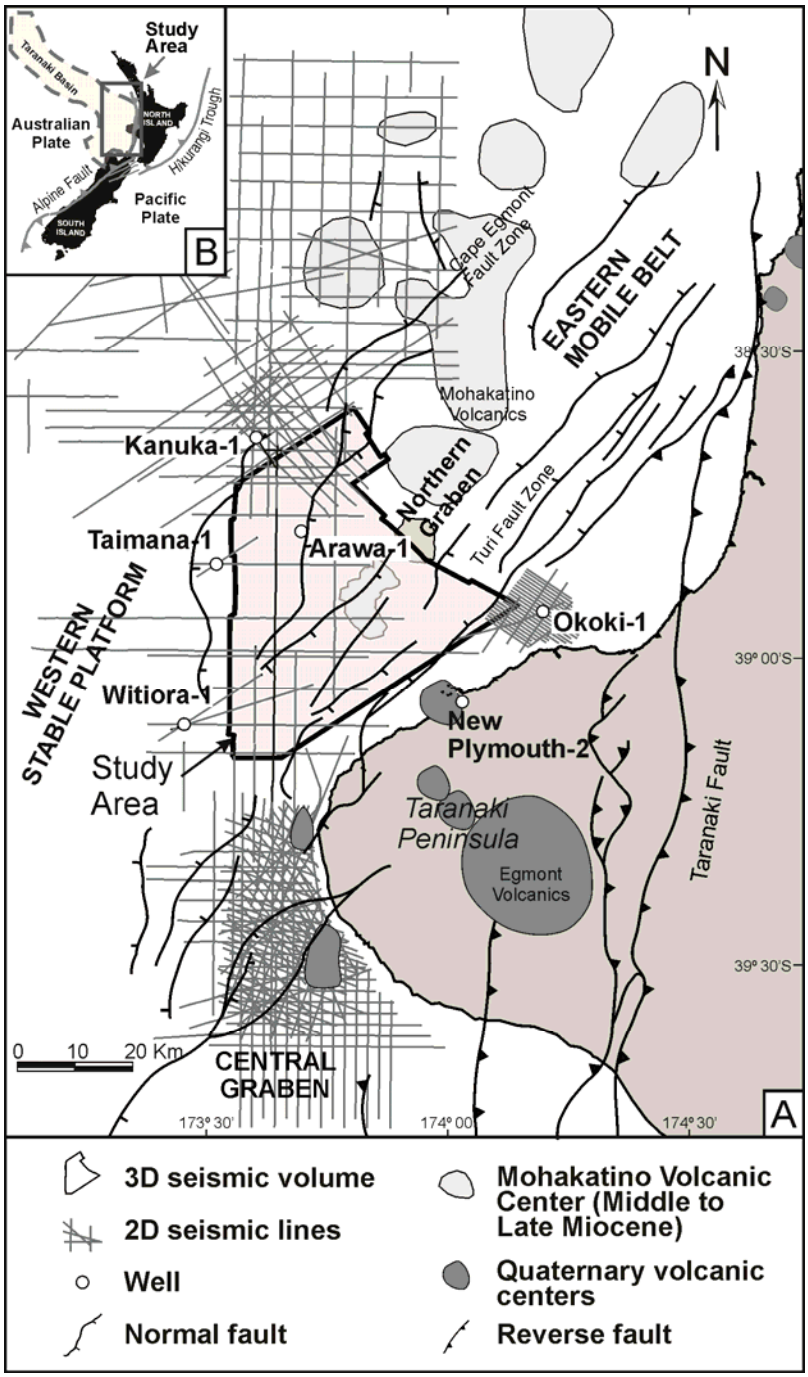

Figure 2.2: (A) Map showing the study area along the western margin of New Zealand's North Island. Light-gray-shadowed area highlights the location of the 3-D seismic volume used in this study. Semiregional 2D seismic lines are also shown. (B) Small map shows relative location of Taranaki Basin, including its northwestern deepwater extension and corresponding tectonic framework along Australian-Pacific plate boundary zone.

Geological Setting

The Taranaki Basin is a Cretaceous to modern sedimentary basin that covers a total area of 330,000 km^2 along the western coast of New Zealand and has both an onshore and offshore component (Figure 2.2). The eastern boundary of the basin is delineated by the Taranaki Fault, part of a system of reverse faults associated with the converging boundary between the Australian and Pacific tectonic plates (King & Thrasher, 1992) (Figure 2.2). To the south, the basin merges with the small subbasins of New Zealand's South Island, and to northwest in the Deepwater Taranaki Basin, the basin merges with the New Caledonian Basin (King & Thrasher, 1992; King & Thrasher, 1996) (Figure 2.2). Within the Taranaki Basin, King & Thrasher (1996) distinguished two main tectonic regions, divided by the Cape Egmont Fault Zone (Figure 2.2): the tectonically active Eastern Mobile Belt, which includes the Central and Northern grabens and an associated buried Miocene andesitic volcanic arc (Mohakatino Volcanic Center, MVC), and the tectonically quiescent and structurally simple Western Stable Platform, which lacks fault activity. The study area includes the Northern Graben and eastern portions of the Western Stable Platform (Figure 2.2).

The basin has undergone a complex and diverse tectonic history that includes phases of rifting and passive margin development overprinted by several stages of foreland evolution and volcanism associated with the evolving Pacific and Australian convergent plate boundary (King & Thrasher, 1992; King & Thrasher, 1996). The Northern Graben, the subject of this study, is a northeast-southwest-oriented structure that opens towards the northeast, where it reaches a maximum width of about 40 km, The Northern Graben was formed during back-arc rifting in the early Pliocene (King & Thrasher, 1996). The Cape Egmont and Turi fault zones constitute its western and eastern boundaries, respectively (Figure 2.2). Extension in the Taranaki Basin was preceded by

mid–late Miocene volcanism (12–16 Ma) (King & Thrasher, 1992; Giba et al., 2010) and the formation of submarine andesitic stratovolcanoes located along the axis of the graben (MVC, Figure 2.2).

The main lithostratigraphic units related to the Pliocene–Recent tectonic event within the Taranaki Basin are associated with the Rotokare Group (King & Robinson, 1988) (Figure 2.3). The Mangaa Formation is the lowermost stratigraphic unit contained within the Northern Graben, and is composed of a series of basin floor fan deposits (Hansen & Kamp, 2002). The Giant Foresets Formation comprises a thick (up to 2,000 m) shelf-to-basin succession of mostly fine-grained sediments (King & Thrasher, 1996; Hansen & Kamp, 2002; Hansen & Kamp, 2004; Morgans, 2006). This succession is characterized by the development of high relief clinoforms (as high as 1,500 m; Figure 2.4a). The approach for this study involves quantification of clinoform architectures within the Giant Foresets Formation in order to address the following set of questions: (1) Are there geomorphological differences among the various clinoform architectures in the Giant Foresets Formation and if so are they controlled by changes in tectonism, sediment supply, fluctuations of relative sea level, or current-controlled processes? If geomorphological differences are controlled by a combination of geologic factors, what are the dominant processes? (2) Can the Giant Foresets Formation clinoforms be categorized quantitatively based on their differing depositional profiles? What can their morphologies tell about sediment supply and transport mechanisms and is there a relationship between clinoform architecture and lithological composition? (3) Does clinoform development, structural domain, and tectonic regime within the Taranaki Basin drive sediment partitioning? Can I predict areas of sediment accumulation along the shelf margin and areas of sediment bypass and accumulation in deep-water regions?

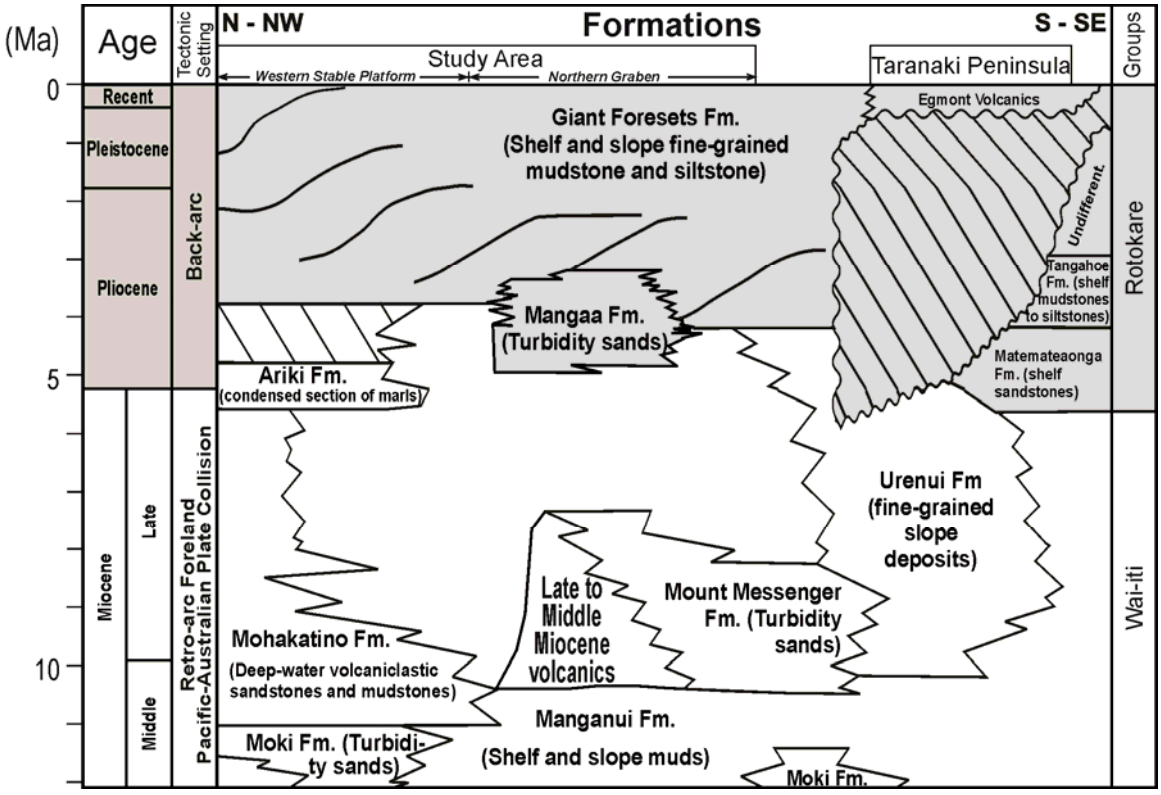

Figure 2.3: Miocene–Recent chronostratigraphic chart for Taranaki Basin (modified from Hansen and Kamp, 2002) including the offshore Pliocene–Recent Giant Foresets Formation of the northern Taranaki Basin composed of continental-scale clinoforms with heights that exceed 100 m.

Figure 2.4

(a) Uninterpreted seismic profile in the northern Taranaki Basin

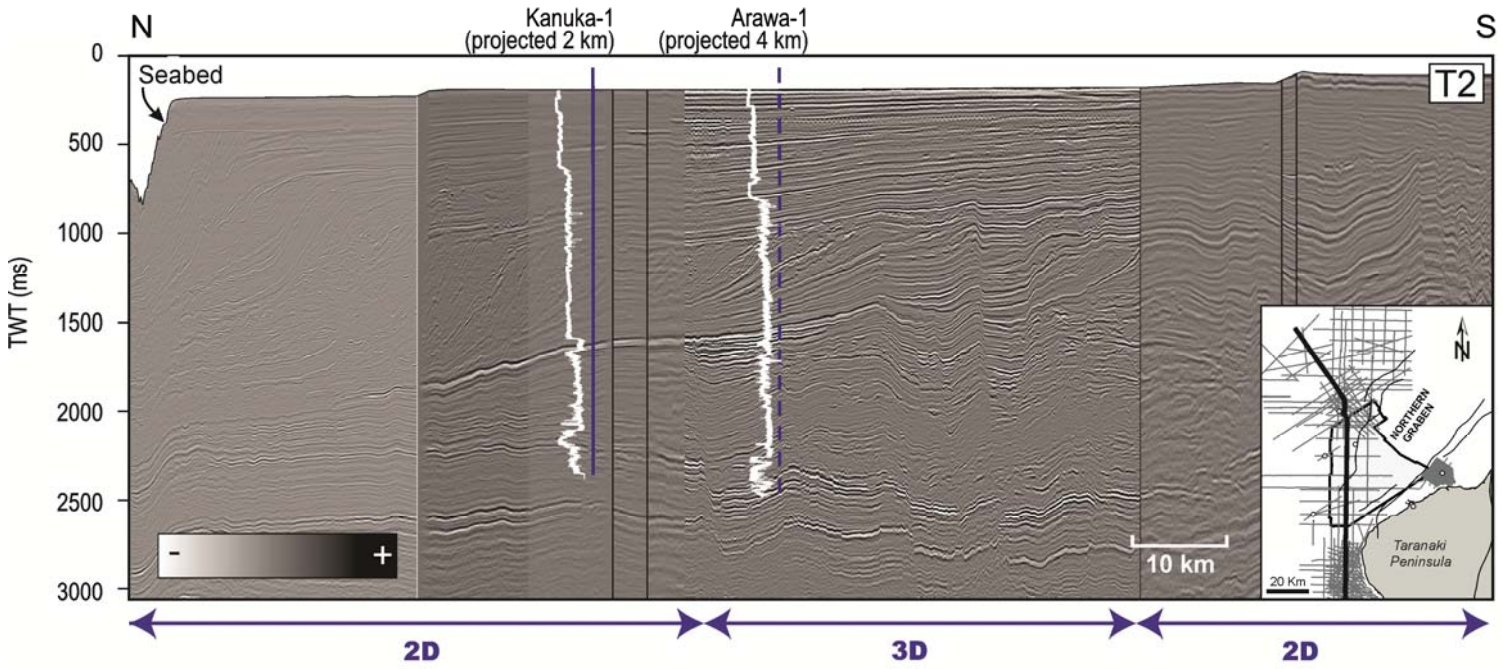

Figure 2.4 (continued)

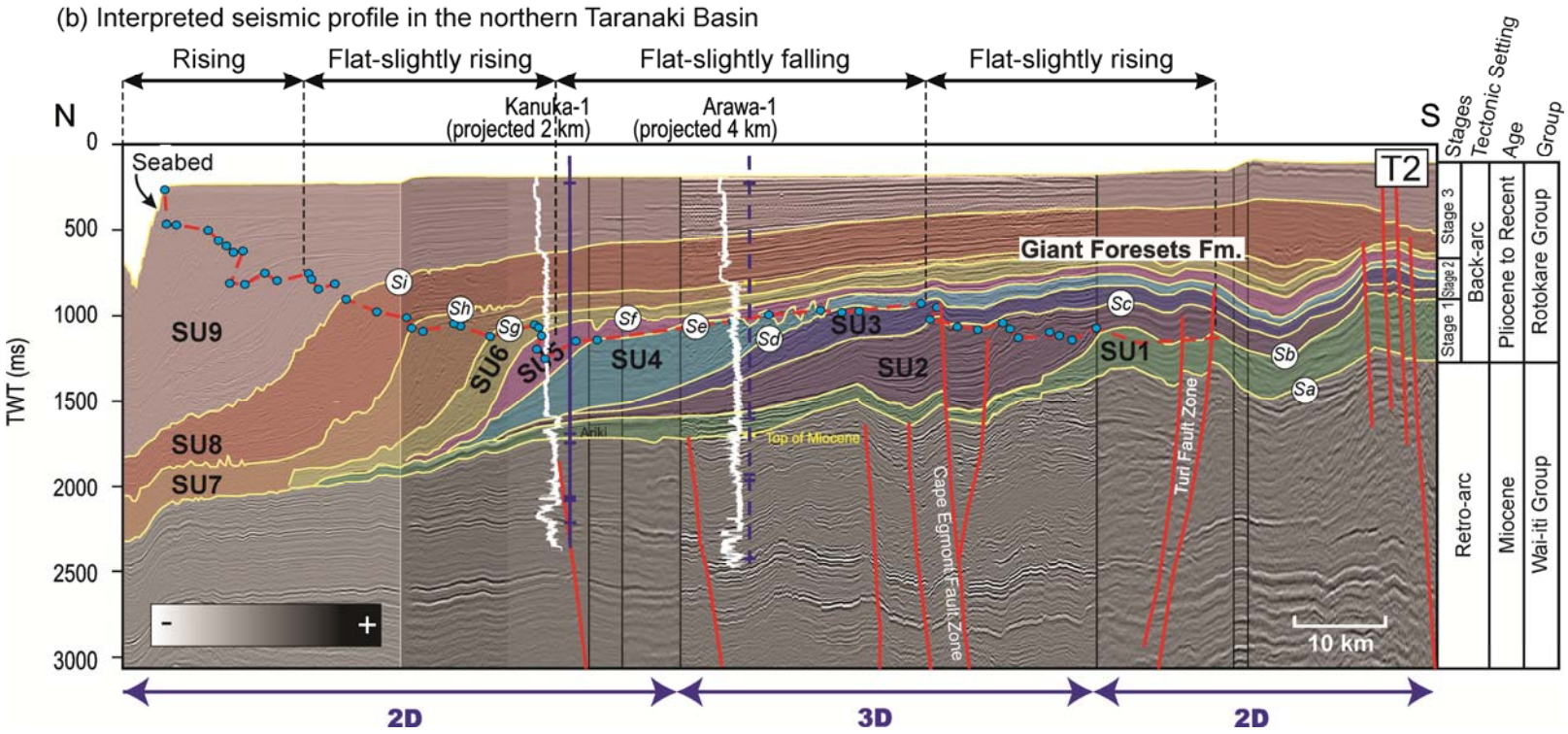

Figure 2.4: Uninterpreted and interpreted composite seismic profile (including 2D and 3D datasets) along depositional dip (see inset map for location). (a) Seismic image showing well-defined clinoforms of the Giant Foresets Formation. (b) Composite seismic line including the interpretations of key surfaces (Sa to Seabed), seismic units (SU1–SU9), stages of clinoform evolution (Stages 1–3), and shelf-edge trajectories. Notice progressive northward migration of shelf break through time and change from mostly progradational (SU1–SU6) to aggradational margin (SU6–SU9).

DATASET AND METHODOLOGY

Seismic and Well Data

The primary datasets used to conduct this study were 2D and 3D seismic reflection data and well data (Figure 2.2). The 3D seismic volume was acquired in 2005 and covers an area of 1,700 km^2, with vertical resolution of about 10–15 m in the Pliocene–Recent section. Four thousand line kilometers of 2D seismic profiles located within the offshore area of the Taranaki Peninsula were also available for this study. The vertical seismic resolution of these 2D seismic lines varies between 20–30 m (Figure 2.4a) in the Pliocene to Recent section. Imaging depths reach a maximum of 7 seconds (s) TWTT across the study area for both the 2D and 3D seismic surveys.

Geophysical logs, biostratigraphic, and lithological information from six exploratory wells (see Figure 2.2 and Table 2.1) were also integrated into this study. One of the wells is located within the 3D seismic volume and the others are located in close proximity to the seismic volume (Figure 2.2). Two-dimensional seismic lines allowed for the correlation of key picks from these adjacent wells into the seismic volume. Two other wells located in the Taranaki Peninsula (Figure 2.2) lack quality biostratigraphic and lithological information and could not be used in the correlation of key picks. Paleoenvironmental and age interpretations, based on existing biostratigraphic zonations (Hoskins & Raine, 1984; Morgans, 1984; Crundwell et al., 1992; Hansen & Kamp, 2004; Morgans, 2006; Crundwell, 2008), were performed within the study area (Figure 2.5). In addition, original micropaleontological counts were used to reinterpret and refine the age control within the stratigraphic interval of interest.

Well	Year	Total Depth (m)	Time/ Depth	GR	Resist.	Sonic	Density	Biostratig. Info.	Litho. Info.	Well Report
Arawa-1	1991	3055	Yes	Yes	Yes	Yes	Yes	Yes	Yes	Yes
Kanuka-1	2007	2879	Yes	Yes	Yes	Yes	Yes	Yes	Yes	Yes
New Plymouth-2	1965	4451	No	Yes	Yes	Yes	Yes	Yes	Yes	Yes
Okoki-1	1989	4250	Yes	Yes	Yes	Yes	Yes	Yes	Yes	Yes
Taimana-1	1983-84	4195	No	Yes	Yes	Yes	Yes	Yes	Yes	Yes
Witiora-1	1984	4229	No	Yes	Yes	Yes	Yes	Yes	Yes	Yes

Table 2.1: Summary table of attributes from available well data in the Taranaki Basin.

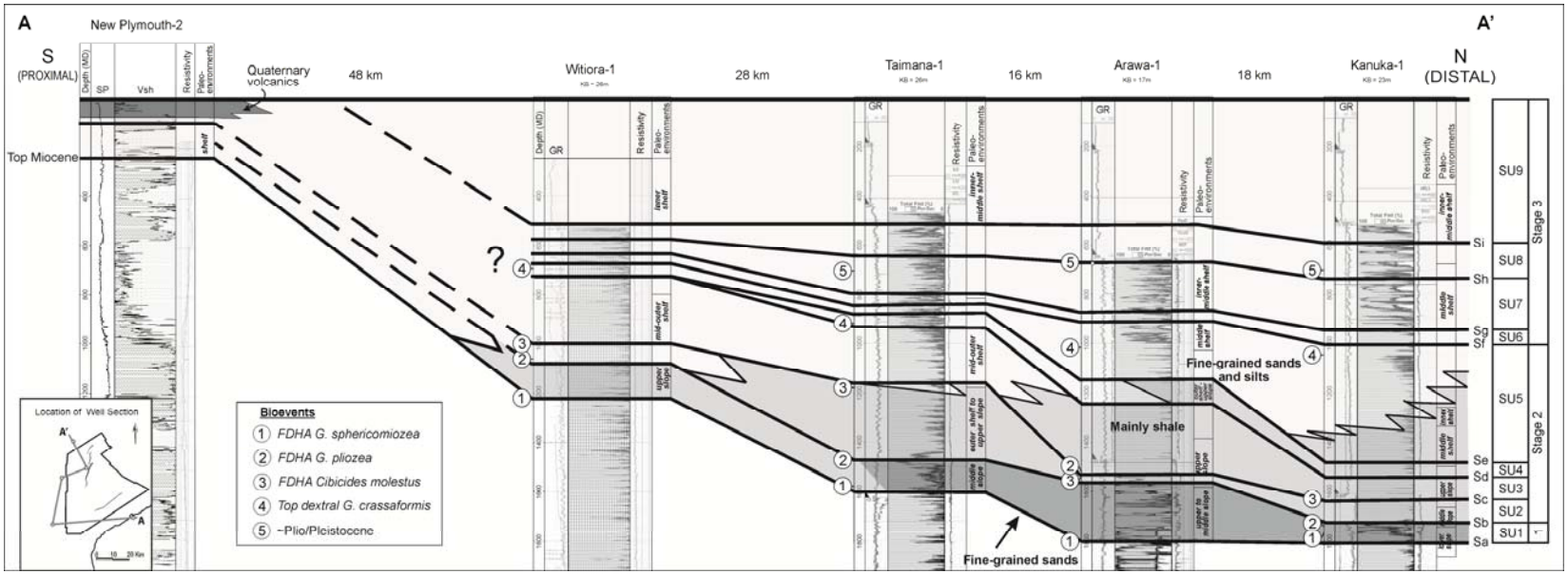

Figure 2.5: Cross section showing the correlation of key wells including Witiora-1, Taimana-1, Arawa-1, and Kanuka-1 (see inset map for locations). Cross section includes bioevents as well as lithostratigraphic and paleoenvironmental interpretations including basin deepening toward north. Biostratigraphic markers originally reported by Morgans (2006) and Crundwell (2008) but reinterpreted in this study.

Velocity information within the study area was available for three key wells in the form of check shots and sonic logs (Table 2.1). Seismic velocity information derived from the wells was calibrated with seismic using the elaboration of four synthetic seismograms (e.g., Figure 2.6). Synthetic seismograms were also used to tie the age and paleoenvironmental interpretations from the wells to seismic data. Approximate time-depth conversion within the interval of interest is 100 milliseconds (ms) two-way-travel-time (TWTT) are equivalent to 100 m. In addition, a velocity model was built using the interpolation of calibrated time-depth curves. This analysis facilitated the depth-conversion of key seismic transects and allowed to describe the true geometric relationships associated with the structural and stratigraphic configuration of the Giant Foresets Formation (Figure 2.7). Backstripping analyses performed in the 3D survey show that the difference between the compacted (measured) and decompacted (calculated) Pliocene–Recent section is no more than 12% (Cardona, 2009; Giba et al., 2012); therefore, no correction was made for burial compaction.

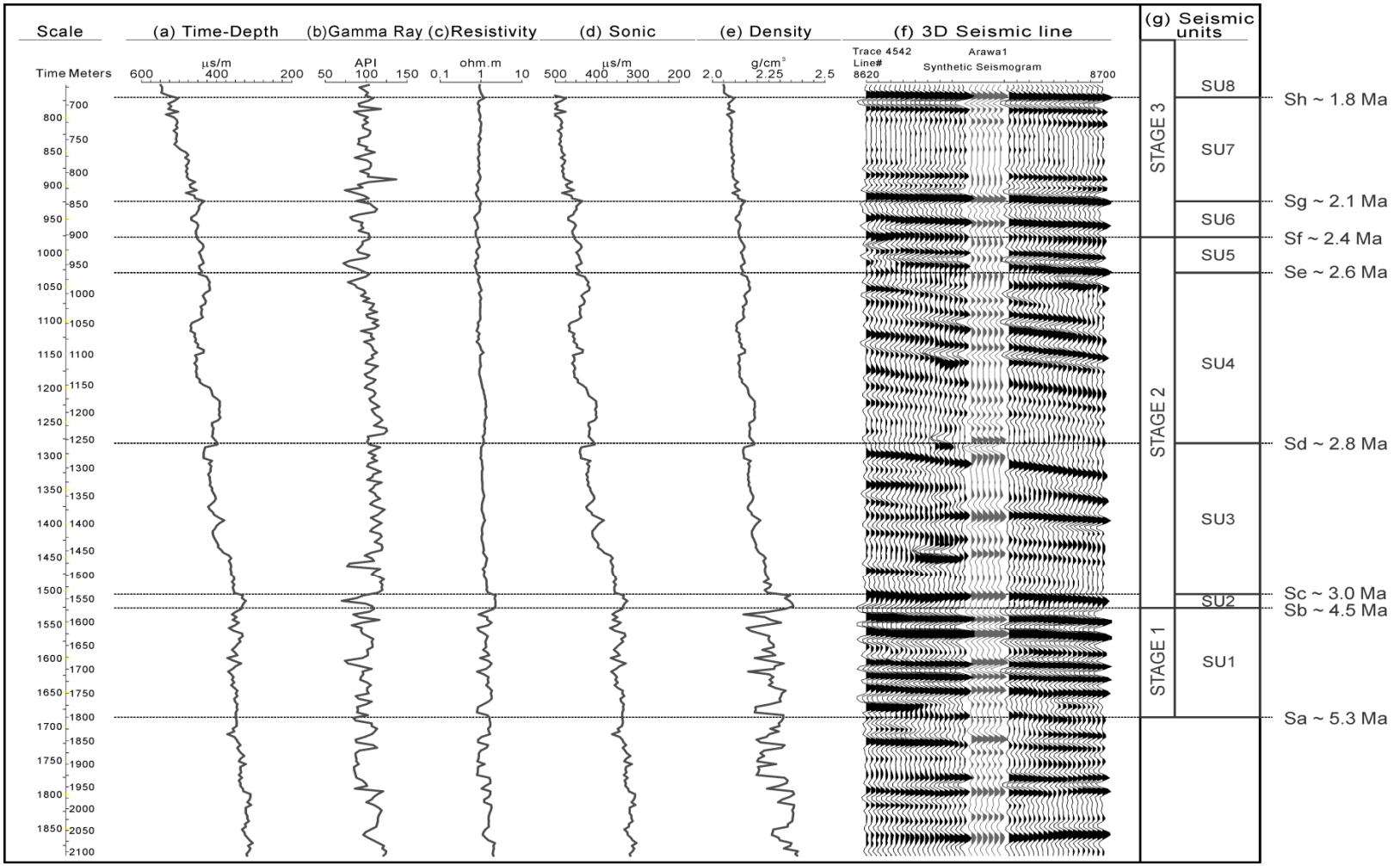

Figure 2.6: Seismic-well calibration using synthetic seismogram generated using Syntool for well Arawa-1. Image includes time-depth, gamma ray, resistivity and density logs, as well as seismic line tied to with well information.

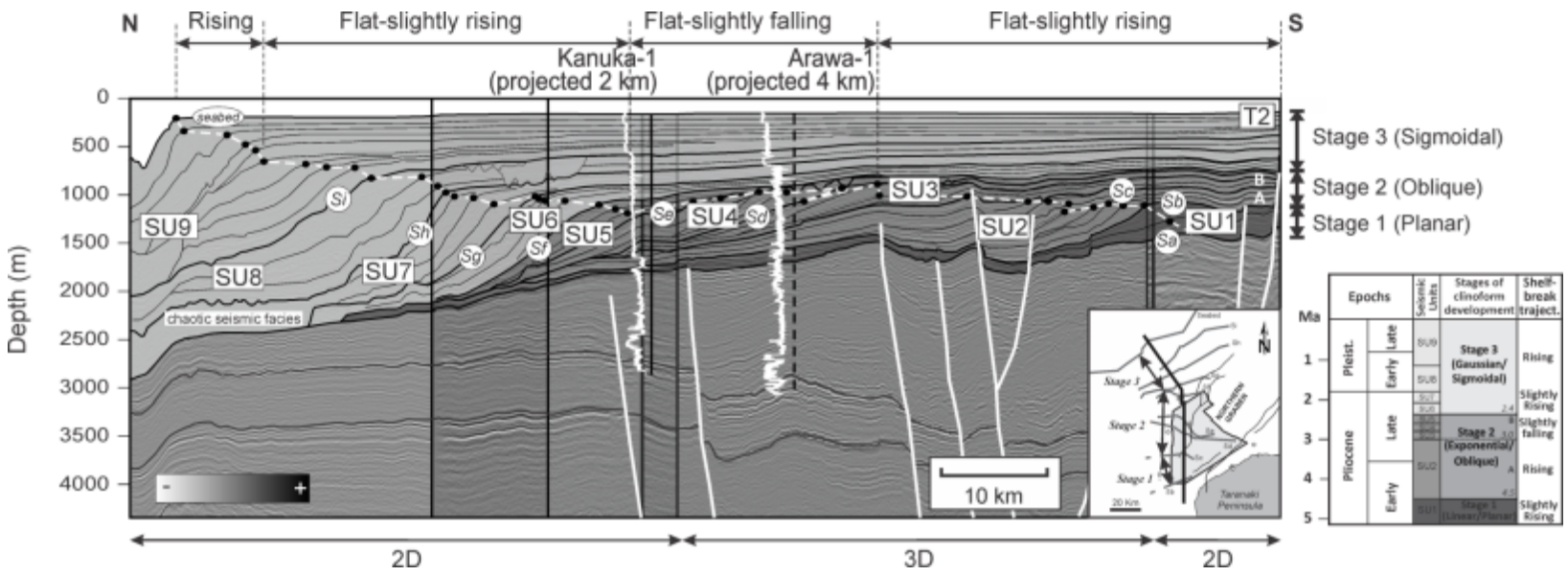

Figure 2.7: Interpreted depth-converted seismic profile, showing the three stages of clinoform development (Stages 1–3) interpreted here. Gamma ray logs are displayed for each well. Vertical exaggeration=9x.

Definition of Seismic Units and Stages of Clinoform Evolution

The Giant Foresets Formation is recorded in the seismic data as a well-developed stacked succession of clinoforms that prograde towards the northwest (King & Thrasher, 1996; Hansen and Kamp, 2002) (Figure 2.4a). Structure maps on key stratigraphic horizons and interval isochron maps of key stratigraphic units were generated using conventional interpretation methods (i.e., seismic facies analysis and identification of reflection terminations; Mitchum & Vail, 1977). Ten key surfaces (including the seabed) were identified and mapped across the study area (surfaces "Sa" to "seabed", Figures 2.4b and 2.7). These surfaces define the top and base of nine major seismic units (SU1 to SU9). Seismic units were defined based on seismic facies analysis and individual clinoform characteristics. I used only data from the 3D seismic survey to generate isochron maps of individual seismic units (SU1 to SU9), because the spacing and resolution of the 2D seismic grid were insufficient to confidently and meaningfully extend the interpretation of bounding surfaces associated with individual seismic units (Figure 2.2). However, seismic packages (SU1 to SU9) were combined into three stages of basin fill and data from both the 2D seismic grid and the 3D seismic volume were used to generate gross isochron maps that represent these three stages of fill (stages 1 to 3). In addition, extraction of root-mean square (RMS) seismic amplitude was also performed using key stratigraphic surfaces. RMS amplitude extractions were used to help in the identification of local amplitude anomalies, lineaments, and any other geological features that might have depositional and/or structural significance (Posamentier & Kolla, 2003; Posamentier, 2005). Paleoenvironmental information obtained from key wells was included in order to generate well-controlled paleogeographic maps.

Definition of Clinoform Morphometric Parameters

The Pliocene–Recent clinoforms from the Giant Foresets Formation were classified according to their morphology. Morphometric parameters of foreset inclination, and foreset height and length, were measured for each clinoform. Progradation and aggradation rates were calculated for each clinoform (Figure 2.1). Restoration of data to pre-faulted/folded stages was necessary before these measurements were confidently determined (Henriksen et al., 2011).

Shelf trajectories were documented through analysis of temporal changes in clinoform rollover points. The shelf-edge position for various stages in a basin's history has been defined as coincident with clinoform rollover points (Adams & Schlager, 2000; Kertznus & Kneller, 2009). Because all clinoforms that form part of the Giant Foresets Formation are defined as continental-scale clinoforms (foreset heights >100 m; Emery, 1981; Helland-Hansen and Hampson, 2009), the shelf-edge position always coincides with the location of the clinoform rollover point at any given time (Figure 2.1). Shelf-edge trajectories were traced in each of the seismic transects by identifying and connecting rollover points of temporally unique units (Figure 2.4b). The base of the slope was defined as the point in a dip profile where a significant decrease in slope occurs (O'Grady & Syvitski, 2002). The foreset inclination is defined as the angle (α) measured on a right angle triangle defined by the foreset height and length, as shown in Figure 2.1. If an important change in slope was observed close to the shelf edge region, measurements of upper-slope inclination (θ) were also taken in order to estimate the degree of incision and deformation affecting the upper slope region of a given clinoform. From these measurements a series of plots showing the relationships between the different parameters inside and outside the Northern Graben were generated. This detailed documentation of individual clinoform geometries and rollover positions within

seismic units (SU1 to SU9) enabled deduction of stacking patterns and shelf-edge trajectories to a high degree of vertical resolution. This level of detail was needed in order to compare the Giant Foresets Formation clinoform morphologies with postulated eustatic (Haq et al., 1987; Miller et al., 2005) and $\delta^{18}O$ isotope curves (Lisiecki & Raymo, 2005), as a means of determining the relative role of eustatic fluctuations in the Taranaki Basin.

DESCRIPTION OF STRUCTURAL AND STRATIGRAPHIC ELEMENTS

A series of maps were created to provide information from which I could assess, for each seismic unit (depositional interval): (1) thickness and distribution, (2) depositional strike and dip, (3) clinoform rollover trajectories, and (4) the location, steepness and orientation of paleoshelf to slope transitions.

Structure maps were created for the top and base of each seismic unit SU1 to SU9 (surfaces Sa to seabed) (Figure 2.8). These maps expose the importance of the Northern Graben in influencing the shelf physiography and clinoform dimensions. The Northern Graben is recognizable in the structural maps by the presence of en echelon faults that are separated by relay ramps in the northern portions of the 3D survey. These en echelon faults form part of the Cape Egmont and Turi fault zones to the west and east, respectively (Figure 2.2). All structural surfaces, except for the seabed, are characterized by a steepening of their contours around the position where the Northern Graben starts (northern portions of the 3D survey; Figure 2.8a–i). This steepening is interpreted to indicate a change in gradient of the paleo-structural slope.

Figure 2.8

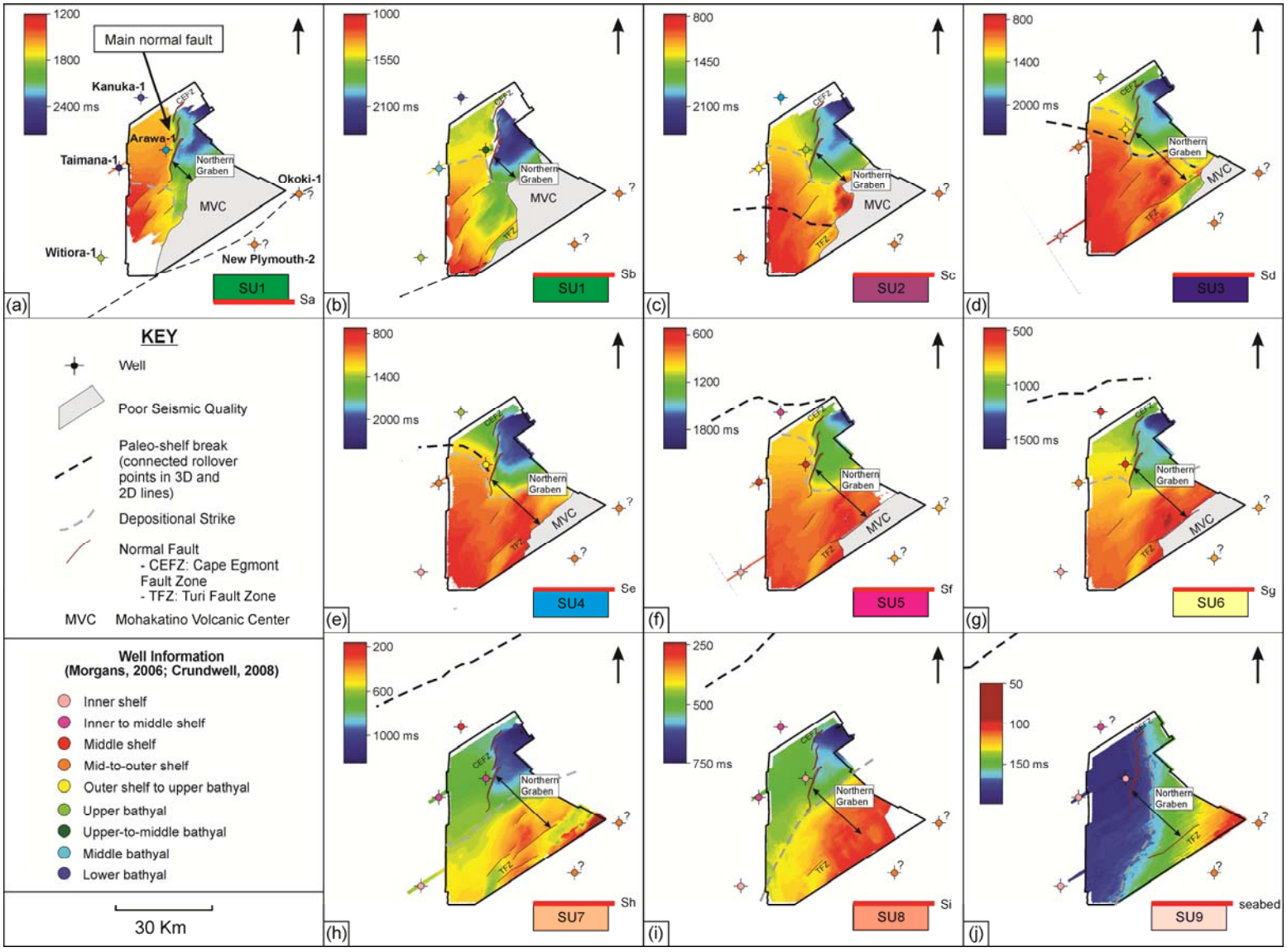
Main normal fault
Kanuka-1
Arawa-1
Taimana-1
Okoki-1
Witiora-1
New Plymouth-2
CEFZ
Northern Graben
MVC
TFZ
SU1
Sa
Sb
SU2
Sc
SU3
Sd
SU4
Se
SU5
Sf
SU6
Sg
SU7
Sh
SU8
Si
SU9
seabed
(a)
(b)
(c)
(d)
(e)
(f)
(g)
(h)
(i)
(j)
KEY
Well
Poor Seismic Quality
Paleo-shelf break (connected rollover points in 3D and 2D lines)
Depositional Strike
Normal Fault
- CEFZ: Cape Egmont Fault Zone
- TFZ: Turi Fault Zone
MVC Mohakatino Volcanic Center
Well Information (Morgans, 2006; Crundwell, 2008)
Inner shelf
Inner to middle shelf
Middle shelf
Mid-to-outer shelf
Outer shelf to upper bathyal
Upper bathyal
Upper-to-middle bathyal
Middle bathyal
Lower bathyal
30 Km

Figure 2.8: Time-structure maps of seismic unit bounding surfaces (Sa to Seabed) in area covered by the 3D seismic volume. Colored well symbols represent paleoenvironmental interpretations based on biostratigraphic assemblages as interpreted by Morgans (2006) and Crundwell (2008).

An additional map compiles the clinoform rollover positions identified in both 2D and 3D seismic transects for all interpreted horizons (Sa to seabed) to help visualize the evolution of paleoshelf edge trajectories through time (Figure 2.9 and dotted black lines in Figure 2.8). Variations in the location of clinoform rollover points across the study area over time also provide a measure of progradation, yielding insight into basin margin history. In addition, isochron maps (Figure 2.10) of individual seismic units (SU1 to SU9) bounded by structural horizons were used to pinpoint depocenter locations, their relation with their main structural elements and to assess their changes over time. The nine seismic units (SU1 to SU9) were separated into three groups (stages 1 to 3) on the basis of similarities in morphologies, seismic facies and their overall trajectories.

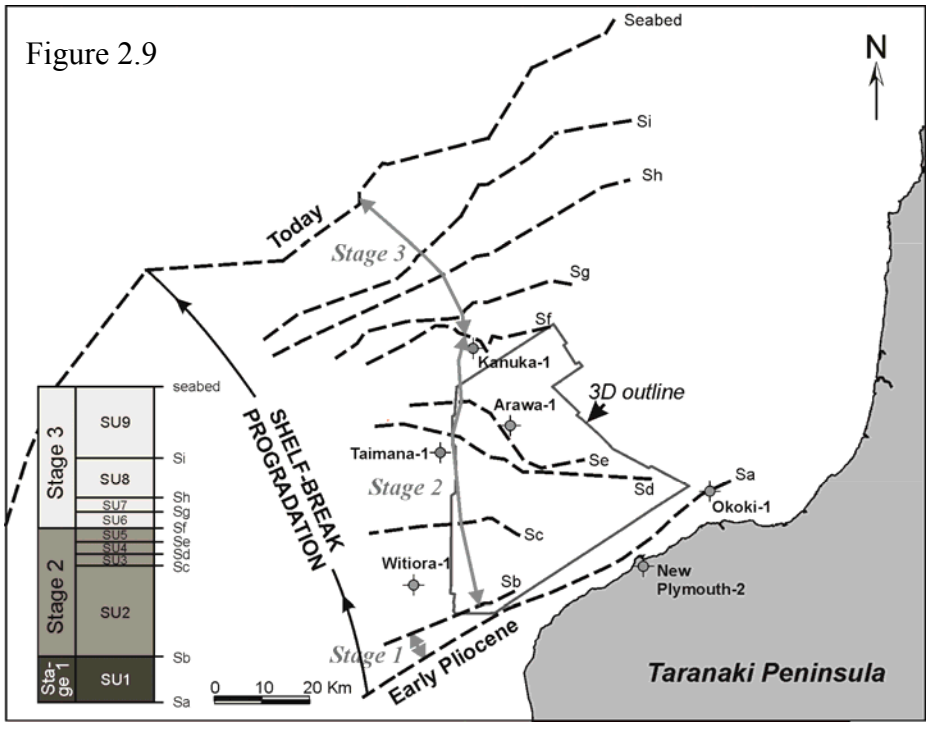

Figure 2.9: Graphic showing the migration of individual shelf edges (Sa - Seabed) from early Pliocene to Holocene. Rollover points were correlated using seismic data as proxies to identify paleoshelf edge locations for base and top of individual seismic units. Note overall northward migration of the shelf edge.

Stage 1: Seismic Unit SU1 (4.5–5.3 Ma)

Seismic reflections associated with individual clinoforms in SU1 are laterally continuous, showing high to moderate amplitudes. In addition, clinoform profiles are characterized by the presence of laterally extensive bottomsets that thin basinward (Figure 2.7). SU1 exhibits a relatively uniform thickness with an apparent increase towards the southeast, near the location of the MVC (Figure 2.10a). The depocenter of SU1 has a northeast-southwest orientation and its location could be related to flexural subsidence associated with the Miocene-active Taranaki Fault. Sediment is inferred to have been derived from the east, where active sediment sources were present between 4.5 to 5.3 Ma. The formation of the mid-to-late Miocene MVC also caused uplift of Eocene and early Miocene strata, forming paleo-bathymetric highs that acted both as additional sources of sediment and as sediment routing systems that partially controlled accommodation in this part of the basin. Structural maps for surfaces Sa and Sb suggest that paleoshelf edges were oriented predominantly southwest-northeast (Figures 2.8a-b and 2.9). The majority of sediments during SU1 accumulated in a position that was close to but outboard of the paleoshelf edge. The orientation of the main depocenter at this time was not completely aligned with the graben, suggesting that SU1 was deposited before the opening of the Northern Graben was complete.

Figure 2.10

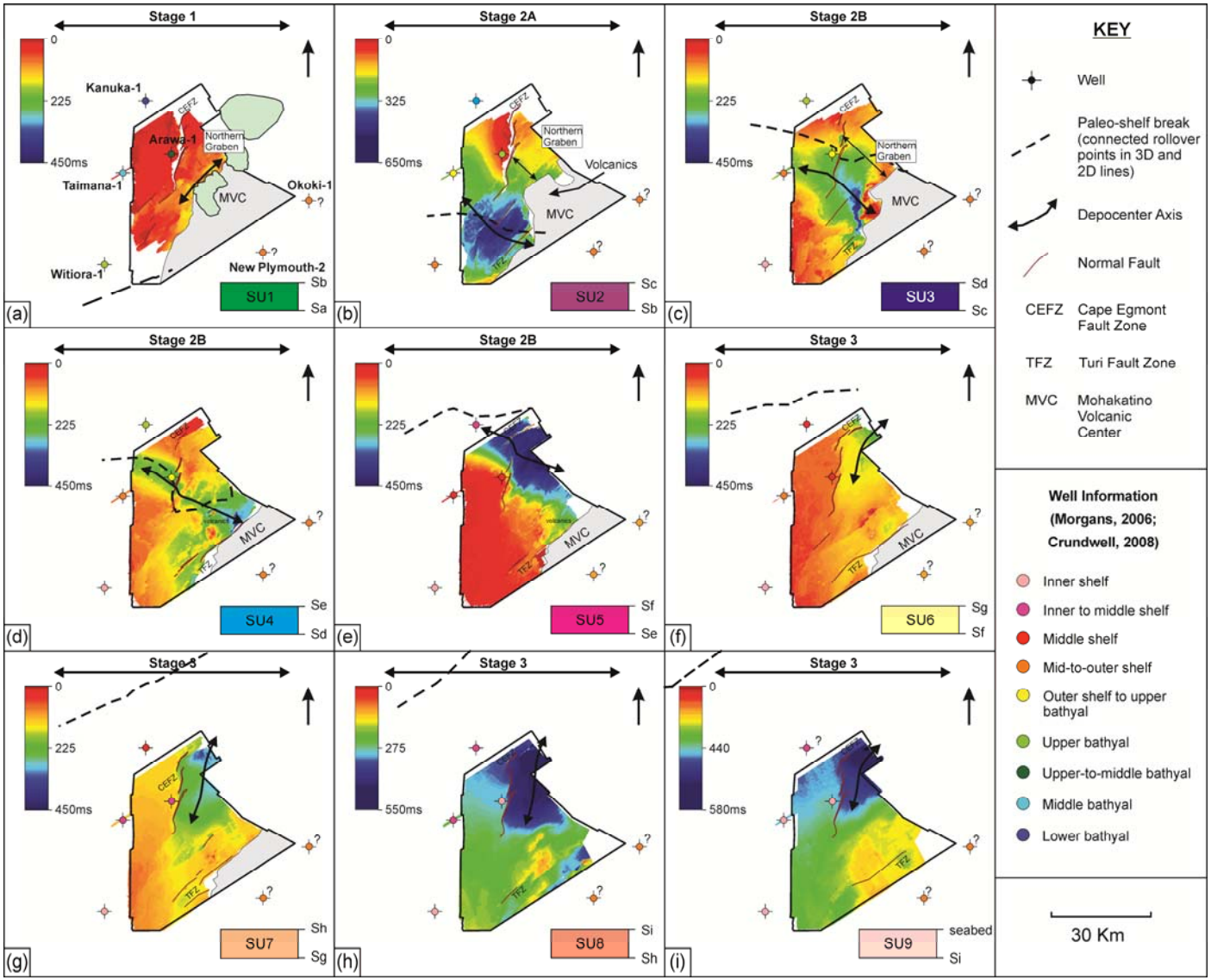
Stage 1
Kanuka-1
Arawa-1
Northern Graben
Taimana-1
MVC
Okoki-1
Witiora-1
New Plymouth-2
CEFZ
0
225
450ms
Sb
Sa
SU1
(a)
Stage 2A
325
650ms
Volcanics
Sc
Sb
SU2
(b)
Stage 2B
Sd
Sc
SU3
(c)
Stage 2B
Se
Sd
SU4
(d)
Stage 2B
Sf
Se
SU5
(e)
Stage 3
Sg
Sf
SU6
(f)
Stage 3
275
550ms
Si
Sh
SU8
(h)
Stage 3
440
580ms
seabed
Si
SU9
(i)
Stage 3
Sh
Sg
SU7
(g)
TFZ
KEY
Well
Paleo-shelf break (connected rollover points in 3D and 2D lines)
Depocenter Axis
Normal Fault
CEFZ Cape Egmont Fault Zone
TFZ Turi Fault Zone
MVC Mohakatino Volcanic Center
Well Information (Morgans, 2006; Crundwell, 2008)
Inner shelf
Inner to middle shelf
Middle shelf
Mid-to-outer shelf
Outer shelf to upper bathyal
Upper bathyal
Upper-to-middle bathyal
Middle bathyal
Lower bathyal
30 Km

Figure 2.10: Isochron maps from seismic units SU1 through SU9 in area covered by 3D seismic volume. Depocenter axes indicated with double-headed arrow for each unit.

Stage 2: Seismic Units SU2–SU5 (2.4–4.5 Ma)

Seismic reflections associated with the topsets of individual clinoforms within SU2 are characterized by a low-amplitude, continuous character while laterally equivalent seismic reflections associated with the foreset and bottomset segments of these clinoforms display a high-amplitude and continuous response (Figure 2.4b). Seismic reflections linked to the topsets of clinoforms associated with seismic unit SU3 continue to show a low-amplitude and continuous character, but their foresets and bottomsets are characterized a low-amplitude and semicontinuous (wavy) response in some areas. Clinoforms contained within seismic unit SU4 show continuous and low- to medium-amplitude topsets that are affected by incisions located near the rollover points to the north while the foreset and bottomset portions of these clinoforms have discontinuous and low-amplitude reflections (Figure 2.4b). Clinoforms associated with seismic unit SU5 are characterized by semicontinuous and low-amplitude reflections, with their topsets filling incisions in the outer shelf and their foresets occupying a relatively restricted area in the upper slope region. In general, the topset portions of clinoforms associated with seismic units SU2 to SU5 tend to be very thin while there is a progressive increase in foreset declivities as the section becomes younger (Figure 2.4).

Structural maps for surfaces Sb to Sf (Figure 2.8b–f) indicate that the orientation of paleoshelf edges progressively shifted from northeast-southwest (Sb) to almost east-west (Sf) during this time (4.5 to 2.4 Ma; Figure 2.9). Mapping of paleoshelf edges through time also shows a progressive northward migration (Figure 2.9). Isochron maps for seismic units SU2–SU5 (Figure 2.10b–e) show a gradual migration of depocenters

toward the northeast. This migration reflects the opening of the Northern Graben and creation of accommodation, allowing for the redistribution of sediments toward the northeast. Depocenters for seismic units SU2–SU5 are northwest-southeast oriented, with the bulk of sediments accumulating on the hanging-wall of faults that bounded the Northern Graben (Cape Egmont and Turi fault zones) (Figure 2.10b–e). The alignment between structural fabric (fault control) and physiographic boundaries (shelf-edge location) reached its maximum during deposition of seismic unit SU4 (2.6 to 2.8 Ma), when interpreted paleoshelf edges for surfaces Sd and Se coincided with the southern boundary of the Northern Graben (Figures 2.8 and 2.10). Structural deformation associated with the activation of the Northern Graben during this period influenced clinoform architectures, sediment distribution, and accommodation within the basin.

Stage 3: Seismic Units SU6–SU9 (0–2.4 Ma)

There is an increased level of sediment preservation on the topsets of clinoforms associated with seismic units SU6–SU9. In addition, deep, channelized incisions are also observed on the distal portion of the topsets near the shelf edge (Figure 2.7). Topsets are characterized by continuous and medium- to high-amplitude reflections that transition to low-amplitude and sometimes chaotic seismic facies on the foresets (Figure 2.4). Clinoform foresets within this interval tend to be steeper than in older seismic units and the foreset to bottomset transition is more evident on seismic profiles. Structural maps of surfaces Sf to the seabed (2.4–0 Ma; Figure 2.8f–j) document a progressive change in paleoshelf edges from an east-west orientation (SU2–SU5) to a northeast-southwest orientation (SU6–SU9) (Figure 2.9). In addition, isochron maps for seismic units SU6–SU9 show the development of a northwest-southeast V-shaped depocenter (Figure 2.10f-i). This depocenter had an opening toward the northeast and likely represented a local minibasin that was infilled by shelfal facies suggested by the predominance of clinoform

topsets (Figure 2.7). The bulk of sedimentation was occurring toward the north, where 2D seismic lines show clinoform profiles covering the outer-shelf, slope, and basin floor portions of the basin (Figure 2.7).

In general structural and isochron maps and well information indicate an overall migration of paleoshelf edges and depocenters toward the north-northwest within the Taranaki Basin during Pliocene–Recent (Figures 2.7 and 2.9).

CLINOFORM ARCHITECTURE AND STACKING

Shelf-Edge Trajectories

Seismic transects inside (T1) and outside (T2) the Northern Graben were used to examine shelf-edge trajectories within these two different structural domains (Figure 2.11). Visual examination of shelf-edge trajectories on the seismic profiles (Figures 2.7 and 2.11) and measurements of aggradational and progradational rates for individual clinoform packages (Figure 2.12a–b and Table 2.2) indicate that there are remarkable differences that occurred inside and outside the graben region.

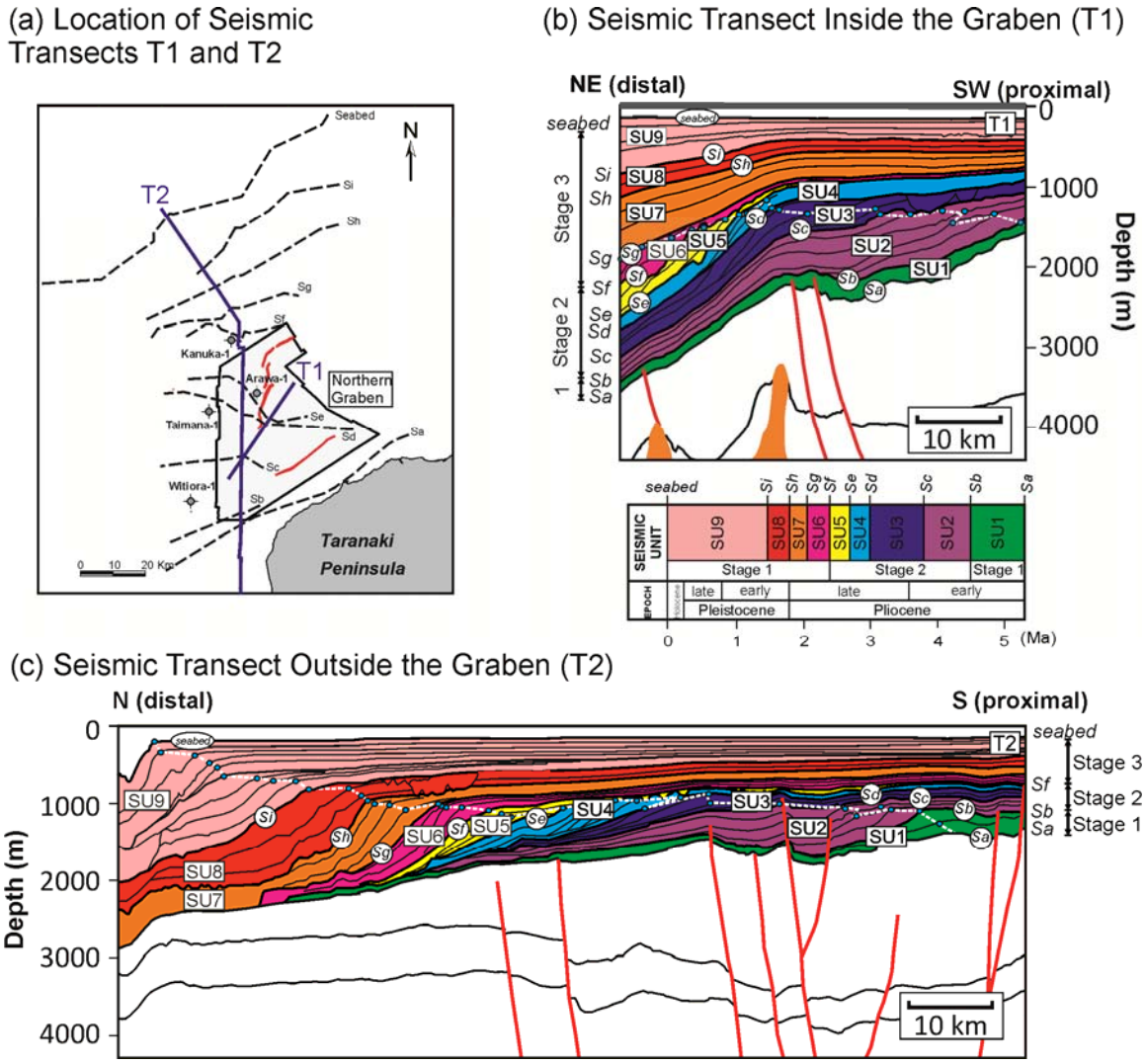

Figure 2.11: Line drawings of two depth-converted seismic lines. Each transect showcases interpretation of seismic units (SU1–SU9), three stages of clinoform evolution (Stages 1–3), and rollover locations for individual clinoforms (blue dots). Rollover points used as proxy to identify paleo shelf-edge locations at specific times. (a) Map showing location of seismic transects (T1 and T2) and location of individual paleoshelf breaks (Sa to Seabed). Shelf-edge trajectories indicate progressive northward migration of continental margin from early Pliocene to Holocene. (b) Seismic transect 1 (T1) located inside graben region; lateral continuity toward northeast hindered by lack of seismic coverage. (c) Seismic transect 2 (T2) located outside graben region. Shelf-edge trajectories for seismic units SU4 through SU6 are falling inside graben (T1) but are flat to slightly rising outside graben region (T2).

Figure 2.12

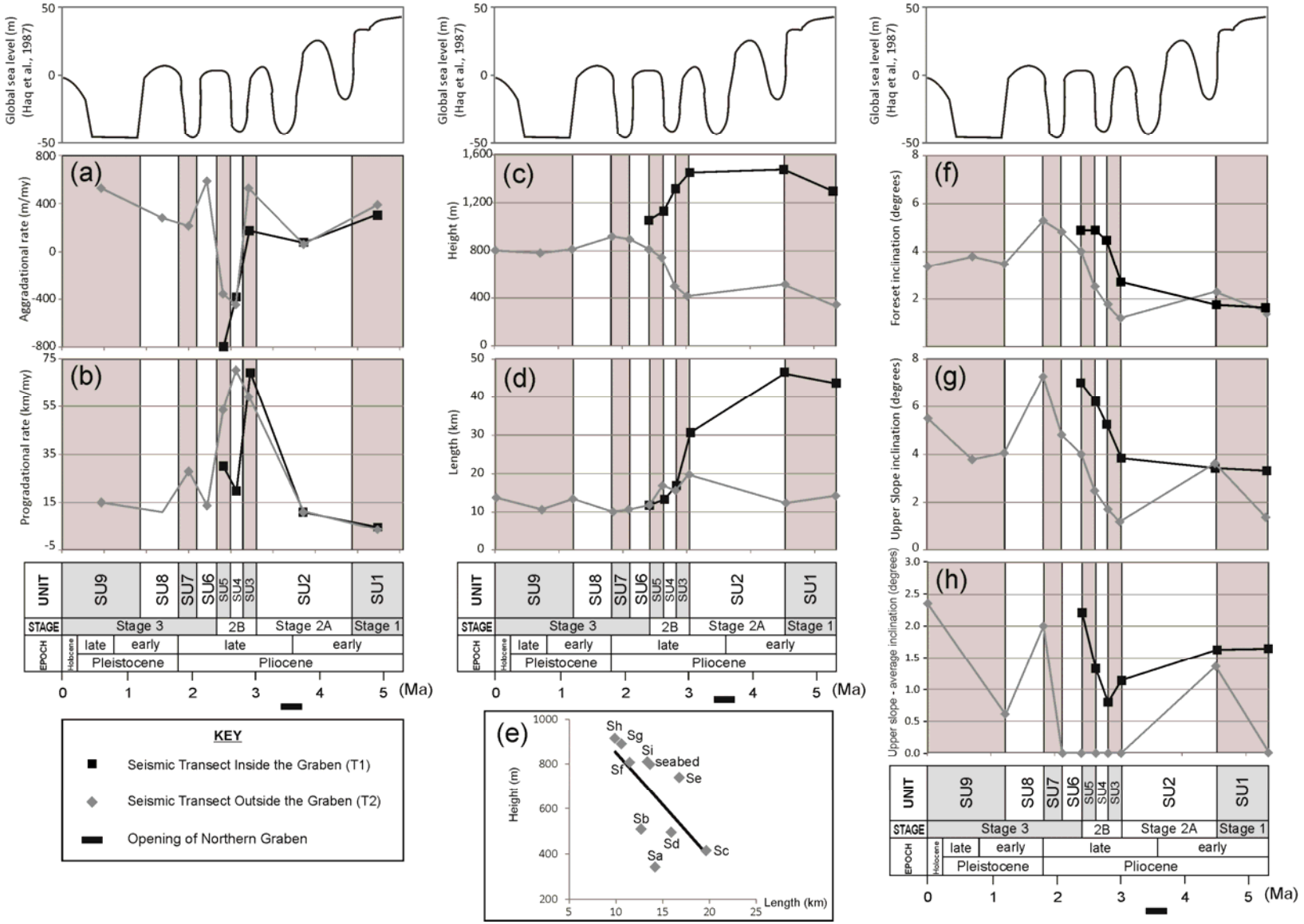
Global sea level (m) (Haq et al., 1987)
(a)
Aggradational rate (m/my)
(b)
Progradational rate (km/my)
(c)
Height (m)
(d)
Length (km)
(e)
Height (m)
Length (km)
Sh
Sg
Si
seabed
Se
Sf
Sb
Sd
Sc
Sa
(f)
Foreset inclination (degrees)
(g)
Upper Slope inclination (degrees)
(h)
Upper slope - average inclination (degrees)
UNIT
SU9
SU8
SU7
SU6
SU5
SU4
SU3
SU2
SU1
STAGE
Stage 3
2B
Stage 2A
Stage 1
EPOCH
Holocene
late
early
Pleistocene
Pliocene
(Ma)
KEY
Seismic Transect Inside the Graben (T1)
Seismic Transect Outside the Graben (T2)
Opening of Northern Graben

Figure 2.12: Graphs illustrating quantitative relationships between morphological parameters through time. Parameters are calculated using measurements of clinoform architectures inside (T1) and outside (T2) Northern Graben. Lack of data coverage inside graben region allowed for only measurements of parameters for seismic units SU1 through SU5. (a) Aggradational rates of shelf-edge trajectories. (b) Progradational rates of shelf-edge trajectories. (c) Clinoform heights. (d) Clinoform lengths. (e) Crossplot of clinoform height versus length outside graben region. (f) Average clinoform foreset inclination values. (g) Upper slope inclination values. (h) Difference between upper slope and average clinoform foreset inclination values.

Transect	Surface	Age (Ma)	Foreset inclin. (degrees)	Upper slope inclin. (degrees)	Height (m)	Length (km)	Stage	Seismic unit	Progra-dation (km)	Aggra-dation (m)	Progradation rate (km/my)	Aggradation rate (m/my)	Ratio of aggradation to progradation (/1000)
Inside Graben	Sa	5.3	2	3	1296	44	1	SU1	4	253	5	317	63
	Sb	4.5	2	3	1477	47	2A	SU2	17	110	11	73	7
	Sc	3.0	3	4	1451	31	2B	SU3	14	35	69	173	3
	Sd	2.8	4	5	1318	17		SU4	4	-77	20	-385	-19
	Se	2.6	5	6	1130	13		SU5	6	-160	29	-800	-28
	Sf	2.4	5	7	1061	12							
	Sg	2.1	NO DATA										
	Sh	1.8											
	Si	1.2											
	seabed	0.0											
Outside Graben	Sa	5.3	1	1	342	14	1	SU1	3	305	4	381	105
	Sb	4.5	2	4	510	13	2A	SU2	17	79	11	53	5
	Sc	3.0	1	1	413	20	2B	SU3	12	104	59	521	9
	Sd	2.8	2	2	495	16		SU4	14	-90	71	-451	-6
	Se	2.6	3	3	739	17		SU5	11	-72	54	-361	-7
	Sf	2.4	4	4	808	12	3	SU6	4	174	14	581	41
	Sg	2.1	5	5	892	11		SU7	8	62	28	207	7
	Sh	1.8	5	7	916	10		SU8	7	164	12	274	23
	Si	1.2	3	4	810	13		SU9	19	625	15	521	34
	seabed	0.0	3	6	800	14							

Table 2.2: Summary of geometrical measurements of seismic units interpreted in the northern Taranaki Basin.

Inside the Graben Region (Seismic Transect T1)

Inside the graben region, shelf-edges show a slightly rising to flat trajectory from SU1 through SU3 (early–late Pliocene) and a falling trajectory from SU3 to SU6 (late Pliocene) (Figure 2.11a). Unfortunately, lack of seismic coverage inside the graben region prevent following shelf-edge trajectories and obtaining quantitative measurements of aggradational and progradational rates for the late Pliocene–Recent interval (SU6 to SU9) (e.g., Figures 2.2 and 2.12). Measurements of aggradational rates for individual clinoform packages were calculated in meters per million years (m/my), showing a consistent decrease from 317 to -800 m/my from the early to late Pliocene (SU1–SU5) (Table 2.2 and Figure 2.12a). Two distinctive aggradational trends were identified for the early–late Pliocene section inside the graben region. The first trend shows positive aggradational rates that decrease from 317 to 73 m/my (SU1–SU2) (Figure 2.12a), and coincide with a slightly rising to flat shelf-edge trajectory (Figure 2.11a). The second trend shows negative aggradational rates that decrease at a faster pace from 173 to -800 m/my (SU3–SU5) (Figure 2.12a), and coincide with a falling shelf-edge trajectory (Figure 2.11a). Negative aggradational rates and falling shelf-edge trajectories indicate an increase in sediment erosion and bypass from the outer shelf to the upper slope region in the late Pliocene (SU3–SU5). Measurements of progradational rates for individual clinoform packages were calculated in kilometers per million years (km/my) for the early–late Pliocene, exhibiting values that range from 5 to 69 km/my (Table 2.2 and Figure 2.12b). Variations on early–late Pliocene progradational rates inside the graben region can again be subdivided into two distinctive trends. The early–late Pliocene period (>3.0 Ma) was characterized by an increase in progradational rates from 5 to 69 km/my, associated with an increase in sediment supply around this time (Figure 2.12a and Table 2.2). The second trend during the late Pliocene (SU3 to SU5) was defined by an abrupt

decrease in progradational rates, from 69 to 29 km/my, indicating a slowdown of the basinward advance of the shelf edge (Table 2.2).

Outside the Graben Region (Seismic Transect T2)

Overall, shelf edges outside the graben region are characterized by flat trajectories from SU1 through SU5 (early–late Pliocene) and a fast-rising trajectories from SU5 through SU9 (late Pliocene–Recent) (Figure 2.11b); however, small variations in these patterns can be discerned. For example, shelf-edge trajectories from SU1 through SU3 are slightly rising, whereas shelf-edge trajectories from SU3 to SU5 are slightly falling (Figure 2.11b). On the other hand, rising trajectories from SU6 through SU8 (late Pliocene–early Pleistocene) are not as steep as rising trajectories recorded within the youngest clinoform package, SU9 (early Pleistocene–Recent) (Figures 2.8b and 2.12a). The magnitude of aggradational and progradational rates inside and outside the graben region appears comparable (Table 2.2 and Figure 2.12). However, aggradational rates inside the graben region during the late Pliocene (SU4–SU5) seemed to experience a sustained decline, while values rebounded outside the graben for time-equivalent units (Figure 2.12a). On the other hand, progradational rates were almost identical during the early Pliocene across the study area, experiencing a notable increase during the late Pliocene. This increase in progradational rates was seen earlier inside the graben region (Figure 2.12b).

Significance of Shelf-Edge Trajectories in the Taranaki Basin

Many authors suggest that shelf-edge trajectories can be used to examine base-level changes through time (e.g., Johannessen & Steel, 2005; Henriksen et al., 2009; Sanchez et al., 2012). Johannessen & Steel (2005) suggest that flat and slightly downward-directed shelf-edge trajectories are associated with a relative sea level that is

stable to slightly falling through time, facilitating optimal delivery of sediment across the shelf to deep-water regions. In contrast, rising shelf-edge trajectories reflect an overall rising relative sea level, implying that a much greater percentage of the sediment budget is stored on the shelf and coastal plains (Johannessen & Steel, 2005). In the case of the Taranaki Basin, I believe that shelf-edge trajectories reflect the combined influence exerted by relative sea-level fluctuations, sediment supply, and underlying structural controls on the development of the Pliocene–Recent stratigraphic succession. During the early–late Pliocene (SU1–SU3), flat to slightly rising shelf-edge trajectories were dominant inside and outside the graben region, supporting the idea of a stable to slightly rising relative sea level that encouraged moderate preservation of sediments on shelfal areas. Negative aggradational rates and falling shelf-edge trajectories during the late Pliocene (Figure 2.12a and Table 2.2) marked the onset of intense erosion on the outer shelf region and an increase in sediment bypass into the upper slope. These conditions are associated with stages of falling relative sea level.

Shelf-edge trajectories as well as aggradational and progradational rates show similar trends inside and outside the graben region (Figures 2.8 and 2.12a–b); however, some differences are evident. For instance, during the late Pliocene (SU3–SU5) erosion and sediment bypass were more intense inside the graben region, as revealed by a steeper fall in shelf-edge trajectory and a sharper decrease in aggradational rates (Figures 2.8 and 2.12a). Progradational rates inside and outside the graben region show similar trends and magnitudes, but variations were first recorded inside the graben region during the late Pliocene (Figure 2.12b). Although the overall decrease in aggradation and increase in progradation during the late Pliocene could have been partially controlled by the overall drop in eustatic sea-level fluctuations (Figure 2.12) (Miller et al., 2005; Lisiecki &

Raymo, 2005), local changes such as an increase in sediment supply within the basin (Tippett & Kamp, 1995) may also have played an important role.

The presence of growth strata along fault systems that define the boundaries of the Northern Graben (Cape Egmont and Turi fault zones) suggests that the opening of the graben was episodic, starting during the early Pliocene (Figure 2.10b) and continuing during the Pleistocene (Figure 2.10i) (Giba et al., 2012).

Clinoform Heights and Lengths

For the early–late Pliocene portion of the succession clinoform heights inside the graben region are significantly larger than those outside the graben region (Figure 2.12c). Clinoform heights inside the graben region during the early–late Pliocene (surfaces Sa to Sf) ranged from 1061 to 1477 m, whereas time-equivalent units outside the graben ranged between 342 and 808 m. In addition, clinoform heights outside the graben region remained constant, around 400 m during the early–late Pliocene (Sa to Sd), although registering a noteworthy increase to 739 m during the late Pliocene (Figure 2.12c). Larger clinoform heights inside the graben are likely a reflection of the influence that the underlying paleobathymetry (controlled by the underlying structures) exerted on the development of clinoform morphologies that must adapt their depositional profiles to the steepness of the margin. In addition, the abrupt changes on clinoform heights that were registered during the late Pliocene in both transects (T1 and T2) appear to coincide with the activation of underlying structures associated with the development of the Northern Graben (Figure 2.12c) suggesting a linkage between these two events. Paleobathymetric reconfiguration of the basin during the late Pliocene as a result of structural deformation caused readjustments in clinoform profiles that were registered as significant changes in clinoform heights (Figure 2.12c).

Inside the graben region, clinoform lengths decreased systematically during the early–late Pliocene, from 44 to 12 km (SU1 to SU5; Figure 2.12d and Table 2.2), indicating narrowing of the slope as a potential response to increased accommodation owing to the activation of the Northern Graben (Figurs 2.8a and 2.12d). However, clinoform lengths outside the graben region stayed more-or-less constant at around 15 km during the early–late Pliocene, experiencing a decrease during the late Pliocene (SU6), at which time values stabilized remaining at around 14 km during the Pleistocene–Recent period (SU8 to SU9; Figure 2.12d). A negative correlation between clinoform heights and lengths outside the graben region, starting during the late Pliocene (SU4), is also observed (Figure 2.12e). This inverse correlation, during which clinoform heights increased while clinoform lengths decreased, reflected the advance of the shelf edge while the steepness of the slope increased (Figure 2.11b).

Average Foreset Inclination and Upper Slope Inclination

During the Pliocene–Recent (SU1–SU9), foreset and upper-slope declivities (see Figure 2.1) increased both inside and outside the graben region (Figures 2.12f-g). In general, clinoform declivities inside the graben region seem to be slightly higher than those outside the graben region, but trends seem similar across both regions (Figure 2.12f). During the early–late Pliocene (SU1–SU2), foreset declivities ranged from 1° to 3° both inside and outside the graben region. A sharp increase in foreset declivities is evident during the late Pliocene (SU3–SU7) (1°–5°). Data from inside the graben region was not available for the upper Pliocene–Holocene section (SU6–SU9), but foreset inclination values calculated outside the graben region vary from 3° to 5° for this interval (Figure 2.12f).

Discrepancies between foreset and upper slope inclination values are due to variations along the depositional profile, where the upper part of the slope is more prone

to gravitational collapse. Foreset and upper slope inclination values throughout the study area seem to follow the same trend, exhibiting increased values through time (Figures 2.12f-g). However, inside the graben region, upper-slope inclination values are higher than foreset declivities (0.5°–2.5° difference; Figure 2.12h), indicating that the upper part of the slope was always steeper than the overall geometry of the depositional profile (Figures 2.1 and 2.12f-g). This shift inside the graben region (separation between upper-slope and foreset inclination values; Figure 2.12h) indicates substantial truncation of strata at the shelf edge. This truncation is likely due to sediment bypass, mass wasting episodes, and potential deposition of fans on the deep basin. On the other hand, upper-slope inclination and average inclination values outside the graben region generally follow the same trend and show similar values for the early–late Pliocene interval, suggesting that truncation and incision of the upper slope were not as pervasive as they were inside the graben region (Figure 2.12h). In the upper succession (SU6-SU9), however, upper-slope inclination values reached 6°–7° (Table 2.2). In cross section these surfaces (Sh and seabed) show clear evidence of slumping having affected the upper part of the slope (Figures 2.8b).

MARGIN CLASSIFICATION AND CLINOFORM INCLINATION VALUES

Several authors have attempted to study the morphology of modern passive continental margins and their associated depositional settings by utilizing measurements of clinoform declivities (e.g., O'Grady et al., 2000; Adams & Schlager, 2000; Kertznus & Kneller, 2009). I apply a similar approach to the Giant Foresets Formations of the northern Taranaki Basin, taking into consideration that this stratigraphic succession was deposited in a back-arc basin and not on a passive margin. Figure 2.13 includes plots of average clinoform declivities versus depth for seismic units both inside and outside the graben region. Measurements were taken from seismic transects T1 and T2, following the

methodology of O'Grady et al. (2000) (Figure 2.11). Average foreset declivities within the study area are, in general, higher than those reported for passive margins (Figure 2.13). This difference can be attributed to oversteepening of clinoform foresets caused by the influence of active tectonics. The initial assumption was that, because the Giant Foresets Formation was deposited in a tectonically active back-arc basin near the zone of collision between the Pacific and Australian plates (Figure 2.2), the distribution of data points on the foreset inclination/depth plots would be dramatically different from the patterns observed on passive margins. This is somewhat true inside the graben area, where foreset inclination values range from 0° to 10° and the distribution of data points is somewhat scattered (Figure 2.13a–f). However, despite these differences, it would not be unreasonable to categorize patterns observed inside the graben region within the deep and steep category defined by O'Grady et al. (2000) for passive margins (Figure 2.13a–f). The deep and steep category indicates conditions of low sediment supply, exposed margins, and the development of abundant canyons (O'Grady et al., 2000). On the other hand, foreset inclination patterns observed outside the graben region in the Taranaki Basin (Figure 2.13g–p) can be more easily correlated to some of the categories that were defined using data from passive margins. For seismic units SU1–SU3 (early–late Pliocene), inclination values outside the graben fluctuated between 0° to 4° and, although data was scarce below the 1 km mark, the pattern seems to be consistent with gentle and smooth morphologies that have been linked to supply-dominated margins with unstable substrates and poor canyon development. For seismic units SU4–SU5 (middle part of the late Pliocene), foreset inclination values outside the graben region fluctuated between 0° to 8° and the pattern resembles a steep and rough geometry, implying conditions of low sediment supply, higher erosional rates, and high canyon development. For seismic units SU6–SU9, inclination values typically range from 0° to 6° with some outliers reaching

10°; in this case a clear pattern associated with the sigmoidal category can be identified, suggesting conditions of high sediment supply and more stable substrates that supported progradation and development of few canyons (Figure 2.13).

Figure 2.13

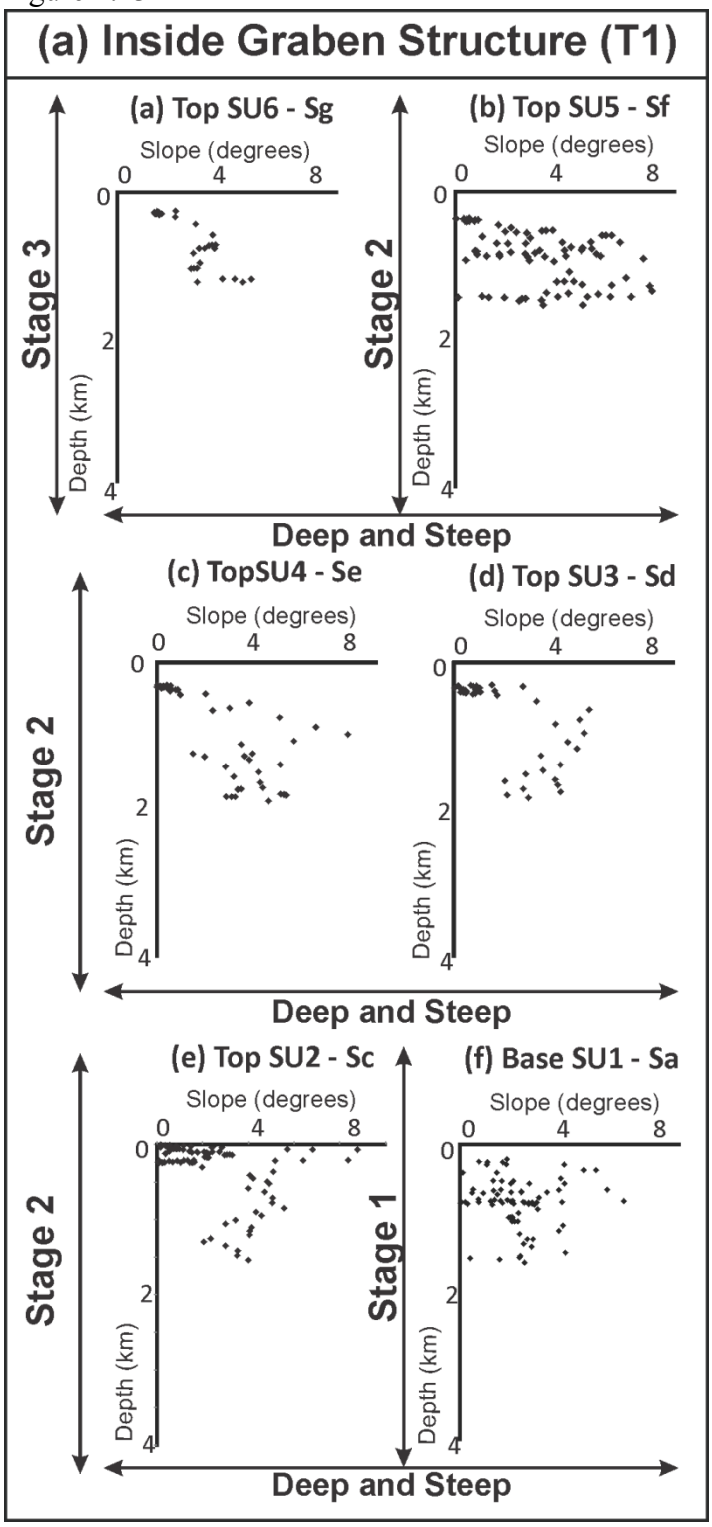
(a) Inside Graben Structure (T1)
(a) Top SU6 - Sg
(b) Top SU5 - Sf
Slope (degrees)
0
4
8
0
2
4
Depth (km)
Stage 3
Stage 2
Deep and Steep
(c) TopSU4 - Se
(d) Top SU3 - Sd
Stage 2
Deep and Steep
(e) Top SU2 - Sc
(f) Base SU1 - Sa
Stage 2
Stage 1
Deep and Steep

Figure 2.13 (continued)

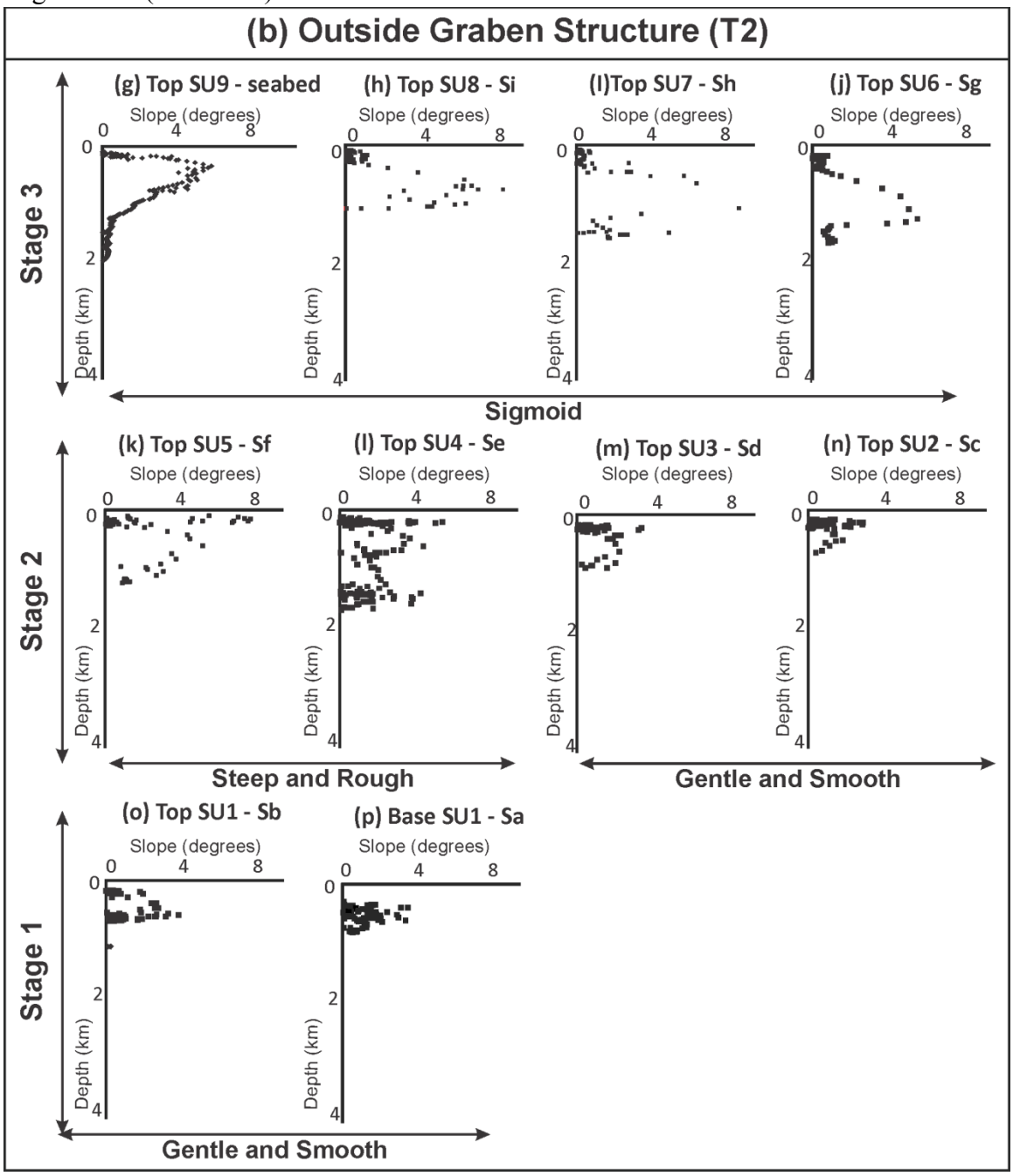

Figure 2.13: Plots showing variations on clinoform inclination values versus depth (a) inside (T1) and (b) outside (T2) the Northern Graben.

I also applied the methodological approach developed by Adams & Schlager (2000), obtaining best-fit curves for the different slope profiles in the Taranaki Basin Giant Foresets Formation (Sa to seabed; Figure 2.14). Table 2.3 shows the main parameters for each equation as well as the goodness of fit (R2). The results indicate that first-order continental margin morphologies, both inside and outside the graben region, are expressed by either linear or exponential functions for the lowest Pliocene interval (SU1; Figures 2.14a–b and h–i) and by exponential functions for the lower to upper Pliocene succession (SU2–SU4; Figures 2.14c–p and j–l). Adams & Schlager (2000) pointed out that linear morphologies have been associated with margins in which sediments rest at an angle of repose that can be disturbed by a minor addition of sediments. Exponential profiles, on the other hand, can form in settings where high rates of sedimentation are dominant, causing rapid progradation with minimal vertical movement of the shelf edge (Adams & Schlager, 2000). This exponential profile configuration also implies active transport of sediments by gravity-induced processes acting on the outer shelf and upper part of the slope. This interpretation, based on foreset inclination patterns as described by Adams & Schlager (2000), fits well with shelf-edge trajectories observed for the lower to upper Pliocene succession (SU1–SU4; Figure 2.11), as well as with the high progradational/low aggradational rates that were recorded for these units (see ratio of aggradation to progradation in Table 2.2). There is not a complete coverage of the upper part of the succession inside the graben region, but morphologies associated with the upper Pliocene–Recent (SU5–SU9) stratigraphic succession inside and outside the graben region (Figures 2.14f–g and m–p) seem to showcase a transitional state from exponential to mainly Gaussian morphologies (Figure 2.14 and Table 2.3). Gaussian morphologies have been linked to continental margins subjected to the modifying effects of extrinsic processes like fluctuations of base level (e.g., changing

tides and seasonal weather and/or high-amplitude changes in sea level) and the action of ocean currents (Adams & Schlager, 2000). Development of Gaussian profiles in the Taranaki Basin during the late Pliocene–Recent could indicate a rapid increase of relative sea level, as well as an increase in the redistribution of sediments by the action of ocean currents (e.g., strong wave action). An overall eustatic sea-level fall is recorded in most of the interval (Miller et al., 2005; Lisiecki & Raymo, 2005); therefore, the increase in accommodation observed in rising shelf-edge trajectories and aggradational patterns may have been generated by a different geological process than eustatic sea-level rise, most likely tectonics.

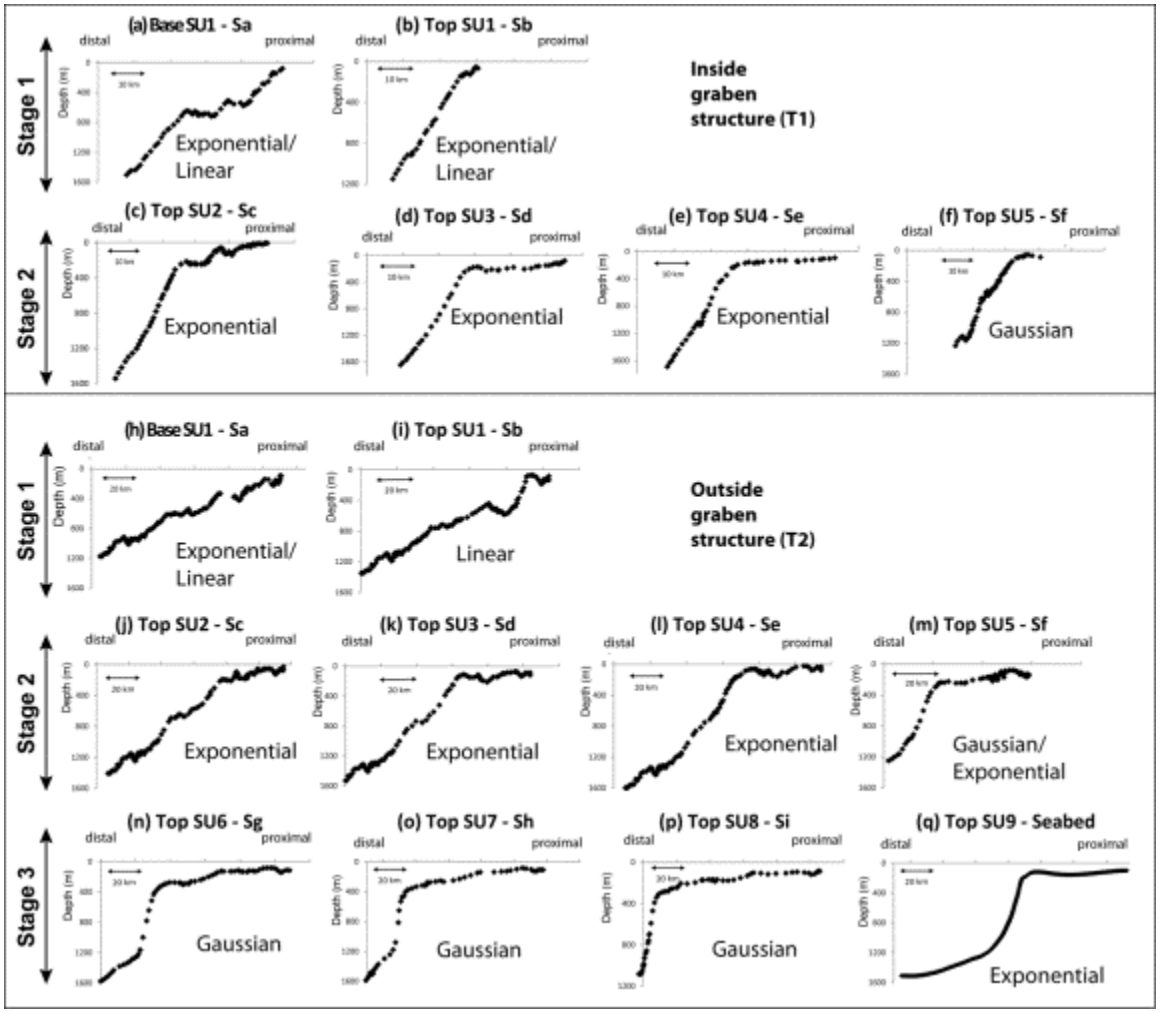

Figure 2.14: Plots of the geometry of individual clinoform profiles (base and top of seismic units) inside (T1) and outside (T2) Northern Graben. Plots fit lineal, exponential, or Gaussian functions.

Seismic Profile	Stage	Seismic Unit	Seismic Unit Upper Boundary	Age (Ma)	Slope average inclination (degrees)	Maximum Slope inclination (degrees)	Best Fit	a (Linear eq.)	b (Linear eq.)	b (Exponential eq.)	V (Gaussian eq.)	R^2
Inside graben structure	2B	SU5	Sf	2.4	4.4	7.0	Gaussian				**0.14**	**0.982**
		SU4	Se	2.6	4.9	6.2	Exponential			**0.028**		0.989
		SU3	Sd	2.8	4.5	5.2	Exponential			**0.001**		0.992
	2A	SU2	Sc	3.0	2.7	3.8	Exponential			**0.132**		0.987
	1	SU1	Sb	4.5	1.8	3.4	Exponential			**0.015**		0.989
			Sa	5.3	1.7	3.3	Linear	**0.054**	**0.102**			0.962
Outside graben structure	3	SU9	Seabed	0.0	3.1	6.0	Exponential			**0.057**		0.987
		SU8	Si	1.2	5.3	5.3	Gaussian			—	**0.17**	**0.995**
		SU7	Sh	1.8	4.1	8.1	Gaussian				**0.16**	**0.993**
		SU6	Sg	2.1	4.0	5.3	Gaussian			—	**0.13**	**0.990**
	2B	SU5	Sf	2.4	4.1	4.7	Exponential			**0.205**		**0.988**
		SU5	Sf	2.4	3.7	5.0	Gaussian				**0.12**	**0.993**
		SU4	Se	2.6	2.3	2.3	Exponential			**0.022**		0.992
		SU3	Sd	2.8	1.9	1.9	Exponential			**0.015**		0.991
	2A	SU2	Sc	3.0	1.1	1.3	Exponential			**0.007**		0.983
	1	SU1	Sb	4.5	2.3	3.6	Linear	**0.015**	**0.004**			0.789
			Sa	5.3	1.4	1.4	Exponential	—	—	**0.018**		0.891

Table 2.3: Fitting parameters for seismic units within the study area. Methodology for data collection and interpretation follows Adams and Schlager (2000).

Adams & Schlager (2000) estimated that the curvature of exponential profiles (b in their Figure 2.2B) has a range of 0.438–2.074 in sand-dominated slopes, compared to a range of 0.043–0.225 in mud-dominated slopes. On the other hand, the peakedness value on Gaussian profiles (V in their Figure 2.2C) ranges from 0.031 to 0.086 in clay-dominated slopes, and from 0.088 to 0.214 in slopes containing sand (Adams & Schlager, 2000; see their Figure 2.2). I applied these criteria to the Giant Foresets Formation and the data suggest that seismic units SU1–SU5 are mainly composed of fine-grained lithologies, whereas seismic units SU6–SU9 contain sandier intervals (Figure 2.15). This lithological prediction seems to also be supported by well log correlations (Figure 2.5).

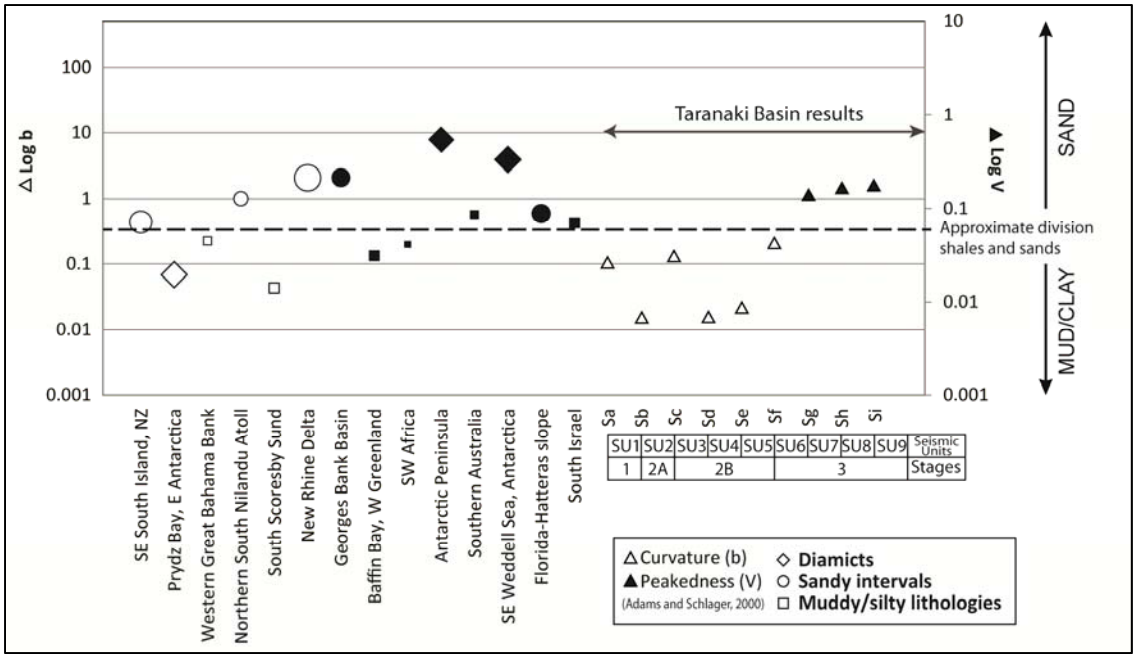

Figure 2.15: Curvature (b) and peakedness (V) for modern continental margins (Adams and Schlager, 2000) and for subsurface of Taranaki Basin (this paper). Curvature and peakedness parameters are linked to lithological composition (Adams and Schlager, 2000).

STAGES OF CLINOFORM EVOLUTION / SUMMARY AND INTEGRATION OF SEISMIC AND MORPHOLOGICAL ANALYSIS

Three stages of clinoform evolution were defined within the region (Figure 2.7) based on geometrical measurements and the analysis of clinoform morphologies (i.e., clinoform trajectories, heights, lengths, and declivities; Figures 2.12, 2.13 and 2.14). In addition, I also incorporated results that were derived from the application of classification systems developed by O'Grady et al. (2000) and Adams & Schlager (2000) into the analysis (Figures 2.13 and 2.14). Stage 1 contains seismic unit SU1, whose individual clinoform profiles display a gentle and smooth architecture, clinoform foresets are low-angle, and rollover trajectories are flat to rising. Stage 2 includes seismic units SU2–SU5; in this unit, individual clinoforms are characterized by concave profiles and rising to flat rollover trajectories . Stage 2A (SU2) and Stage 2B (SU3–SU5) were defined based on variations in shelf-edge trajectories, progradational rates and degree of topset incision Finally, Stage 3 contains seismic units SU6–SU9, characterized by sigmoidal clinoforms with a convex-to-concave geometry and mostly rising rollover trajectories.

Isochron maps for Stages 1 through 3 are shown in Figure 2.16. Unlike isochron maps derived from individual seismic units (SU1–SU9; Figure 2.10), these maps were generated by incorporating data points from the 2D seismic survey, and therefore provide a semi regional view of the Pliocene–Recent stratigraphic infilling of the Taranaki Basin.

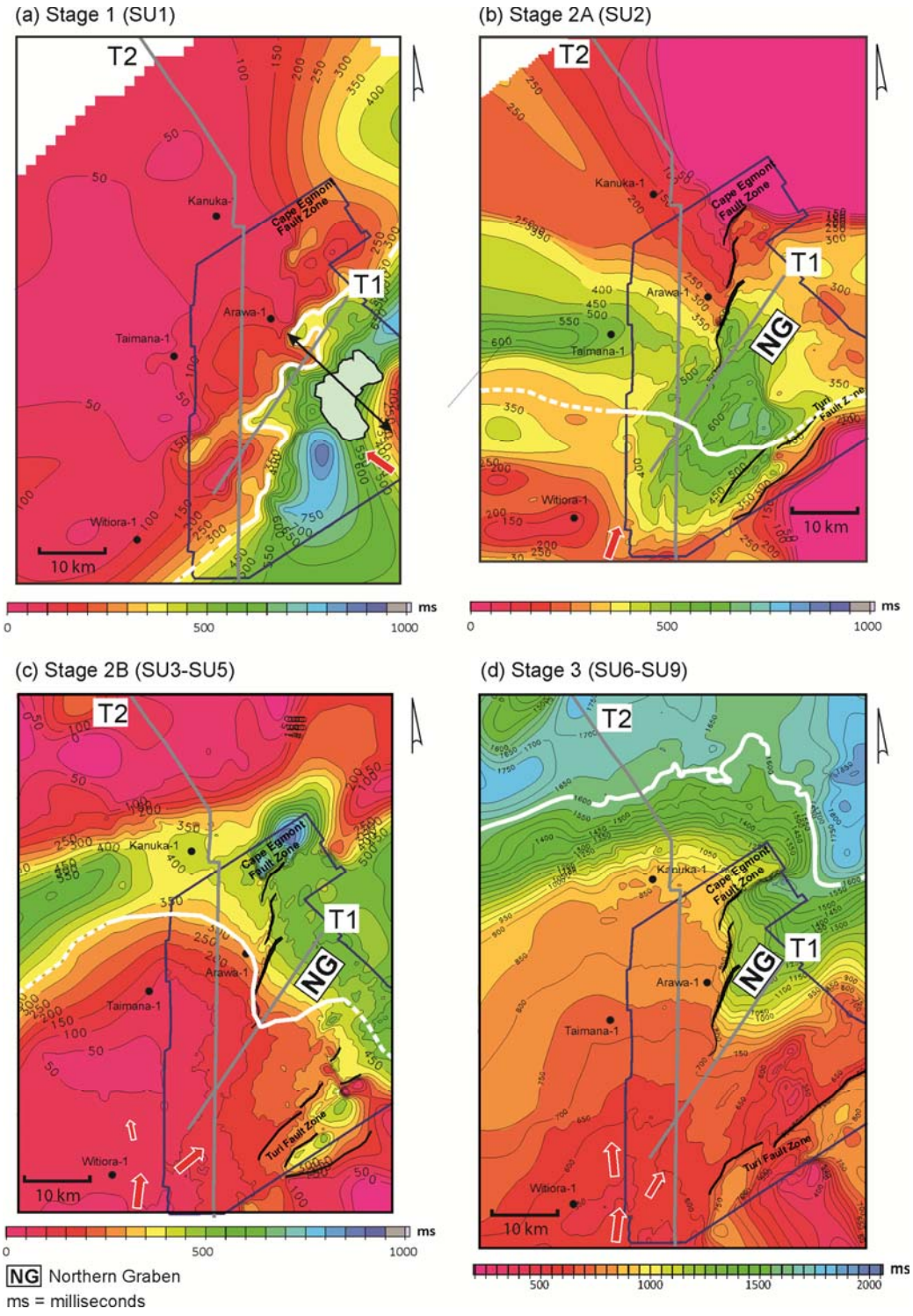

Figure 2.16: Semiregional isochron maps, generated using 2D and 3D seismic surveys (a) during Stage 1, (b) Stage 2A, (c) Stage 2B, and (d) Stage 3.

Stage 1 (SU1)–Deposition of planar clinoforms (early Pliocene)

Shelf-edge trajectories within Stage 1 are mainly flat to ascending (Figure 2.7). Margin aggradational rates range from 317 to 381 m/my across the study area, and progradational ranges from 4 to 5 km/my (transect T1). Clinoform heights and lengths are larger to the east (T1), with foreset inclination values ranging between 1° and 2° across the study area (Figure 2.12). Clinoform morphologies to the west (transect T2) were classified as gentle and smooth, owing to their low foreset angles and the lack of irregularities associated with canyon incisions. On the other hand, steeper clinoform morphologies to the east (T1) were tentatively classified as deep and steep (O'Grady et al., 2000). Clinoform profiles across the study area fitted either linear or exponential functions according to the Adams & Schlager (2000) classification system (Figure 2.14). Curvature parameters suggest that units within Stage 1 are mainly of a fine-grained nature (mudstones and claystones) (Figure 2.15).

The isochron map of Stage 1 indicates that the paleoshelf edge had a northeast-southwest orientation (Figures 2.9 and 2.16a). Thick intervals can be observed along the outer shelf, suggesting that sediments were retained in this region. No clear indication exists of structural deformation affecting the geometry of the margin at this time (Figure 2.16a). The RMS attribute extraction map of Stage 1 shows two distinctive zones separated by a northeast-southwest-oriented moderate-amplitude region (Figure 2.17a) that may indicate the orientation and position of the paleoshelf edge. The two zones are interpreted as the outer-shelf and upper-slope regions (Figure 2.17b). To the southwest and within the shelf-edge region, localized high amplitude bodies can be seen, arranged in a semilinear pattern which have been interpreted to represent deposits of a series of channels. These channels bypassed sediments from the outer shelf to the upper part of the slope. Just down dip of the paleoshelf edge, a broad zone of high-amplitude reflections

with a fan-like plan form is observed (Figure 2.17). These reflectors have been interpreted as a slope fan. Distributary channels are also interpreted to occur on the fan as semilinear, thin, high amplitude streaks trending parallel to the fan axis (Figure 2.17a). Well Arawa-1 shows sand-rich lithologies deposited in upper to middle bathyal depths that may correspond to fan sands (Figure 2.18). In well Witiora-1, located to the south, this interval is reported to have been deposited in upper-bathyal environments, whereas wells Taimana-1, Arawa-1, and Kanuka-1, to the north, contain middle- to lower-bathyal environments (Morgans, 2006; Crundwell, 2008), which support the paleogeographical interpretation proposed in this work. The morphometric analysis (Adams & Schlager, 2000; O'Grady et al., 2000) suggesting limited canyon development in this region agrees with these observations. The lack of canyons suggests that sediments were fed to the slope and sequestered in a stable environment as slope aprons. Only in areas where sudden fluxes of sediment addition destabilized the slope (northeast), slope fans were disrupted and moved downslope.

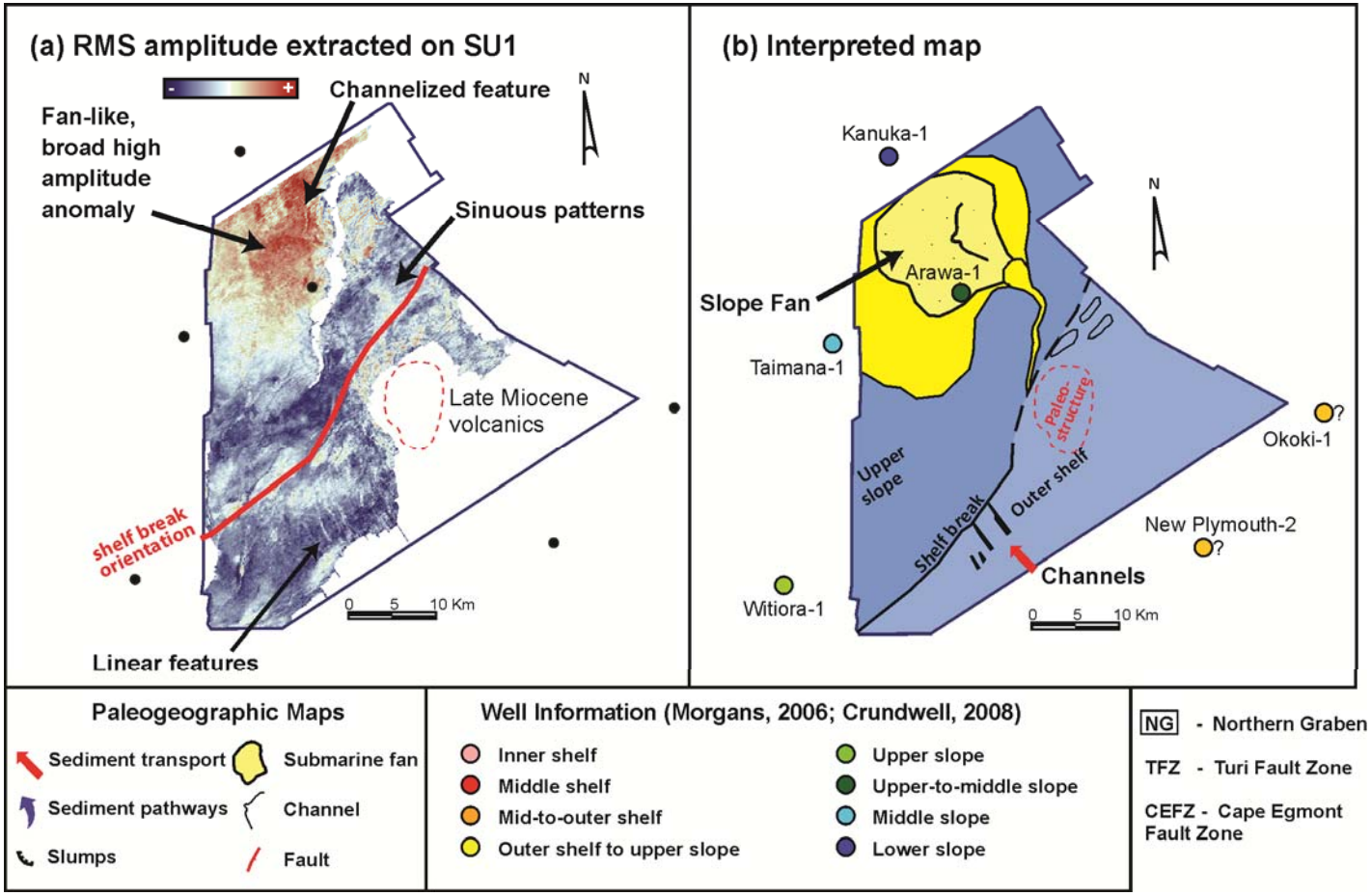

Figure 2.17: (a) RMS amplitude extraction map of seismic unit SU1 (early Pliocene) in area covered by 3D seismic survey. Extraction window is 20 ms below Sb. (b) Paleoenvironmental interpretation of seismic unit SU1 showing location of paleoshelf break and deepwater fan connected by slope channels to outer shelf.

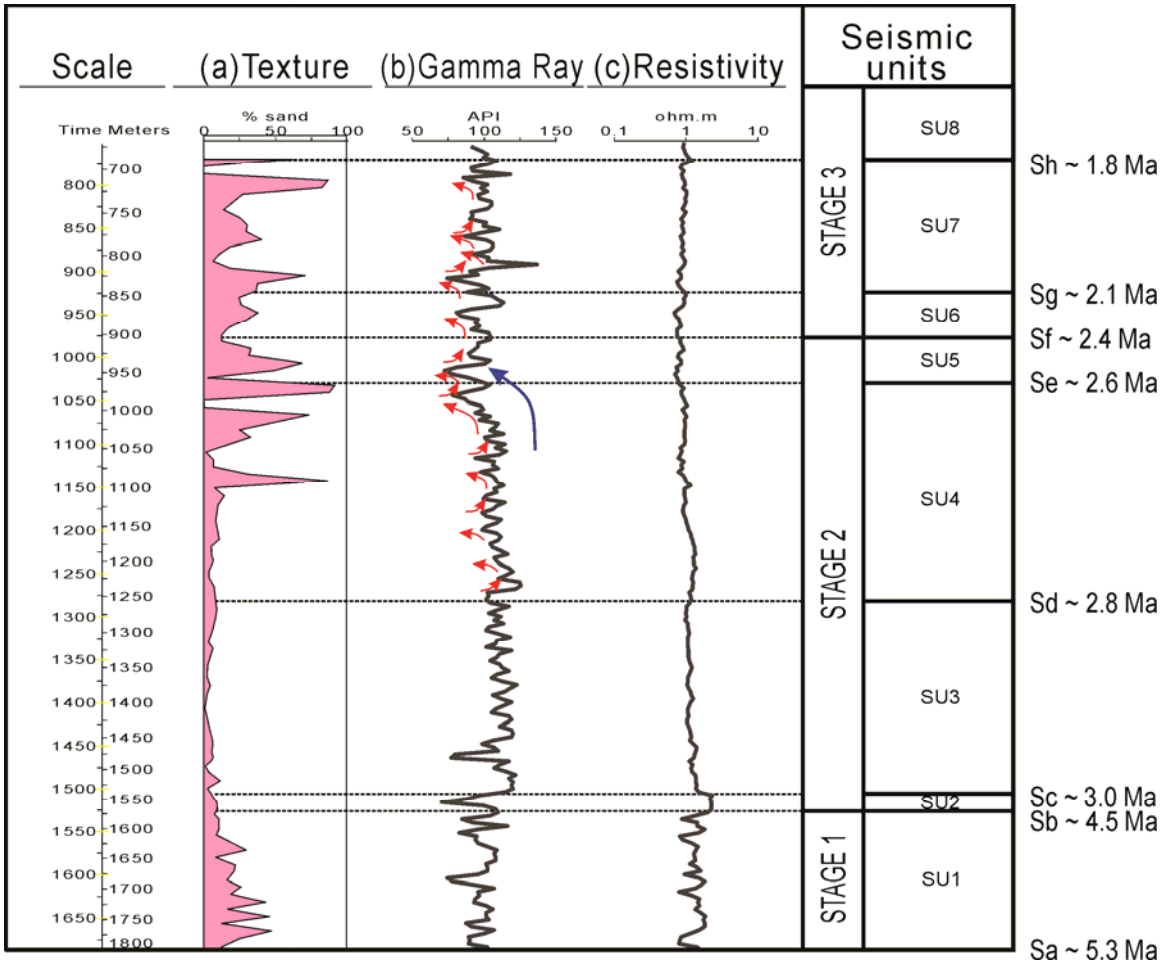

Figure 2.18: Lithological information, Gamma Ray and Resistivity logs for well Arawa-1

Stage 2A (SU2)–Deposition of oblique clinoforms (early–late Pliocene)

Shelf-edge trajectories within Stage 2A are flat to slightly rising (SU2 in Figure 2.7); aggradational rates range from 53 to 73 m/my, and progradational rates are close to 11 km/my. Structural deformation associated with the emplacement of the Northern Graben seems to have started at this time (Figure 2.16b). Clinoform heights and lengths are larger inside the graben region (transect T1; Figures 2.12c-d), and foreset inclination values are slightly higher than in Stage 1 (Figure 2.12f). Clinoform morphologies outside the graben can be categorized as gentle and smooth (O'Grady et al., 2000; Figure 2.13) and clinoform profiles, both inside and outside the graben region, fit exponential

functions (Adams & Schlager, 2000; Figure 2.14). Curvature parameters predict dominance of fine-grained lithologies for this interval (Figure 2.15). The isochron map of Stage 2A reflects the influence of the fault system on sediment accumulation. The fault system is associated with the development of the Northern Graben at this time (Figure 2.16b). Thicker intervals on the isochron map correspond to areas where accommodation was created as a response to graben evolution-associated normal faulting. Development of the Northern Graben triggered a change in the orientation of the paleoshelf edge compared to the previous stage (Stage 1; Figure 2.16). During Stage 2A, the western portion of the paleoshelf edge developed an approximately east-west orientation that deflected toward the south as it approached the Northern Graben (Figure 2.16b). Two main depocenters existed at this time: one parallel to the east-west-oriented paleoshelf edge to the west, and an eastern depocenter contained within the Northern Graben (Figure 2.16b).

RMS amplitude attribute maps for Stage 2A (Figure 2.19) show two distinct zones of unique amplitude character. The southwestern corner of the 3D seismic volume is a zone with moderate to high amplitude seismic response. Low-amplitude, narrow and sinuous ribbon-shaped features with a southwest-northeast orientation are arranged in a dendritic pattern. Based on the geomorphological features observed in RMS maps, this zone is likely the topset portion of the margin (Figure 2.18b), where high-amplitude responses are believed to correlate with shelfal deposits. The background seismic response of the zone located to the northeast is dominated by low- to moderate-amplitude reflections. High-amplitude channelized features in this area have a northeast-southwest orientation; these features are moderately sinuous and are interpreted as slope channels (Figure 2.19) that branch out in the downslope direction and connect with high-amplitude, lobate features that are interpreted as possible slope fans (Figure 2.19b). In

addition, straight and narrow, high-amplitude lineations are also observed and interpreted as slope gullies (Figure 2.19b). There is an apparent connection between the dendritic-channelized system in the southern zone and the slope channels observed towards the north. The boundary between these two zones of different seismic response defines the paleoshelf edge for the interval, when sediments were transported from the southwest to the northeast by subaqueous mechanisms from the inboard area to the shelf edge, developing slope channels and fans (Figure 2.19b). Seismic profiles also show the development of continental-scale clinoforms prograding to the north.

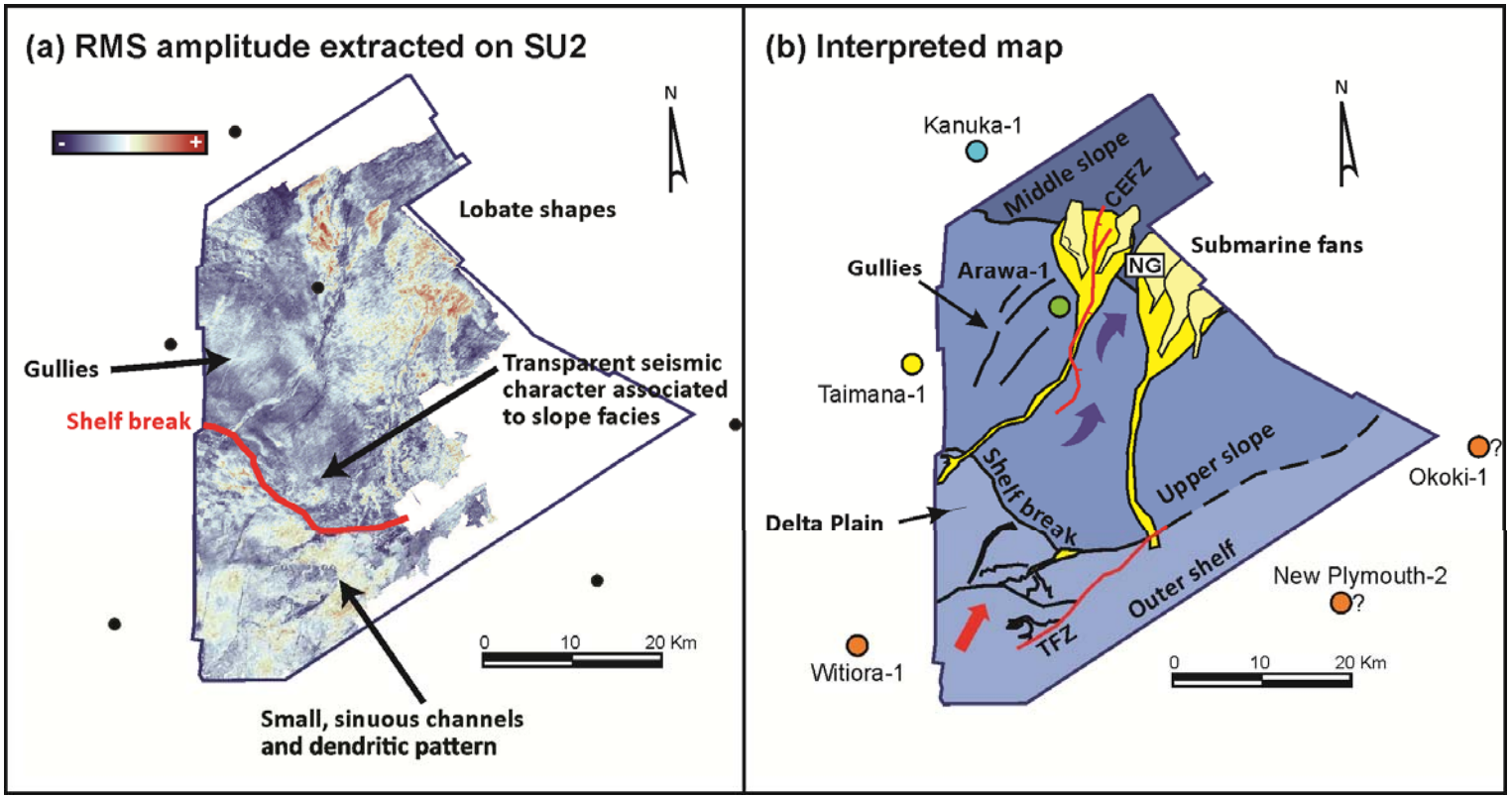

Figure 2.19: (a) RMS amplitude extraction map of seismic unit SU2 (early–late Pliocene) in area covered by 3D seismic survey. Extraction window is 20 ms below Sc. (b) Paleoenvironmental interpretation of seismic unit SU2 (Stage 2A) showing location of paleoshelf break and outer-shelf deltaic channels that transferred sediments into two deepwater fans through slope channels.

Stage 2B (SU3-SU5)– Deposition of oblique clinoforms (late Pliocene)

Shelf-edge trajectories were remarkably flat outside the graben region, while flat-to-falling trajectories were dominant inside the graben (Figure 2.11). There are also significant differences during Stage 2B in aggradational and progradational rates inside and outside the graben region. Progradational rates increased significantly during this time, especially outside the graben region, reaching a peak during the late Pliocene (71 km/my for SU4; Table 2.2). In contrast, aggradational rates across the study area registered their lowest values, with values reaching -800 m/my inside the graben region (Figure 2.12a; Table 2.2). The negative aggradational rate indicates a decreasing shelf-edge trajectory that may be associated with both a relative sea level fall and subsequent erosion of topsets. Clinoform heights outside the graben increased from 413 to 808 m whereas clinoform heights inside the graben decreased from 1451 to 1061 m. Foreset and upper-slope declivities also registered increases from 2° to 5° across the region (Figure 2.12). Outside the graben region, clinoform morphologies transitioned from gentle and smooth (SU3) to steep and rough (SU4 to SU5; Figure 2.13) while functions that fit clinoform profiles transition from exponential (SU3–SU4) to Gaussian (SU5) (Figure 2.14f; O'Grady et al., 2000; Adams & Schlager, 2000). Curvature parameters suggest that lithologies in this interval are composed mainly of mudstones and claystones (Figure 2.15).

The isochron map of Stage 2B shows the deflection in the orientation of the paleoshelf edge associated with the development of the Northern Graben (Figure 2.16c). When looking at a series of seismic profiles, it also can be seen the advance of the paleoshelf edge toward the north (Figure 2.9). Two different segments associated with the paleoshelf edge are identified on the isochron map: a western segment with a northeast-southwest orientation and an eastern segment with a northwest-southeast orientation.

Depocenters shifted outboard toward the north, where most sediments were deposited under slope water depths in relatively narrow troughs (10 to 15 km wide). The change in geometry registered in the eastern segment of the paleoshelf edge from Stages 2A to 2B was likely related to the progressive infilling of the southeastern portion of the Northern Graben by sediments coming from the southwest (Figure 2.16).

The RMS amplitude map of seismic unit SU4 (Figure 2.20a) exhibits a series of linear, high amplitude, narrow amplitude threads trending perpendicular to the interpreted shelf edge. These are interpreted to represent deposits of a dendritic, outer shelf channel system with a northeast-southwest orientation in the southern portion of the 3D seismic survey. Toward the north, a different pattern is observed in which high-amplitude and elongated bodies have a west-northwest to east-southeast orientation parallel to the paleoshelf edge (Figure 2.20b). Patterns within this area are interpreted as mass wasting deposits derived from the eastern and western flanks of the graben structure (Figure 2.20b). It is possible that the geometry of these deposits was influenced by current-controlled processes.

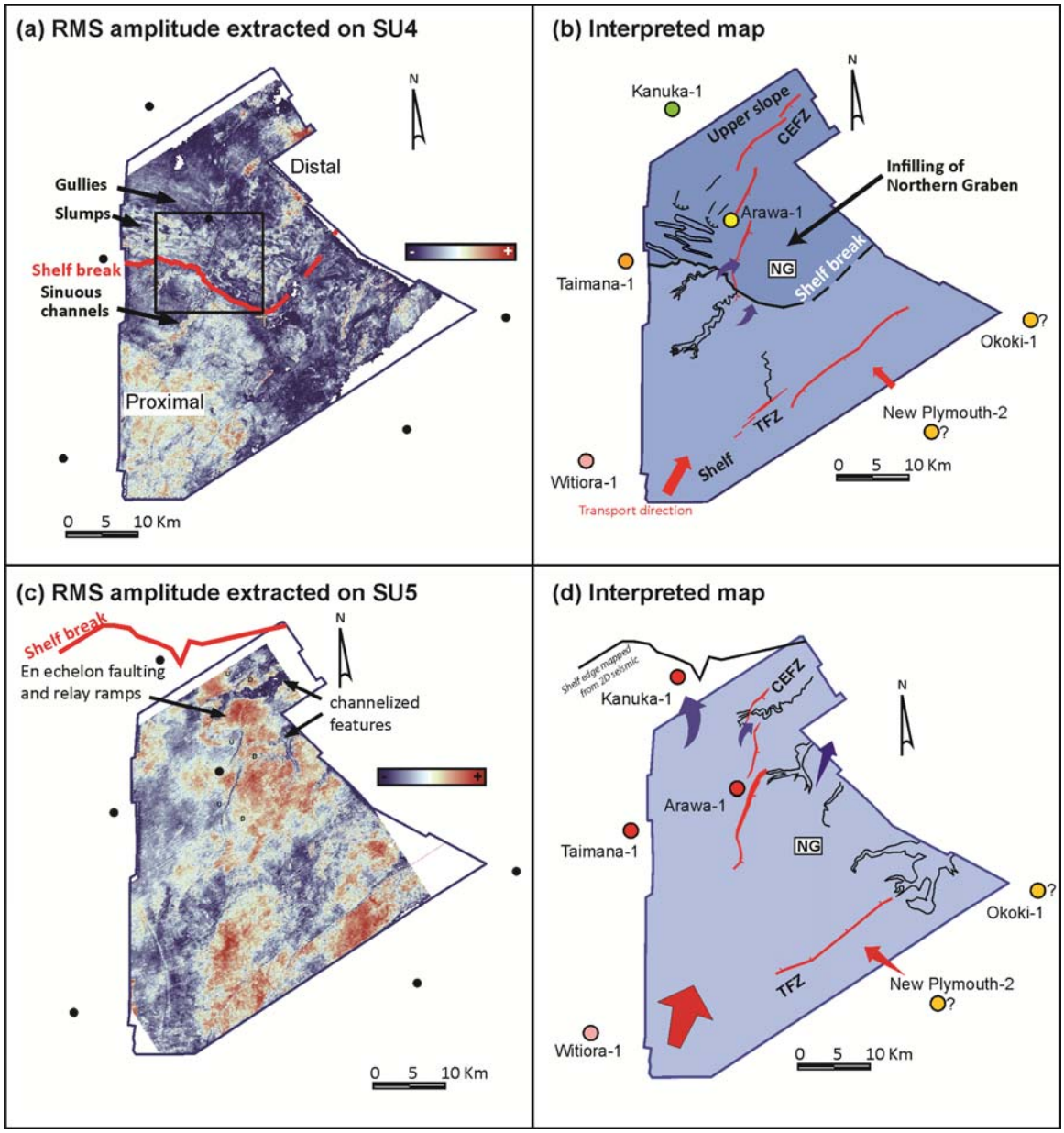

Figure 2.20: (a) RMS amplitude extraction map of seismic unit SU4 (late Pliocene) in area covered by 3D seismic survey. Extraction window is 20 ms below Se. (b) Paleoenvironmental interpretation of seismic unit SU4 (early Stage 2B) showing location of paleoshelf break, sinuous channels in outer shelf, and slumped material and gullies in upper part of slope. (c) RMS amplitude extraction map of seismic unit SU5 (late Pliocene) in area covered by 3D seismic survey. (d) Paleoenvironmental interpretation showing location of paleoshelf break to north of well Kanuka-1 and dendritic channels occupying topset portions of clinoforms.

The RMS amplitude extraction map of seismic unit SU5 (Figure 2.20c) represents a later stage of infilling, when the paleoshelf edge was located to the northeast and outside the coverage of the 3D seismic volume. This RMS amplitude extraction map (SU5) images the topsets of highly progradational clinoforms that already infilled most of the pre-existing accommodation (Figure 2.20c). The attribute extraction map of SU5 also contains a series of linear, highly sinuous amplitudes that amalgamate into broad regions of high amplitude response. Individual threads exhibit a dendritic pattern. These seismic morphologies are interpreted to represent channels >2 km wide that migrated on the outer shelf. Individual channels are arranged in a well-defined dendritic pattern, and seismic lines show that the channels are highly incised. In addition, en-echelon faults and associated relay ramps appear to have controlled the location and geometry of these channelized systems (Figure 2.20d). By the time seismic unit SU5 was deposited, the entire area covered by the 3D seismic volume was occupied by a highly progradational system that was associated with low sea level conditions (Figure 2.20).

Stage 3 (SU6–SU9)—Deposition of sigmoidal clinoforms (late Pliocene–Recent)

Clinoform packages associated with Stage 3 are characterized by high aggradation-to-progradation ratios that translate into a higher degree of sediment preservation on the shelf (Table 2.2 and Figure 2.7). Aggradational rates outside the graben region reached 521 m/my during deposition of the younger section (SU9; Figure 2.12). Clinoform heights and lengths were relatively constant at this time, displaying an inverse relationship (Figure 2.12e). Clinoform morphologies were classified as sigmoidal outside the graben region (O'Grady et al., 2000; Figure 2.13), but clinoform profiles mainly fitted Gaussian distribution curves across the entire study area (Adams & Schlager, 2000; Figure 2.14). Curvature parameters predict the presence of sandstones

(Figure 2.15). However, none of the available wells drilled the foresets of these clinoforms and, therefore, the increase of sand content cannot be verified (Figure 2.5).

The isochron map of Stage 3 shows thickening of the sediment wedge toward the north-northwest, where depocenters now covered the entire outboard region (Figure 2.16d). The paleoshelf edge had advanced more than 30 km toward the north, developing two distinctive segments: a western portion with a northeast-southwest orientation, and an eastern segment with an almost north-south alignment (Figure 2.16d). A later stage of tectonic subsidence affected the southern end of the graben, generating accommodation on the shelf and a fault-bounded v-shaped depocenter (Figure 2.16d). The RMS attribute extraction map from SU6 (Figure 2.21a) shows narrow and high-amplitude linear trends that are interpreted as deposits of dendritic channels active to the west of the fault system that defines the western boundary of the graben structure. These channels were located within the topsets of the clinoforms and were transporting sediments from the southwest to the northeast into the v-shaped shelfal depocenter through graben relay ramps (Figure 2.21b). High-amplitude reflections are ubiquitous to the east of the Cape Egmont Fault Zone, which defines the western boundary of the graben structure (Figure 2.21c). Southwest-northeast-oriented anomalies are aligned with the graben structure and may indicate a preferential direction of sediment transport. In addition, the progradation of clinoforms into deeper basin positions allowed the deposition of progressively steeper clinoforms that most likely triggered slope collapse as observed in seismic sections. The lack of connection of this features and shelf incisions also suggest that they are not related to sea level falls. Consequently, deep water deposits are most likely fine grained.

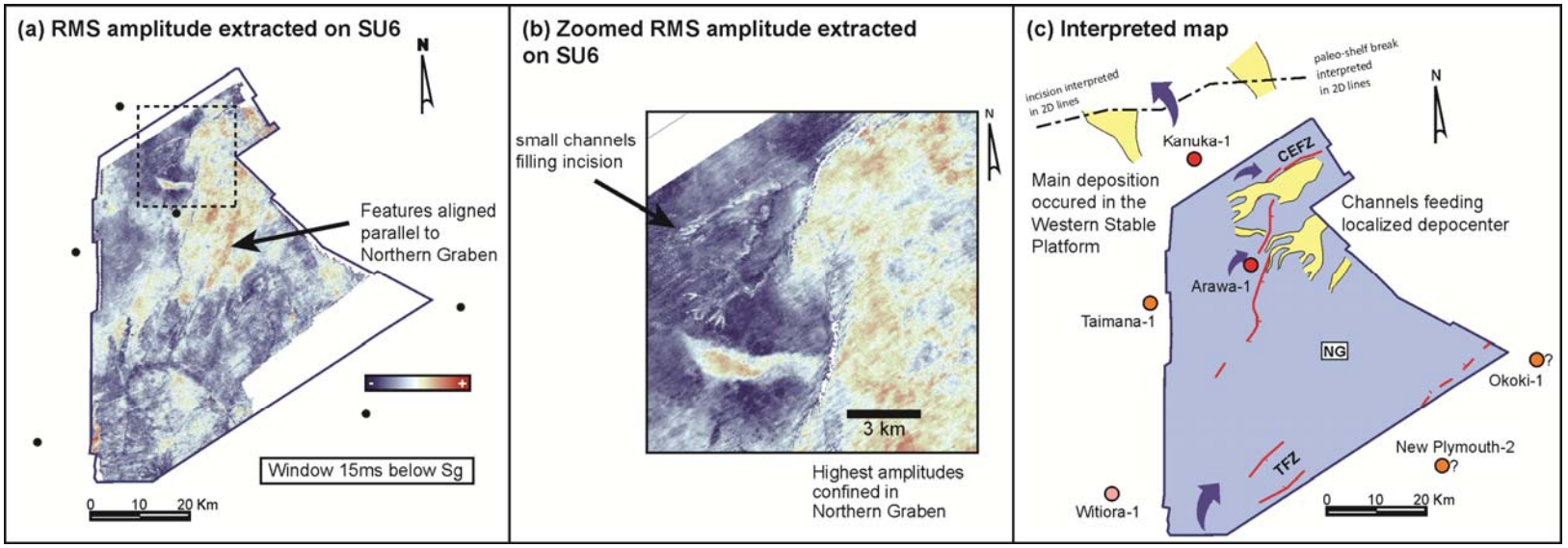

Figure 2.21: (a) RMS amplitude extraction map of seismic unit SU6 (late Pliocene) in area covered by 3D seismic survey. Extraction window is 15 ms below Sg. (b) Detailed area showing higer-resolution image of dendritic-channelized systems on shelf. (c) Paleoenvironmental interpretation of seismic unit SU6 (early Stage 3) indicating location of paleoshelf break to north of well Kanuka-1. Image also shows northeast-southwest dendritic channels on shelf feeding localized shelfal depocenter.

DISCUSSION

Role of sea-level fluctuations in the development of the Giant Foresets Formation clinoform morphologies

During Stage 1, sea-level curves show the initiation of a falling trend in eustatic sea level (Figure 22e–g; Miller et al, 2005; Lisiecki and Raymo, 2005). However, flat to slightly rising shelf-edge trajectories are dominant inside and outside the graben region suggesting that other factors likely controlled sedimentation (Figures 2.22h). I suggest that the fact that the Northern Graben started to open in the late Miocene in northern positions of the North Island coast (Giba et al., 2010) could have manifested itself in the form of generation of low to moderate accommodation in the study area. Regardless, most sediment was bypassed toward deeper waters during Stage 1 (Figures 2.7 and 2.22).

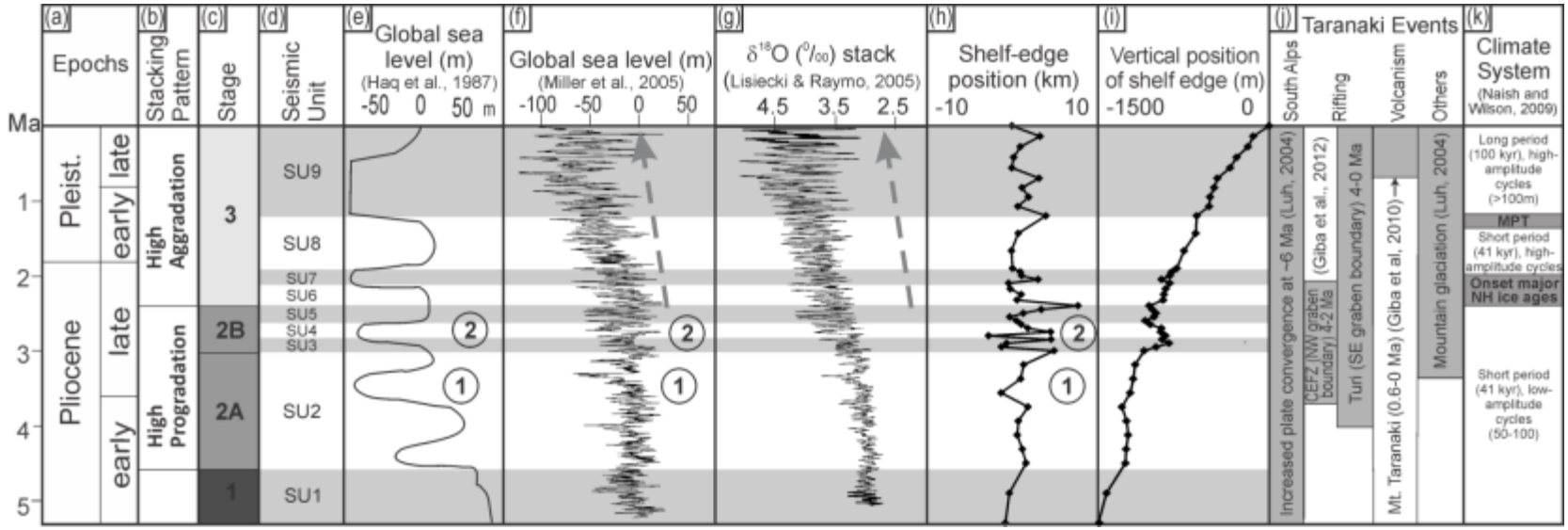

Figure 2.22: (a) Chronologic framework. (b) Stacking pattern from seismic data. (c) Seismic stages (Stages 1–3). (d) Seismic units (SU1–SU9) (e) Global sea-level curve from Haq et al. (1987). (f) Global sea-level curve from Miller et al. (2005). (g) $\delta^{18}O$ excursions based on benthic foraminifera from Lisiecki and Raymo (2005). (h) Paleoshelf edge trajectories from seismic data in the Taranaki Basin (this study). (i) Vertical position of paleoshelf break in Taranaki Basin presented as cumulative aggradation (this study). (j) Principal tectonic events affecting Taranaki Basin during Pliocene–Recent. (k) Climate systems affecting the Taranaki Basin during Pliocene–Recent times.

During Stage 2, a correlation between aggradation/progradation curves and postulated global sea levels is observed, except at the beginning of Stage 2A, when rising shelf-edge trajectories might reflect initial and very rapid graben subsidence rates (Giba et al., 2012) (Figure 2.22). The good correlation between relative sea-level curves and the shelf-edge position during Stage 2 is evident in the two peaks of eustatic sea-level fall (indicated by circled numbers in Figure 2.22) occurring around 2.4 and 3.8 Ma. Stage 2 developed during a general lowering in global sea level. This trend started during the late Pliocene and was influenced by the growth of ice sheets in the southern and then northern hemispheres (Haq et al., 1987; Miller et al., 2005; Naish & Wilson, 2009). This period of relative sea-level fall may have acted as a major driver of margin progradation and siliciclastic shelf building across the Taranaki Basin during the lower and mid-Pliocene. However, high tectonic subsidence rates, associated with the opening of the Northern Graben, were already present and may have been responsible for the apparent transgressive pulses observed in the interval. High rates of sediment supply, intensified by the increasing Southern Alps relief (Tippett & Kamp, 1995), and reorientation of sediments by the Northern Graben caused sediment supply to outpace tectonic subsidence, resulting in progradational stacking patterns and flat-to-falling shelf-edge trajectories. Consequently, clinoform stacking patterns observed in the seismic units within Stage 2 are attributed to a combination of both global sea-level drop and sediment bypass associated with the Northern Graben activity.

Sea-level curves and shelf-edge trajectories show different trends during Stage 3. Sea-level curves exhibit an overall falling sea-level, whereas aggradational patterns recorded during most of the period are indicative of sea-level rise (Figure 2.22; Johannessen & Steel, 2005). The onset of major Northern Hemisphere glaciations occurred in the late Pliocene, close to the Stage 2/Stage 3 boundary (~2.5 Ma), and this

period is characterized by greater climatic variability and higher amplitude sea-level change than previous periods (Figure 2.22g; Naish & Wilson, 2009). Eustatic amplitudes during the last 0.8–0.9 my were greater than 100 m, in contrast to Neogene (Miocene and early Pliocene) amplitudes of 50–100 m (Williams, 1988).

Increased convergence rate of the Pacific-Australian plates in the Pleistocene and the migration of the subduction zone towards the west (Tippett & Kamp, 1995) generated rapid uplift of the Southern Alps and greater availability of sediment to the northwest. The mid-Pleistocene transition (MPT) records fundamental changes in the Earth's climate, when shorter 41-ky obliquity-dominated cycles gave way progressively to the 100 ky fluctuations that characterize the later Pleistocene and Holocene, beginning around one million years ago (Hayward et al., 2012). High aggradation-to-progradation ratios in SU9 (Table 2.2) may be related to this event and could be responsible for the slight increase in variability observed in the shelf edge trajectory when compared with SU7 and SU8 (see smoother character in Figure 2.22h). On the other hand, asymmetrical "saw-tooth" patterns of climate cycles after about 700 ka (Hayward et al., 2012) indicate slow buildup of ice and subsequent rapid melting that, in the case of the Taranaki Basin, translated into rapidly rising sea levels and slow sea-level falls. Slow sea level fall was likely compensated for by subsidence related to sediment loading (Holt and Stern, 1991), generating an overall rising shelf-edge trajectory and higher aggradation-to-progradation ratios (Figures 2.7 and 2.22i). Individual sea-level falls were probably insufficient to expose the entire shelf because of the high rate of basin subsidence, explained by sediment loading on the Western Platform (Holt and Stern, 1991; Cardona, 2009), which increased after ~3 Ma with compacted sedimentation rates of 300–400 m/my (Baur, 2012; King & Thrasher, 1996).

Role of the Northern Graben in sediment partitioning and physiography of the margin

The analyses suggest that the Northern Graben played a key role in defining the geometry and location of sediments and sedimentary pathways in the shelf-edge region. Development of the graben through time also controlled (1) the location and migration of local and regional depocenters, and (2) changes in its depositional conditions from the shelf to deep-water. The architecture of channelized features interpreted from attribute maps (Figures 2.17 to 2.20) suggests that sediment was preferentially funneled to the northeast through the Northen Graben. Lower progradational rates recorded inside the graben region during Stage 2B suggest that at the time of deposition of these units, accommodation was already created by the graben (Figure 2.23). The 3D perspective in Figure 2.23 helps visualize how the sediment, sourced from the southwest, may have been redirected to fill the space generated by the graben. Relay ramps, formed between fault segments, acted to "funnel" channels, down toward the graben center in Figures 2.19a and 2.19d.

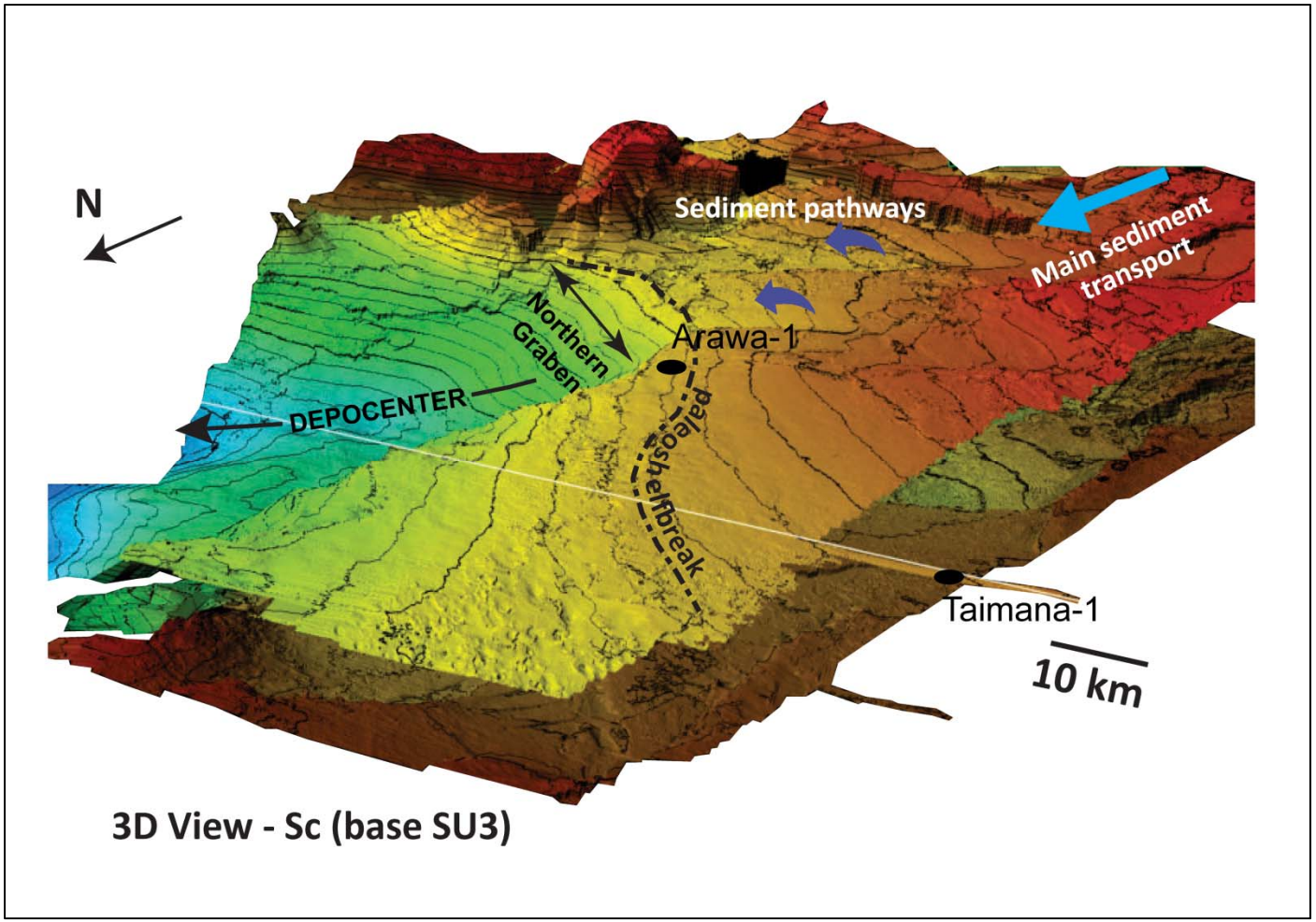

Figure 2.23: Three-dimensional visualization of surface Sc (clinoform defining base of seismic unit SU3), looking from west to east. Image shows character of sedimentary pathways on shelf that transported sediments from southwest to northeast.

CONCLUSIONS

The application of several techniques of clinoform morphology characterization in the early Pliocene–Recent succession of the northern Taranaki Basin allows identifying three stages of margin evolution. These stages are primary associated with variations in the shelf edge transition, clinoform trajectory, incision location and clinoform dimension that reflect long-term changes in relative sea level; size and position of sediment sources; mechanisms of sediment transport; and different episodes of graben activity.

Comparison of clinoform architectures and global sea level fluctuations indicate that low stand conditions dominated during the first two stages and relative sea level fall played the main role in shaping the observed geometries. However, a different mechanism had to prevail in the last stage, when both high accommodation and sediment supply were needed to developed "Giant" clinoforms. I propose that these increases were generated by the migration of the Pacific-Australian subduction zone and associated uplifting of the Southern Alps.

This study shows that the analysis of clinoform morphologies can help predict the occurrence of prospective deep-water deposits in the distal parts of the basin. The presence of sharp and deeply incised shelf edges and flat clinoform trajectories are likely associated with sediment bypass and the transport of sediment into deeper-water positions as expected in Stage 2. Smoother shelf edge transitions, slope incisions not connected with the shelf, and rising clinoform trajectories suggest that potential deep-water deposits may be associated with slope failure and collapse and are most likely fine grained as proposed for Stage 3.

The presence of underlying structures is also crucial in the development of stratigraphic sequences in continental margins and prediction of deep-water deposits. The

opening of the Northern Graben at the beginning of Stage 2 played an important role in defining the position of the shelf edge as well as funneling sediment into the structure towards the northeast. Reactivation of the graben faults during Stage 3 may have also played an important role in storing coarser grained sediment on the shelf as suggested by high amplitude anomalies aligned with the graben.

CHAPTER 3: 2D STRATIGRAPHIC FORWARD MODELING OF CLINOFORMS TO DEDUCE DRIVING MECHANISMS OF STRATA FILL, NORTHERN TARANAKI BASIN, NEW ZEALAND

ABSTRACT

Clinoforms, the basic large-scale architectural form within which sediments are stored and eventually fed down depositional dip in clastic wedges, are found in many shapes and sizes. Extremely large clinoforms, or "giant" clinoforms, are found on both modern and ancient continental margins. Understanding how these clinoforms form, evolve, and degrade is critical to understanding how transport mechanisms affect the shelf margin and sediment partitioning in any given basin. The Neogene stratigraphic succession of the Taranaki Basin in New Zealand contains clinoform packages that display a variety of architectures. Quantitative characterization of this unit was used to unravel the processes by which clinoforms evolve along a tectonically active margin that was under the influence of tectonic- and isostatic-driven subsidence, sea-level change, and sediment supply fluctuations. Nine different clinoform packages were identified on the basis of changes in their seismic stratigraphic characteristics, and two-dimensional stratigraphic forward modeling was used to define which geologic controls were influencing their genesis. The results of this study show that during the early to late Pliocene, clinoform architectures were influenced by the opening of a back-arc rifting structure in the Taranaki Basin (Northern Graben) that controlled sediment redistribution and partitioning. At the same time a drop in global sea level allowed sediment bypass to distal portions of the basin. During the late Pliocene, changes in the Australian-Pacific subduction zone forced rapid uplifting of the Southern Alps, generating a significant increase in sediment supply. Model simulations suggest that clinoform architectures during the late Pliocene were controlled by this increase in sediment supply and loading.

INTRODUCTION

Clinoforms are the basic depositional morphology for sedimentary accumulations at scales ranging from bars to deltas and continental margins. Deposits bounded by clinoform surfaces are referred to as clinothems (Rich, 1951; Figure 3.1). Clinoforms are found in many shapes and sizes but are always characterized by three geometric elements (Pirmez et al., 1998): topset, foreset, and bottomset (Figure 3.1). Continental-scale clinoforms have slope reliefs on the order of hundreds of meters, and their depositional profile covers the entire shelf, slope, and basin-floor transitions (Wolinsky and Pratson, 2007; Helland-Hansen and Hampson, 2009). Extremely large continental-scale clinoforms (>700 m), termed "giant" clinoforms by some workers, are observed on both modern and ancient continental margins (Hubbard et al., 2010). Changes in basin architectures and clinoform morphologies can be the result of interactions between different geological variables at any given time (global and relative sea-level fluctuations, changes in the location of sedimentary sources, variations in sediment supply, tectonic subsidence, isostatic compensation, changes in physiography, and oceanic currents, etc.) (Martinsen and Helland-Hansen, 1995; Cathro et al., 2003; Burgess et al., 2006; Boyd et al., 2008). Identifying which factors exert the predominant control on clinoform architecture in a particular basin is not an easy task. Sequence stratigraphic models do not always capture the complexities associated with the processes operating in a given basin; instead these models focus too much on the impact of accommodation and eustatic sea-level changes as primary controls to predict basin architectures and sediment distribution (e.g., Mitchum et al., 1977; Posamentier and Vail, 1988; Johannenssen and Steel, 2005). One of the main caveats of the sequence stratigraphic model is that sediment supply, which can vary significantly and rapidly in tectonically active regions, is commonly considered as a constant or quasi-constant variable (Burgess et al., 2006). In addition, the

effects of sediment loading and isostatic compensation are typically neglected (Reynolds et al., 1991).

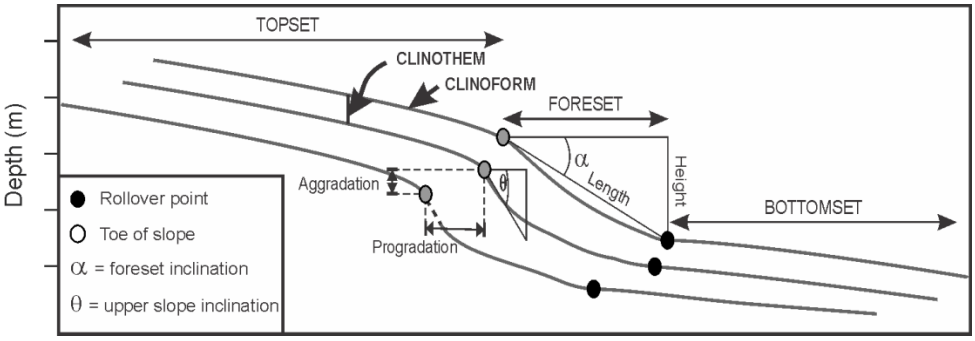

Figure 3.1: Sketch showing clinoform geometrical elements (topset, foreset, and bottomset) and parameters collected in this study for each seismic unit. Deposits bounded by clinoform surfaces are referred to as clinothems (Rich, 1951).

In Chapter 2, seismic stratigraphic interpretations and paleontological studies were combined to understand the framework and history of the Pliocene to Recent stratigraphic succession within the northern Taranaki Basin, where "giant" clinoforms (Giant Foresets Formation, GFF) were deposited. Chapter 2 highlights how the systematic description of clinoform architectures can be coupled with process-oriented interpretations associated with paleoenvironmental and tectonic conditions. In this study, the quantitative characterization of the architectural elements of the GFF performed in Chapter 2 is used as input to generate 2D stratigraphic forward models. This study uses clinoform architectures from the GFF and stratigraphic forward-modeling techniques to bridge the limitations commonly encountered when using sequence stratigraphic models and to obtain a more accurate picture of the geologic conditions that controlled the architecture and sediment partitioning within this basin during the Pliocene to Recent time. To achieve this goal, the models that are presented in this paper (1) demonstrate the expected stratigraphic/clinoform response of the northern Taranaki Basin to eustatic sea-

level variations while keeping sediment flux and subsidence rates constant, (2) consider a dynamic basin model in which subsidence and sediment supply are not kept constant through time but instead respond to changing tectonics and evolving topography, comparing and contrasting the stratigraphic signatures of variable eustasy and variable tectonics, (3) demonstrate the importance of sediment loading and isostatic compensation on clinoform development, and (4) analyze the impact of back-arc rifting and the opening of the Northern Graben on clinoform architectures. Key questions that this study seeks to answer are (1) What were the dominant geologic controls (e.g., tectonics, sediment supply, and global sea-level fluctuations) that influenced the character of the different clinoform architectures that are observed within the GFF, and did these controls vary through time? (2) Are there any architectural differences between clinoforms that developed inside and outside the Northern Graben structure, and was the opening of the graben capable of producing changes in both clinoform morphology and basin physiography? and (3) Did the uplift of the Southern Alps generate an important source of sediments for the Taranaki Basin during the Pliocene to Recent time, and if so, is there any geomorphological signature within the GFF's clinoforms that could be linked to this event?

Stratigraphic Forward Models

Quantitative forward modeling of the stratigraphic record is a form of prediction that presupposes prior understanding of the processes of erosion, transport, and deposition, and attempts to predict facies distribution and basin architectures at some time in the future (Griffiths, 2001). Stratigraphic forward modeling represents a powerful tool to understand depositional processes within a basin, which results in the prediction of realistic depositional products (e.g., clinoform geometries) and provides insights into the influence and relative weight that different geologic processes (tectonic subsidence,

eustasy, and sediment flux) have in defining stratigraphic geometries (Jordan and Flemings, 1991; Pirmez et al., 1998). Numerical models can simulate sedimentation on continental margins at different scales and provide a means to examine the response of morphology to changing sedimentary and geologic conditions (O'Grady and Syvitski, 2002). Three main types of stratigraphic models are recognized on the basis of different assumptions: geometric models (Jervey, 1988; Reynolds at al., 1991), process-based models (Tetzlaff and Harbaugh, 1989), and diffusion models (Kenyon and Turcotte, 1985; Jordan and Flemings, 1991; Paola et al., 1992) (Table 3.1). This study uses a 2D diffusion-based model (STRATA; Flemings and Grotzinger, 1996) to predict basin depositional processes. Diffusion-based models are derived from the equations of slope-driven motion and conservation of mass (Eq. 1; Flemings and Grotzinger, 1996). They assume that erosion, transport, and deposition occur via linear diffusion, meaning that sediment transport is proportional to the topographic slope (Kenyon and Turcotte, 1985; Jordan and Flemings, 1991; Flemings and Grotzinger, 1996). The diffusivity coefficient (K) in these models refers to the efficiency with which mass is transported over a given topographic slope (Flemings and Grotzinger, 1996; Kaba, 2004). In the equation below, *h* is the elevation of the point on the clinoform, *t* is any given time, and *x* is the horizontal position of the point (Jordan and Flemings, 1991; Paola et al., 1992). Although important to the final modeling effort of this paper, the details of the derivation of these parameters will not be discussed here. For further discussion, the reader is referred to Jordan and Flemings (1991), Paola et al. (1992), and Flemings and Grotzinger (1996).

$$\frac{\partial h}{\partial t} = K\frac{\partial^2 h}{\partial x^2} \qquad (1)$$

Type of model	Approach	Strengths	Weaknesses
Geometric models (Jervey, 1988; Reynolds at al. 1991)	Equilibrium profiles of sediment distribution modified by the competing effects of subsidence and erosion.	Capable of producing reasonable approximations to observed stratal geometry. Computationally simple. Useful to understand the effects of sea level, sediment supply, and tectonism at large regional scales.	Depositional surface does not evolve according to the actual stratigraphic processes of sediment transport and deposition. Unable to create small-scale stratal geometries.
Process-based or hydraulic models (Tetzlaff and Harbaugh, 1989)	Numerical approximations to the equations of fluid flow.	Useful at small scales such as understanding the internal geometry of reservoirs and predicting grain-size distributions.	Necessity to specify a large number of input parameters that may make it computationally intensive to simulate flow and sediment transport at the continental margin scale.
Diffusion models (Kenyon and Turcotte, 1985; Jordan and Flemings, 1991)	Derived from the equations of slope-driven motion and conservation of mass.	Use of a few assumptions and simple equations. Useful at larger scales including simulations of stratal geometries in semi-regional seismic sections.	Diffusion coefficients are hard to define and relate to physical processes. Only models slope-driven processes (e.g., creep, sliding, and slumping), cannot model other processes such as effects of waves and currents.

Table 3.1: Comparison of the different types of stratigraphic forward models

The software STRATA was created at the Massachusetts Institute of Technology (MIT) by Peter Flemings and John Grotzinger (1996) to determine reasonably quickly the relative importance of various transport conditions (e.g., tectonic subsidence, sediment flux, and eustasy) that control the geometries of clinoforms. STRATA has been successfully used in modeling high-relief clinoforms similar in size to those in the GFF (e.g., North Slope, Alaska; Kaba, 2004). STRATA uses sediment flux instead of sediment rate as the input parameter to constrain boundary conditions for stratigraphic models. Sediment flux refers to the amount of sediment delivered to a basin, whereas

sedimentation rate refers to a measure of the flux of sediment being deposited or preserved in a certain point or area (Petter et al., 2013).

GEOLOGIC SETTING AND TECTONIC HISTORY

The Taranaki Basin is a Cretaceous- to Recent-age sedimentary basin having a stratigraphic infill more than 10,000 m in thickness in the deepest parts of the basin (King and Thrasher, 1996). The Taranaki Basin, located along the western coast of New Zealand's North Island, has a total area of 330,000 km^2 when including its deeper water portions (called the Deepwater Taranaki Basin; Figure 3.2). The Taranaki Fault is a north-south-oriented reverse fault that delineates the eastern boundary of the basin (Figure 3.2). The origin of this fault is linked to the converging boundary between the Pacific and Australian tectonic plates (King and Thrasher, 1992). The other borders of the Taranaki Basin are not clearly defined: to the south, the basin merges with the small subbasins of the northwestern coast of the South Island, and to the northwest and north, it merges with the bathyal New Caledonia and Northland Basins, respectively (King and Thrasher, 1996) (Figure 3.2). The Cape Egmont Fault Zone (CEFZ) defines the boundary between two well-defined tectonic regions within the Taranaki Basin (King and Thrasher, 1996): (1) the tectonically active Eastern Mobile Belt that includes the Central and Northern Grabens and their associated buried Miocene andesitic volcanic arc and (2) the tectonically quiescent Western Stable Platform, where fault activity was mostly absent (Figure 3.2). The area covered by this study includes offshore portions of both the Eastern Mobile Belt, where the Northern Graben is located, and its continuation into the Western Stable Platform to the west (Figure 3.2).

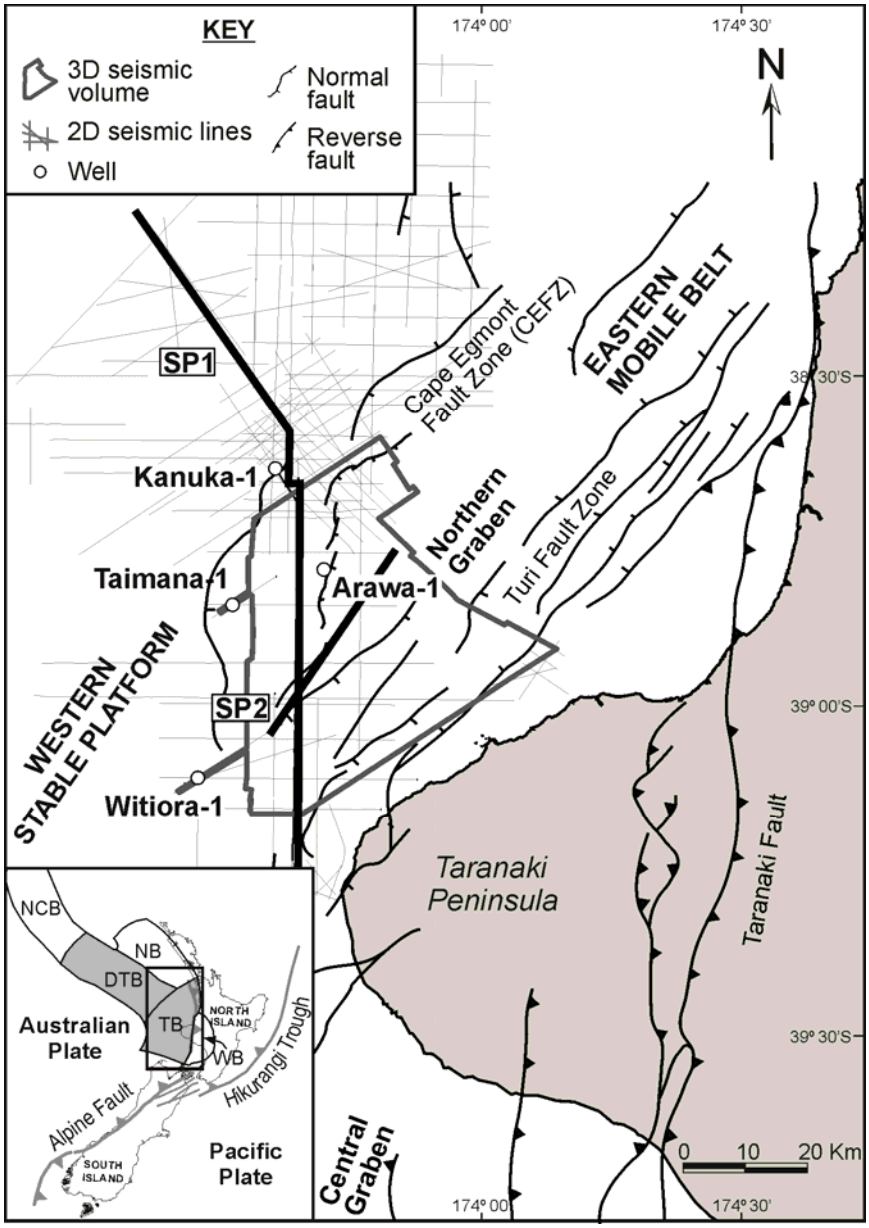

Figure 3.2: Map showing area of study, located in the western margin of New Zealand's North Island. The 3D seismic volume that was used in this study is outlined. Semiregional 2D seismic lines and modeled seismic profiles are also shown. SP1: Seismic profile 1 is located outside the Northern Graben. SP2: Seismic profile 2 is located inside the Northern Graben. Location of the Taranaki Basin, relative to the tectonic framework along Australian-Pacific plate boundary, is presented in the index map at the lower left corner of the figure. NCB = New Caledonia Basin; DTB = Deepwater Taranaki Basin; TB = Taranaki Basin; NB = Northland Basin; WB = Wanganui Basin.

The tectonic history of the basin is complex and includes rifting, passive margin development, and several stages of foreland evolution associated with the evolving Pacific-Australian convergent plate boundary (King and Thrasher, 1992, 1996). The Northern and Central Grabens formed during back-arc rifting from the early Pliocene to Recent time (King and Thrasher, 1996; Giba et al., 2010). The Northern Graben is a northeast-southwest-oriented graben that opens toward the northeast, reaching a maximum width of about 40 km. The Turi and Cape Egmont Fault Zones define the eastern and western boundaries of the Northern Graben (Figure 3.2). This graben represents an important structural element that greatly influenced the character of the stratigraphic infilling within the northern Taranaki Basin during Pliocene to Recent time (Chapter 2).

The Rotokare Group is the main stratigraphic unit deposited in the Taranaki Basin under back-arc rifting conditions during Pliocene to Recent times (King and Robinson, 1988; Figure 3.3). The Mangaa and the Giant Foresets Formations (GFF) are part of the Rotokare Group, but this work is only concerned with the study of the younger GFF (Figure 3.3). In the study area, the GFF is as much as 2 km thick and is composed of mostly fine-grained shelf to basin-floor deposits (King and Thrasher, 1996; Hansen and Kamp, 2002, 2004; Morgans, 2006).

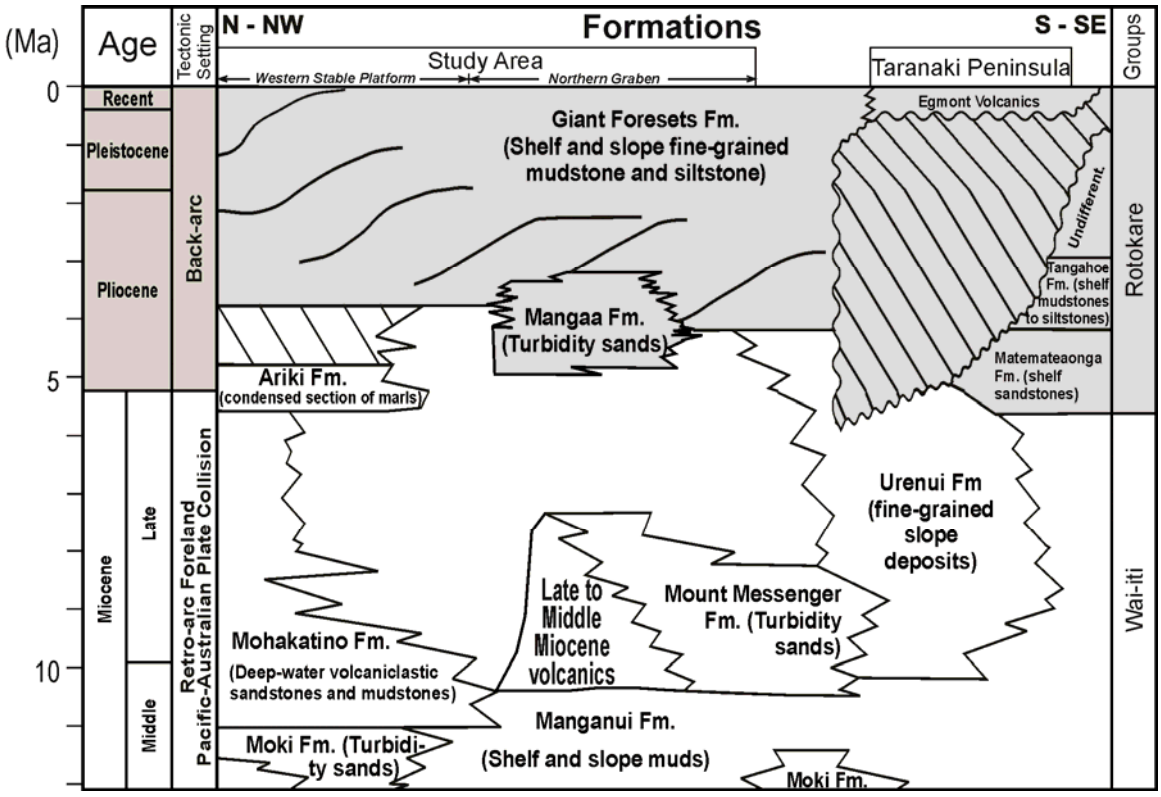

Figure 3.3: Miocene to Recent chronostratigraphic chart for the Taranaki Basin (modified from Hansen and Kamp, 2002). Interval of interest covers offshore Pliocene to Recent GFF of the northern Taranaki Basin. Giant Foresets Formation is composed of continental-scale clinoforms with heights that exceed 100 m.

DATA AND METHODS

Data

Seismic reflection datasets (2D and 3D) and well information were used in this study (Figure 3.2). The 3D seismic volume covers an area of about 1,700 km^2 and has a vertical resolution of 10 to 15 m within the Pliocene to Recent interval; 4,000 km of 2D seismic data was also available (Figure 3.2). The seismic resolution of the 2D lines ranges between 20 and 30 m within the Pliocene to Recent stratigraphic interval. Imaging depths reach a maximum of 7 s two-way travel time (TWTT) for both the 2D and the 3D seismic surveys. Geophysical logs, as well as biostratigraphic and lithological

information from four exploratory wells (Witiora-1, Taimana-1, Arawa-1, and Kanuka-1; Figure 3.2), were available and integrated into the study. Well Arawa-1 is the only well located within the 3D seismic survey. Wells Taimana-1, Witiora-1, and Kanuka-1 are located close to the western boundary of the seismic volume and were either projected or tied into the 3D volume using 2D lines (Figure 3.2). Age and paleoenvironmental interpretations were based on existing biostratigraphic zonations (Hoskins and Raine, 1984; Morgans, 1984; Crundwell et al., 1992; Hansen and Kamp, 2004; Morgans, 2006; Crundwell, 2008). Check shots and sonic logs provided velocity information. The approximate time-depth conversion within the interval of interest is 100 ms (TWTT) equivalent to 100 m. Synthetic seismograms were used to tie chronostratigraphic and paleoenvironmental interpretations from the wells to the seismic data, and they were also used to depth-convert key seismic lines that revealed the true geometry related to the structural and stratigraphic configuration of the GFF clinoform system.

Methods

Two seismic profiles normal to the shelf edge that were previously interpreted in Chapter 2 were selected. The first profile (SP1) is located outside the graben structure and captures clinoform morphologies in an area that was not intensively affected by structural deformation (Figure 3.4). The second profile (SP2) is located inside the graben structure and captures architectures from an area affected by intense structural deformation and tectonic subsidence (King and Thrasher, 1996; Figure 3.5). Nine seismic units (SU1 to SU9) and ten key surfaces (Sa to seabed) were defined on the basis of seismic facies analysis and individual clinoform characteristics (Chapter 2). Foreset declivities, clinoform heights and lengths, and progradation and aggradation rates were measured and calculated for each clinoform unit (Figure 3.1, Table 3.2). A systematic

description of how these parameters were collected is provided in Chapter 2. I focus here on using these previously collected data for modeling purposes.

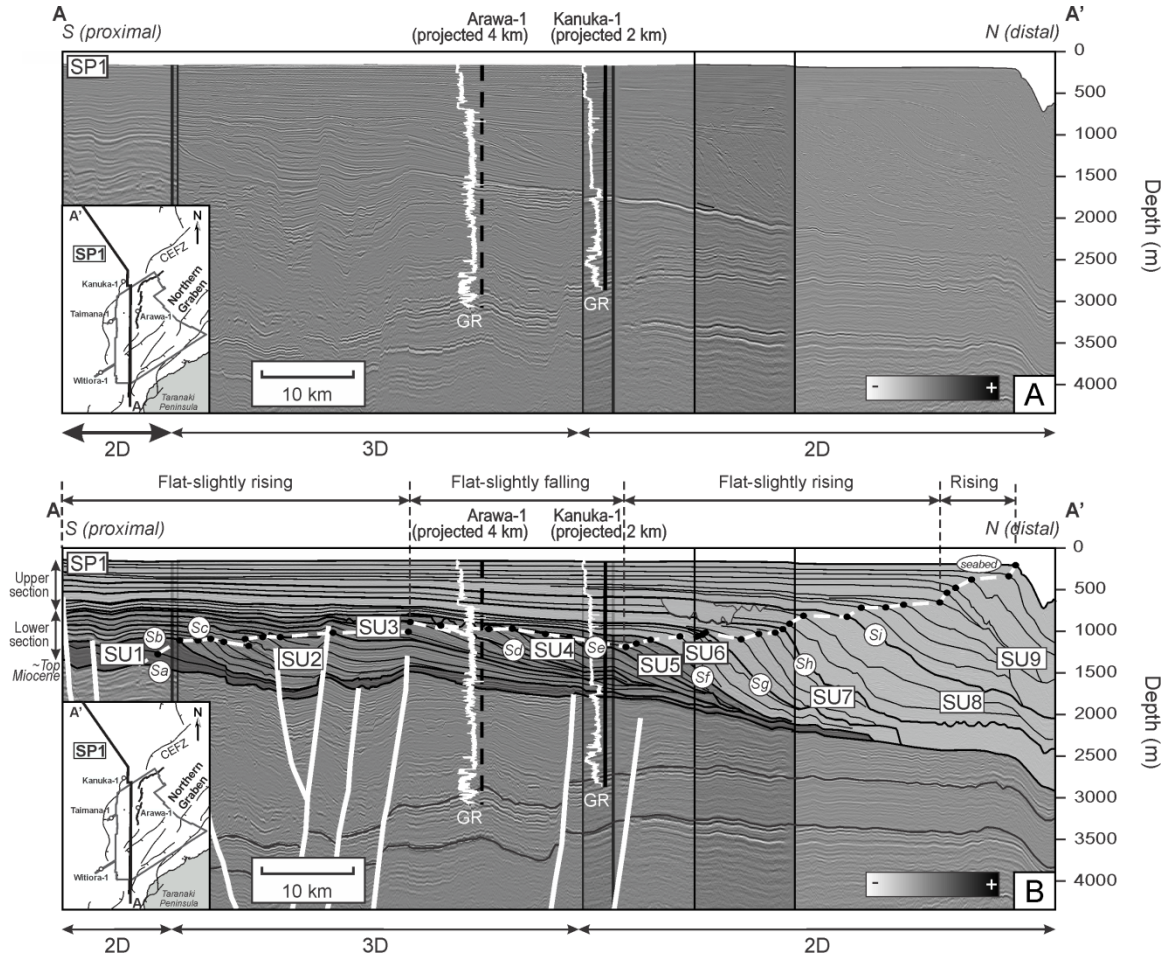

Figure 3.4: Uninterpreted and interpreted composite seismic profile along depositional dip outside the graben structure (SP1) (see index map for location). (A) Seismic image shows well-imaged clinoforms that developed during Pliocene to Recent times and are part of the GFF. Wells Arawa-1 and Kanuka-1 are projected onto this line. (B) Composite seismic line showing interpretation of key surfaces (Sa–seabed), seismic units (SU1–SU9), and shelf-edge trajectories. Notice progressive northward migration of the shelf edge through time and change from mostly progradational (Sa–Sf) to aggradational margin (Sf–seabed).

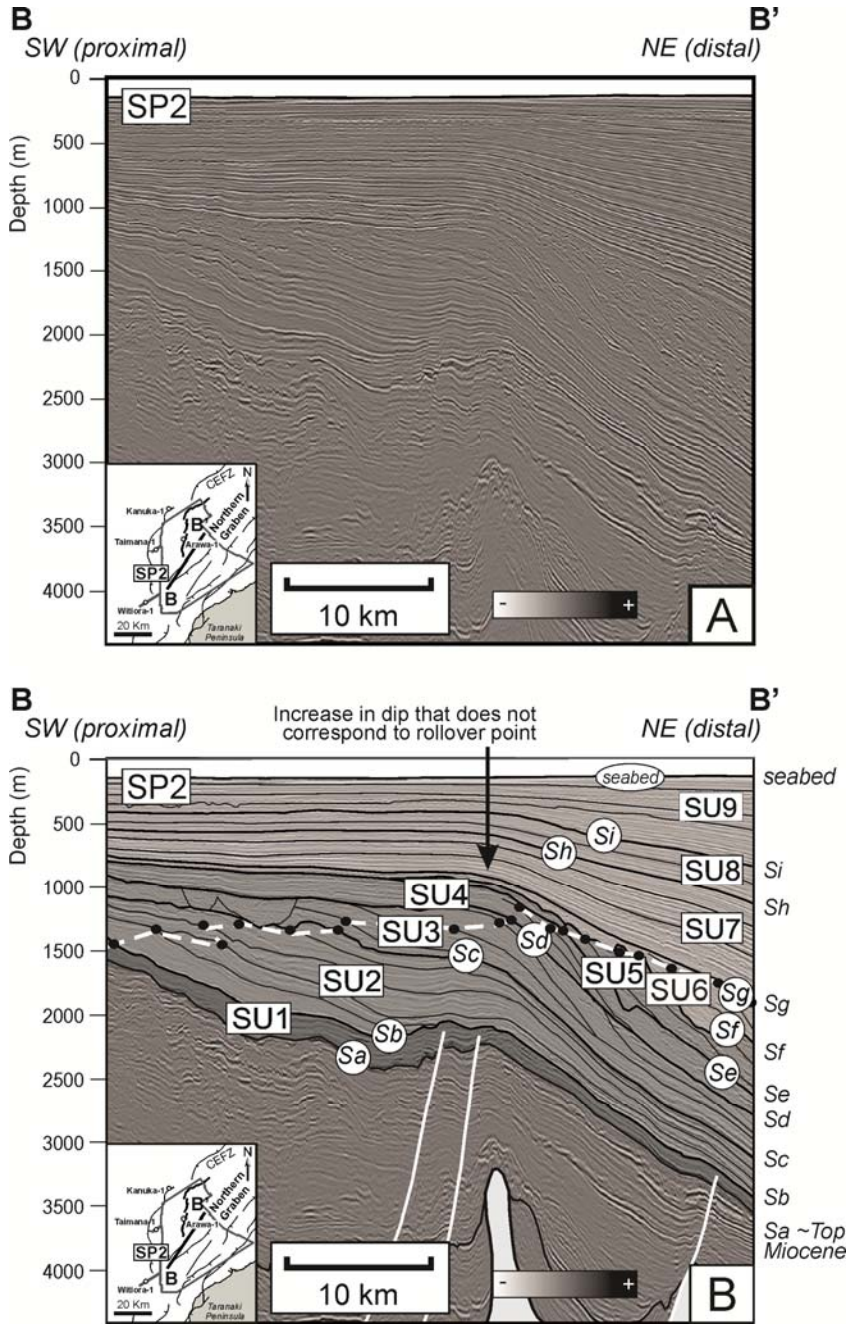

Figure 3.5: Uninterpreted and interpreted composite seismic profile along depositional dip inside the Northern Graben (SP2) (see index map for location). (A) Seismic image shows well-imaged clinoforms that developed during Pliocene to Recent times and are part of the GFF. (B) Composite seismic line showing interpretation of key surfaces (Sa–seabed), seismic units (SU1-–SU9), and shelf-edge trajectories. Notice progressive northward migration of shelf break through time.

Seismic Profile	Surface	Age (Ma)	foreset decliv. (°)	upper slope decliv. (°)	height (m)	length (km)	Section	Seismic Unit	Progradation* (km)	Aggradation* (m)	Progradation rate (km/my)	Aggradation rate (m/my)
SP1 (Outside Graben)	Sa	5.3	1	1	342	14	Lower	SU1	3	305	4	381
	Sb	4.5	2	4	510	13		SU2	17	79	11	53
	Sc	3.0	1	1	413	20		SU3	12	104	59	521
	Sd	2.8	2	2	495	16		SU4	14	-90	71	-451
	Se	2.6	3	3	739	17		SU5	11	-72	54	-361
	Sf	2.4	4	4	808	12	Upper	SU6	4	174	14	581
	Sg	2.1	5	5	892	11		SU7	8	62	28	207
	Sh	1.8	5	7	916	10		SU8	7	164	12	274
	Si	1.2	3	4	810	13		SU9	19	625	15	521
	seabed	0.0	3	6	800	14		--	--	--	--	--
SP2 (Inside Graben)	Sa	5.3	2	3	1296	44	Lower	SU1	4	253	5	317
	Sb	4.5	2	3	1477	47		SU2	17	110	11	73
	Sc	3.0	3	4	1451	31		SU3	14	35	69	173
	Sd	2.8	4	5	1318	17		SU4	4	-77	20	-385
	Se	2.6	5	6	1130	13		SU5	6	-160	29	-800
	Sf	2.4	5	7	1061	12	Upper	N.D.	N.D.	N.D.	N.D.	N.D.
	Sg	2.1	N.A.	N.A.	N.A.	N.A.		N.D.	N.D.	N.D.	N.D.	N.D.
	Sh	1.8	N.A.	N.A.	N.A.	N.A.		N.D.	N.D.	N.D.	N.D.	N.D.
	Si	1.2	N.A.	N.A.	N.A.	N.A.		N.D.	N.D.	N.D.	N.D.	N.D.
	seabed	0.0	N.A.	N.A.	N.A.	N.A.		--	--	--	--	--

N.D. = no data
* See text for explanation of how values are measured

Table 3.2: Measurements of geometrical parameters on clinoforms outside (SP1) and inside (SP2) the Northern Graben

2D Stratigraphic Forward Modeling

The geometry of the GFF clinoforms was modeled two-dimensionally using the software STRATA (Flemings and Grotzinger, 1996). Subsidence values, relative sea-level fluctuations, flexural rigidities, and diffusivity coefficients are input parameters to perform the simulations of STRATA. These parameters were obtained from studies performed in the Taranaki Basin by previous authors (Holt and Stern, 1991; King and Thrasher, 1996; Cardona, 2009) and from publications covering clinoform development in general, as well as the application of stratigraphic modeling techniques (Jordan and Flemings, 1991; Reynolds et al., 1991; Paola et al., 1992; Pirmez et al., 1998). Several models were run to test the influence of a variety of geologic controls on the development of clinoform geometries. First, I explored the nature of the stratigraphic response of a geometrically simple margin to eustatic sea-level variations (Haq et al., 1987; Miller et al., 2005) to try to reproduce the geometries observed in seismic profile SP1. I run these simulations using a steady-state basin having constant subsidence and sediment flux. Secondly, I examined dynamic basin models where subsidence and sediment flux were not kept constant through time but responded to the tectonic settings (e.g., the opening of the Northern Graben back-arc basin, the migration of the Australian-Pacific plate subduction zone, and changes in the Southern Alps uplift). Thirdly, I considered the effects of isostatic compensation on the creation of accommodation. Finally, I analyzed the geometric differences between the profiles inside and outside the graben (SP1 and SP2) and evaluated different conditions hypothesized to reproduce the profile outside the graben (SP2).

For each model, input parameters were varied individually to isolate the relative effects that sea-level fluctuations, sediment flux, subsidence, and isostatic compensation had on clinoform geometries and margin architectures. Table 3.3 summarizes the range of

values for the different parameters used in each set of models. In order to quantify the goodness of the fit between the real GFF clinoform architectures and the simulation results, the parameters that were measured or calculated directly from the seismic lines were used (foreset declivities, heights and lengths, progradation and aggradation rates) (Figure 3.1). Iterative simulations were run until the closest geometric matches were produced for each case. To simplify this comparison process, the GFF clinoforms were divided into an upper and a lower section (Figures 3.4 and 3.5) according to their geometric characteristics. The lower GFF section contains seismic units SU1 and SU5 (Figures 3.4 and 3.5), which are characterized by clinoforms that present oblique and linear geometries having abrupt topset to foreset transitions (Chapter 2). The upper GFF section contains seismic units SU6 and SU9 (Figures 3.4 and 3.5), which are characterized by sigmoidal shapes and smoother topset to foreset transitions (Chapter 2).

	Set of Models 1	Set of Models 2	Set of Models 3	Set of Models 4
	Fig. 3.14	Fig. 3.15	Fig. 3.16	Fig. 3.18
Marine diffusivity coefficient K_m (m^2/y)	100-500	100-500	100-500	100-500
Non marine diffusivity coefficient K_{nm} (m^2/y)	10,000-50,000	10,000-50,000	10,000-50,000	10,000-50,000
Sediment flux (m^2/y)	Constant through time (5-100)	Variable through time, results from Petter et al. (2013) in SP1 (9-79)	Variable through time, results from Petter et al. (2013) in SP1 (9-79)	Variable through time, results from Petter et al. (2013) in SP2 (17-76)
Subsidence rate (m/my)	Constant through time (100-500)	Variable through time (backstripped subsidence curves from wells Witiora-1, Arawa-1, and Kanuka-1)	Variable through time (backstripped subsidence curves from wells Witiora-1, Arawa-1, and Kanuka-1)	Variable through time (backstripped subsidence curves from wells Witiora-1, Arawa-1, and Kanuka-1)
Sea level curve	Miller et al. (2005) and Haq et al. (1987)	Miller et al. (2005)	Miller et al. (2005)	Miller et al. (2005)
Flexural rigidity (Nm)	None	None	$5.6x10^{22}$-$15x10^{22}$	$5.6x10^{22}$-$15x10^{22}$

Table 3.3: Range of values of the input parameters used in strata

Model Design

Time and Length of the Modeling

Although the GFF was deposited between 5.3 and 0 Ma, simulations presented in this study were extended to cover the last 7.5 m.y. of basin evolution. Extending the simulation period was necessary to generate enough accommodation to form the surface that defines the base of the GFF clinoform package (top Miocene horizon) toward the south and to allow for proper development of clinoforms in the focus area (Kaba, 2004). Additional modifications were made to the reference lines in order to properly condition the simulation. For instance, seismic profile SP1 (outside graben structure) was originally 114 km long but was extended to 400 km to remove a blanking distance that is automatically generated by STRATA (10% of total section length at the proximal end of the model) and any residual boundary effect at the distal end of these profiles (Kaba, 2004). Likewise, the length of seismic profile SP2 (inside graben structure) was increased from ~45 to 400 km to standardize the length of the lines and to allow for proper simulation of the topset geometries of clinoforms contained within the Plio-Pleistocene section.

Sea-Level Fluctuations

Two global sea-level curves were used to simulate changes in sea level through time for these models: the Haq et al. (1987) global sea-level curve and the Miller et al. (2005) sea-level curve that was derived by performing backstripping in the coast of New Jersey.

Sediment Flux

Sediment flux was kept constant through time in the steady-state model, using the values shown in Table 3.3 for different STRATA runs. For the dynamic models, the

approach proposed by Petter et al. (2013) was applied to the Taranaki Basin GFF clinoforms in order to estimate sediment flux. This method simplifies the computation of sediment fluxes because it uses parameters that are easily estimated from 2D seismic profiles (clinoform height, thickness, and progradation and aggradation rates) (Figures 3.1 and 3.6).

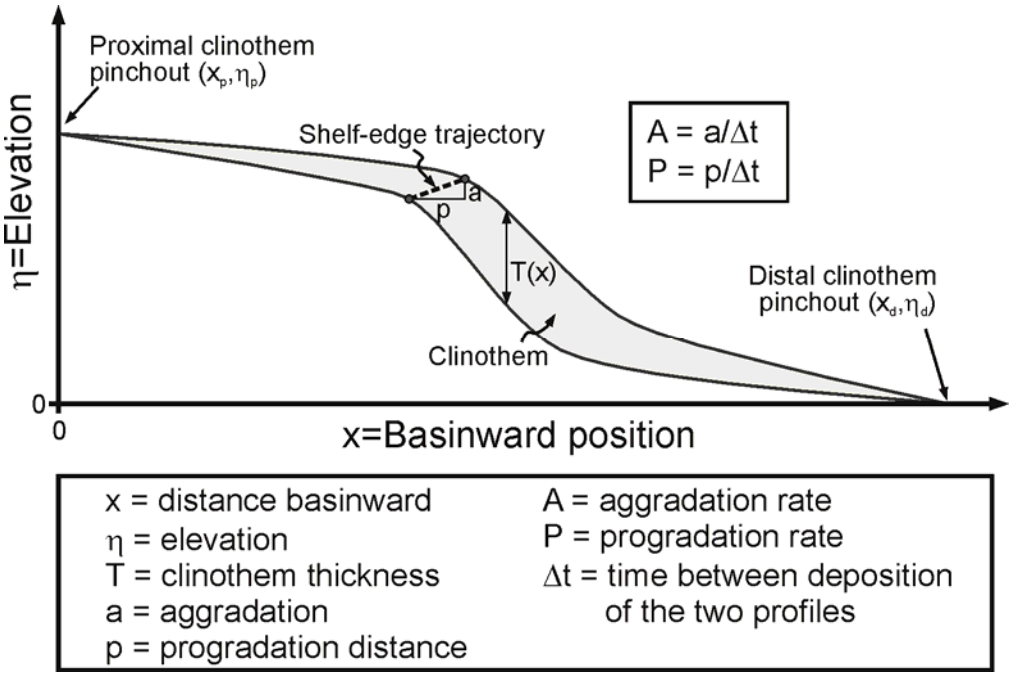

Figure 3.6: Sketch illustrating the parameters used for calculations of sediment flux according to Petter et al. (2013). The datum (h=0) corresponds to the surface onto which the profiles downlap, and the coordinate origin (x=0) is located at the clinothem proximal pinchout.

Three main steps were followed to calculate sediment flux in the Taranaki Basin (Petter et al., 2013) and summarized in Figure 3.7: (1) progradation and aggradation rates for seismic profiles SP1 and SP2 were calculated following the shelf-edge trajectory as defined by clinoform rollovers (Table 3.2); (2) the distal clinothem pinchout positions (Figure 3.6) were calculated as defined by Petter et al. (2013)—this procedure involved plotting both the clinothem thickness and the elevation against basinward position

(Figures 3.8 to 3.11) in order to find the best-fitting exponential equations (Figure 3.7); and finally, (3) sediment flux was calculated using the relationship established by Petter et al. (2013; Figure 3.7). Table 3.4 shows the final product with sediment flux estimates associated with each seismic unit inside and outside the Northern Graben.

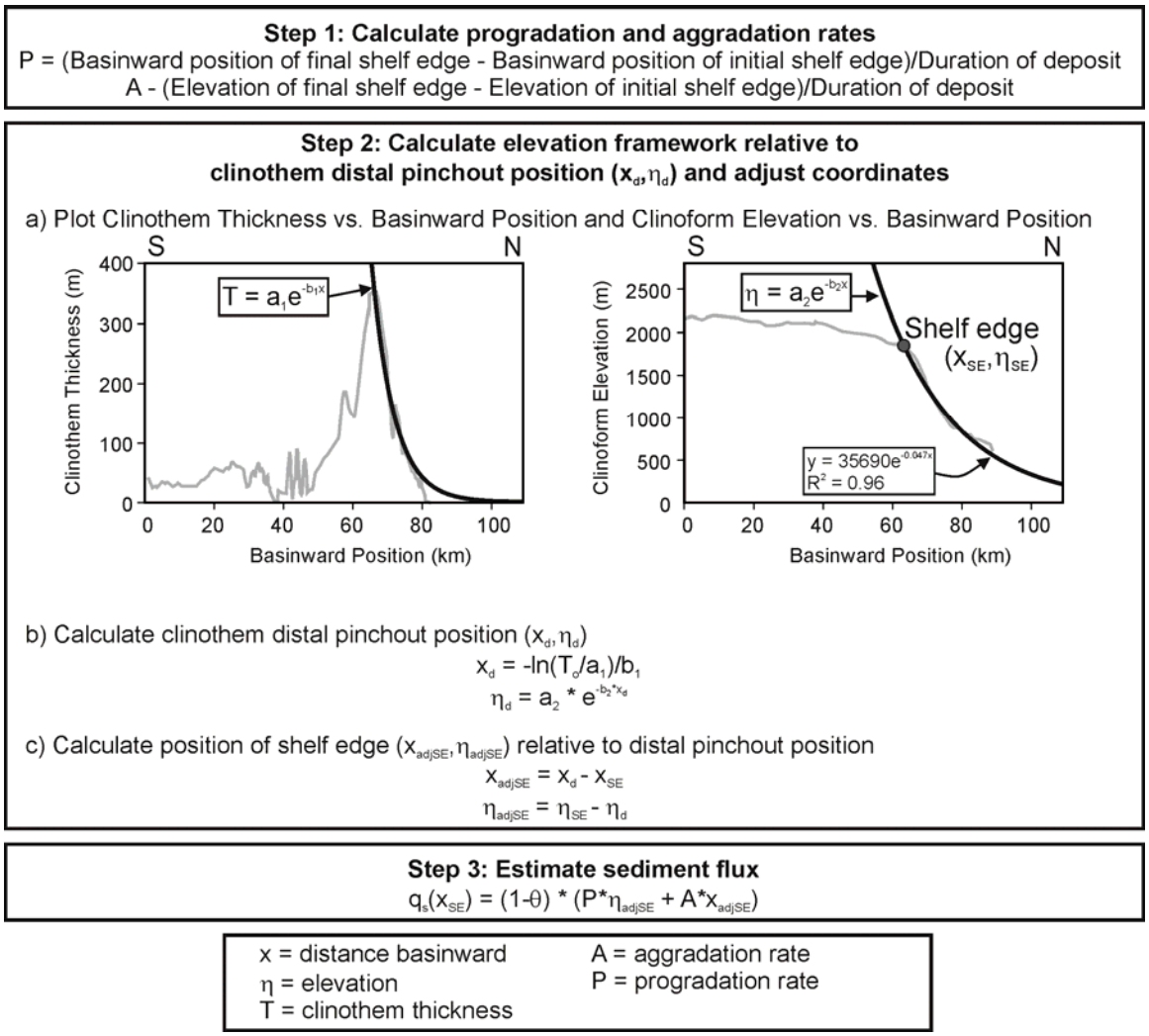

Figure 3.7: Steps to estimate shelf-edge sediment flux (modified from Petter et al., 2013).

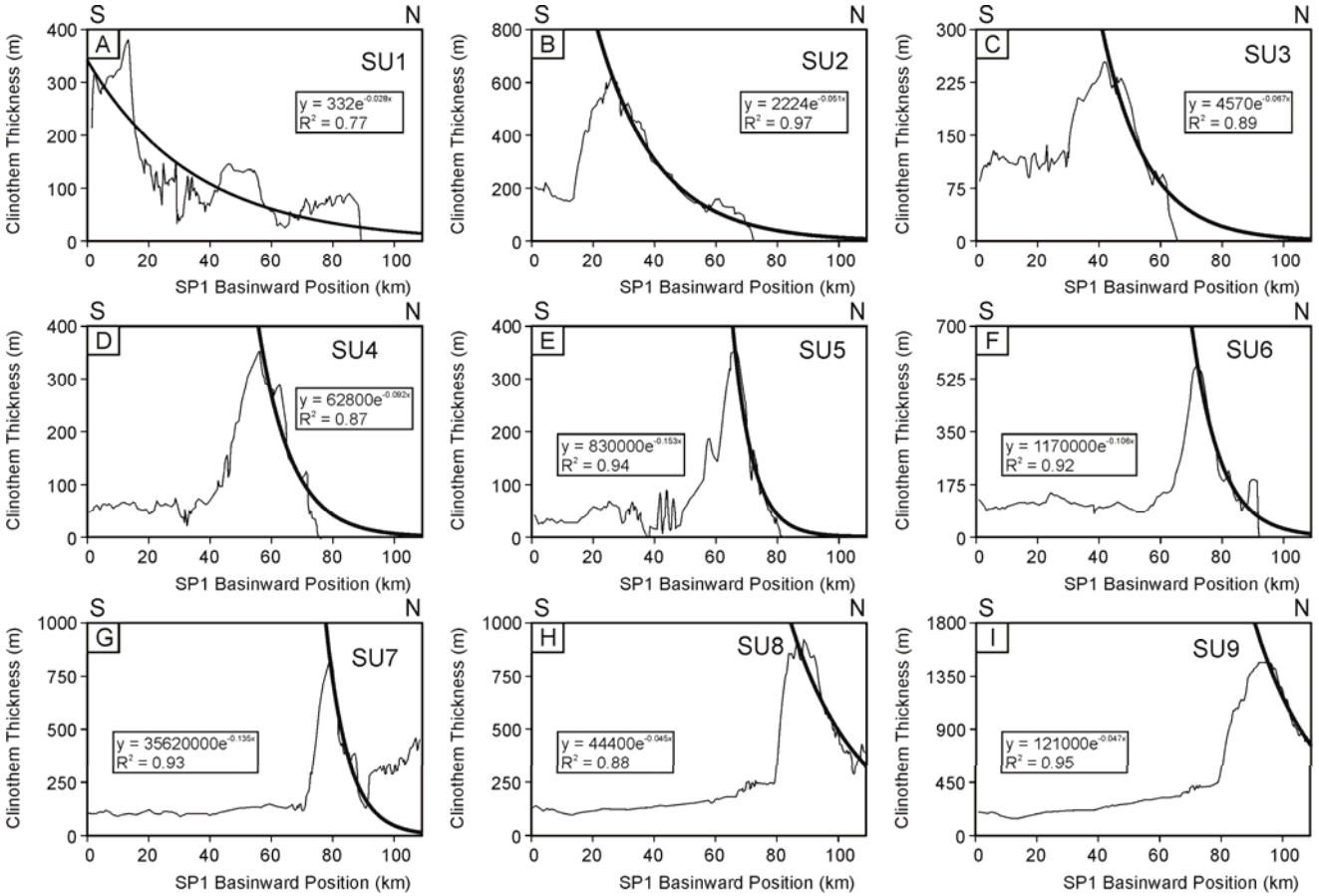

Figure 3.8: Plots showing the change in clinoform thickness (m) along the seismic profile located outside the graben (SP1) for different seismic units (SU1–SU9). The thin black line shows the variation in thickness. The thick black line represents exponential functions fitting the general trends. Seismic profile SP1 is ~100 km long, and the origin (0 m) is defined in its southern end.

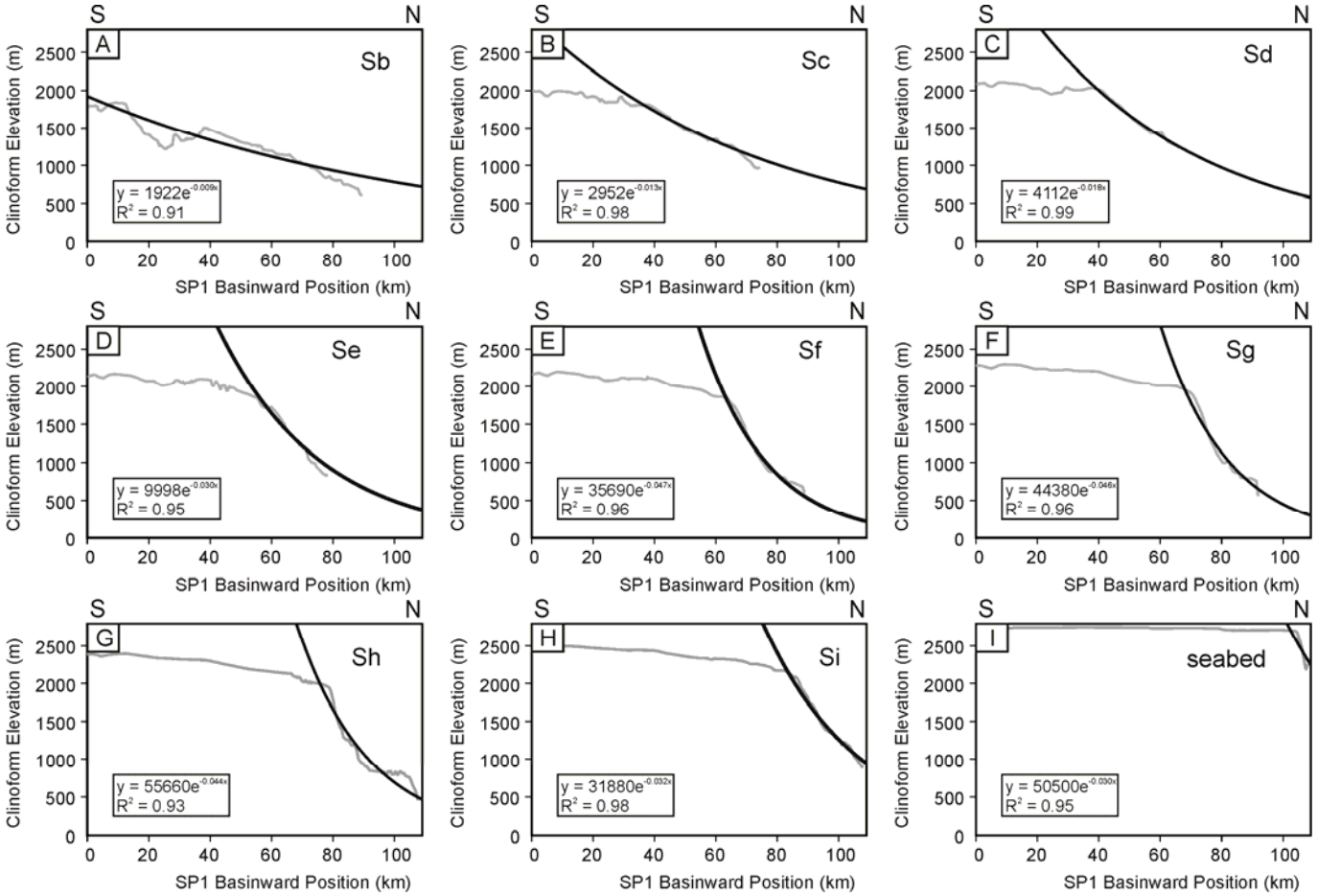

Figure 3.9: Plots showing the change in clinoform elevation (m) along the seismic profile located outside the graben (SP1) for different seismic unit boundaries (Sb–seabed). The thin black line shows the variation in thickness. The thick black line represents exponential functions fitting the general trends. Seismic profile SP1 is ~100 km long, and the origin (0 m) is defined in its southern end.

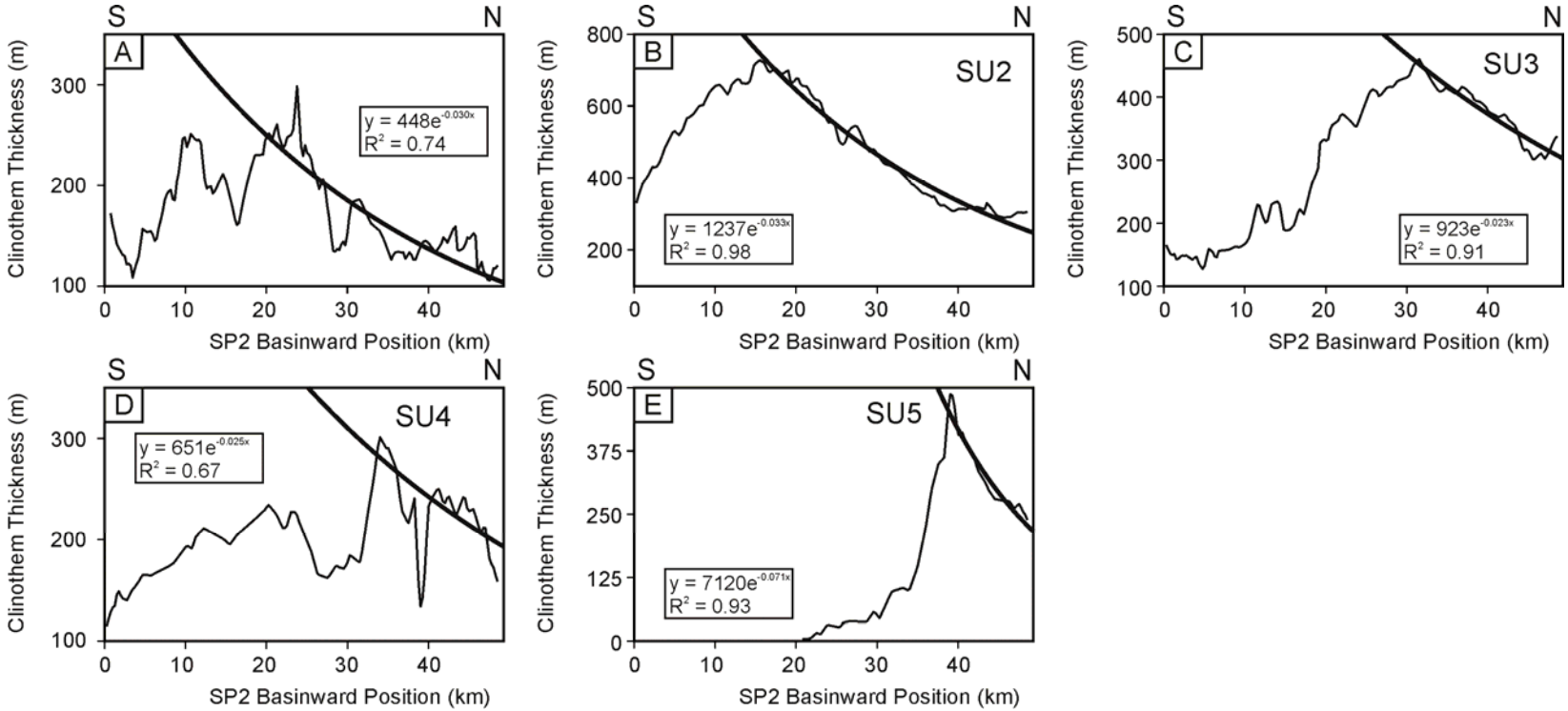

Figure 3.10: Plots showing the change in clinoform thickness (m) along the seismic profile located inside the graben (SP2) for different seismic units (SU1–SU5). The thin black line shows the variation in thickness. The thick black line represents exponential functions fitting the general trends. Seismic profile SP1 is ~100 km long, and the origin (0 m) is defined in its southern end. Lack of data coverage inside the graben region only allowed registering parameters for seismic units SU1 to SU5.

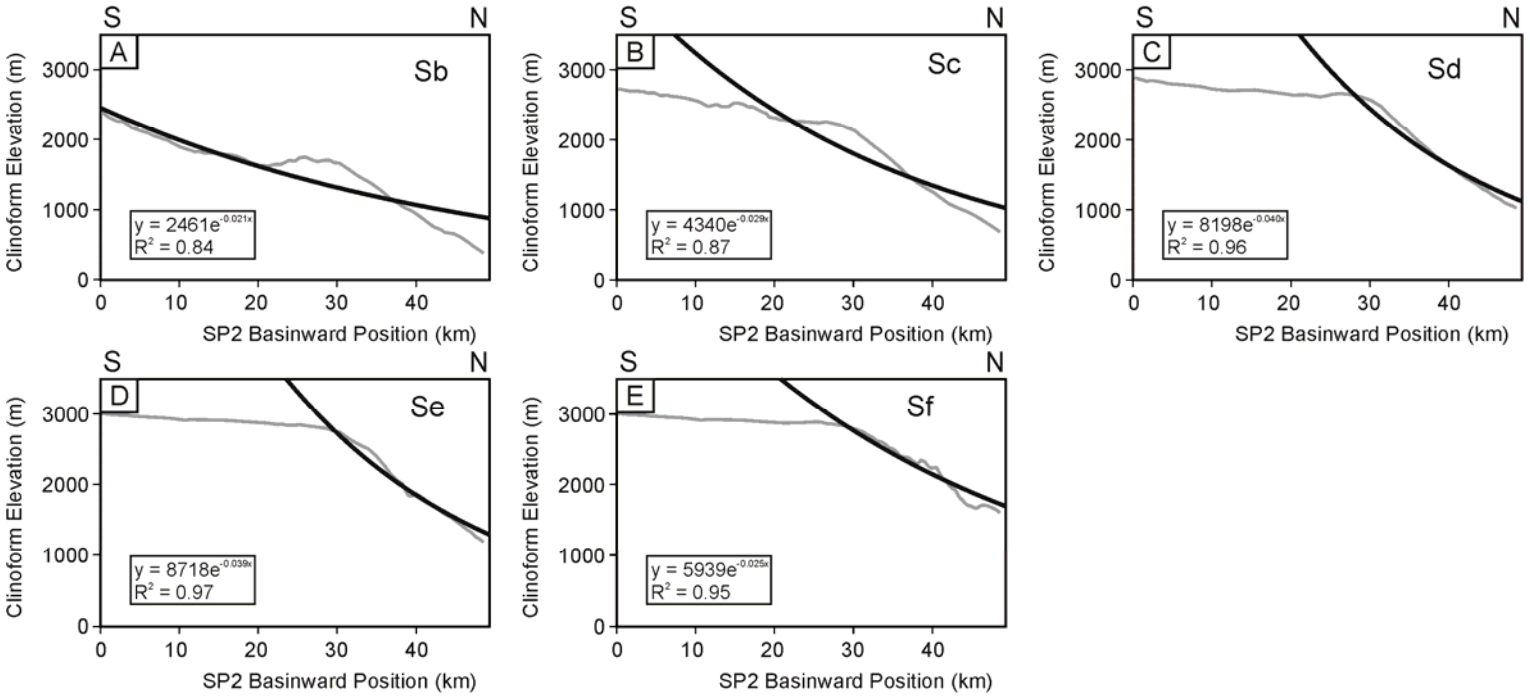

Figure 3.11: Plots showing the change in clinoform elevation (m) along the seismic profile located inside the graben (SP2) for different seismic unit boundaries (Sb–Sf). The thin black line shows the variation in thickness. The thick black line represents exponential functions fitting the general trends. Seismic profile SP1 is ~100 km long, and the origin (0 m) is defined in its southern end. Lack of data coverage inside the graben region only allowed registering parameters for surfaces Sa to Sf.

Seismic Profile	Unit	Porosity	Progradation rate (km/my)	Aggradation rate (m/my)	Thickness vs. Basinward position (exponential parameters)			Surface	Age (Ma)	XSE* (km)	ηSE* (km)	Elevation vs. Basinward position (exponential parameters)			Distal pinchout position Xd (km)	Distal pinchout position ηd (m)	XadjSE† (km)	ηadjSE† (m)	q(XSE)* (m^2/y)
					a	b	R^2					a	b	R^2					
SP1 (Outside Graben)	SU1	0.2	4	381	332	-0.028	0.77	Sb	4.5	13	1819	1922	-0.009	0.91	89	604	77	1215	27
	SU2	0.2	11	53	2242	-0.051	0.97	Sc	3	38	1807	2952	-0.013	0.98	72	1020	34	787	9
	SU3	0.2	59	521	4570	-0.067	0.89	Sd	2.8	41	1981	4112	-0.018	0.99	65	1263	24	718	44
	SU4	0.2	71	0	62840	-0.092	0.87	Se	2.6	56	1836	9998	-0.030	0.95	75	942	19	894	50
	SU5	0.2	54	0	8304000	-0.153	0.94	Sf	2.4	64	1835	35690	-0.047	0.96	89	607	25	1228	53
	SU6	0.2	14	581	1165000	-0.106	0.92	Sg	2.1	70	1902	44380	-0.046	0.96	92	555	22	1347	25
	SU7	0.2	28	207	35620000	-0.135	0.93	Sh	1.8	79	1925	55660	-0.044	0.93	117	333	38	1592	42
	SU8	0.2	12	274	44370	-0.045	0.88	Si	1.2	86	2082	31880	-0.032	0.98	202	47	116	2035	44
	SU9	0.2	15	521	121100	-0.047	0.95	seabed	0	104	2662	50500	-0.030	0.95	217	69	113	2593	79
SP2 (Inside Graben)	SU1	0.2	5	317	448	-0.030	0.74	Sb	4.5	0	2397	2461	-0.021	0.84	89	604	89	1793	30
	SU2	0.2	11	73	1237	-0.033	0.97	Sc	3	16	2526	4340	-0.029	0.87	72	1020	57	1506	17
	SU3	0.2	69	173	923	-0.023	0.91	Sd	2.8	30	2560	8198	-0.040	0.96	65	1263	35	1297	76
	SU4	0.2	20	0	651	-0.025	0.67	Se	2.6	30	2749	8718	-0.039	0.97	75	942	45	1807	29
	SU5	0.2	29	0	7120	-0.071	0.93	Sf	2.4	39	2348	5939	-0.025	0.95	89	607	51	1741	40

***XSE = Basinward position of shelf edge; ηSE = Elevation of shelf edge; q(XSE) = Sediment flux at shelf edge position**
***XadjSE = Basinward position of shelf edge relative to clinothem pinchout position; ηadjSE = Elevation of shelf edge relative to clinothem pinchout position**

Table 3.4: Sediment flux calculation for SP1 and SP2 using the procedure of Petter et al. (2013)

Tectonic Subsidence

For the steady-state models, subsidence values were assumed to be constant over the entire depositional period, but they were gradually increased for each simulation (Table 3.3) in order to find the values that produced the best matches to the seismic section. For the dynamic models, curves of tectonic subsidence were obtained from the geohistory analyses performed by Cardona (2009) in wells Arawa-1, Taimana-1, and Witiora-1, and by Bates and Heid (2007) in well Kanuka-1. The subsidence trends observed in the wells were not uniform across the basin (Figure 3.12), as expected in a basin affected by a variety of underlying structural features. Therefore, individual well curves were used. Subsidence curves from wells close to the seismic profiles were used directly in the projected position of the well whereas, when the wells were too far from the seismic profiles, only general trends of subsidence could be assumed through the interpolation of the curves. On the basis of this criterion, wells Kanuka-1 and Arawa-1 were projected into seismic profile SP1 and their curves used in those positions whereas an average of subsidence rates that included data from wells Arawa-1 and Witiora-1 was used in the southern end of seismic profiles SP1 and SP2.

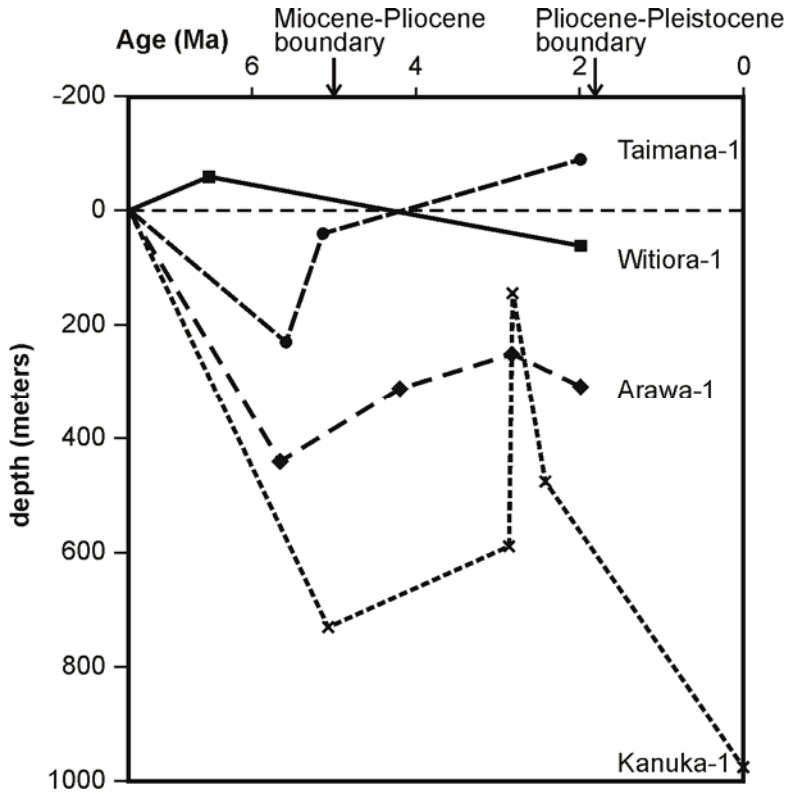

Figure 3.12: Subsidence curves for wells Witiora-1, Taimana-1, Arawa-1, and Kanuka-1 compiled from Cardona (2009) and Bates and Heid (2007). Locations of wells on which subsidence curves are based are shown in Figure 3.1.

Flexural Rigidity

The flexural rigidity that was used ranged from 5.6×10^{22} to 15×10^{22} Nm. These values were obtained from previous studies that performed forward modeling of the gravity and isostatic responses of the Plio-Pleistocene sedimentary load in the northern Taranaki shelf margin (Holt and Stern, 1991). This range includes the values of 8×10^{22} Nm obtained by Stern (1990) in southern positions of the Taranaki Basin and 7.5×10^{22} Nm reported by Stern and Davey (1990) in the adjacent Wanganui Basin (Figure 3.2).

RESULTS

First set of models: steady-state models. Variations in sea level.

The global sea-level curves derived by Haq et al. (1987) and Miller et al. (2005) were used to extract the values of relative sea level. Both curves produced similar results in terms of dimensions (height and length of clinoforms) and stacking patterns (progradation and aggradation amounts), as shown in Figure 3.13. However, model runs using the curve of Miller et al. (2005) generated smoother, convex shelf-edge regions, whereas the curve of Haq et al. (1987) produced sharper shelf-edge regions (Figure 3.13). The modeling indicates that lower resolution sea-level curves (e.g., Haq et al., 1987) fail to reproduce sigmoidal clinoform morphologies (rounded and smoother shelf breaks) such as those observed in the upper section of the GFF (>2.4 Ma). As suggested by Adams (2001), these sigmoidal geometries can be better reproduced by using curves that record smaller sea-level fluctuations (e.g., Miller et al., 2005). Models performed in this study confirmed this observation. Consequently, I used the global sea-level curve of Miller et al. (2005) as input for all the models. Subsidence profiles using passive-margin basal topographies were chosen to run the models because, although the Taranaki Basin is not considered a passive margin, the topography of the top Miocene horizon (base of the GFF clinoform packages) shows a passive margin as defined by STRATA (deepening basinward; Figures 3.4 and 3.5). Subsidence profiles associated with the formation of foreland basins and cratonic conditions were also used, but these runs generated unrealistic saglike basins and flat basements that do not match the geometries observed in the study area.

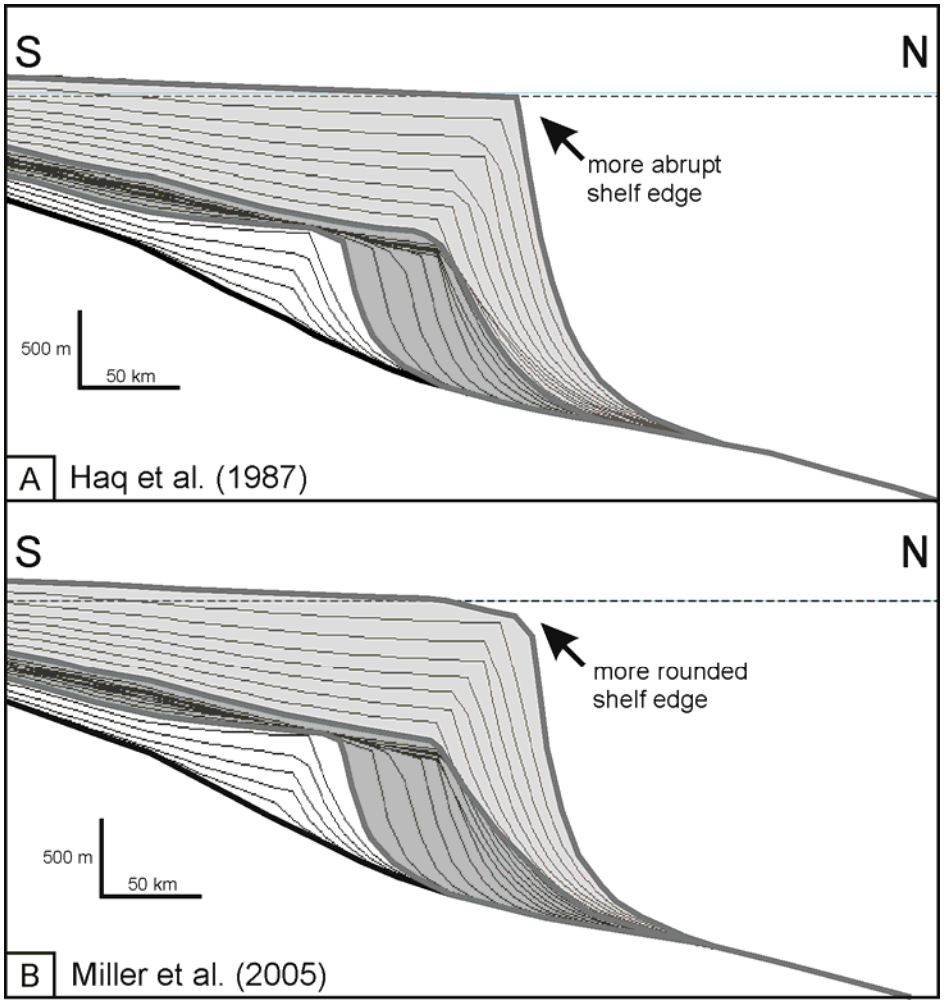

Figure 3.13: Clinoform morphologies obtained from (A) Haq et al. (1987) and (B) Miller et al. (2005). Modeling results are very similar. However, the curve of Haq et al. (1987) generates abrupt topset to foreset transitions, whereas the curve of Miller et al. (2005) generates smoother transitions and more oblique shelf-edge geometries. Input sediment flux and subsidence rates were taken from the Taranaki Basin well and seismic information for SP1.

To reproduce the topset and foreset declivities observed in the seismic profiles, the nonmarine and marine diffusivity values were gradually increased (Knm and Km), with the result that lower diffusivity values were associated with higher declivities. The values of diffusivity coefficients changed slightly depending on the sediment flux and subsidence rates that were used as input; however, values that better reproduce the GFF

geometries ranged from 40,000 to 50,000 m^2/y for the nonmarine diffusivity coefficient (Knm) and from 100 to 200 m^2/y for the marine case (Km). The high foreset declivities observed in the upper section (late Pliocene to Recent succession) were better reproduced when low marine diffusivity coefficients were used in the models. However, simulations using higher values of the marine diffusivity coefficient better matched the lower section (early to late Pliocene succession). I found that establishing a very low inclined basement configuration at the beginning of the simulation slightly increased slope values in the lower section.

Variations in sediment flux and subsidence rates were introduced systematically (Figure 3.14) to determine if sea-level fluctuations alone could reproduce observed clinoform architectures in the northern Taranaki Basin. Simulations of the GFF clinoform system were initiated with the minimum values of tectonic subsidence and sediment flux. An initial approach was to estimate the maximum subsidence rate on the basis of the seismic profiles. To achieve this goal, the height of the youngest clinoform was measured (difference in elevation between the clinoform rollover point and the topography of the base of the clinoform package, top Miocene horizon), and this value was divided by the estimated depositional period (5.3 m.y.), obtaining a maximum subsidence rate of 428 m/m.y. on SP1 and 509 m/m.y. on SP2. The subsidence values that were considered cover a range from 100 to 500 m/m.y. (Table 3.3) to include subsidence rates published for the Plio-Pleistocene succession of the Taranaki Basin by previous authors (King and Thrasher, 1996; Cardona, 2009; Baur, 2012). Similar to subsidence values, the sediment flux was kept constant for the depositional period, but a range of values were used to run multiple models (Table 3.3). The initial values for sediment flux were estimated using the progradation and aggradation rates calculated from the clinoform geometries observed in the seismic data (Chapter 2). Progradation rates were multiplied by aggradation rates, and

then the product was divided by the time in which these units were deposited to obtain the minimum sediment flux needed to reproduce the GFF architectures. For SP1 the estimated minimum sediment flux necessary to reproduce these geometries was 25 m^2/y, whereas a value of 15 m^2/y was obtained for SP2. Despite these estimates for minimum sediment fluxes, smaller values (5 m^2/y) were also used in the modeling to evaluate the impact that little sediment input could have on the generation of clinoform architectures. To appreciate the sensitivity of the model to changes in sediment flux, these values were increased gradually until reaching a maximum value of 100 m^2/y (Table 3.5). In general, increases in subsidence rates produced higher relief clinoforms (larger clinoform heights), increases in aggradation rates, and decreases in progradation rates (Figure 3.14; Table 3.5). Alternatively, increases in sediment flux generated higher progradation rates (Figure 3.14; Table 3.5).

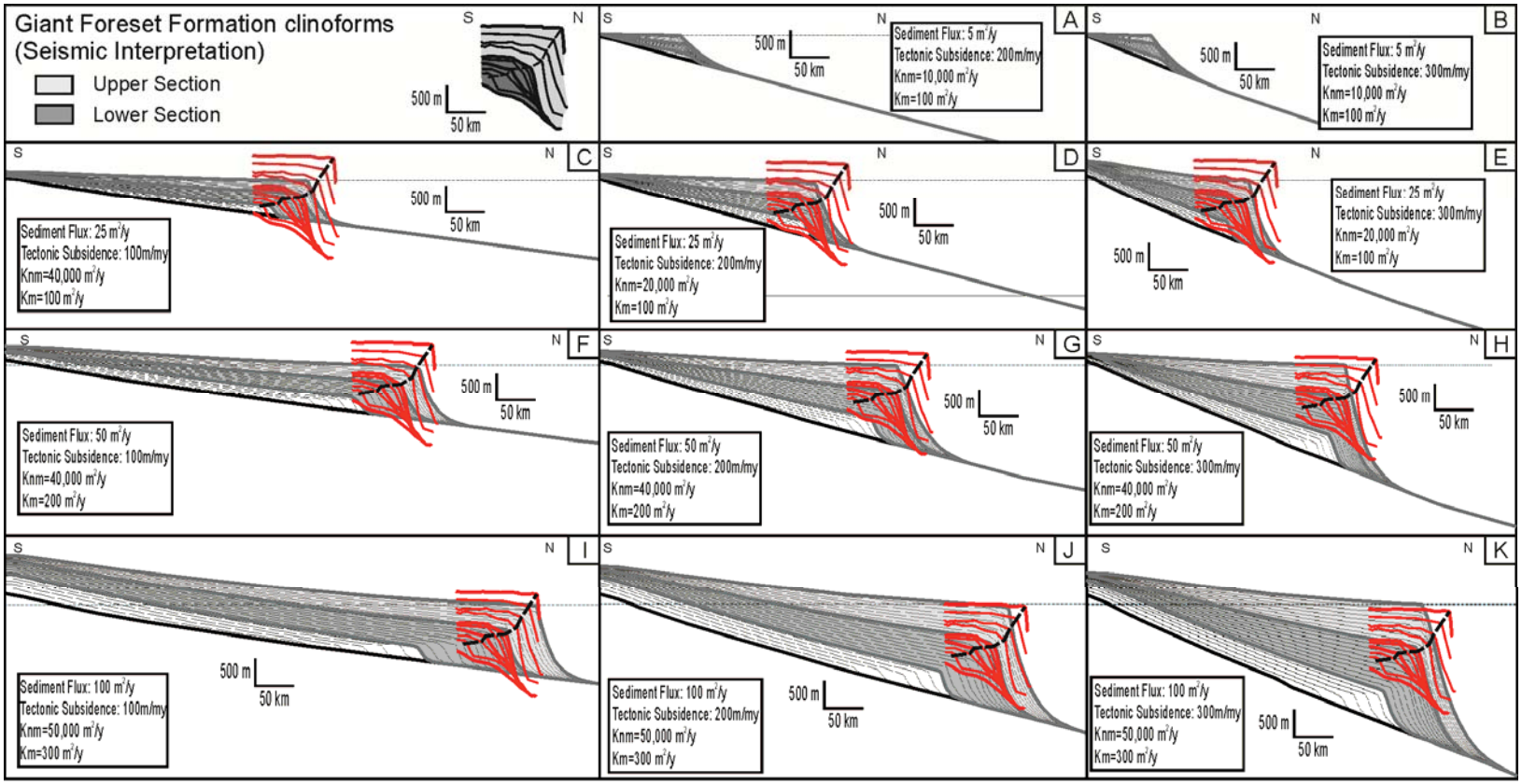

Figure 3.14: Results for set of models 1. The figures illustrate clinoform growth and progradation simulated outside the graben (SP1) under values of sediment supply and tectonic subsidence constant through time (red lines). For different model runs, sediment flux values increase in the vertical direction and tectonic subsidence values increase in the horizontal direction. Sea-level fluctuations were simulated using the curve of Miller et al. (2005). No isostatic compensation due to sediment loading was included. Constant values of sediment flux and tectonic subsidence did not simultaneously reproduce the geometry of the lower and upper sections of the GFF in SP1.

Figure	*Knm* (m^2/y)	*Km* (m^2/y)	Tectonic subsidence (m/y)	Sediment flux (m^2/y)	Flexural rigidity (Nm)	Aggrad. Lower (m)	Aggrad. Upper (m)	Total Agrad. (m)	Prog. Lower (km)	Prog. Upper (km)	Total prog. (km)	Height Lower (m)	Length Lower (km)	Angle Lower (degrees)	Height Upper (m)	Length Upper (km)	Angle Upper (degrees)
GFF	N.A.	N.A.	N.A.	N.A.	N.A.	291	738	1030	64	40	104	655	23	2	940	20	3
3.14A	10,000	100	200	5	None	161	175	337	0	-7	-7	304	27	1	599	57	1
3.14B	10,000	100	300	5	None	275	147	421	-8	-4	-13	490	33	1	727	50	1
3.14C	40,000	100	100	25	None	206	267	473	40	8	48	435	20	1	702	30	1
3.14D	40,000	100	200	25	None	351	321	672	16	1	16	720	29	1	1018	37	2
3.14E	40,000	100	300	25	None	365	411	776	23	5	28	848	26	2	1314	37	2
3.14F	50,000	200	100	50	None	234	283	517	64	24	88	597	25	1	946	39	1
3.14G	50,000	200	200	50	None	474	522	995	33	0	33	969	36	2	1619	64	1
3.14H	50,000	200	300	50	None	674	619	1293	21	0	21	1314	31	2	2064	50	2
3.14I	50,000	300	100	100	None	321	438	759	114	40	154	747	24	2	1300	47	2
3.14J	50,000	300	200	100	None	493	703	1195	68	19	87	1188	37	2	2012	59	2
3.14K	50,000	300	300	100	None	831	782	1613	41	8	48	1726	47	2	2711	76	2

Note: “Lower” refers to the lower section (early-late Pliocene), including seismic units SU1 to SU5 whereas “Upper” refers to the upper section (late Pliocene-recent), including seismic units SU6 to SU9.

N.A. = not applicable

Aggrad. = Aggradation; Prog. = Progradation

Table 3.5: Input parameters and geometrical measurement for clinoforms produced by set of models 1 (modeling of SP1 with only sea-level variations)

A small sediment flux (e.g., 5 m^2/y) produced smaller relief clinoforms than the GFF clinoforms (Figures 3.14A to 3.14B; Table 3.5). Progressive increases in sediment flux and/or subsidence rates in the computer models generated clinoform morphologies that started to resemble those observed in the basin. However, none of the models could reproduce in the same run a carbon copy of the geometries observed for both the lower (early to late Pliocene) and the upper (late Pliocene to Recent) clinoform packages. When the sediment flux was increased to 25 m^2/y and tectonic subsidence rates to 300 m/m.y., the models successfully reproduced the dimensions (i.e. height and length; Table 3.5) of the lower, early to late Pliocene clinoforms in the Taranaki Basin, but they failed to mimic their shelf-edge trajectories (Figure 3.14E). For sediment fluxes of 50 m^2/y and tectonic subsidence rates of 100 m/m.y., the position and trajectory of the shelf edge gets a better match, and the modeled clinoform dimensions are still very close to the GFF lower section (Figure 3.14F) with regards to the upper, late Pliocene to Recent unit, a sediment flux of 100 m^2/y increased the accuracy of the shelf-edge position and trajectory, as well as the clinoform morphologies (Figure 3.14I; Table 3.5). These results indicate that a sediment flux of 50 m^2/y, combined with a tectonic subsidence of 100 m/m.y. generated the best match both for shelf-edge positions and trajectories and for clinoform morphologies of the lower stratigraphic package (Figure 3.14F). However, an increase of sediment flux to 100 m^2/y was needed to generate the best match for clinoform morphologies of the upper stratigraphic package (Figure 3.14I).

The set of models discussed above allows me to conclude that (1) sediment flux and tectonic subsidence rates have to be greater than 25 m^2/y and 100 m/m.y., respectively, to form continental-scale clinoforms in the Taranaki Basin; (2) the lack of a unique solution to reproduce clinoform morphologies simultaneously in both the lower and the upper stratigraphic succession suggests that a time-variable sediment flux model

is necessary where sediment flux increases with time; (3) the basal surface over which clinoforms are reproduced in these models does not resemble the real geometry observed in the seismic profiles, making a nonuniform lateral subsidence function using well data necessary; and (4) despite some of the limitations inherent in this set of models, results indicate that under this set of conditioning factors, the GFF clinoforms could have been formed when tectonic subsidence rates were similar or greater than 100 m/m.y., and sediment flux between 25 and 100 m^2/y.

Although this set of models did not generate a carbon copy of the geometries for both the lower and the upper clinoform packages, results provided valuable insights into the influence that sediment flux and subsidence had in the development of clinoform stacking patterns within the Taranaki Basin. Because global sea-level curves show an overall sea-level drop for the interval of interest (ending in the latest Pleistocene), it was expected that the models would produce low aggradation/progradation ratios, thin topset successions, and flat to slightly descending shelf-edge trajectories (Johannessen and Steel, 2005; Carvajal and Steel, 2009) in most of the section. The models clearly showed that low sediment fluxes (e.g., 5 m^2/y) could not generate these patterns and that instead landward movement of the shelf edge was produced. It was when sediment fluxes were increased (e.g., sediment flux must be higher than 50 m^2/y when subsidence is 300 m/m.y., but higher than 100 m^2/y when subsidence is 400 m/m.y.) that the observed patterns in the basin could be better reproduced (Figure 3.14).

Second set of models: dynamic models. Variations in sediment flux and subsidence.

A separate set of models was run by applying the procedure as described by Petter et al. (2013) to seismic profile SP1 to estimate sediment flux values that ranged from 9 to 79 m^2/y (Table 3.4). In this case, the average values for the lower and the upper section are 20 m^2/y and 59 m^2/y, respectively, which are considerably smaller (40–60%) than the

values that produced the best results in the previous set of models (50 m^2/y and 100 m^2/y). Despite this difference in terms of the magnitude of sediment flux between the previous set of models and the Petter et al. (2013) simulation, overall results continued to indicate a considerable increase in sediment flux through time for the study section. Several values of marine and nonmarine diffusion coefficients were tested again to see if any changes were observed in the newly generated clinoform geometries. Values of 50,000 m^2/y and 100 m^2/y worked the best for the nonmarine and marine coefficients, respectively, and produced the best matches in terms of declivities and topset thicknesses (Figure 3.15; Table 3.6).

Figure 3.15

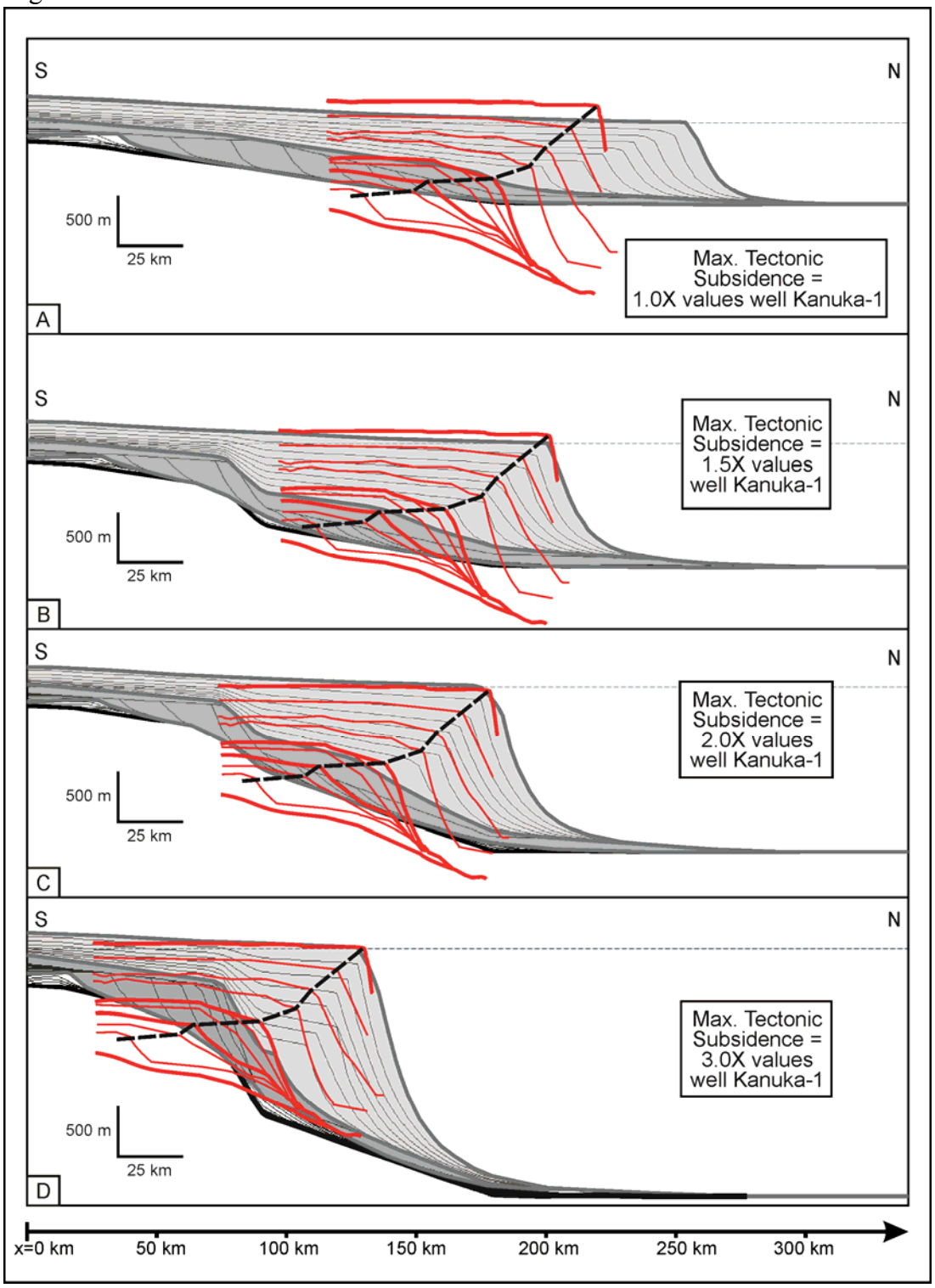
S
N
500 m
25 km
Max. Tectonic Subsidence = 1.0X values well Kanuka-1
A
S
N
Max. Tectonic Subsidence = 1.5X values well Kanuka-1
500 m
25 km
B
S
N
Max. Tectonic Subsidence = 2.0X values well Kanuka-1
500 m
25 km
C
S
N
Max. Tectonic Subsidence = 3.0X values well Kanuka-1
500 m
25 km
D
x=0 km
50 km
100 km
150 km
200 km
250 km
300 km

Figure 3.15: Results for set of models 2. The figures illustrate clinoform growth and progradation simulated outside the graben (SP1) under values of sediment supply and tectonic subsidence variable through time. Clinoforms were modeled using the tectonic subsidence curves of key wells (Witiora-1, Arawa-1, and Kanuka-1). Subsidence at the end of SP1 was varied from one to three times the values of the Kanuka-1 well to reproduce the geometry of the GFF. Clinoforms modeled using tectonic subsidence values of Kanuka-1 have lower relief than those of the GFF (A). Clinoforms developed higher reliefs using tectonic subsidence 1.5 times higher than the values reported in Kanuka-1, but still smaller than those of the GFF (B). Clinoforms modeled using tectonic subsidence 2.0 times higher than the values of Kanuka-1 have geometries similar to those of the GFF (C). Clinoforms modeled using tectonic subsidence 3.0 times higher than the values of Kanuka-1 are bigger than the GFF (D). All simulations used the sea-level curve of Miller et al. (2005) and diffusivity coefficients of 50,000 m^2/y (knm) and 100 m^2/y (km). The abrupt deepening of the base of the clinoform package does not properly replicate what is observed in the seismic transect SP1.

Third set of models: dynamic models. Simulation of sediment loading and isostatic compensation.

Isostatic compensation was introduced into this set of models through variations in the input parameter of flexural rigidity (Table 3.7), generating considerable increases in clinoform heights and aggradation/progradation ratios (Figure 3.16). Flexural rigidity values from 5.6×10^{22} to 15×10^{22} Nm produced good results. However, smaller values of flexural rigidity generated narrower and thicker clinoform packages (compare Figures 3.16A and 3.16B). The larger value of the range (15×10^{22} Nm) better reproduced the GFF geometry, generating a wider configuration and a gradual increase in depth basinward (Figure 3.16A). Subsequent runs used this value as input.

Figure	*Knm* (m^2/y)	*Km* (m^2/y)	Tectonic subsidence curve	Sediment flux input (Table 3.4)	Flexural rigidity (Nm)	Agrad. Lower (m)	Agrad. Upper (m)	Total Agrad. (m)	Prog. Lower (km)	Prog. Upper (km)	Total Prog. (km)	Height Lower (m)	Length Lower (km)	Angle Lower (degrees)	Height Upper (m)	Length Upper (km)	Angle Upper (degrees)
GFF	N.A.	N.A.	N.A.	N.A.	N.A.	291	738	1030	64	40	104	655	23	2	940	20	3
3.15A	50,000	100	Witiora-1, Arawa-1 and Kanuka-1	Results from Petter et al. (2013)	none	-383	502	119	139	80	219	180	23	0	784	30	1
3.15B	50,000	100	Witiora-1, Arawa-1 and 1.5x Kanuka-1	Results from Petter et al. (2013)	none	-561	682	121	110	60	171	384	46	0	1099	34	2
3.15C	50,000	100	Witiora-1, Arawa-1 and 2x Kanuka-1	Results from Petter et al. (2013)	none	-613	745	132	97	49	147	685	51	1	1468	41	2
3.15D	50,000	100	Witiora-1, Arawa-1 and 3x Kanuka-1	Results from Petter et al. (2013)	none	-128	367	238	59	52	111	1031	28	2	2160	42	3

Note: "Lower" refers to the lower section (early-late Pliocene), including seismic units SU1 to SU5 whereas "Upper" refers to the upper section (late Pliocene-recent), including seismic units SU6 to SU9.
N.A. = not applicable
Aggrad. = Aggradation; Prog. = Progradation

Table 3.6: Input parameters and geometrical measurement for clinoforms produced by set of models 2 (modeling of SP1 with variations in sediment flux and subsidence rates through time)

Figure 3.16

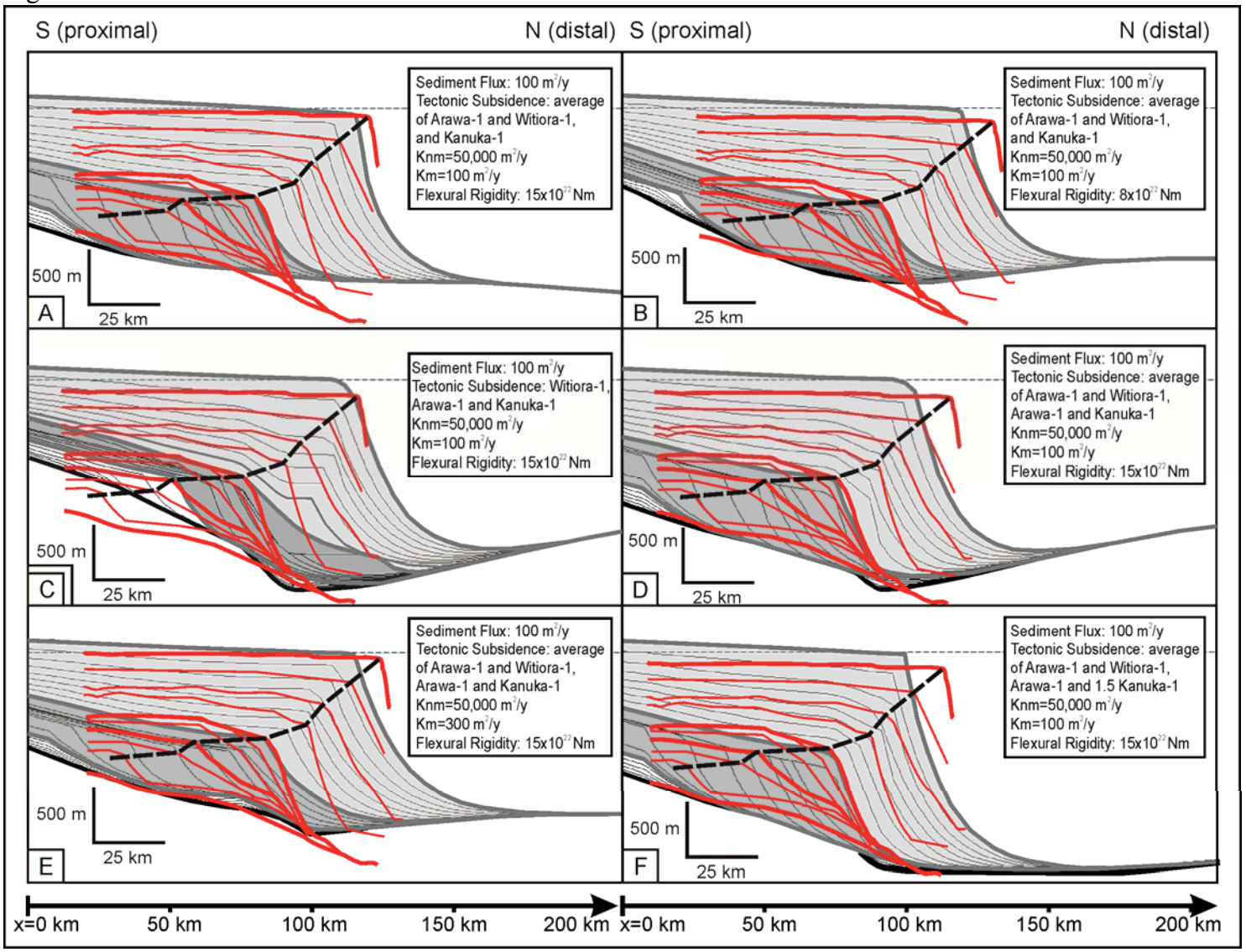
S (proximal)
N (distal)
S (proximal)
N (distal)
Sediment Flux: 100 m²/y
Tectonic Subsidence: average of Arawa-1 and Witiora-1, and Kanuka-1
Knm=50,000 m²/y
Km=100 m²/y
Flexural Rigidity: 15x10²² Nm
500 m
25 km
A
Sediment Flux: 100 m²/y
Tectonic Subsidence: average of Arawa-1 and Witiora-1, and Kanuka-1
Knm=50,000 m²/y
Km=100 m²/y
Flexural Rigidity: 8x10²² Nm
500 m
25 km
B
Sediment Flux: 100 m²/y
Tectonic Subsidence: Witiora-1, Arawa-1 and Kanuka-1
Knm=50,000 m²/y
Km=100 m²/y
Flexural Rigidity: 15x10²² Nm
500 m
25 km
C
Sediment Flux: 100 m²/y
Tectonic Subsidence: average of Arawa-1 and Witiora-1, Arawa-1 and Kanuka-1
Knm=50,000 m²/y
Km=100 m²/y
Flexural Rigidity: 15x10²² Nm
500 m
25 km
D
Sediment Flux: 100 m²/y
Tectonic Subsidence: average of Arawa-1 and Witiora-1, Arawa-1 and Kanuka-1
Knm=50,000 m²/y
Km=300 m²/y
Flexural Rigidity: 15x10²² Nm
500 m
25 km
E
Sediment Flux: 100 m²/y
Tectonic Subsidence: average of Arawa-1 and Witiora-1, Arawa-1 and 1.5 Kanuka-1
Knm=50,000 m²/y
Km=100 m²/y
Flexural Rigidity: 15x10²² Nm
500 m
25 km
F
x=0 km
50 km
100 km
150 km
200 km
x=0 km
50 km
100 km
150 km
200 km

Figure 3.16: Results for set of models 3 in SP1. The figures illustrate clinoform growth and progradation simulated outside the graben (SP1) using isostatic compensation. Overall, considerable increases in clinoform heights and aggradation/progradation ratios that better match the GFF are observed. Flexural rigidity values of 15×10^{22} Nm produced better results than smaller values that did not reproduce well the base of the clinoform package (A and B). The use of the average tectonic subsidence of Witiora-1 and Arawa-1 at x = 0 km better reproduced the southern end of seismic profile SP1 (C and D). Diffusivity coefficients (Km) of 100 m^2/y and 300 m^2/y produced good matches to the GFF; however, 300 m^2/y is slightly better in the lower section (C and E). An increase of tectonic subsidence at the end of the profile generated higher clinoforms than those of the GFF (F). All simulations used the sea-level curve of Miller et al. (2005).

Figure	*Knm* (m^2/y)	*Km* (m^2/y)	Tectonic subsidence curve	Sediment flux input (Table 3.4)	Flexural rigidity (Nm)	Aggrad. Lower (m)	Aggrad. Upper (m)	Total Aggrad. (m)	Prog. Lower (km)	Prog. Upper (km)	Total Prog. (km)	Height Lower (m)	Length Lower (km)	Angle Lower (degrees)	Height Upper (m)	Length Upper (km)	Angle Upper (degrees)
GFF	N.A.	N.A.	N.A.	N.A.	N.A.	291	738	1030	64	40	104	655	23	2	940	20	3
3.16A	50,000	100	Average Witiora-1 and Arawa-1 and Kanuka-1	Results from Petter et al. (2013)	1.50E+23	126	739	865	72	36	108	601	27	1	1437	29	3
3.16B	50,000	100	Average Witiora-1 and Arawa-1 to Kanuka-1	Results from Petter et al. (2013)	8.00E+22	-129	882	753	71	28	99	631	22	2	965	34	2
3.16C	50,000	100	Witiora-1, Arawa-1 and Kanuka-1	Results from Petter et al. (2013)	1.50E+23	12	836	848	24	36	60	823	53	1	1060	56	1
3.16D	50,000	100	Average Witiora-1 and Arawa-1, Arawa-1 and Kanuka-1	Results from Petter et al. (2013)	1.50E+23	72	890	962	68	24	92	820	16	3	1442	39	2
3.16E	50,000	300	Average Witiora-1 and Arawa-1, Arawa-1 and Kanuka-1	Results from Petter et al. (2013)	1.50E+23	4	738	742	75	33	108	743	37	1	1394	47	2
3.16F	50,000	100	Average Witiora-1 and Arawa-1, Arawa-1, Kanuka-1 and 1.5xKanuka-1	Results from Petter et al. (2013)	1.50E+23	-117	854	738	70	29	100	597	22	2	1270	29	3

Note: “Lower” refers to the lower section (early-late Pliocene), including seismic units SU1 to SU5 whereas “Upper” refers to the upper section (late Pliocene-recent), including seismic units SU6 to SU9.
N.A. = not applicable
Aggrad. = Aggradation; Prog. = Progradation

Table 3.7: Input parameters and geometrical measurement for clinoforms produced by set of models 3 (modeling of SP1 with the introduction of isostatic compensation)

Fourth set of models: dynamic models. Modeling conditions inside the graben.

Estimates of sediment flux inside the graben structure along seismic profile SP2 show a similar value to that calculated outside the graben during the earliest Pliocene time (~5.3–4.5 Ma; see SU1 values in Figure 3.17). These similarities are thought to be indicative of graben inactivity in this part of the basin. This observation agrees with previous interpretations that suggest the activation of the CEFZ faults started around 3.4 to 3.7 Ma (Giba et al., 2012). However, differences in sediment flux become increasingly larger inside the graben structure (SP2) during the late Pliocene (~4.5–2.8 Ma; Figure 3.17) when sediment influx increases in the zone of higher subsidence that is linked to the opening of the Northern Graben. Sediment flux decreased again during the deposition of seismic units SU4 and SU5 (~2.8 Ma; Figure 3.17). This decrease could be associated with a variety of causes, including shifting of sediment sources and feeding systems associated with the Northern Graben dynamics.

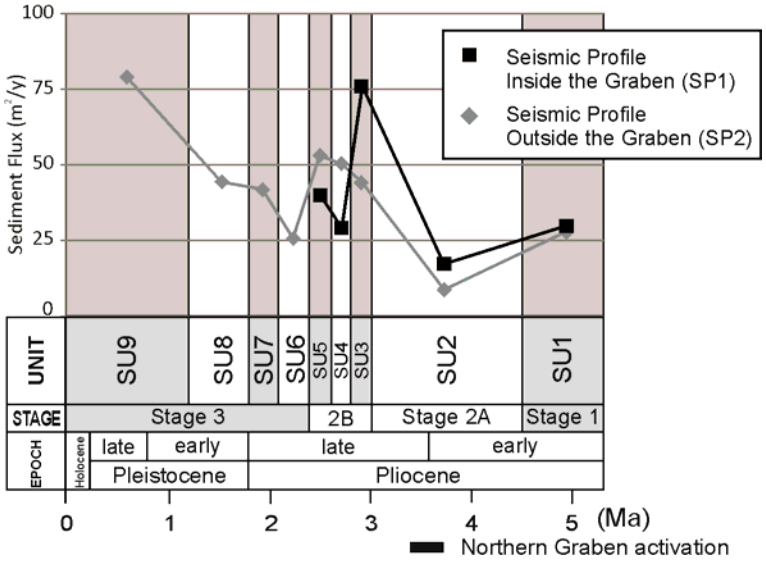

Figure 3.17: Graph illustrating sediment flux through time. Values calculated using geometrical measurements of clinoform outside (SP1) and inside (SP2) the Northern Graben. Lack of data coverage inside the graben region only allowed registering parameters for seismic units SU1 to SU5.

In the modeled sections, generation of accommodation in the proximal portions (southern end) of seismic profile SP2 was reproduced well by using the average subsidence curves of the Witiora-1 and Arawa-1 wells (Figure 3.18). Even though well Arawa-1 is located relatively close to the distal end (northern end) of seismic profile SP2 (Figure 3.2), subsidence of this well failed to reproduce clinoform morphologies inside the graben structure because the well is located in a different structural block (Figures 3.2 and 3.18A; Table 3.8). Because data from wells inside the graben structure were not available (Figure 3.2), gradual increments of subsidence were applied to the original subsidence curve of the Arawa-1 well to model conditions that could have generated the clinoform morphologies inside the graben region. Subsidence values that were 2.0 times larger than the reported values in well Arawa-1 generated clinoforms having shorter lengths and overall geometries that did not resemble the morphology of the GFF clinoforms inside the graben (Figure 3.18B; Table 3.8). However, the model successfully replicated these clinoform morphologies and associated shelf-edge trajectories when subsidence values were increased to 3.5 times the original values reported by well Arawa-1 (Figures 3.18C and 3.18D; Table 3.8). These subsidence values ranged between 150 and 400 m/m.y., which are comparable to the subsidence reported in a variety of synrift areas worldwide (Allen and Allen, 2005; Xie and Heller, 2009). However, the resulting clinoforms in the upper section had an average height of 2,250 m (Figure 3.18C), making them considerably larger than those measured on the seismic profile outside the graben. To reproduce clinoforms having similar foreset heights, subsidence values of the Kanuka-1 well were used in the distal portions of seismic profile SP2 (southern end). Resulting clinoforms had average heights of 1,500 m, but an unusual “saglike” geometry was generated in the base of the clinoform system (~top Miocene horizon; Figure 3.18D). Without any further information, both solutions are possible and

suggest that clinoforms in the upper section of SP2 are considerably larger than those observed in SP1. Finally, the abrupt increase in dip that shows the stratigraphic section in the middle portions of SP2 (Figure 3.5) and that does not correspond to the shelf edge was also modeled. To reproduce this geometry, a rapid increase in tectonic subsidence from an average of 150 to 200 m/m.y. was simulated close to that position.

Figure 3.18

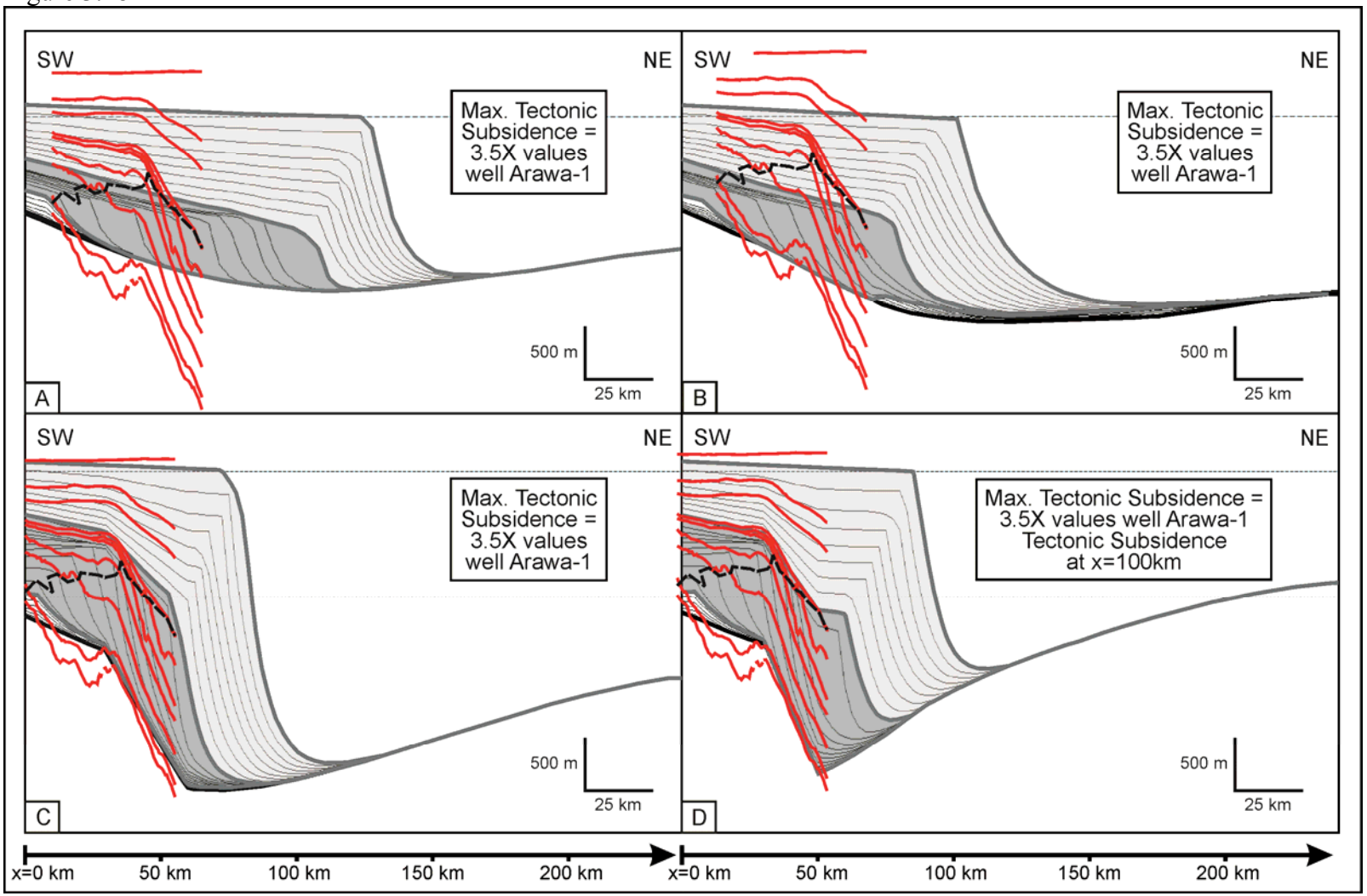
SW
NE
Max. Tectonic Subsidence = 3.5X values well Arawa-1
500 m
25 km
A
SW
NE
Max. Tectonic Subsidence = 3.5X values well Arawa-1
500 m
25 km
B
SW
NE
Max. Tectonic Subsidence = 3.5X values well Arawa-1
500 m
25 km
C
SW
NE
Max. Tectonic Subsidence = 3.5X values well Arawa-1 Tectonic Subsidence at x=100km
500 m
25 km
D
x=0 km
50 km
100 km
150 km
200 km
x=0 km
50 km
100 km
150 km
200 km

Figure 3.18: Results for set of models 4. The figures illustrate clinoform growth and progradation simulated inside the Northern Graben (SP2) using isostatic compensation. Tectonic subsidence of Arawa-1 failed to reproduce clinoform morphologies inside the graben because the well is located in a different structural block (A). Clinoforms modeled using values of tectonic subsidence 2.0 times larger than the reported values in Arawa-1 generated clinoforms having shorter lengths and overall geometries that did not resemble the morphology of the GFF clinoforms (B). Clinoforms modeled using values of tectonic subsidence 3.5 times the original values reported by Arawa-1 successfully replicated clinoform morphologies and shelf-edge trajectories of the GFF (C). Clinoforms modeled using values of tectonic subsidence of Kanuka-1 at the southern end of SP2 developed smaller heights and a “saglike” geometry (D).

Figure	*Knm (m2/y)*	*Km (m2/y)*	Tectonic subsidence curve	Sediment flux input (Table 3.4)	Flexural rigidity (Nm)	Agrad. Lower (m)	Agrad. Upper (m)	Total Agrad. (m)	Prog. Lower (km)	Prog. Upper (km)	Total Prog. (km)	Height Lower (m)	Length Lower (km)	Angle Lower (degrees)	Height Upper (m)	Length Upper (km)	Angle Upper (degrees)
GFF	N.A.	N.A.	N.A.	N.A.	N.A.	326	1026	1352	57	38	95	1683	33	4	No info.	No info.	No info.
3.18A	50,000	100	Average Witiora-1 and Arawa-1 at x=0 km, Arawa-1 at x=75 km and Kanuka-1 at x=100 km	Results from Petter et al. (2013) – SP2	1.50E+23	-312	1065	753	92	24	116	548	17	2	1460	27	3
3.18B	50,000	300	Average Witiora-1 and Arawa-1 at x=0 km, 2x Arawa-1 at x=75km	Results from Petter et al. (2013) - SP2	1.50E+23	-211	991	780	70	24	93	739	19	2	1721	49	2
3.18C	50,000	100	Average Witiora-1 and Arawa-1 at x=0 km, 3.5x Arawa-1 at x=75km	Results from Petter et al. (2013) - SP2	1.50E+23	541	522	1063	26	59	85	1665	19	5	1771	21	5
3.18D	50,000	100	Average Witiora-1 and Arawa-1 at x=0 km, 3.5x Arawa-1 at x=75 km, Kanuka-1 at x=100 km	Results from Petter et al. (2013) - SP2	1.50E+23	514	627	1142	25	54	80	1345	20	4	1810	18	6

Note: "Lower" refers to the lower section (early-late Pliocene), including seismic units SU1 to SU5 whereas "Upper" refers to the upper section (late Pliocene-recent), including seismic units SU6 to SU9.
N.A. = not applicable
Aggrad. = Aggradation; Prog. = Progradation

Table 3.8: Input parameters and geometrical measurement for clinoforms produced by set of models 4 (modeling of SP2)

By creating a series of crossplots I established some relationships between clinoform morphologies and geologic processes. For example, crossplots of progradation rate vs. sediment flux indicate that, in general, higher sediment flux translates to higher progradation rates both outside and inside the graben (SP1 and SP2 in Figures 3.19A and 3.19B). However, inside the graben region (SP2) an almost linear correlation exists between these two parameters, whereas data are more scattered outside the graben (SP1) (Figures 3.19A and 3.19B). Some outliers are observed in the upper section of the profile outside the graben (SP1) where a high sediment flux, due to isostatic compensation, translated into higher aggradation rates instead of higher progradation rates (Figure 3.19A). Crossplots of progradation rate vs. height inside the graben (SP2) (Figure 3.19D) generally show an inverse linear correlation (progradation rates decrease, whereas heights increase) because tectonic subsidence generated enough accommodation to increase clinoform heights but their progradation distance is decreased in order to conserve mass. SU3 is also an outlier point associated with a considerable increase in sediment flux (Figure 3.17, Table 3.4), which is reflected as an increase in progradation rates. In contrast, no relationship is apparent in the profile outside the graben (SP1) (Figure 3.19C). In the lower section, increases in progradation rates are associated with small increases in clinoform heights that may also result from a regional sediment flux increase (Figure 3.17). Nevertheless, increases in clinoform height outside of the graben were not as large as those inside the graben. Small increases in sediment flux could therefore keep steady or even increase progradation rates outside the graben; however, a very large increase in sediment flux, such as is seen during the deposition of SU3, would be required to do the same in SP2.

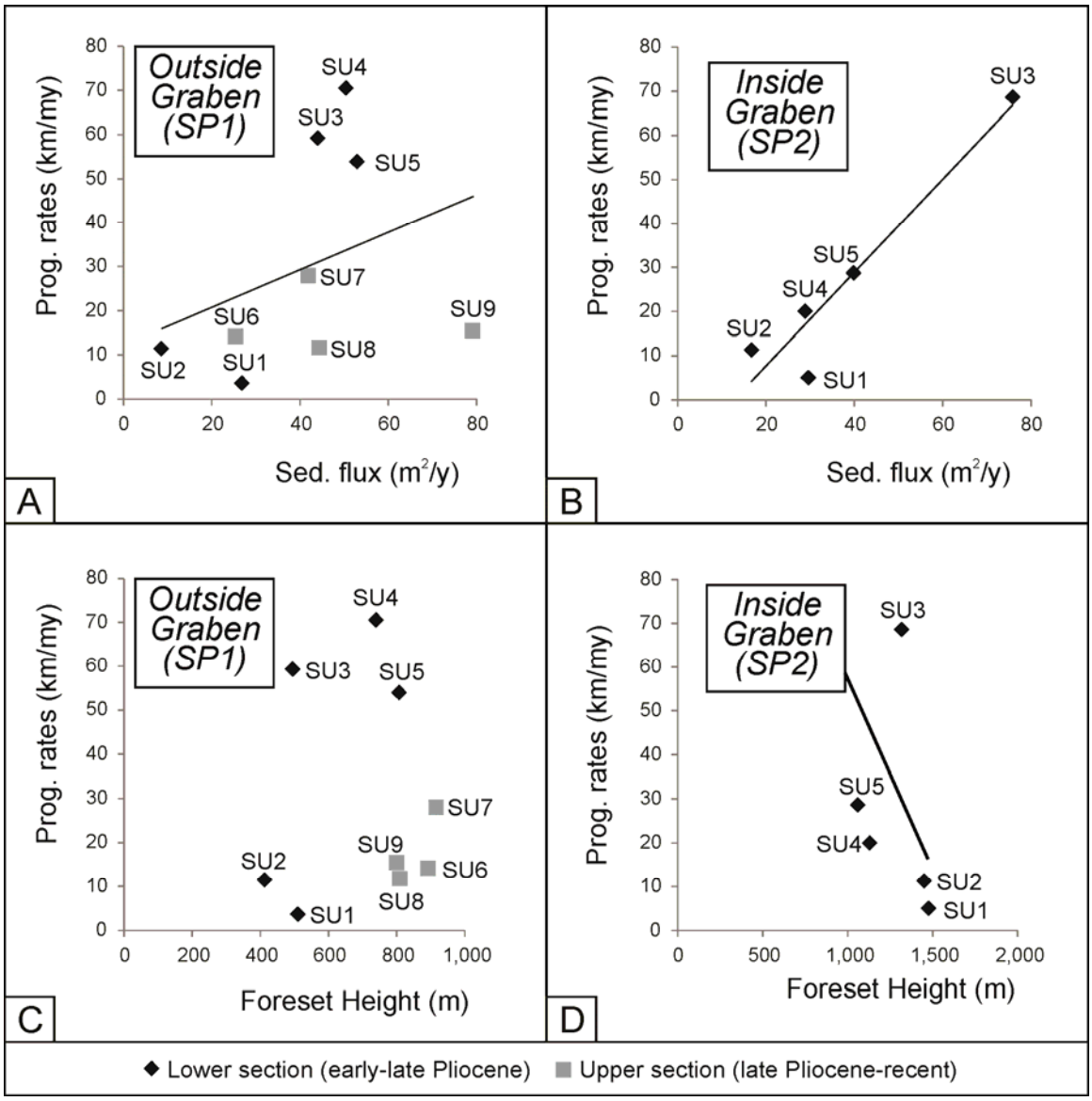

Figure 3.19: Crossplots of (A) progradation rate vs. sediment flux outside the graben; (B) progradation rate vs. sediment flux inside the graben; (C) progradation rate vs. foreset height outside the graben; and (D) progradation rate vs. foreset height inside the graben.

DISCUSSION: CONTROLS ON BASIN ARCHITECTURES AND CLINOFORM MORPHOLOGIES IN THE NORTHERN TARANAKI BASIN

The clinoforms of the GFF show morphological variations through time (lower vs. upper section) that suggest that transport conditions varied during progradation of the

clinoforms. One of the objectives was to use forward-modeling techniques to determine if eustatic sea-level fluctuations alone could reproduce the changes in clinoform morphologies within the Taranaki Basin, with little to no variations in sediment flux and tectonic subsidence. A unique solution for both the lower (early to late Pliocene) and the upper (late Pliocene to Recent) section was not found by modeling only sea-level fluctuations (Figure 3.14). Instead, results suggest that a considerable increase in sediment flux during deposition of the upper section was needed to reproduce the GFF geometries. Sediment flux estimates using the procedure described by Petter et al. (2013) also suggest that increases in sediment flux occurred from the early Pliocene to the present day (Figure 3.17).

Most of the studied stratigraphic interval developed during a general lowering of global sea level (Miller et al., 2005). This trend began during the Pliocene and was most likely influenced by ice sheet growth in the Southern and then Northern Hemisphere (Naish and Wilson, 2009). The lower section (early to late Pliocene) is characterized by geometries that might be associated with this sea-level drop because of the development of flat to descending shelf-edge trajectories, thin topset thicknesses, and low aggradation/progradation ratios, which are expected in this kind of scenario (Johannessen and Steel, 2005). On the basis of this scenario, I conclude that relative sea-level fall most likely acted as a major driver of clinoform and margin progradation across the Taranaki Basin during the early to late Pliocene. This influence is even more evident inside the graben (SP2), where high tectonic subsidence rates associated with the opening of the Northern Graben were made less significant by the interplay of sea-level fall and increased sediment supply, resulting in progradational stacking patterns and flat to falling shelf-edge trajectories. The effect of sea-level change on clinoforms is not as easily identified in the upper section. Although the effect of sea-level fall should manifest itself

in this interval, stacking patterns reflect an apparent increase in relative sea level with increasingly higher aggradation/progradation ratios, higher topset thicknesses, and ascending shelf-edge trajectories (Johannessen and Steel, 2005). Simulations demonstrate that the development of transgressive/progressive patterns in clinoforms was sensitive not only to sea-level fluctuations but also to changes in the magnitude of sediment flux and the rate of subsidence within the basin. Figure 3.14 illustrates how variations in sediment flux and subsidence can influence clinoform stacking patterns using the same global sea-level curve. The relevance of this finding is that the end configuration for each case scenario could be interpreted differently from a sequence stratigraphic perspective. For example, simulations using very small sediment flux inputs (e.g., 5 m^2/y; Figures 3.14A and 3.14B) generated geometries that reflect apparent transgressive conditions (movement of the shelf edge landward) and sea-level rise. To obtain progradational patterns, increases in sediment flux had to be applied to the model. In the case of the northern Taranaki Basin, architectures interpreted in the upper clinoform section were only reproduced successfully when sediment supply was increased considerably and isostatic compensation due to sediment loading was included as a mechanism to generate accommodation. These results suggest that sediment flux might have been a major control on clinoform architecture and the development of high-relief clinoforms during the late Pliocene to Pleistocene in the Taranaki Basin.

Sediment flux in the northern Taranaki Basin

Investigating the tectonic history of the region may clarify the increase in sediment flux that must have occurred in the Taranaki Basin for the models to be correct. An increased convergence rate between the Pacific and Australian plates and the migration of the associated subduction zone toward the southwest generated rapid uplift of the Southern Alps, creating a potential sediment source to the southwest (Tippett and

Kamp, 1995; Allis et al., 1998). After deposition of the Miocene section the main source of sediment shifted from the eastern North Island (Taranaki Fault and highs) to the southern South Island (Southern Alps; Tippett and Kamp, 1995). In addition to this change in source, an adjustment to sediment pathways and clinoform progradation toward the northeast was observed, most likely generated by the opening of the Northern Graben (Chapter 2). Thicknesses of different clinoforms were mapped in Chapter 2 to identify the source of the clastic influx since the Pliocene. That study suggested that most of the sediment was derived from the South Island, an area associated with uplift of the Southern Alps. A secondary sediment source may have been located along the eastern margin of the Taranaki Basin (North Island), but it was probably smaller and has little contribution owing to the presence of the Turi Fault highs (Nodder, 1995; King and Thrasher, 1996), reinforcing the idea that sediment was transported from the southwest to the northeast.

Subsidence in the northern Taranaki Basin

There is great variability from well to well in the subsidence curves observed in the study area. Variability such as this is expected in active rift zones and may be associated with different rates and timing of fault segment development, and the location of the wells in different fault blocks (Steckler et al., 1988). The southwest migration of the Pacific-Australian convergence zone and episodes of uplifting of both the Taranaki Peninsula and the Southern Alps may also have added to the effects of individual faults on subsidence. Figure 3.12 shows the results from the geohistory analysis of several wells in the northern Taranaki Basin performed by Bates and Heid (2007) and Cardona (2009). Subsidence curves in all the wells show generally consistent patterns; however, the changes in subsidence rates do not occur at the same time, and the amount of increase is highly variable (increasing basinward). Characteristics common to the Northern Graben

wells (except for the Witiora-1 well) include a period of high tectonic subsidence (7.5 to 5.5–5 Ma), an interval showing uplifting (5.5–5 to 3 Ma), and renewal of subsidence to the present day. Stern and Davey (1990) suggested similar stages for the Wanganui area, where rifting was followed by thermal contraction and then a signature of thrusting and loading. Well Witiora-1 shows completely different subsidence trends, its area having undergone uplifting from 7.5 to 6.5 Ma and showing relatively low subsidence rates thereafter.

The early phase of subsidence occurs during the latest Miocene to the earliest Pliocene (7.5 to 5.5–5 Ma), when tectonic subsidence rates were high. Subsidence values from the wells (120 to 300 m/m.y.) are too high to be considered the result of thermal subsidence. In fact, thermal subsidence values found by Baur et al. (2013) in the Caledonian and Deepwater Taranaki Basin are much smaller (~20 m/m.y.), as are other global values for the thermal cooling phase of many continental rifted basins (Xie and Heller, 2009). Because most contractional deformation in the basin (~90%) was located near the subduction thrust that is located east of the Taranaki Fault (Nicol et al., 2007; Baur, 2012), there is not an uplifting component affecting subsidence of this area at this time of the basin history. However, flexural subsidence related to the Australia-Pacific subduction zone and eastern uplifting (Taranaki Fault highs) may have played an important role in generating these high subsidence values.

During the second tectonic phase in the early to late Pliocene (5.5–5 to 3 Ma), tectonic subsidence rates are negative, implying uplifting that was linked to tectonic convergence affecting the region. This event could be linked to the uplifting of the Taranaki Peninsula and the Southern Alps as a result of the migration of the Pacific-Australian plate subduction zone toward the west (Stern et al., 1992; Holt and Stern, 1994; Stern and Holt, 1994; Allis et al., 1998; Bache et al., 2012; Baur et al., 2013). On

the basis of studies in mudstone porosities, Stern et al. (2006) estimated as much as 1,000 m of Pliocene uplift in the proximity of the study area (see their Figure 3.8). Although the CEFZ became active by 3.7 to 3.4 Ma (Giba et al., 2012), its effects are not easily distinguished in the tectonic subsidence curves, most likely because the wells are positioned outside the zone of maximum graben subsidence.

Tectonic subsidence rates increased abruptly (68 to 198 m/m.y.) during the deposition of the late Pliocene to Recent section (3 to 0 Ma; Figure 3.12). Increasing subsidence curves may indicate the migration of uplifting farther toward the southwest and a higher effect of both flexural (associated with the migrating subduction zone) and graben subsidence. During this stage, subsidence increased toward the north, with the highest tectonic subsidence observed in the northern well (Kanuka-1) and lowest values in the southern well (Witiora-1). Well Taimana-1 does not show renewed subsidence in the analyzed interval, but a relative uplifting that may be associated with its position in a graben footwall block.

Although there is no well information on Northern Graben subsidence, the modeling results indicate subsidence values between 150 and 400 m/m.y. This subsidence range is consistent with syn-rift predictions based upon lithosphere thinning by moderate factors of <2 (McKenzie, 1978) and worldwide compilations (Allen and Allen, 2005; Xie and Heller, 2009). In addition, the abrupt increase in the dip of the stratigraphic section that required an increase in tectonic subsidence to be modeled suggests that the Northern Graben formed in segments instead of during a single event and that the northern fault segments are younger than the southern segments, which agrees with previous observations (Giba et al., 2012).

Role of Northern Graben in GFF clinoform morphologies and sediment redistribution

Tectonic subsidence rates obtained inside the Northern Graben generated enough accommodation to develop higher relief clinoforms and smaller progradation rates (SU4–SU5) compared with time-equivalent clinoforms outside the graben. However, in the initial stages of evolution of the graben, higher progradation rates (when compared with SP1) are observed (SU2–SU3, Table 3.3). The increase in progradation rates can be explained by evoking an increase in sediment flux (Figure 3.17), which may be the result of initial reorientation of sediment pathways toward the recently formed structure, following the graben axis. This scenario suggests that the graben opened around 3 to 4 Ma. High rates of sediment supply, intensified by the increasingly higher relief of the Southern Alps (Tippett and Kamp, 1995), and funneling of sediments by the Northern Graben outpaced high tectonic subsidence rates, resulting in the increase in progradation rates and flat to falling shelf-edge trajectories observed on seismic lines. By the time of deposition of SU4, however, activation of northern CEFZ segments and deactivation of southern segments allowed for more accommodation that, at the same time, generated a decrease in progradation rates. The apparent decrease in sediment flux (Figure 3.17 and Table 3.4) by this time might suggest increased bypass associated with an active Northern Graben and potential deposition of deeper water fans.

CONCLUSIONS

Two-dimensional stratigraphic forward-modeling techniques, in conjunction with the analysis of clinoform geometries, can be important tools to identify the main controls on basin development and assess the relative importance of eustatic sea-level fluctuations, tectonics, and sediment flux on clinoform morphologies. The ability to

match models to seismically interpreted geometries allowed constraining the conditions needed for the development of the GFF high-relief clinoforms.

The methodology to calculate sediment flux as provided by Petter et al. (2013) proved effective in calculating sediment flux, generating clinoform morphologies similar to those found in seismic profiles. Values of sediment flux were constrained considerably using this procedure, obtaining a maximum value of 79 m^2/m.y.

GFF clinoforms show different geomorphological characteristics in the early to late Pliocene section (lower section) and the late Pliocene to Pleistocene section (upper section) that could not be successfully modeled using only eustatic sea-level variations but could be successfully modeled when time-variable sediment flux and time- and space-variable subsidence rates were introduced. Eustatic sea-level fluctuations and the opening of the graben structure most likely played the main roles controlling basin architectures during the early to late Pliocene. High sediment flux derived from the uplifting of the Southern Alps and associated sediment loading played a major role in basin architectures since the late Pliocene, making possible the development of high-relief clinoform packages.

Stratigraphic forward modeling allowed the estimation of realistic graben subsidence values, obtaining values around three to four times larger than in the profile outside the graben. Implications in terms of mechanisms associated with graben development were also found, such as that the Northern Graben evolved under conditions where individual fault segments dominated at different times.

These results demonstrate the power of stratigraphic forward-modeling techniques, especially where data are scarce. They can provide valuable information about the relative importance of basin controls (sea level, subsidence, sediment supply) and guide predictions of clinoform geometries and sediment partitioning.

CHAPTER 4: IMPLICATIONS OF ALONG STRIKE CHANGES IN CLINOFORM DEVELOPMENT AND LOCAL MORPHOLOGICAL VARIABILITY: A CASE STUDY FROM EASTERN OFFSHORE TRINIDAD

ABSTRACT

The geometries and stratigraphic relationships that characterize the last maximum glacial lowstand shelf margin succession in eastern Trinidad offer the opportunity for an expanded assessment of the complex interactions between external and local geological processes in controlling continental-margin depositional architectures, sediment partitioning, and sediment delivery to the basin. Two along-dip seismic transects were chosen from different structural domains of the eastern Trinidad margin and analyzed with respect to clinoform morphologies in order to examine the depositional history of the continental margin and how deposits change along strike. The Northern Structural Domain (NSD) is influenced by transpressional tectonics linked to the Caribbean Plate Boundary Zone (CPBZ). The Southern Structural Domain (SSD) is influenced by growth faulting and paleo-Orinoco dynamics. Temporal variations in clinoform morphologies are linked to the formation of an underlying paleo-canyon in the NSD and to changes in sediment supply from the Orinoco delta in the SSD. Along-strike variations (south to north) in clinoform morphologies include an increase in clinoform height and earlier development of shelf edge deltas associated with the paleocanyon in the NSD. Sediment distribution is also influenced by the presence of structural elements. In the NSD, the paleocanyon produced a narrower shelf that allowed sediment transport into deep water areas whereas in the SSD the location of growth faults on the shelf forced most sediment to be stored there. When compared with the Taranaki Basin of western New Zealand, another basin containing a variety of clinoform morphologies, the Trinidad margin

exhibits more pronounced lateral variations that highlight the role that deltaic systems play in the delivery of sediment.

INTRODUCTION

A clinoform is defined as a depositional shape, which in dip section is characterized by a gently sloping topset, a steeply sloping foreset, and a gently sloping bottomset (Rich, 1951; Pirmez et al., 1998) (Figure 4.1). Clinoforms are found in nature at different scales and include delta front clinoforms (tens of meters high) and continental margin clinoforms (hundreds of meters high) (Wolinzky and Pratson, 2007; Helland-Hansen and Hampson, 2009). The point where the topset and foreset intersect is called the rollover point and corresponds to the shelf edge in continental scale clinoforms. The intersection between the foreset and bottomset is known as the toe of the slope (Figure 4.1). When a delta has prograded as far as the shelf edge, the delta front typically coincides with the upper slope of the shelf margin (Johannessen and Steel, 2005). These systems are called shelf-edge deltas. Because clinoforms are the basic architectural form by which sediments are stored and eventually fed down depositional dip along the continental margin, several authors have used clinoform characteristics to infer paleoenvironmental and paleotransport conditions (O'Grady et al., 2000; Adams and Schlager, 2000; Kertznus and Kneller, 2009; Salazar et al., in review) as well as temporal and spatial fluctuations. Shelf-edge trajectories (the pathway taken by the shelf edge during the development of accreting clinoforms; Steel and Olsen, 2002) have also been used to predict sediment partitioning and sediment volumes in deep-water settings (Johannessen and Steel, 2005): flat to slightly downward trajectories suggest a stable to slightly falling relative sea level and optimal delivery of sediment across the shelf; rising shelf-edge trajectories reflect an overall rising relative sea level, and less or even no sand delivery into deepwater areas. The Taranaki Basin of New Zealand is well known for the

variety of clinoform architectures that characterize its Neogene margin (Hansen and Kamp, 2002). Clinoform classification techniques were used in Chapter 2 to identify three stages of clinoform development associated with the interplay between eustacy, tectonics and sediment supply. The continental margin of eastern Trinidad is also characterized by a variety of clinoform morphologies and dimensions. In this study, I use a method which includes seismic stratigraphic interpretations and a detailed clinoform morphological analysis to document and interpret the last maximum glacial low-stand shelf-margin succession along the eastern Trinidad margin. Herein, I deduce the relationships between clinoform development and the variables that influenced sediment movement in the shelf edge and slope region, including sea-level fluctuations, sediment input, and tectonics. I also evaluate the validity of this analysis in areas with characteristics dissimilar to those observed in the northern Taranaki Basin. These characteristics include different (1) regional tectonic settings, (2) sediment supply sources, (3) time intervals (3rd vs. 4th order stratigraphic intervals), and (4) degrees of clinoform geometry preservation.

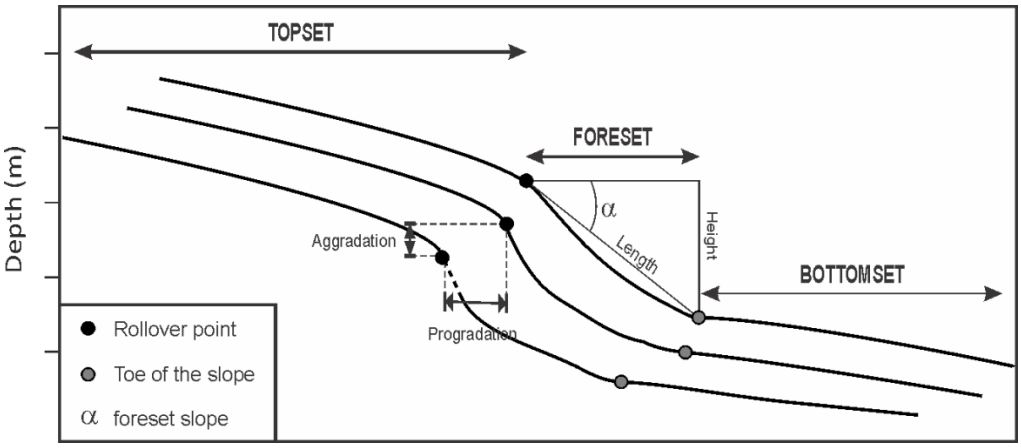

Figure 4.1: Graphic showing idealized clinoform morphologies and geometric parameters recorded for each seismic unit.

Geologic Settings

The study area is located in the southeastern region of the tectonically active Caribbean Plate Boundary Zone (CPBZ) in eastern offshore Trinidad (Figure 4.2A). It is characterized by different structural styles. Moscardelli et al. (2012) defined two different structural domains: the Northern Structural Domain (NSD) and the Southern Structural Domain (SSD) (Figure 4.2B). Transpressional tectonics associated with the CPBZ control the faulting style and the geometry of deposits along the NSD. The Darien Ridge, which limits the NSD towards the north (Figure 4.2B), is a northeast-southwest uplift composed of folded and thrusted Cretaceous and lower Tertiary carbonates and clastics deformed during the Miocene (Wood, 2000; Garciacaro et al., 2011). The presence of this ridge confined sediment transport to areas immediately southwest of the uplift, contributing to the formation of a Pliocene-Pleistocene incised paleocanyon (Figures 4.2B and 4.3) that funnelled sediments downslope during the last maximum glacial lowstand (Moscardelli et al., 2006). In the SSD, the main structural elements developed along the southern continental margin are a series of Pliocene-Pleistocene northwest-southeast regional and counterregional growth faults and their associated rollover anticlines (Figures 4.2B and 4.4). These structures are controlled by extensional and gravitational tectonics (Moscardelli et al., 2012). Similar to the NSD paleocanyon, these growth fault structures played an important role in constraining the position of the shelf edge through time because subsidence in the hanging wall generated accommodation (Sydow et al., 2003; Moscardelli et al., 2012). Along with accommodation enhanced by tectonics, high sediment supply, associated with the Orinoco delta system, allowed the filling of these depocenters and the deposition of thick, prograding megasequences in the margin (Wood, 2000).

Figure 4.2

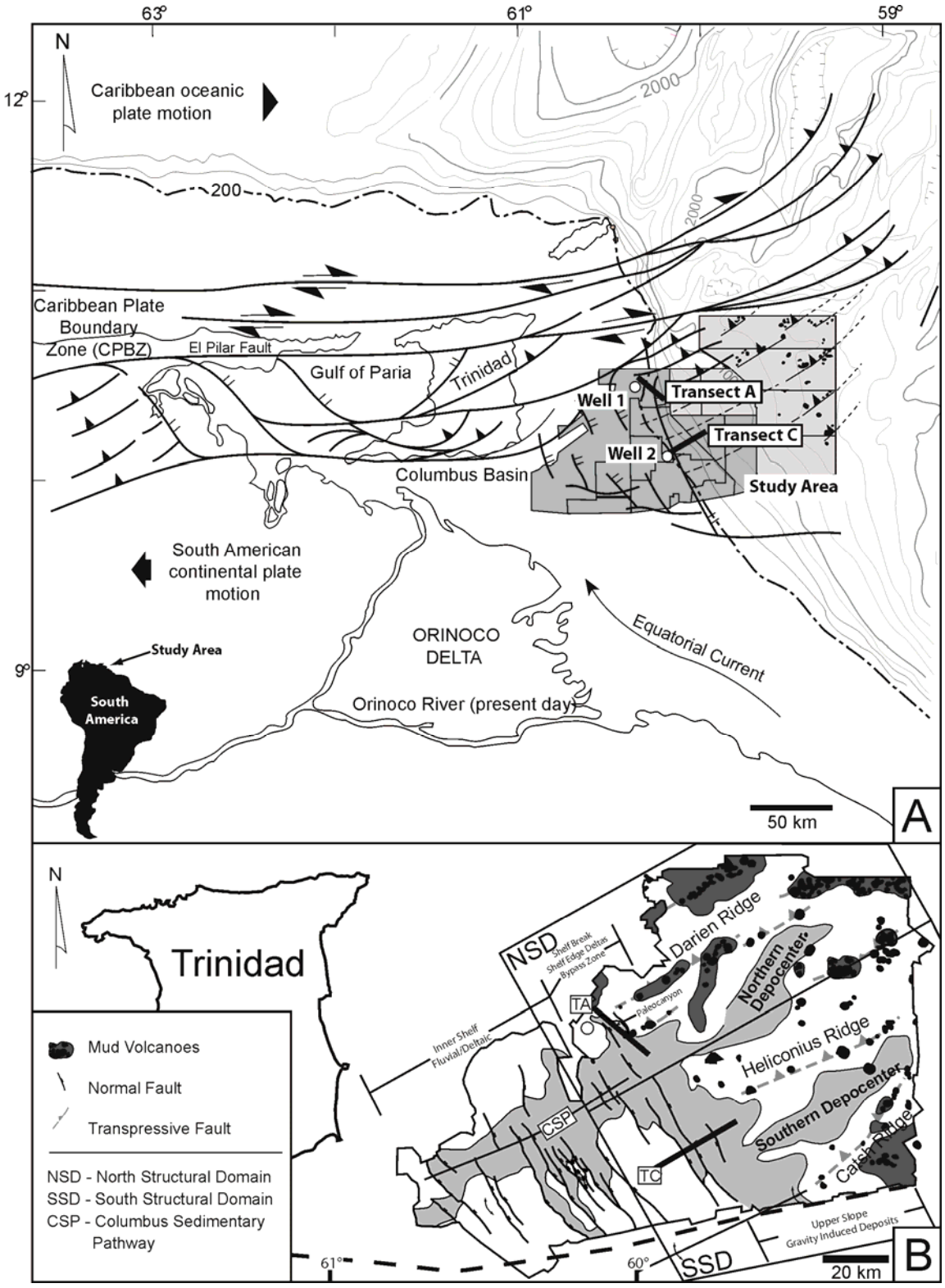
63°
61°
59°
N
12°
Caribbean oceanic plate motion
2000
200
Caribbean Plate Boundary Zone (CPBZ)
El Pilar Fault
Gulf of Paria
Trinidad
Well 1
Transect A
Transect C
Well 2
Columbus Basin
Study Area
South American continental plate motion
ORINOCO DELTA
Equatorial Current
Study Area
South America
9°
Orinoco River (present day)
50 km
A
N
Trinidad
Mud Volcanoes
Normal Fault
Transpressive Fault
NSD - North Structural Domain
SSD - South Structural Domain
CSP - Columbus Sedimentary Pathway
NSD
Shelf Break
Shelf Edge Deltas
Bypass Zone
Darien Ridge
Northern Depocenter
TA
Paleocanyon
Inner Shelf
Fluvial/Deltaic
Heliconius Ridge
CSP
Southern Depocenter
Caley Ridge
TC
Upper Slope
Gravity Induced Deposits
61°
60°
SSD
20 km
B

Figure 4.2: (A) Map showing the area of study located in northeastern South America along the Caribbean plate boundary zone (CPBZ). Contours represent bathymetry in meters. The area of three-dimensional (3-D) seismic data is outlined. The light-gray–shadowed area in the map highlights the deep-water blocks where gravity-induced deposits were studied and documented by Moscardelli et al. (2006) and Moscardelli and Wood (2008). The dark-gray–shadowed area highlights the 3-D seismic data that have been incorporated into this work and where fluvial and deltaic sequences were documented by Maher (2007) and Moscardelli et al. (2012). Transects A and C represent the location of two seismic transects used in this study located in the northern and southern structural domains, respectively. (B) Map highliting the main structural elements and the location of the North and South Structural Domains. Modified from Moscardelli et al. (2012).

Figure 4.3

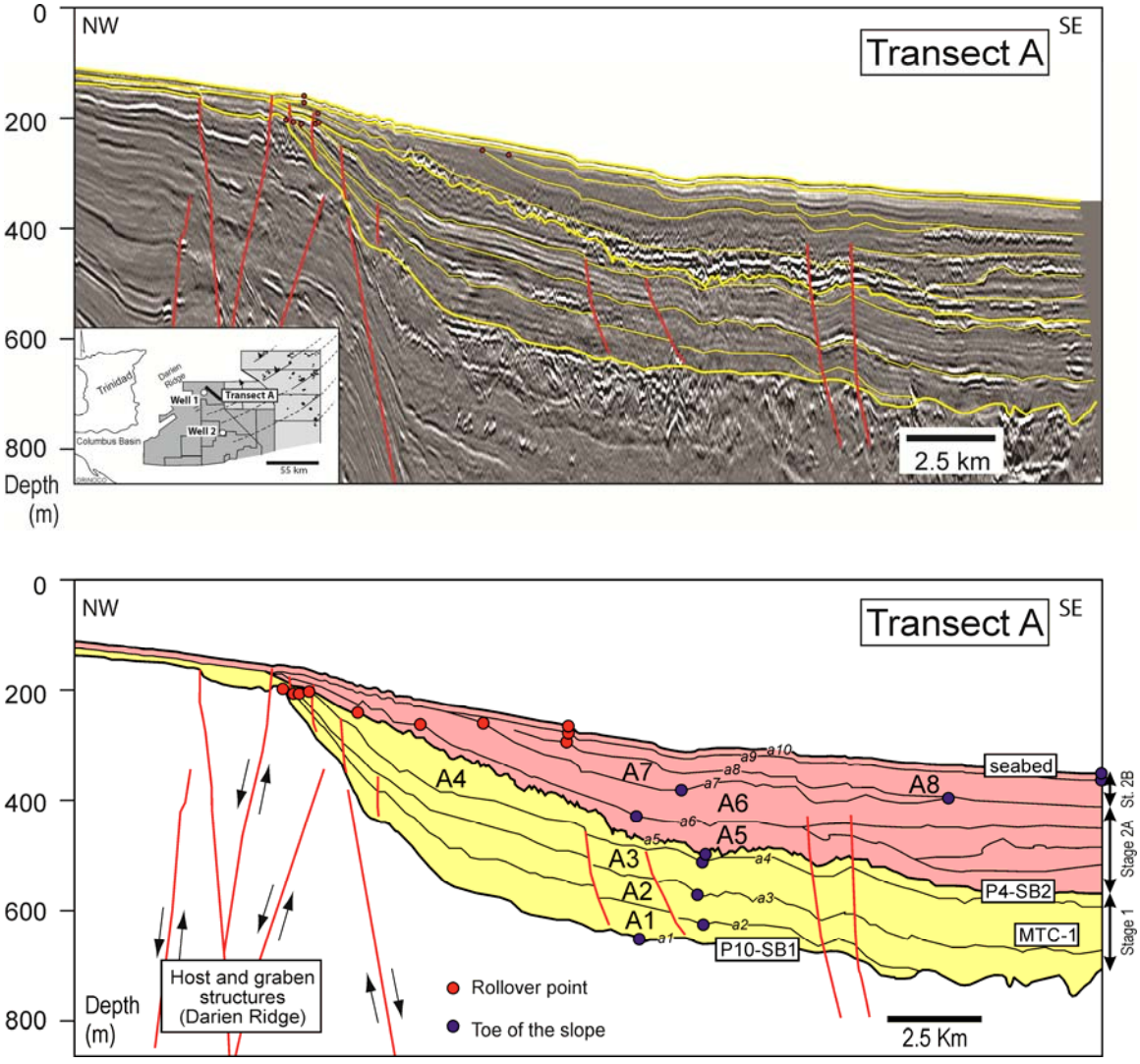

Figure 4.3: Seismic Transect A (TA) along the main axis of a paleocanyon located in the NSD (erosional shelf margin). (A) Three-dimensional seismic transect taken from the NSD of the eastern offshore Trinidad continental margin and (B) interpretation showing key surfaces (a1 to a10), clinoform packages (A1 to A9), stages of basin evolution (stages 1-2), and clinoform trajectories (see Figure 4.1 for location). LST = lowstand systems tract; TST = transgressive systems tract; MTC = mass-transport complex.

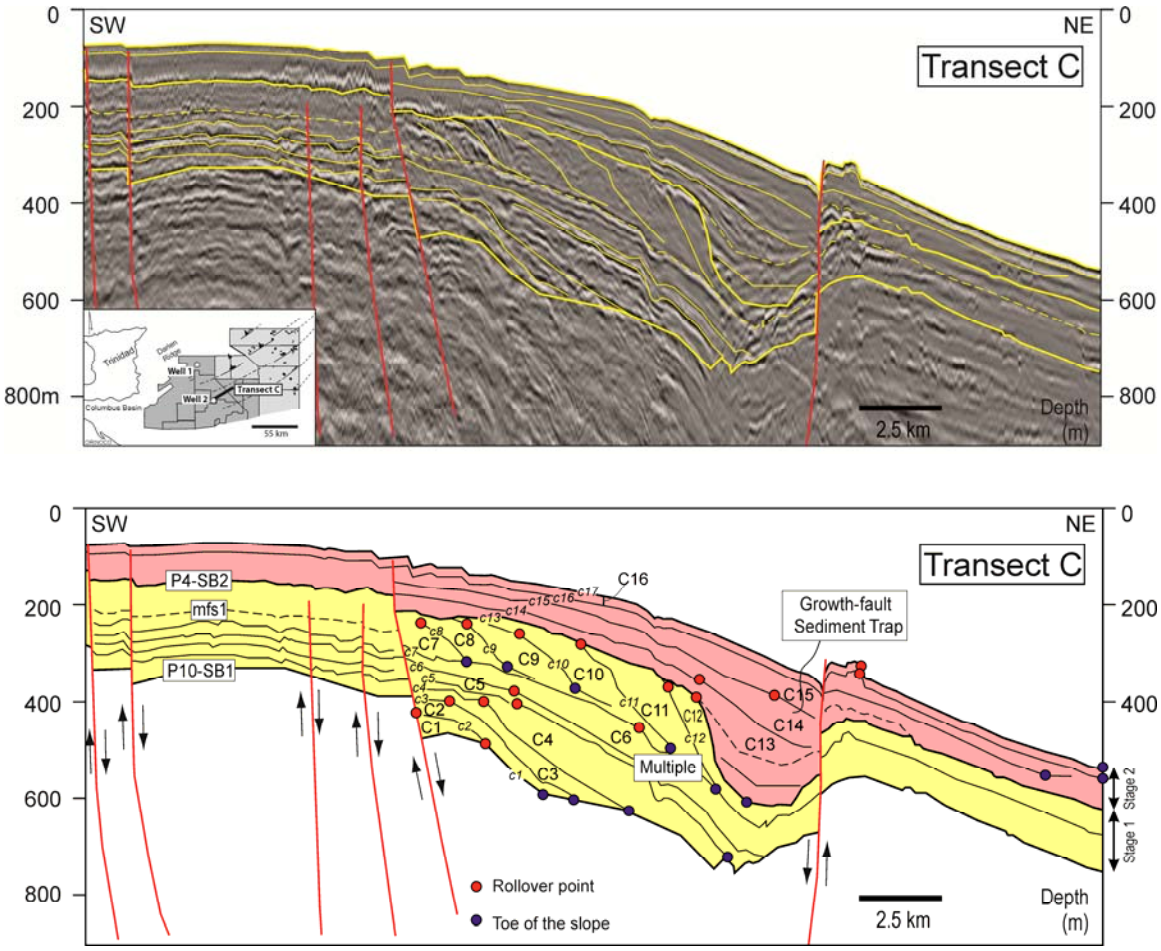

Figure 4.4: Seismic Transect C (TC), showing growth-fault sediment traps in the SSD. (A) Three-dimensional seismic transect taken from the NSD of the eastern offshore Trinidad continental margin and (B) interpretation showing key surfaces (c1 to c17), clinoform packages (C1 to C16), stages of basin evolution (stages 1-2), and clinoform trajectories (see index map for location). LST = lowstand systems tract; HST = highstand systems tract; TST = transgressive systems tract; mfs = maximum flooding surface.

DATASET AND METHODOLOGY

Seismic and Well Data

3D seismic reflection data was the primary dataset used for this study (Figure 4.2A). Six unique 3D seismic volumes were acquired and merged into a single continuous volume, covering a total area of 15,000 km^2. The average vertical resolution in the interval of interest (<120 ky) is approximately 10-15 m with imaging depths reaching a maximum of 5 seconds (s) TWTT. Two seismic transects previously interpreted by Moscardelli et al. (2012) were reconstructed and reinterpreted in this study. Transect A (TA) is a dip line that was recorded across the main axis of the paleocanyon located in the NSD (Figures 4.2 and 4.3). Transect C (TC) is a dip line located to the south of the outlet of the Columbus sedimentary pathway (Figure 4.2B), which captures active growth and counterregional faults that form sediment traps in the SSD (Figure 4.4). Several exploratory wells have been drilled through the interval of interest; however, geophysical logs and core were not available because the section is shallow and is not of commercial interest to the oil industry. Velocity information, in the form of check shots and sonic logs, was available for two key wells (wells 1 and 2, Figure 4.2A) close to each of the selected seismic transects, TA and TC. Approximate time-depth conversion within the interval of interest is 100 ms (TWTT) equivalent to 75 m. This analysis facilitated the depth-conversion of the seismic transects and allowed to describe the real geometrical relationships associated with the structural and stratigraphic configuration of the study area clinoform packages.

Definition of Seismic Units and Age Estimation

Clinoform packages were interpreted individually in each of the two seismic transects on the basis of seismic facies and individual clinoform characteristics. Ten key surfaces, including the seabed (clinoform a10), were identified and digitized in TA

(clinoforms a1 to a10, Figure 4.3). These surfaces define the top and the base of nine major seismic units (A1 to A9, Figure 4.3). For TC, seventeen key surfaces were identified and digitized (clinoforms c1 to c17, Figure 4.4), defining the top and base of sixteen major seismic units (C1 to C16).

The studied stratigraphic section is shallow (<800m) and lacks biostratigraphic markers. Age estimations for the youngest section are based on the occurrence of a regional erosional surface that has been identified by numerous authors as the last glacial maximum lowstand surface (P4-SB2 sequence boundary) with an assigned age of 18-20 ky (Moscardelli et al., 2006; Maher, 2007; Moscardelli et al., 2012). Clinoforms a5 and c13 correspond to this erosional surface in seismic transects TA and TC, respectively (Figures 4.3 and 4.4). Another sequence boundary (P10-SB1) corresponding to the base of a mass-transport complex has been mapped by several authors (Moscardelli et al., 2006; Maher, 2007; Moscardelli et al., 2012); however, no age for this surface has been put forth. Wood (2000) provided age control for a seismic transect within the study area with the youngest horizon (TD in Wood, 2000) dated at 500 ky. This horizon is considerably deeper in the stratigraphy than the interval used for this study, indicating that the section of interest is younger than 500 ky. Also, sequence stratigraphic interpretations of the area (Sydow, 2003; Moscardelli et al., 2012) suggest the presence of fourth order cycles (40-100 ky), indicating that the section between sequence boundaries P4-SB2 and P10-SB1 was deposited during a 40 to 100 ky time period with an approximate age between 60 and 120 ky for P10-SB1. 120 ky may be the best candidate for P10-SB1 because it corresponds to an important sea level fall seen in eustatic sea level curves (Miller et al., 2005) which may have generated a regional sequence boundary. Because the focus of this study is the analysis of clinoform morphologies and their relative temporal and spatial variations, an accurate estimation of age is preferred,

although not mandatory. Because of the data presented above, I chose to use 60 and 120 ky as boundary values to estimate the ranges of progradation, aggradation, and sediment flux rates within the section. It is, however, important to note that estimates of progradation, aggradation and sediment rates within the interval may contain a significant error due to erosion, specifically in the interval directly below P4-SB2.

Clinoform Classification

Clinoforms interpreted in TA and TC are classified according to their morphologies. Restoration of data to pre-faulted stages was necessary in TC in order to obtain accurate measurements. I define the rollover position (Figure 4.1) as the point that shows the first significant change in curvature along a depositional dip profile (Adams and Schlager, 2000; Kertznus and Kneller, 2009) and the foreset to bottomset transition as the point in a dip profile where a significant decrease in the foreset inclination occurs (O'Grady and Syvitski, 2002). Morphometric parameters, including foreset height, length and inclination (Figure 4.1) were measured for each clinoform (Table 4.1). Rollover trajectories, as well as aggradation and progradation distances, were documented through analysis of temporal changes in clinoform rollover points (Table 4.1 and Figures 4.3 and 4.4). Progradation and aggradation rates were calculated for each clinoform package, using the estimated age for the individual package. Clinoforms were classified on the basis of their morphologies using the methodologies developed by O'Grady et al. (2000) and Adams and Schlager (2000). The method of Adams and Schlager (2000) was also used to estimate potential variations in lithology within the study area.

Seismic Transect	Stage		Age for shorter period (years)	Age for longer period (years)	Clinoform	Height (m)	Length (km)	Inclination (°)	Seismic Unit	Progradation for shorter period (km/my)	Aggradation for shorter period (m/my)	Progradation for longer period (km/my)	Aggradation for longer period (m/my)
A	1		70000	120000	a1	454	9.5	2.7	A1	23	-716	11	-358
			57500	95000	a2	419	10.9	2.2	A1	23	-716	11	-358
			45000	70000	a3	364	10.6	2.0	A2	12	55	6	28
			32500	45000	a4	309	10.5	1.7	A3	21	363	11	182
			20000	20000	a5	256	9.3	1.6	A4	104	-3050	52	-1525
	2	A	17000	17000	a6	167	5.8	1.7	A5	556	-7158	556	-7158
			9000	9000	a7	121	5.3	1.3	A6	210	292	210	292
		B	6000	6000	a8	102	10.2	0.6	A7	741	-11287	741	-11287
			3000	3000	a9	85	14.2	0.3	A8	16	5368	16	5368
			0	0	a10	85	14.2	0.3	A9	5	4405	5	4405
C	1	A	70000	120000	c1	105	1.8	3.3	C1				
			65833	111667	c2	168	3.9	2.5	C1	-505	15361	-253	7681
			61667	103333	c3	205	3.8	3.1	C2	244	5715	122	2858
			57500	95000	c4	227	4.4	2.9	C3	249	-264	125	-132
			53333	86667	c5	318	6.4	2.8	C4	244	-1090	122	-545
			49167	78333	c6	332	6.8	2.8	C5	-21	6310	-10	3155
			45000	70000	c7	208	3.7	3.3	C6	904	-17938	452	-8969
		B	40833	61667	c8	80	1.4	3.3	C7	-1585	51634	-793	25817
			36667	53333	c9	88	1.2	4.1	C8	336	-496	168	-248
			32500	45000	c10	112	1.7	3.8	C9	384	-4889	192	-2445
			28333	36667	c11	214	2.7	4.5	C10	448	-5187	224	-2593
			24167	28333	c12	215	1.5	8.2	C11	637	-21142	318	-10571
			20000	20000	c13	217	1.5	8.1	C12	205	-5054	103	-2527
	2		10500	10500	c14	139	3.4	2.3	C13	10	3854	10	3854
			7000	7000	c15	251	8.3	1.7	C14	652	-9360	652	-9360
			3500	3500	c16	277	8.9	1.8	C15	321	5820	321	5820
			0	0	c17	257	8.6	1.7	C16	80	905	80	905

Table 4.1: Summary of geometrical measurements for clinoforms interpreted in seismic transects TA and TC. Values measured using the procedure described in Figure 4.1. Progradational and aggradational rates were calculated using estimated ages for the area. Two cases of shorter and longer periods are provided before 20ky.

Estimations of Sediment Flux

Sediment flux for individual seismic packages was estimated using the method of Petter et al. (2013). First, progradation and aggradation rates were calculated for each seismic unit. Secondly, the distal clinothem pinchout positions were calculated as defined by Petter et al. (2013; Figure 3.6) —this procedure involved plotting both the clinothem thickness and the elevation against basinward position (Figures 3.7, 4.5, 4.6, 4.7 and 4.8). To obtain thickness graphs valid to calculate sediment flux it was necessary to group some of the clinoforms into thicker packages. Average values were calculated and assigned to each clinoform in the group. In the case of TA, units A1-A2, A3-A4 and A7-A9 were grouped together and the parameters for the fitting equations were used for each unit in the same group (Figure 4.5; Table 4.2). Only the data points associated with the first order geometry of the margin profile were considered for the calculations. High values of thickness in the basinward direction (Figure 4.5b-e) indicate the presence of mass transport complex deposits associated with seismic units A3 to A9. In the case of TC, only units C5-C6 and C15-C16 were grouped together to obtain valid thickness graphs, and the same method was applied (Figure 4.6; Table 4.2). Finally, sediment flux was calculated using the relationship established by Petter et al. (2013; Figure 3.7). Table 4.3 shows all data with sediment flux estimates associated with each seismic unit in TA and TC. Because sediment flux calculations have a potential error associated with the uncertainty in age estimations (e.g. the interval between P10-SB1 and P4-SB2), I chose to assess relative temporal and spatial changes in this parameter, rather than report absolute values.

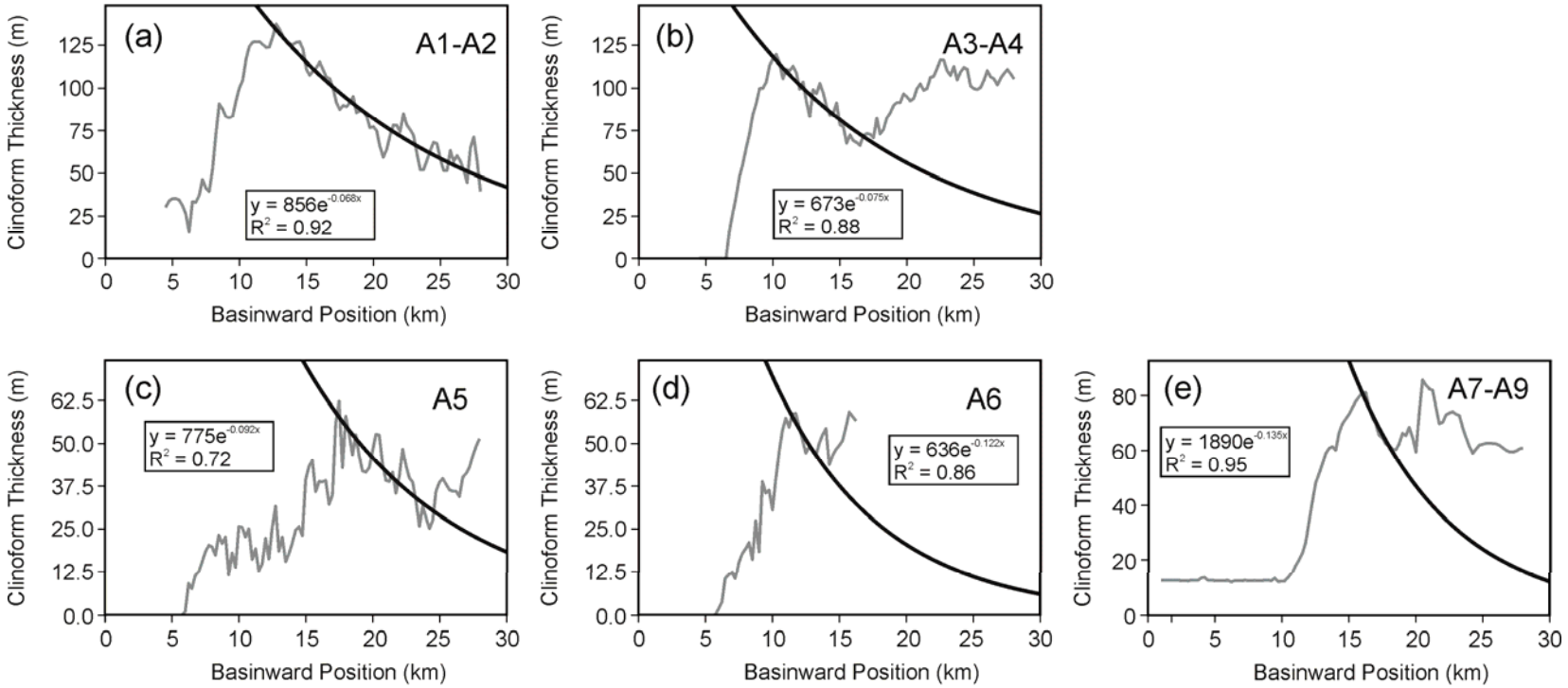

Figure 4.5: Clinothem thickness vs basinward position in TA.

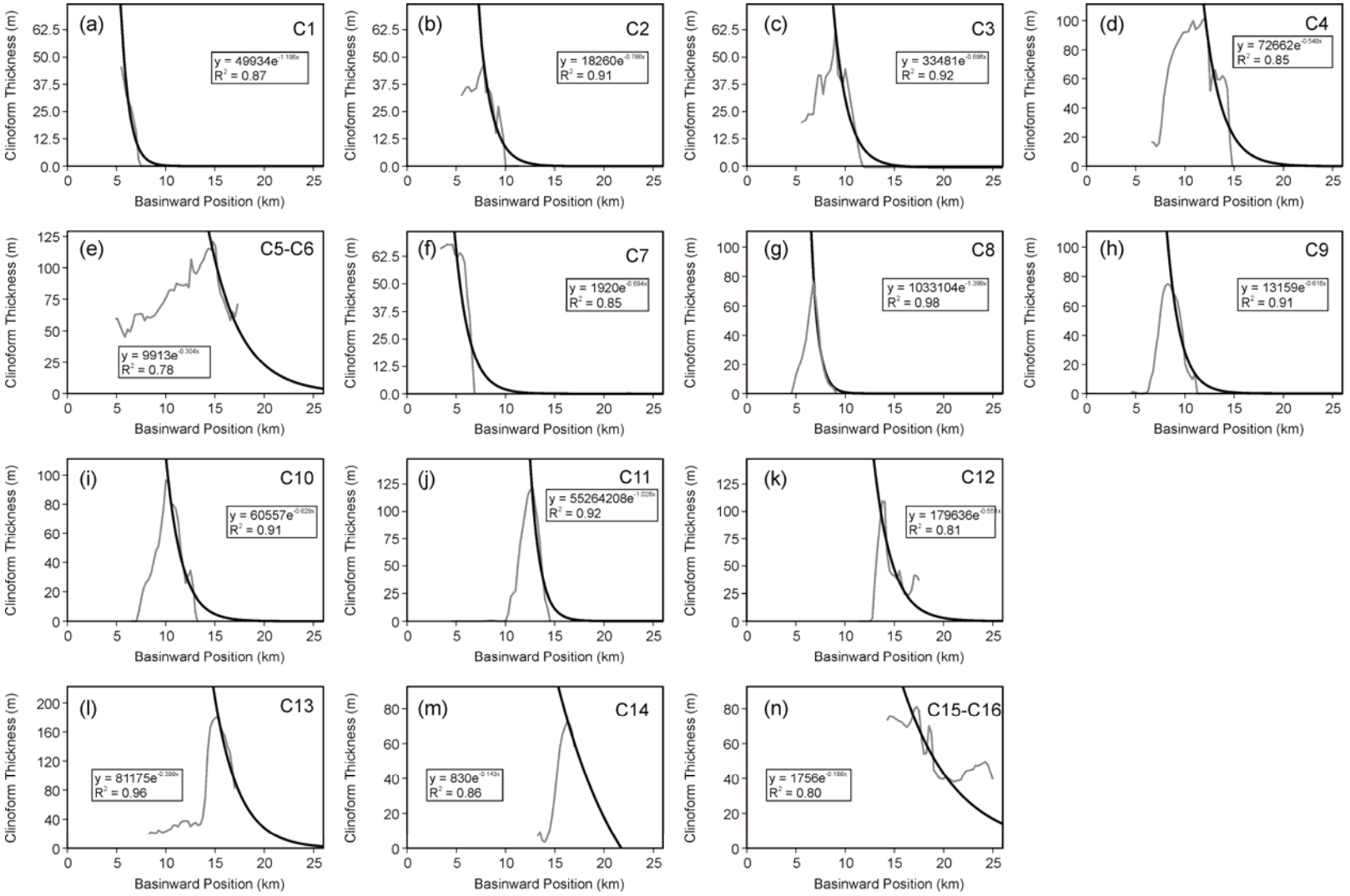

Figure 4.6: Clinothem thickness vs basinward position in TC.

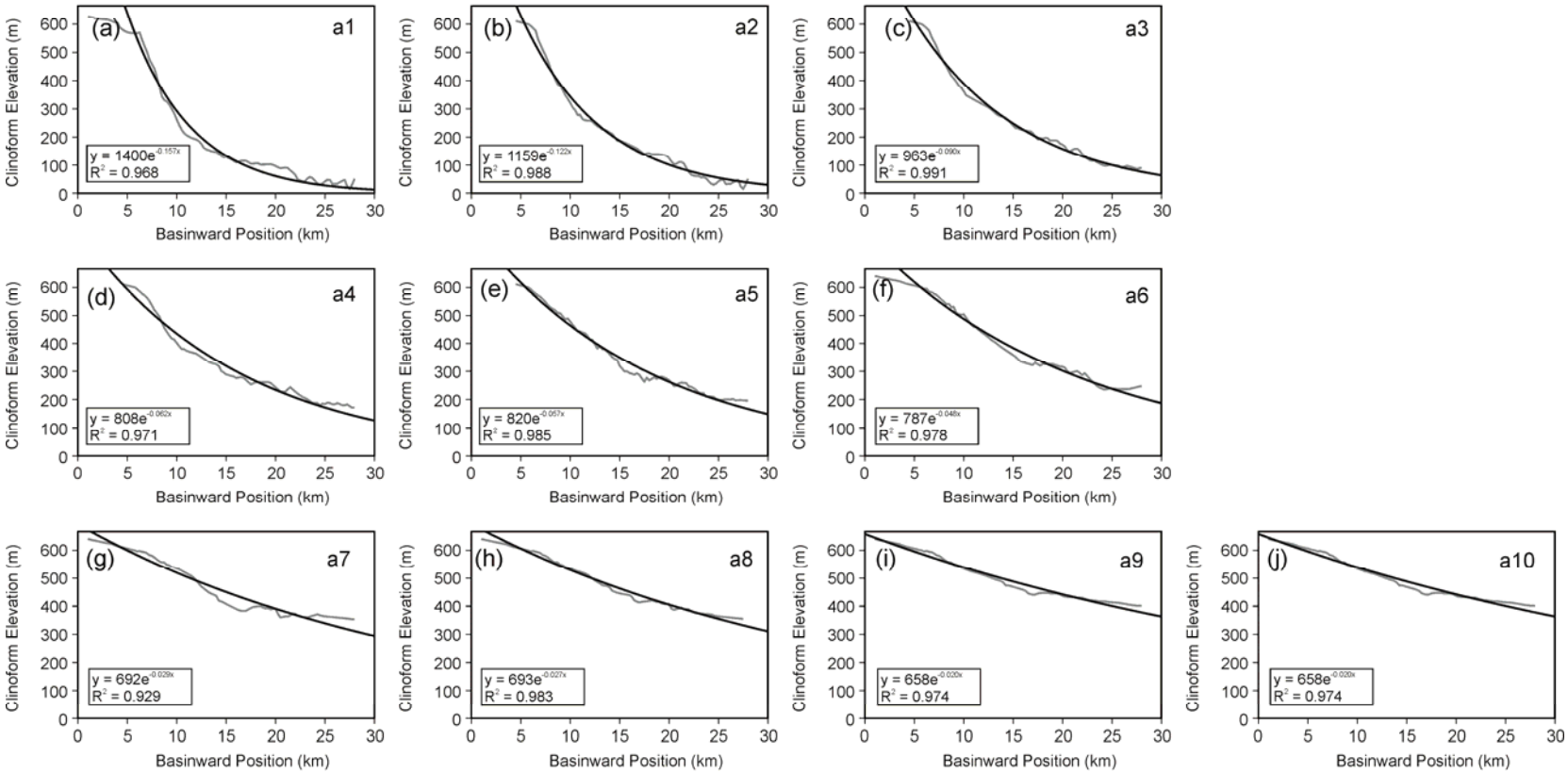

Figure 4.7: Clinoform elevation vs. basinward position in TA. Fitting equation parameters were used to calculate sediment flux according to Petter et al. (2013) procedure.

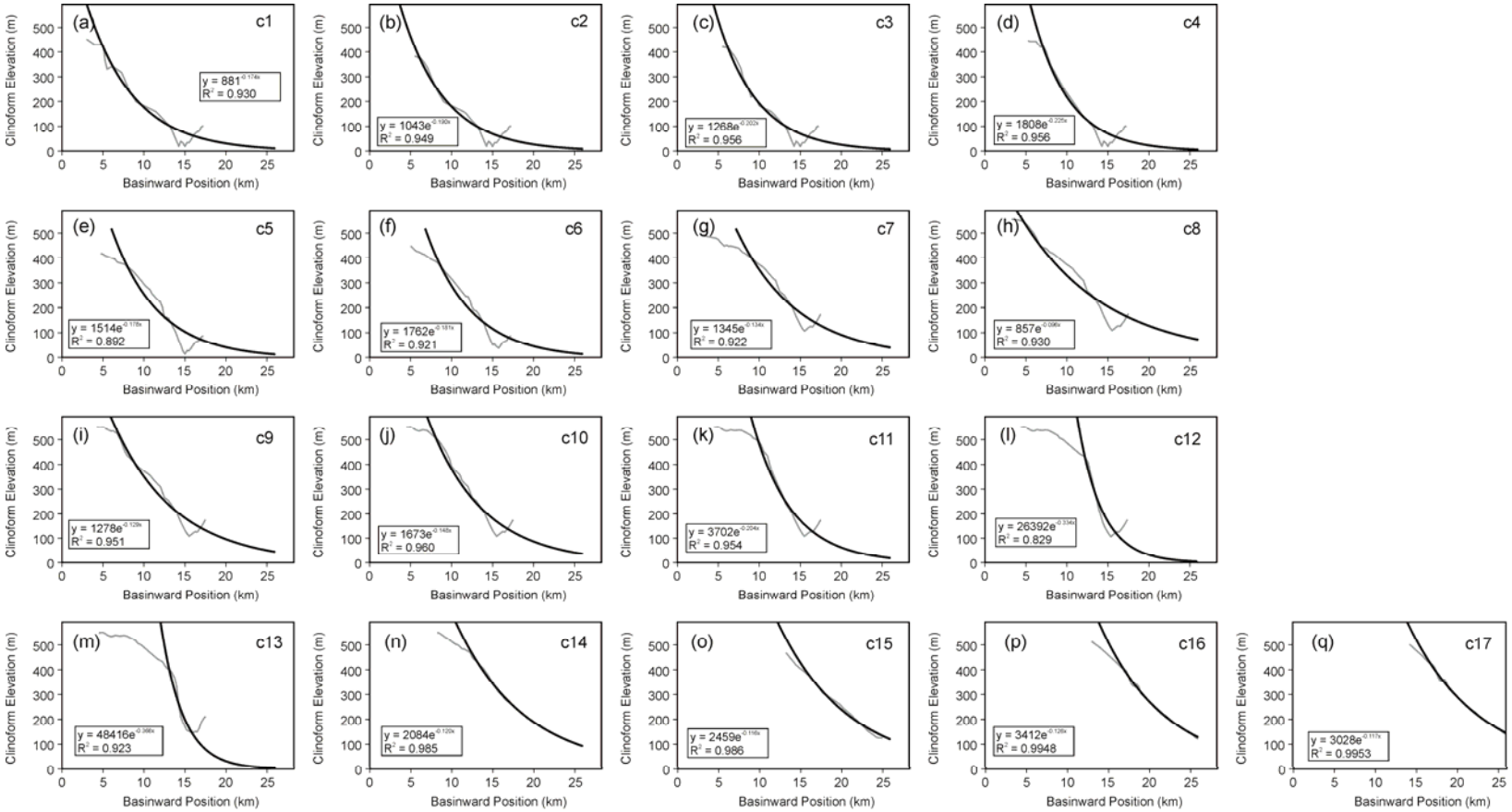

Figure 4.8: Clinoform elevation vs. basinward position in TC. Fitting equation parameters were used to calculate sediment flux according to Petter et al. (2013) procedure.

Seismic Transect	Seismic Unit	a	b	R^2
A	A1-A2	856	-0.068	0.920
	A3-A4	673	-0.075	0.882
	A5	775	-0.092	0.721
	A6	636	-0.122	0.860
	A7-A9	1890	-0.135	0.952
C	C1	134900	-1.198	0.868
	C2	49330	-0.766	0.911
	C3	90450	-0.698	0.915
	C4	196300	-0.549	0.851
	C5-C6	26780	-0.304	0.783
	C7	5186	-0.694	0.854
	C8	2791000	-1.399	0.978
	C9	35550	-0.618	0.909
	C9	118900	-0.735	0.876
	C10	163600	-0.629	0.905
	C11	149300000	-1.028	0.918
	C12	485300	-0.551	0.811
	C13	219300	-0.399	0.962
	C14	2242	-0.143	0.858
	C15-C16	4744	-0.186	0.804

Table 4.2: Fitting parameters for thickness of seismic units in seismic transects TA and TC. Notice that seismic units A1-A2, A3-A4, A7-A9, C5-C6 and C15-C16 were grouped together because individual curves did not show typical thickness trends. The values obtained for each individual unit is the average of the group.

Seismic Transect	Stage		Seismic Unit	Shorter Period		Longer Period		Thickness			Clino-form	Shorter Age (years)	Longer Age (years)	XSE (km)	hSE (m)	Elevation			Xd (km)	hd (m)	XadjSE (km)	hadjSE (m)	Shorter q(XadjSE) (m2/y)	Longer q(XadjSE) (m2/y)
				P (km/my)	A (m/my)	P (km/my)	A (m/my)	a	b	R^2						a	b	R^2						
A	1		A1	23	0	11	0	330	-0.070	0.937	a2	63750	107500	6.67	557	1159	-0.122	0.988	23	56	17	501	9	5
			A2	12	55	6	28	330	-0.070	0.937	a3	51250	82500	6.82	557	963	-0.090	0.991	60	4	53	553	8	4
			A3	21	363	11	182	265	-0.079	0.880	a4	38750	57500	7.09	561	808	-0.062	0.971	50	36	43	524	21	11
			A4	104	0	52	0	265	-0.079	0.880	a5	26250	32500	8.39	523	820	-0.057	0.985	50	47	42	476	40	20
	2	A	A5	556	0	556	0	287	-0.092	0.722	a6	18500	18500	10.05	502	787	-0.048	0.978	44	95	34	407	181	181
			A6	210	292	210	292	235	-0.122	0.860	a7	13000	13000	11.73	504	692	-0.029	0.929	32	281	20	223	42	42
		B	A7	741	0	741	0	688	-0.134	0.926	a8	7500	7500	13.95	470	693	-0.027	0.983	24	371	10	99	59	59
			A8	16	5368	16	5368	688	-0.134	0.926	a9	4500	4500	14.00	487	658	-0.020	0.974	37	317	23	169	100	100
			A9	5	4405	5	4405	688	-0.134	0.926	a10	1500	1500	14.01	500	658	-0.020	0.974	37	317	23	182	81	81
C	1	A	C1	0	15361	0	7681	49934	-1.198	0.868	c2	67917	115833	5.26	338	1043	-0.190	0.949	7	277	2	61	25	12
			C2	244	5715	122	2858	18260	-0.766	0.911	c3	63750	107500	6.27	362	1268	-0.202	0.956	10	161	4	201	56	28
			C3	249	0	125	0	33481	-0.698	0.915	c4	59583	99167	7.31	361	1808	-0.225	0.956	12	131	4	230	46	23
			C4	244	0	122	0	72662	-0.549	0.851	c5	55417	90833	8.33	356	1514	-0.178	0.892	15	33	6	323	63	31
			C5	0	6310	0	3155	9913	-0.304	0.783	c6	51250	82500	8.24	382	1762	-0.181	0.921	16	40	7	343	38	19
			C6	904	0	452	0	9913	-0.304	0.783	c7	47083	74167	12.05	307	1345	-0.134	0.922	25	48	13	259	187	94
		B	C7	0	51634	0	25817	1920	-0.694	0.854	c8	42917	65833	5.40	523	857	-0.096	0.930	9	378	3	145	131	66
			C8	336	0	168	0	1033104	-1.399	0.978	c9	38750	57500	6.80	521	1278	-0.129	0.951	9	412	2	109	29	15
			C9	384	0	192	0	13159	-0.618	0.909	c10	34583	49167	8.40	500	1673	-0.148	0.960	13	254	4	246	76	38
			C10	448	0	224	0	60557	-0.629	0.905	c11	30417	40833	10.27	479	3702	-0.2044	0.954	15	175	5	304	109	54
			C11	637	0	318	0	55264208	-1.028	0.918	c12	26250	32500	12.92	391	26392	-0.3341	0.829	16	136	3	255	130	65
			C12	205	0	103	0	179636	-0.551	0.811	c13	22083	24167	13.78	370	48416	-0.3664	0.923	19	45	5	324	53	27
	2		C13	10	3854	10	3854	81175	-0.399	0.962	c14	15250	15250	13.87	406	2084	-0.1199	0.985	24	113	10	294	35	35
			C14	652	0	652	0	830	-0.143	0.858	c15	8750	8750	16.16	374	2459	-0.1164	0.986	36	38	20	335	175	175
			C15	321	5820	321	5820	1756	-0.186	0.804	c16	5250	5250	17.28	393	3412	-0.1263	0.995	32	63	14	330	151	151
			C16	80	905	80	905	1756	-0.186	0.804	c17	1750	1750	17.56	397	3028	-0.1168	0.995	32	76	14	321	31	31

P = Progradation rate; A = Aggradation rate; XSE = Shelf Edge distance; hSE = Shelf Edge elevation; Xd = Distal pinchout distance hd = Distal pinchout elevation; XadjSE = Xd - XSE; hadjSE = hSE - hd.

Table 4.3: Sediment Flux estimated for seismic units in transects TA and TC.

RESULTS

Clinoform Morphometrics

Transect TA

Seismic transect A is located across the Darien Ridge (Figures 4.2B and 4.3) and contains the major structural elements within the NSD, including regional and counterregional growth faults, high-angle thrusts arranged in a flowerlike structure (core of the structural high associated with the Darien Ridge; Garciacaro et al., 2011; Moscardelli et al., 2012), and a series of high angle normal faults associated with mud-volcano ridges in the southeastern portion (slope region) of TA (Sullivan et al., 2004; Moscardelli and Wood, 2008; Figure 4.2B). Sequence boundary P10-SB1 (clinoform a1) represents the base of the paleocanyon. A visual examination of TA reveals an important change in height, length and inclination around clinoform a5 that allow to classify TA into two sections: a lower section bounded by clinoforms a1 to a5 (seismic units A1 to A4; Figure 4.3), and an upper section bounded by clinoforms a5 to a10 (seismic units A5 to A9; Figure 4.3). Both sections are characterized by high-amplitude, continuous reflectors (Figure 4.3); however, the upper section exhibits more gently dipping clinoforms (average of 2.0° in Table 4.1) than the lower section (average of 0.8° in Table 4.1; Figure 4.3). This seismic character was defined by Moscardelli et al. (2012) as *Sigmoid Clinoform Package* seismic facies, whose geometries are commonly associated with the development of shelf-edge deltas. In both the lower and upper sections, the toe of the slope is difficult to identify, but the rollover point, which corresponds to the shelf edge, is relatively easy to identify because of the abrupt transition between topsets and foresets. Moscardelli et al. (2006; 2012) suggest that these abrupt transitions are associated with a series of slumps and slides that indicate the rollover point of clinoform

packages at the paleocanyon head, and signify sediment bypass toward deep-water depocenters. As sediments were transported downslope, the system evolved into a regional mass transport complex (MTC-1 in Figure 4.3; Moscardelli et al., 2006; 2012).

In figure 4.9, geometrical parameters in TA, including clinoform height, length, inclination, progradation and aggradation rates, and sediment flux are plotted. TA exhibits a progressive decrease in height from the oldest (a1) to the youngest (a10) clinoform (Figure 4.9a). Length trends from clinoforms a1 to a5 (Figure 4.9b) are similar to height trends, indicating that clinoform height decreases are accompanied by slight decreases of length and that clinoforms are becoming smaller. Clinoforms reflecting the youngest part of the section (clinoforms a8-a10) show the highest length values although their heights are the smallest. Foreset declivities (Figure 4.1) in TA show a slight decrease from clinoform a1 to a7 (Figure 4.9c). A larger decrease is observed during deposition of clinoform a8.

Figure 4.9

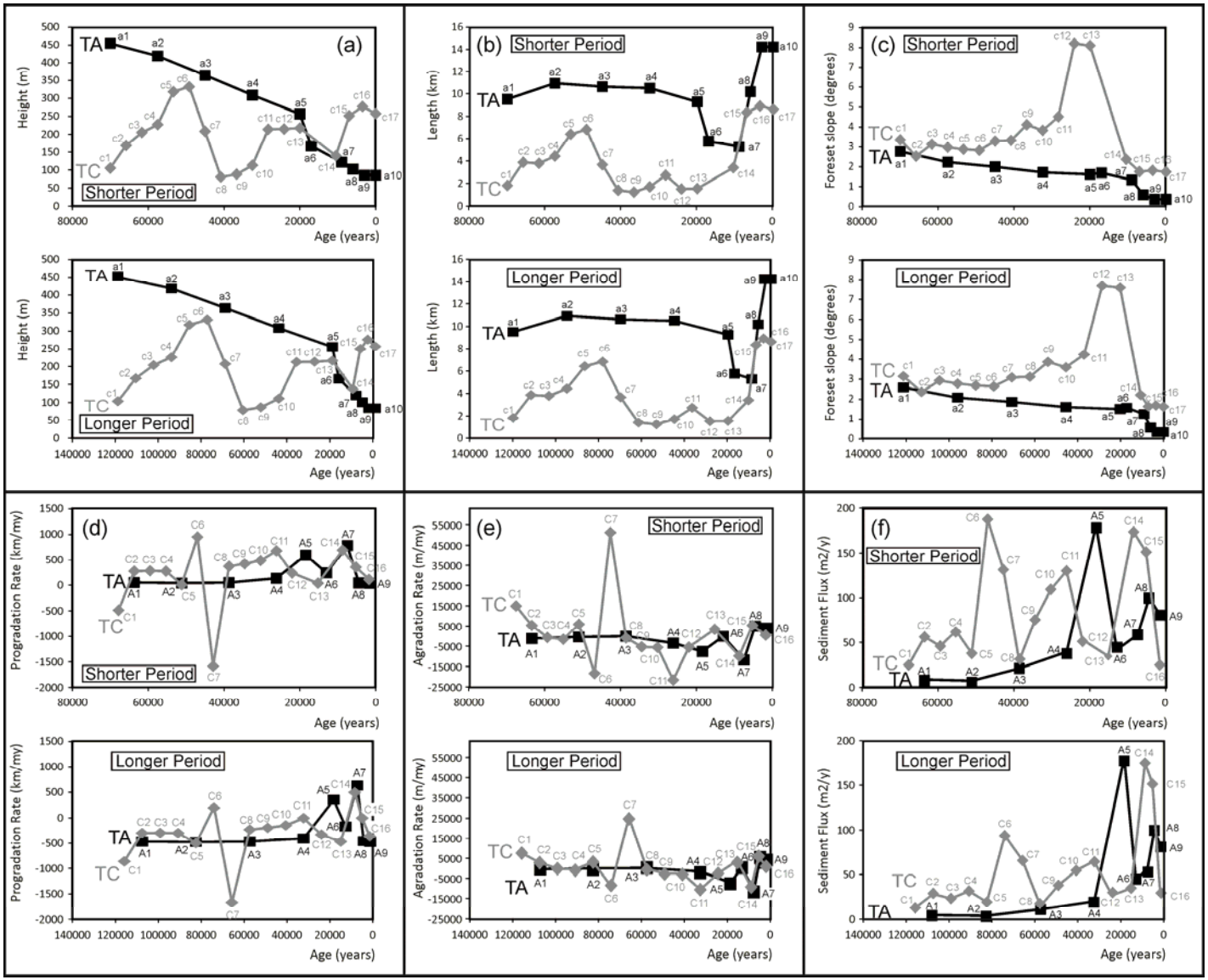
(a)
(b) Shorter Period
(c) Shorter Period
Longer Period
Height (m)
Length (km)
Foreset slope (degrees)
Age (years)
TA
TC
(d)
(e)
(f)
Progradation Rate (km/my)
Agradation Rate (m/my)
Sediment Flux (m2/y)

Figure 4.9: Graphs illustrating quantitative relationships between morphological parameters through time in the NSD (TA) and in the SSD (TC) including (a) Clinoform heights. (b) Clinoform lengths. (c) Average clinoform foreset inclination values. (d) Progradational rates. (e) Aggradational rates. (f) Sediment flux. Results using the shorter and longer periods are shown.

Determining the absolute values of progradation and aggradation rate within units A1 to A4 was not possible due to the lack of biomarkers in the interval and, thus the high level of uncertainty associated with age estimations. Regardless, graphs were constructed for the purpose of comparing relative rates between the different clinoform packages rather than absolute rates. Progradation rates in the lower section of TA (A1 to A4) are relatively steady (average of 40 km/my or 20 km/my, depending on the selected time period; Figure 4.9d; Table 4.1). An relative increase in progradation rate is recorded during deposition of clinoform package A5 (~550 km/my; Figure 4.9d; Table 4.1) that was most likely controlled by increased sediment flux (Figure 4.9f). A relatively larger increase in progradation rate (~740 km/my; Figure 4.9d; Table 4.1) occurs during the deposition of seismic unit A7.

Intensive slope erosion and the presence of mass transport deposits in TA (Moscardelli et al., 2006; 2012) produced trends in clinoform thickness different to those predicted using the method of Petter et al. (2013), where maximum thicknesses are located close to the shelf edge and decrease until reaching the clinoform pinchout position. For TA (both shorter and longer time periods) plots of sediment flux (Figure 4.9f) show: (1) a general increase in sediment flux with time from A1 to A4 (Table 4.3); and (2) two peaks in sediment flux during deposition of clinoform packages A5 and A8. The values for A5 are the highest for the entire section, reaching 181 m^2/y. The increase in sediment flux during A8 is not as large as A5, reaching 100 m^2/y, and might be related to the Saddler effect (Saddler, 1981). The Saddler effect proposes that the longer the time interval measured, the lower the sedimentation rate will appear to be because of the likely

occurrence of more erosional surfaces (and times of non-deposition) that reduce the overall calculated values for sedimentation rate. Also, aggradation and sediment flux calculations in the younger, upper section may result larger than in the older, lower section because of the small effect of compaction.

Transect TC

Seismic transect C is located in the southern continental margin of eastern offshore Trinidad (Figure 4.2). The main structural elements in the SSD correspond to a series of Plio-Pleistocene northwest-southeast–oriented regional and counter-regional growth faults as well as their associated rollover anticlines (Figures 4.2B and 4.4). Sediment sequestration in the outer shelf and upper slope region could have been favored by the presence of the landward-dipping counter-regional faults (Figure 4.4). Through visual examination, it is easy to distinguish three sections based on seismic character. The lower section (C1-C6) is characterized by high-amplitude, continuous and parallel seismic reflectors that dip gently towards the east (up to 3°; Table 4.1, Figure 4.4). Clinoforms units within this section have average heights of 220 m, and thicknesses of up to 180 m. This interval has been identified by Moscardelli et al. (2012) as *Continuous and Parallel* seismic facies and is interpreted as prodelta to upper slope deposits, associated with fine-grained deposition (Sydow et al., 2003; Moscardelli et al.; 2012). In this section the toe of the slope is easy to identify, but the rollover point is not. The presence of a seafloor multiple at similar depths (Sydow et al., 2003; Moscardelli et al.; 2012) makes it difficult to image the interval properly. The middle section of TC (C7-C12) is characterized by clinoforms with steeper inclines (up to 8°, Table 4.1, Figure 4.4), and smaller heights (average of 150 m, Table 4.1, Figure 4.9). Moscardelli et al. (2012) identified this section as *Steep Clinoform Package* seismic facies, which are constrained mainly to the SSD. These seismic facies have been correlated with outer-

shelf deposits found near the shelf edge and associated with the northeasterly migration of the paleo-Orinoco delta system (Moscardelli et al., 2012). The topsets of the older clinoforms (c8-c10) are characterized by low-angle, high-amplitude, and relatively continuous reflectors (Figure 4.4); however, the topsets of clinoforms c10 to c13 present a low-amplitude and discontinuous character that may indicate a higher degree of incision (Figure 4.4). Clinoform foresets in C7-C12 are the steepest of all the sections of TC, reaching up to 8° (Table 4.1). The rollover point and toe of the slope are both easy to identify. The upper section of TC (C13-C16) is characterized by the most gently dipping reflectors (up to 2°, Table 4.1, Figure 4.4). This section was defined by Moscardelli et al. (2012) as *Sigmoid Clinoform Package* seismic facies, which occur in both the NSD and SSD (Figures 4.3 and 4.4). Clinoform heights for *Sigmoid Clinoform* seismic facies typically exceed 200 m in TC (Table 4.1). The toe of the slope and the rollover point are both difficult to identify because of the lack of significant inclination changes, but mat be better recognized by seismic facies (occurrence of chaotic reflectors associated with MTC and other deeper basin conditions) instead of changes in the clinoform profile (e.g., inclination).

Clinoform heights within TC (Figure 4.9a) exhibit three periods of high values (clinoforms c5-c6, c11-c13 and c15-c17, with average values of 325, 215 and 260 m, respectively; Table 4.1). Length plots (Figure 4.9b) also show three zones with similar values of length: clinoform packages c1-c7, c8-c13 and c14-c17, with average values of 4.4, 1.7 and 7.3 km, respectively (Table 4.1). Inclination values in TC show a slight increase from clinoforms c1 to c7 (average of 3°, Figure 4.9c). Inclination values then increases in a faster rate until reaching 8° in clinoforms c12 and c13 (with a slight dip at c10). Clinoform c14 shows an abrupt decrease in the foreset inclination that reflects a inclination that is kept relatively constant for the rest of the transect (average of 1.9°;

Figure 4.9c). Clinoform packages with the highest foreset declivities (c8 to c13) are characterized by *Steep Clinoform Package* seismic facies (Moscardelli et al., 2012), which are associated with outer shelf deltas. Delta clinoforms in this study are usually steeper than their counterparts along the continental margin (compare clinoforms of TA and TC). Unit C6 is characterized by a high progradation rate (452 or 904 km/my, depending on the selected time period) and negative aggradation rates whereas unit C7 is characterized by negative progradation rates and extremely high aggradation rates (25,000 or 50,000 m/my). For both time periods, sediment flux estimates (Figure 4.9f) also exhibit three peaks with maximum values in clinoform packages C6, C11, and C14. I suggest that the longer period produces more realistic sediment flux values than the shorter period (Figure 4.9l) for several reasons: (1) sediment flux plots reproduce better the trends observed in the graphs of height and length (Figures 4.9a and b) in that the peak centered at C11 has relatively small values of sediment flux, and therefore does not generate an important increase in foreset lengths when increases in height occur; (2) the values of sediment flux in the younger section (<20 ky) are higher than all of the others in the loger period case (Figure 4.9f), which is in accordance with the Saddler effect (in the shorter period case, C6 has higher values); and (3) the range of aggradation values obtained in the shorter period (up to 51,000 m/my) appears to be high when compared with other average worldwide ranges (e.g., average of 5,000-6,000 m/my in Syvitsky et al., 2009; Saddler, 1981).

Quantification of clinoform morphologies using the methodology of O'Grady et al. (2000)

O'Grady et al. (2000) generated plots of seafloor slope (equivalent to foreset declivities in this study) versus depth on passive margins and the observable patterns were classified into five morphological categories: 1) gentle and smooth; 2) sigmoid; 3)

steep and rough; 4) deep and steep and 5) stepped (O'Grady et al., 2000; Figure 4.10). Each of these morphological patterns was linked to environmental conditions at the time of deposition including sediment supply, erosiveness of the margin and degree of canyon development (O'Grady et al., 2000; see their Table 4.1). Although the eastern Trinidad margin is found in a complex tectonic setting, I systematically collected foreset clinoform declivities from the seismic units that were defined within seismic transects TA and TC (Figure 4.11). Based on these results, I identified three different geometries within TA: (1) *Steep and Rough* (clinoforms a1-a5), (2) *Gentle and Smooth* (clinoform a7), and (3) *Sigmoid* (clinoforms a7-a10). *Steep and Rough* geometries are associated with conditions of low sediment supply and erosive slopes with many canyons (O'Grady et al., 2000). Calculations from this study support low values of sediment flux in the interval of deposition of seismic units A1 to A4 (Figure 4.9f). Clinoforms a1 and a5 exhibit what I would consider to be erosion, reflected in high and variable values of inclination and sequence boundaries (P10-SB1 and P4-SB2) bounding that interval (Figures 4.11a and 4.11e). *Gentle and Smooth* and *Sigmoid* geometries of O'Grady et al. (2000) are associated with supply dominated settings and the development of few canyons, but with different substrates. The onset of these geometries correlates with increased values of sediment flux.

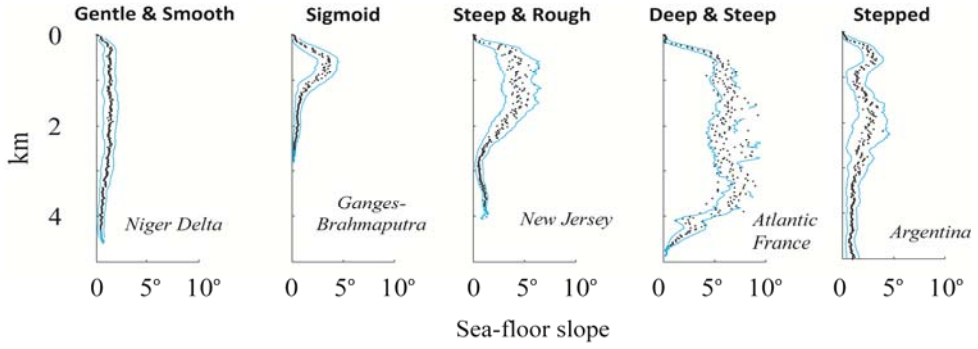

Figure 4.10: Generalized slope profiles of modern margins identified by O'Grady et al. (2000).

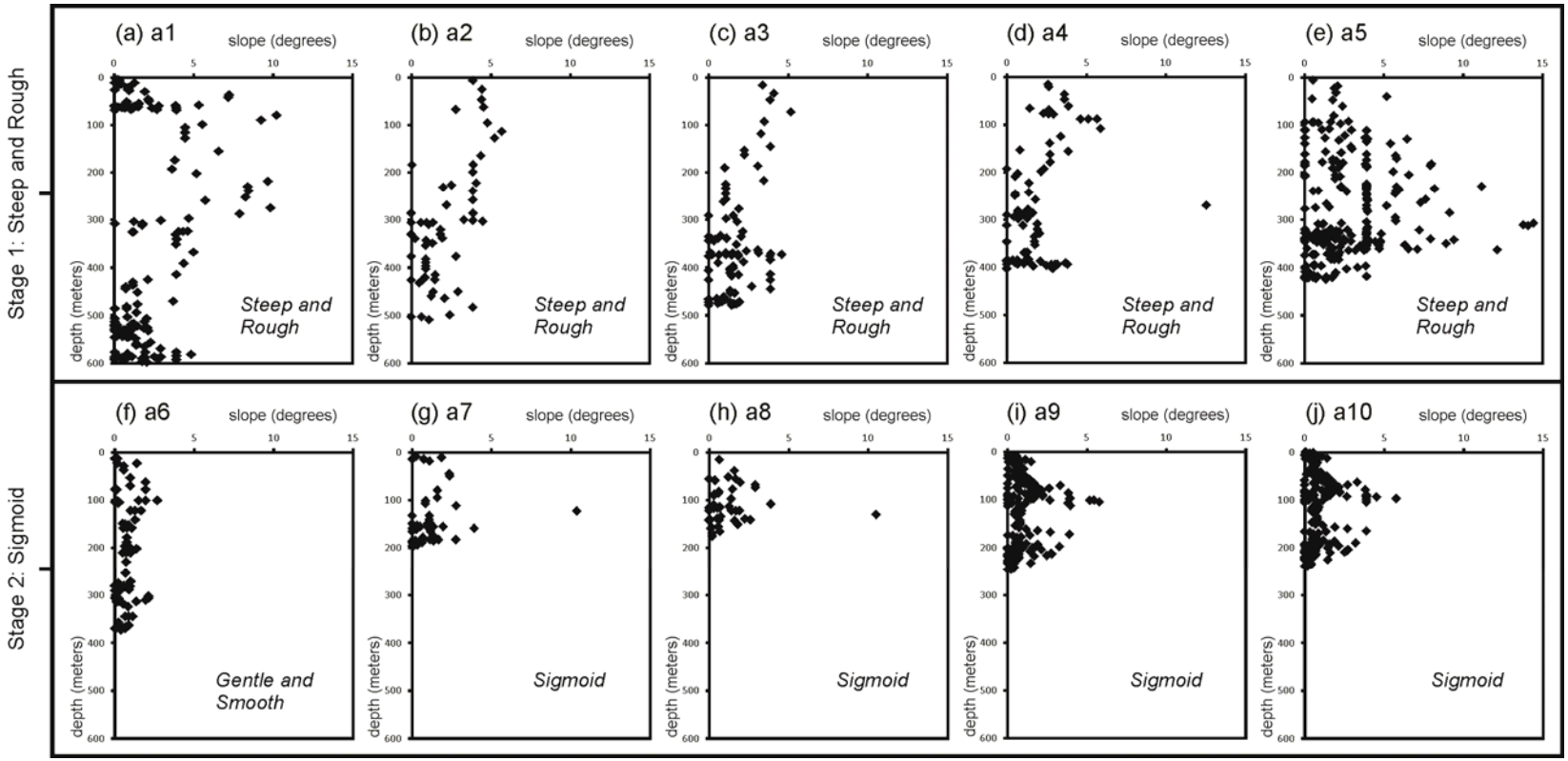

Figure 4.11: Plots of variations in clinoform inclination values with depth in the NSD (TA). Each stage of basin evolution (Stages 1 and 2) is characterized by a specific trend: steep and rough (Stage 1) (a-e), and sigmoid (Stage 3) (f–j) following the methodology of O'Grady et al. (2000).

O'Grady et al. (2000) type plots for TC show that clinoforms within TC can be broken down into different geometries. *Sigmoid* geometries best described clinoforms c1 to c4 (Figure 4.12a-d). However, *Steep and Rough* geometries are most common in clinoforms c5 to c7, associated with higher relief and higher degree of erosion (Figure 4.12e-g). A new transition from *Sigmoid* to *Steep and Rough* geometries is observed in the middle interval of TC. Clinoforms c8 to c10 (Figure 4.12h-j) are characterized by *Sigmoid* geometries associated with smaller values of height and small levels of erosion whereas clinoforms c11 to c13 are characterized by *Steep and Rough*, associated with the largest values of both height and inclination of the entire stratigraphic section (Figure 4.12k-m). The increase in clinoform dimensions is explained by the increase in sediment flux, observed during the deposition of C10 and C11 (Figure 4.9l). Clinoforms c14 to c17 are characterized by higher and longer clinoforms (increase in foreset heights and length), with low inclination values (with the exception of several outliers that are likely associated with faulting). Using O'Grady et al.'s (2000) classification scheme, these clinoforms are defined as *Gentle and Smooth* with their geometries possibly related to a high sediment supply, unstable substrate, and few modern canyons.

Figure 4.12

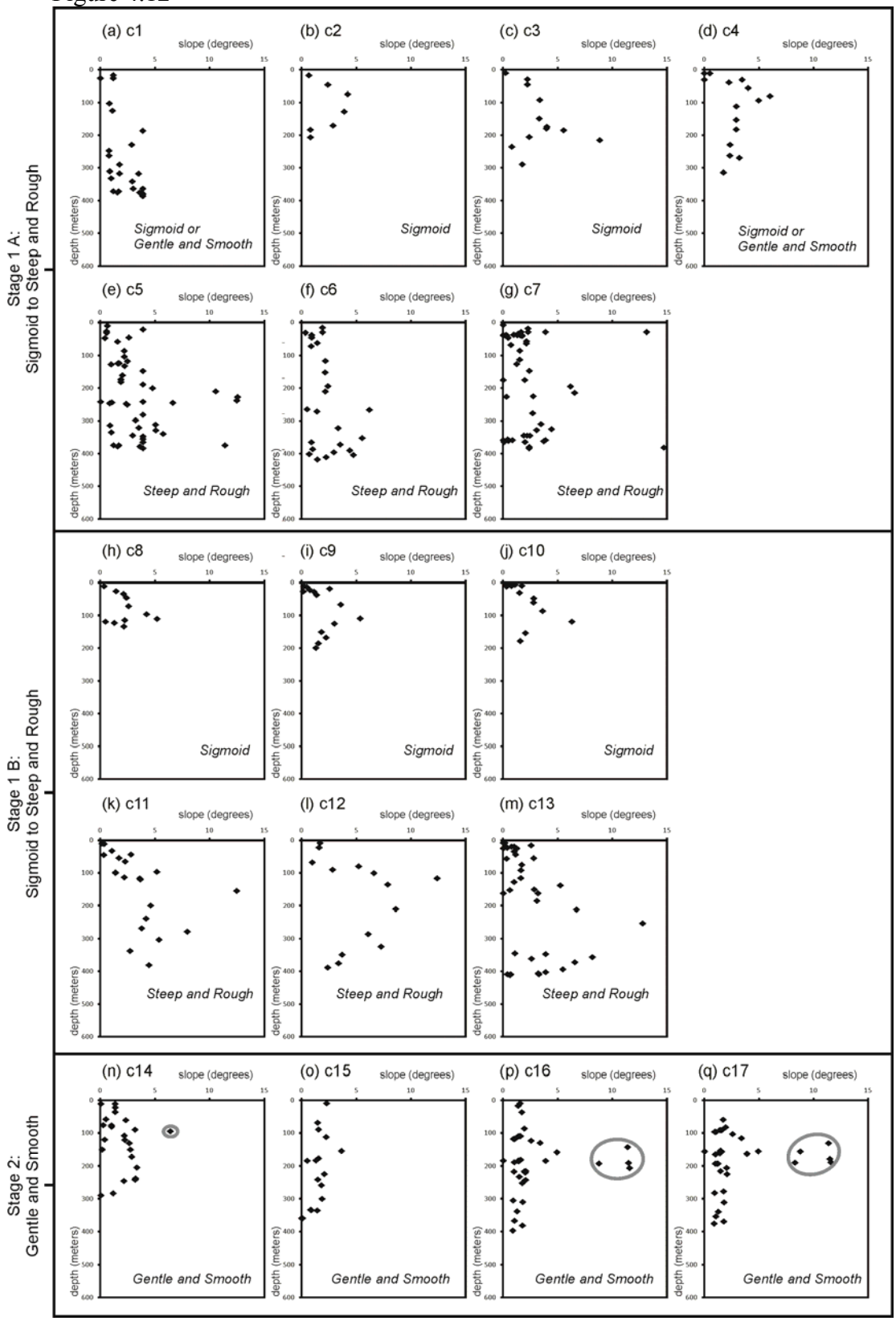
Stage 1 A:
Sigmoid to Steep and Rough
Stage 1 B:
Sigmoid to Steep and Rough
Stage 2:
Gentle and Smooth
(a) c1
(b) c2
(c) c3
(d) c4
(e) c5
(f) c6
(g) c7
(h) c8
(i) c9
(j) c10
(k) c11
(l) c12
(m) c13
(n) c14
(o) c15
(p) c16
(q) c17
slope (degrees)
depth (meters)
Sigmoid or Gentle and Smooth
Sigmoid
Steep and Rough
Gentle and Smooth

Figure 4.12: Plots of variations in clinoform inclination values with depth in the SSD (TC). Each stage of basin evolution (Stages 1 and 2) is characterized by a specific trend or combination trend: sigmoid to steep and rough (Stage 1) (a-g and h-m), and gentle and smooth (Stage 2) (n–q) following the methodology of O'Grady et al. (2000).

Quantification of clinoform morphologies using on the methodology of Adams and Schlager (2000)

Adams and Schlager (2000) also developed a methodology to classify the first-order morphology of continental margins and concluded that these morphologies could be mathematically described by linear, exponential or Gaussian distribution functions (Adams and Schlager, 2000; Figure 4.13). Applying this procedure to TA and TC, the results show that clinoforms in the NSD (TA) are best represented by exponential equations, except for the two youngest reflectors, a9 and a10, that are better defined by Gaussian distributions (Figure 4.14). I suggest that the presence of the paleocanyon generated an abrupt topographic change (deepening of the basin) that controlled the position of the rollover point and controlled a sharp break from topset to foreset. Although the overall section is better represented by exponential equations (Table 4.4), Gaussian distributions also give acceptable solutions for the younger section (A5-A9), suggesting complete filling of the structure by this time.

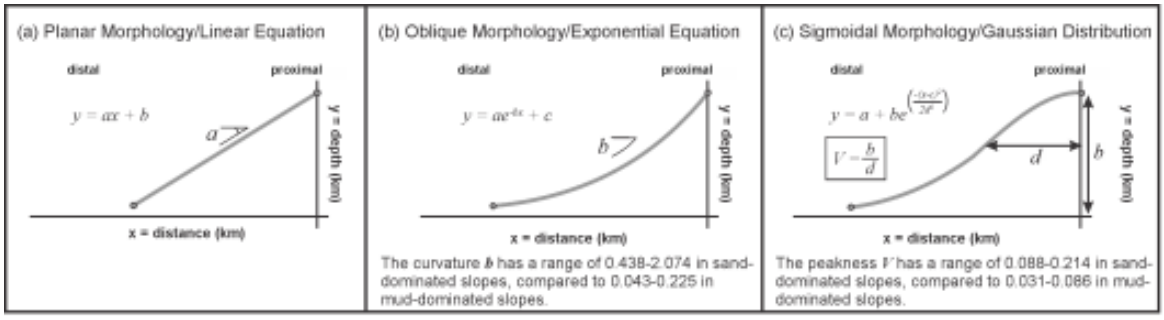

Figure 4.13: Slope types and their governing equations according to Adams and Schlager's classification (2000): (a) planar morphology, (b) oblique curvature, and (c) sigmoidal morphology.

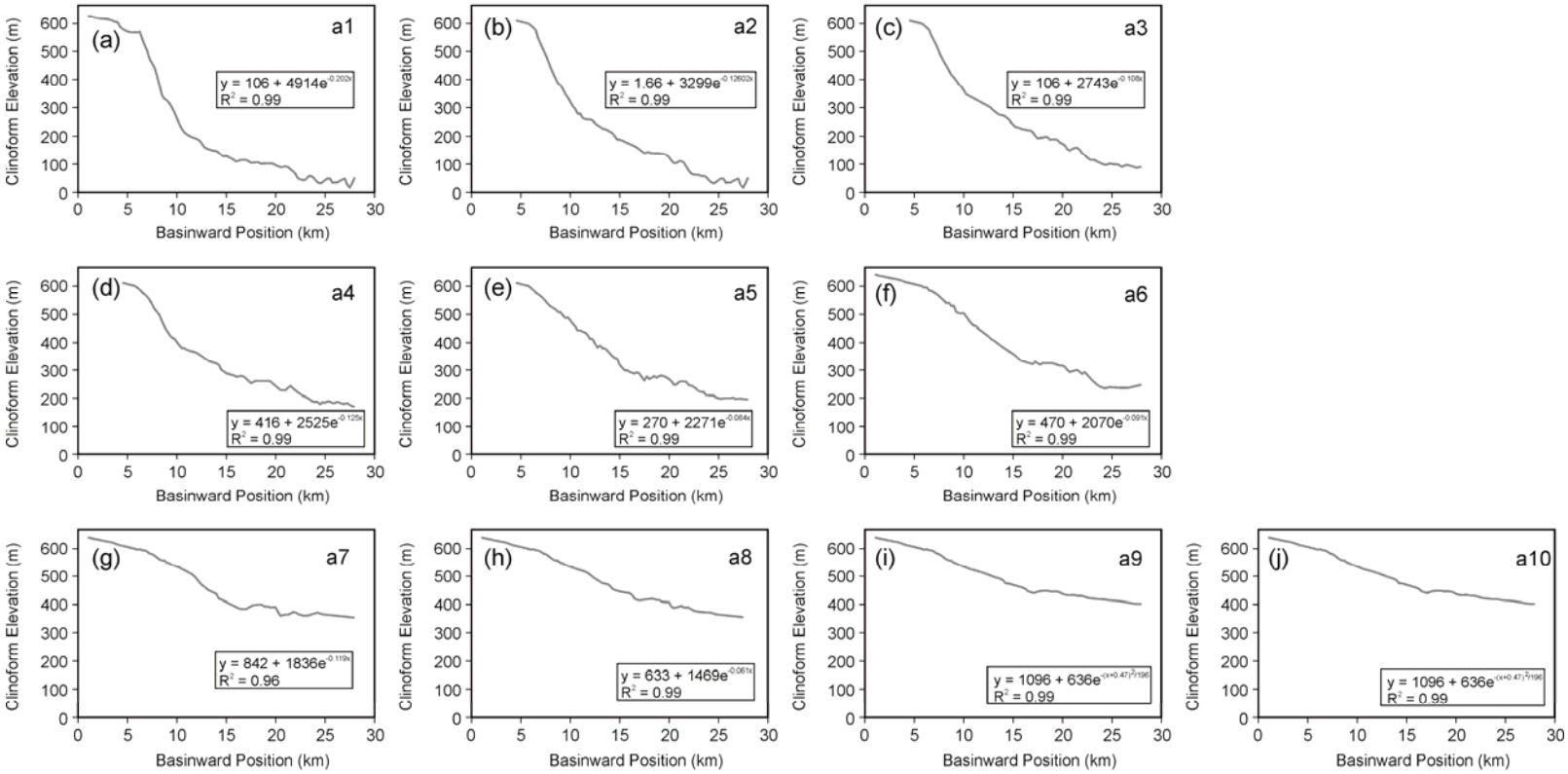

Figure 4.14: Geometry of individual clinoform profiles (base and top of seismic units) in the NSD (TA). Plots fit exponential functions. Collection and interpretation of data points followed methodology described by Adams and Schlager (2000) (See text for discussion).

Transect	Clinoform	Type	a exp	b exp	c exp	Rsq	a1	a2	b2	c2	V	Rsq
A	a1	Exponential	2848	-0.276	88	0.997						
	a2	Exponential	1633	-0.191	94	0.996						
	a3	Exponential	1246	-0.168	146	0.995						
	a4	Exponential	842	-0.109	143	0.989						
	a5	Exponential	793	-0.076	94	0.988						
	a6	Exponential	778	-0.080	141	0.986						
	a7	Exponential	629	-0.091	272	0.960						
	a8	Exponential	538	-0.067	262	0.988						
	a9	Exponential	422	-0.098	382	0.994						
	a10	Exponential	426	-0.100	395	0.994						
C	c1	Exponential	4703	-0.300	195	0.985						
	c1	Gaussian					170	148	6.29	2.13	0.098	0.999
	c2	Gaussian					170	184	5.85	2.33	0.112	0.999
	c3	Gaussian					160	221	6.05	2.62	0.119	0.996
	c4	Gaussian					60	396	4.07	6.32	0.089	0.997
	c5	Gaussian					-84	378.9	9.97	4.89	0.110	0.986
	c6	Gaussian					-2380000	2638000	3.56	961	3.882	0.996
	c7	Gaussian					-4111500	4116000	3.48	1280	4.548	0.996
	c8	Gaussian					573.9	-116	7.36	1.68	0.097	0.996
	c9	Gaussian					599.5	-196	9.71	2.87	0.097	0.981
	c10	Gaussian					272.9	281	6.82	4.05	0.098	0.996
	c11	Gaussian					44.52	510	8.15	5.60	0.129	0.997
	c12	Gaussian					112.6	343	12.10	1.93	0.251	1.000
	c13	Gaussian					163.2	270	13.11	1.26	0.302	0.985
	c14	Gaussian					199.4	310.9	10.59	5.63	0.078	0.998
	c15	Gaussian					87.39	230.6	17.15	6.16	0.053	0.996
	c16	Gaussian					100.7	453.8	10.76	10.09	0.064	0.998
	c17	Gaussian					117.4	464.3	10.49	10.32	0.064	0.997

Table 4.4: Fitting parameters for different seismic units interpreted in study area. Methodology for data collection and interpretation as described by Adams and Schlager (2000).

Best fitting equations for clinoforms in the SSD (TC) (Figure 4.15) are Gaussian, although the youngest section (c16 and c17) could have been fit with exponential functions with slightly lower R-square values. Clinoform slopes best represented by Gaussian distributions indicate margins with sigmoidal profiles (Adams and Schlager, 2000). The development of this type of profile is associated with (1) highly aggradational margins where fluctuations of the wave base and changes in sea level produce redistribution and erosion of sediment at the shelf break, and/or (2) strong influence of ocean currents on the morphology of slopes which round the shelf break during progradation. In the case of the SSD, high sediment supply associated with activity pulses in the paleo-Orinoco, in conjunction with moderate-to high aggradation rates associated with the activation of growth faults may have produced conditions suitable for the development of sigmoidal clinoforms.

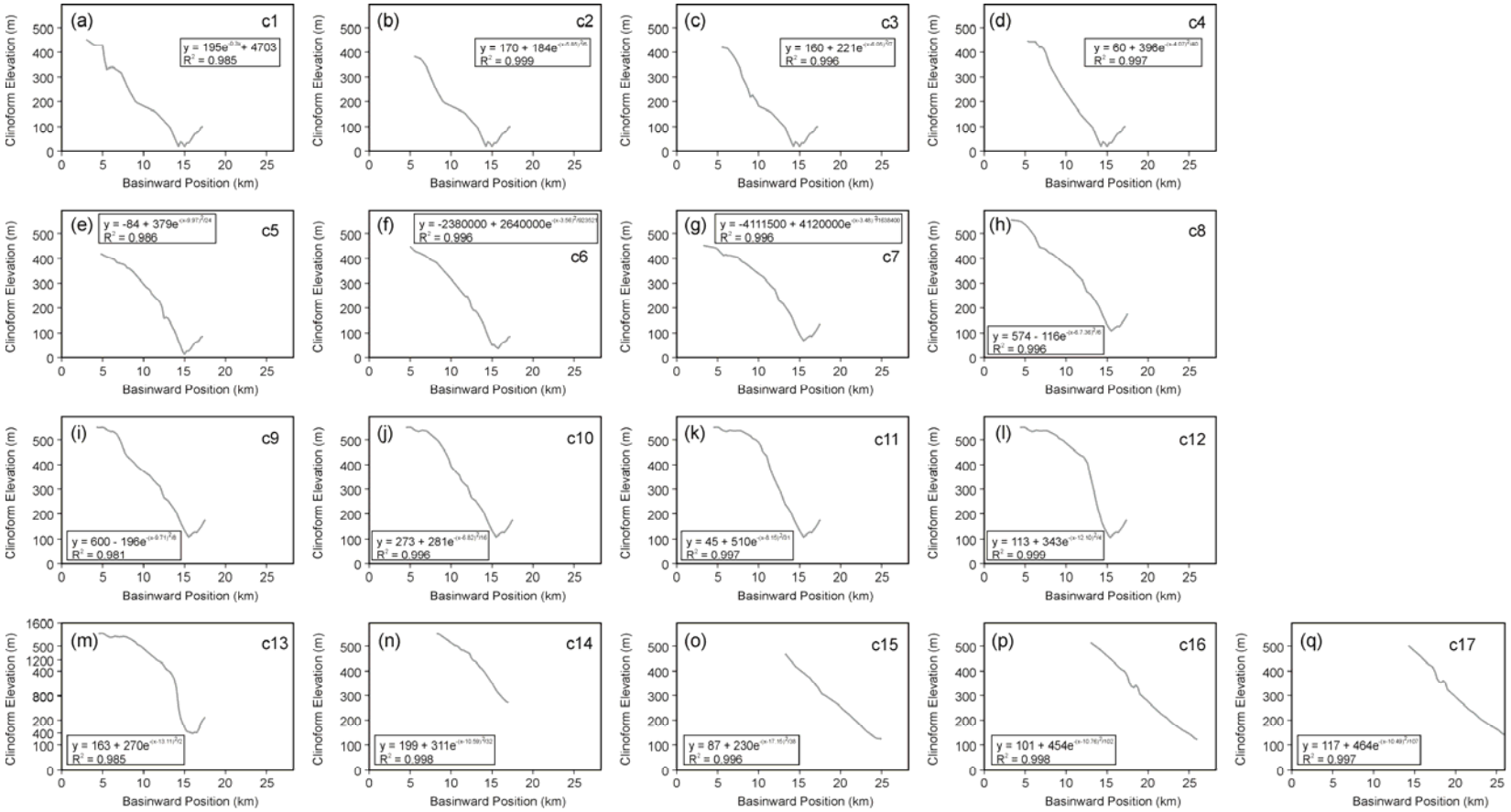

Figure 4.15: Geometry of individual clinoform profiles (base and top of seismic units) in the SSD (TC). Plots fit Gaussian distribution functions. Collection and interpretation of data points followed methodology described by Adams and Schlager (2000) (See text for discussion).

Stages of Clinoform Development

Changes in the morphology of clinoforms and seismic facies through time suggest at least two stages of clinoform development in the basin: stage 1 (~120-20 ky) and stage 2 (~20-0 ky). Stage 1 includes seismic units A1 to A4 in TA and seismic units C1 to C12 in TC. Stage 2 contains seismic units A5 to A9 in TA and C13 to C16 in TC. However, local changes that are particular to each of the structural domains, and that indicate a series of changes of transport and deposition conditions in the basin from north to south, allowed the subdivision of these stages in substages: substages 1A (C1-C6) and 1B (C7-C12) in TC, and substages 2A (A5-A6) and 2B (A7-A9) in TA.

DISCUSSION

Lithological Composition

According to Adams and Schlager (2000), the geometry of slopes (i.e. planar, oblique and sigmoidal) gives information about depositional environments whereas the shape parameters of the three fitting equations (i.e. curvature and peakedness of the curve; Figure 4.13) provide information to deduce sediment composition. Overall, mud-dominated slopes have lower slope angles, curvatures in oblique profiles (b in Figure 4.13b), and peakednesses in sigmoidal profiles (V in Figure 4.13c) than sand-dominated slopes. Adams and Schlager (2000) concluded that the curvature for exponential profiles has a range of 0.438–2.074 in sand-dominated slopes, compared with a range of 0.043–0.225 in mud-dominated slopes. On the other hand, the peakedness range in Gaussian distributions for clay-dominated slopes is less than for slopes containing sand: 0.031–0.086 and 0.088–0.214, respectively.

As mentioned in the previous section, TA is best represented by exponential equations (Figure 4.14). Coefficient of curvature b, which was determined for each

clinoform using Matlab algorithms, varies from 0.067 to 0.276, with averages of 0.164 for the lower section, and 0.087 for the younger section (Table 4.4). These values are within the range of muddy slopes. However, the decrease in the value of b from the older (0.164) to the younger (0.087) section suggests an apparent decrease in grain size to the period when the paleocanyon became filled. These results are in accordance with an abrupt topography generated by the paleocanyon that allowed bypass of coarser-grained sediment. Best fitting equations for TC are always Gaussian (Figure 4.15), indicating that this section is characterized by sigmoidal profiles (Adams and Schlager, 2000). Coefficients of peakedness V found for the entire section have a wide range from 0.057 to 4.548 (Figure 4.16). All profiles have peakedness values below 0.300 except for clinoforms c6 and c7 that were fit by curves with extremely higher values of peakedness (3.882 and 4.548, respectively; Table 4.4). These values are above the range mentioned by Adams and Schlager (2000) and indicate either that the packages are very sandy or that the profiles cannot be represented by the approximations proposed by Adams and Schlager (2000). When compare with geometrical measurements for the same section (Figure 4.9), I notice that this section is characterized by anomalously high progradation and aggradation rates, which are responsible for the high estimates of sediment flux. Clinoforms pakages c1-c5 and c8-c11 have very similar values of peakedness (with an average of 0.105), separated by the anomalous values of clinoforms c6 and c7 (Figure 4.16). At the moment of deposition of clinoforms c12 and c13, coefficient values increase to an average of 0.267 to finally decrease abruptly to an average of 0.065 from clinoform c14 to c17 (Figure 4.16). According to the values presented by Adams and Schlager (2000), most of the section is sandy, except for this youngest interval (clinoforms c14-c17), which is below the sand-mud division in Figure 4.16.

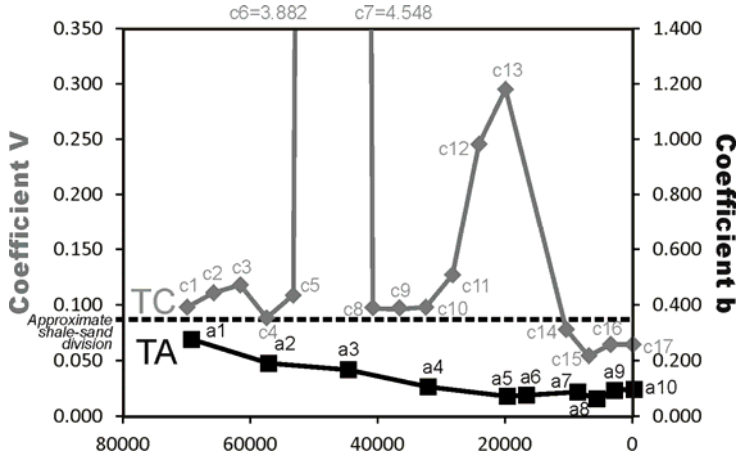

Figure 4.16: Parameters associated with curvature (b) and peakedness (V) for subsurface of the eastern offshore Trinidad margin (this paper). Curvature and peakedness parameters have been linked to lithological composition (Adams and Schlager, 2000). Curvature and peakedness values within the study area indicate the northern seismic transect (TA) is muddier than the southern transect (TC), except for the youngest clinoforms, whose values of peakedness (V) indicate seismic units C14 through C16 are composed of lithologies rich in mud and clay.

Comparing the results for the two seismic transects (Figure 4.16), TA seems much muddier than equivalent units in TC. Outer shelf deltas (as those observed in TC) are generally more sand-rich than shelf-edge deltas (as those observed in TA). There is no apparent correlation between sediment composition in the NSD and SSD, except perhaps that in both sections the muddier interval corresponds with the younger units (<10.5 ky), which indicates that this particular parameter may have been controlled by local processes within the basin.

The classification of the eastern Trinidad margin clinoforms applying Adams and Schlager's technique (2000) shows small changes in the general conditions of the basin through this short period of time (<120 ky). The most important changes most likely occurred along strike, indicating important differences in the transport conditions in the

NSD and SSD, such as general higher sediment flux and sand content in the southern region (TC).

Clinoform morphologies along strike

The analysis of Adams and Schlager (2000) suggests there is a relationship between shelf-edge/outer-shelf deltas and oblique/sigmoidal clinoform morphologies. Shelf-edge deltas show oblique morphologies because of the abrupt change in topography (deepening of the basin) when the delta reaches the shelf edge, which in the case of the NSD is controlled by the position of the paleocanyon. Alternatively, outer shelf deltas developed in areas where accommodation has been gradually generated by growth faulting and sediment supply is high (Paleo-Orinoco discharge). Tidal action that may have helped in the development of sigmoidal morphologies has also been suggested for the SSD (Moscardelli et al., 2012).

During Stage 1, shelf-edge delta facies (*Sigmoid Clinoform* seismic facies) are dominant in the NSD (A1 to A9; Figure 4.3) because the paleocanyon development created a narrower shelf in this region. However, in the SSD a wider shelf did not allow the foresets of the clinoforms to merge with the continental slope and the system did not become a shelf-edge delta, instead prodelta and upper slope facies (*Continuous and Parallel* seismic facies), and outer shelf delta facies (*Steep Clinoform* seismic facies) developed during Stage 1A (C1-C6; Figure 4.4) and stage 1B (C7-C12), respectively. During Stage 2A, the NSD is still characterized by the deposition of shelf-edge delta facies. However, these clinoforms differ considerably from the ones of stage 1 in that they have much smaller heights (average of 110 m compared with 360 m in the lower section) and lengths (average of 6 km compared with 10 km in the lower section), and much higher sediment flux (average of 181 m^2/y compared with 10 m^2/y in the lower section). The development of smaller clinoforms under high sediment supply conditions

can be explained by the lack of accommodation and increased rates of progradation observed in the succession. This stage is also characterized by the presence of mass transport deposits identified in seismic (Figure 4.3). Towards the south, Stage 2A is also characterized by the presence of shelf-edge delta facies, indicating that the delta front reached the continental slope. Clinoforms in this section show decrease in height, slight increase in length, abrupt decrease in inclination as well as, and unlike TA, a slight decrease in progradation, increase in aggradation (accommodation) and slight decrease in sediment flux (Figure 4.9f). Finally, Stage 2B clinoform packages are characterized by shelf-edge delta facies (*Sigmoid Clinoform* seismic facies) in both TA and TC. However, the morphology of clinoforms differs in that clinoform packages in TA (a7 to a10) show a progressive decrease in height (from 121 to 85 m), abrupt increase in length (from 5 to 14 km) and sediment flux (from 40 up to 100 m^2/y) as well as variable progradation and aggradation rates (Figure 4.9). These changes may be associated with the final stage of infill of the structure generated by the paleocanyon. Towards the south (Figure 4.4), clinoforms show an important increase in height, length, decrease in inclination, decrease in progradation rate, increase in aggradation rates and abrupt decrease in sediment flux that may be associated with the generation of accommodation space by normal growth faulting.

Eustatic/Climatic Controls

Sequence stratigraphic analysis of the eastern Trinidad margin (Sydow et al., 2003; Maher, 2007) allowed the interpretation of two 4th order cycles in the interval of interest, separated by a sequence boundary that has been interpreted as the last glacial maximum lowstand surface (P4-SB2), and has an age close to 18-20 ky (Maher, 2007; Moscardelli et al., 2012). These cycles represent the two stages of clinoform development, stage 1 and stage 2, interpreted in this study. The analysis of the

configuration and terminations of seismic reflectors in TC suggests the first cycle (stage 1) is composed of a transgressive system track (TST1, Figure 4.4), usually characterized by *Continuous and Parallel* seismic facies, and a highstand system track (HST1, Figure 4.4), characterized by *Steep Clinoform* seismic facies and observed only in the SSD (Moscardelli et al., 2012). TST1 includes seismic units C1 to C6. The base of this transgressive system is defined by clinoform c1, which corresponds to a sequence boundary (P10-SB1; Figure 4.4), whereas the upper boundary is clinoform c7, whose seismic character corresponds to a maximum flooding surface (MFS1; Figure 4.4). HST1 includes seismic units C7-C12. Its lower boundary is defined by MFS1 (clinoform c7) and its upper boundary by sequence boundary P4-SB2 (clinoform c13), associated with the last glaciation event. The period of deposition of the first cycle (~120-20 ky) is characterized by two trends in the global sea level curve, a warm period followed by a cool period, both characterized by low global sea level values (e.g., Lisiecki and Raymo, 2005; Miller et al., 2005). Great variation in clinoform morphologies compared to those expected from the global sea level trend implies that, besides sea level, other factors played a key role in controlling the shape and dimension of the margin. The stacking patterns associated with transgressive and highstand system tracts observed in the basin, and specifically in the SSD, indicate the generation of accommodation probably associated with extremely rapid subsidence in the Columbus Basin growth fault provenance (Sydow et al., 2003). In fact, TC shows major normal growth faults that may be responsible of part of this accommodation (Figure 4.4). However, toward the NSD, a transgressive character is not recognized in the section (Figure 4.3), most likely because of the lack of growth faults and other changes in accommodation and sediment supply associated with the CBTZ, and regressive patterns are recorded during stage 1 (seismic units A1 to A4).

Following sequence stratigraphy analysis, the second cycle (Stage 2) is interpreted as a lowstand system track (LST2), followed by a very thin transgressive system track (TST2). In both TA and TC, the stratigraphic succession deposited during stage 2 presents most of the elements that have been defined as components of lowstand systems tracts in the classical sequence-stratigraphic model (van Wagoner et al., 1990; Mitchum et al., 1993) (Figures 3 and 4). For instance, architecture of reflectors between clinoforms a6 and a7 and clinoforms c13 and c14 (Figures 3 and 4, respectively) reflect that of lowstand system track submarine fans, characterized by the presence of downlapping terminations against the younger reflector in both directions. The clinoform packages used for the geometrical analysis (A6-A8 and C13-C15) correspond to a regional lowstand wedge, composed of a southwest-northeast progradational to aggradational clinoform packages that were part of a shelf-edge delta (paleo-Orinoco) (Moscardelli et al., 2012). Global sea level curves (e.g., Miller et al., 2005) show a rise in sea level that followed the last lowstand maximum (~18-20 ky). Therefore, regressive patterns shown within this succession are indicative of high sediment supply, enough to counteract the effect of rising sea level. High sediment flux values and the deposition of shelf-edge deltas are associated with high sediment delivered by the paleo-Orinoco delta (Sydow et al., 2003). In addition, changes in stacking patterns from regressive to transgressive in the youngest section (A9 and C16; Figures 3 and 4) reflect a progressive decrease in sediment supply within the overall sea level rise.

Tectonic Control

Abrupt changes from outer shelf deltas to shelf-edge deltas from south to north during Stage 1 suggest that basin physiography and specifically the location of the paleocanyon controlled the position of the shelf edge in the NSD, allowing the relatively rapid development of shelf-edge deltas in that part of the basin. This configuration might

have influenced sediment partitioning in that most sediment in the SSD appears to have been stored on the shelf, where the deltas are located (Figure 4.4), whereas sediment in the NSD was most likely deposited downdip in deeper water positions, associated with mass transport deposits (Figure 4.3).

Clinoform geometries in the NSD present less variations through time (Figure 4.9) because they are primarily controlled by the activation and infilling of the paleocanyon. The great accommodation developed by this structure allowed the development of higher relief clinoforms (Figure 4.3), oblique morphologies, and probably a preferential direction of sediment transport. On the other hand, morphologies in the SSD present a higher degree of variation through time because they were controlled by different episodes of activation of a series of growth faults and the paleo-Orinoco dynamics. Higher values of sediment flux in the SSD can be explained by its proximity to the Orinoco delta, characterized by having one of the largest discharges on Earth (Diaz de Gamero, 1996; Moscardelli et al., 2012). Facies transition from prodelta and upper slope (stage 1A) to outer-shelf delta (stage 1B), as well as the eventual reaching of the shelf edge and deposition of shelf edge deltas (stage 2) can be partially attributed to these high values of sediment flux. Overall, three main episodes of high sediment flux were identified in TC that may correspond to the activation of Orinoco's lobes near this section. Accommodation was generated by growth faults, but gradually. Therefore, clinoform foresets are not as high as in the NSD.

CONCLUSIONS

This study demonstrated that detailed morphological analysis of clinoforms can be an important tool to infer the conditions of sediment transport and deposition in a basin. However, it is important to know the limitations of the methodology and the dataset. Estimations of sediment flux (Petter et al., 2013) and slope composition (Adams

and Schlager) may be misleading when clinoforms are not well preserved and/or important mass transport deposits are present.

The stratigraphic interval studied in the eastern Trinidad margin is too short to recognized important changes in first order morphology through time (oblique vs. sigmoidal). However, changes in individual geometrical parameters (i.e., height, inclination, rates of progradation and aggradation) allowed for a better understanding of the margin evolution, including activation of underlying structures, changes in sediment supply, and paleo-Orinoco dynamics. Changes in accommodation, physiography and sediment supply linked to different tectonic conditions (transtension vs. growth faulting and the Orinoco dynamics), on the other hand, made it possible to develop important changes in clinoform morphologies along strike, including (1) oblique morphologies in the NSD versus sigmoidal morphologies in the SSD; and (2) shelf-edge deltas in the NSD versus outer-shelf deltas in the SSD.

The analysis of clinoform morphologies, including the study of rollover trajectories, helped to infer sediment partitioning within the basin. In the Trinidad margin, the steeper, sigmoidal clinoform packages in the SSD represent outer shelf deltas that stored most of the sediment coming from the Trinidad mainland. The NSD clinoforms, on the other hand, have flatter rollover trajectories that suggest a significant portion of the sediment was deposited into deeper water positions. Paleostructures also play an important role in redistribution of sediment and the location of sediment pathways (bypassing vs. storage in the NSD and SSD, respectively). For instance, the presence of the paleocanyon in the NSD might have triggered deep water deposition in that region as it played a key role in defining the location and geometry of sedimentary pathways, bypass zones, and depocenters.

The presence of a regressive system where accommodation is being created by the paleocanyon (TA) indicates a possible underestimation of the values of sediment flux associated with this system and suggests that Petter et al.'s procedure (2013) may not be adequate for areas where the degree of preservation of the slope is low. Mass wasting in clinoform foresets may generate thickness responses different to those expected in average margins, and may have a big impact on the measurements. Therefore, I propose that this methodology be used only in areas with good preservation of clinoform architectures and the absence (or low influence) of mass transport deposits.

Clinoform development and architectures vary along the northern Taranaki and eastern Trinidad continental margins because of the interaction of deltas and sediment supplies along with different structural elements alongstrike. In the case of the Taranaki Basin, those elements include normal faults, relay ramps and graben development. In the eastern Trinidad margin, growth faults in the SSD and a paleocanyon in the NSD were the most important structural elements controlling clinoform architectures. Although both basins show an important tectonic control, tectonic conditions most likely determined sediment availability in the Taranaki Basin, especially the Southern Alps uplifting, whereas the Orinoco delta dynamics played a major role in the eastern Trinidad margin.

CHAPTER 5: COMPARISON OF CLINOFORM GEOMORPHOLOGICAL ANALYSES PERFORMED IN THE NORTHERN TARANAKI BASIN AND THE EASTERN TRINIDAD MARGIN

INTRODUCTION

A brief comparison of the results obtained in the northern Taranaki Basin and eastern Trinidad margin are presented in this section. Table 5.1 shows a summary of the main differences between the two continental margins. Both regions are characterized by continental margins having a variety of clinoform architectures (Chapters 2 and 4). Although their important tectonic and stratigraphic differences, in both areas, it was possible to classify clinoforms according to their morphology and to infer the predominant controls on clinoform development, including the effects of tectonics, paleostructures and sediment supply. However, one element of consideration is that the eastern Trinidad margin, and especially the northern transect TA, shows a high degree of incision and development of mass transport complexes that could affect estimations of lithology (Adams and Schlager, 2000) and sediment flux (Petter et al., 2013).

	Northern Taranaki Basin	**Eastern Trinidad margin**
Regional tectonic setting	Western margin of the Australia-Pacific plate boundary deformation	Southeastern margin of the tectonically active Caribbean Plate Boundary Zone (CPBZ)
Major structural elements	Northern Graben (backarc rifting structure) close to the shelf edge area	North and east: slope and deep basin affected by several ridges and depocenters associated to the regional tectonic framework South and west: growth faulting on the shelf
Age of stratigraphic interval	Pliocene-Recent (6 Ma-present)	Quaternary (< 120 ky)
Major source of sediment	Several small, muddy rivers from (1) Southern Alps (major) and (2) Taranaki Peninsula (minor)	Paleo-Orinoco River
Depositional system	Clastic Depositional System; inner to outer shelfal conditions	Clastic Depositional System; deltaic systems

Table 5.1: Comparison of tectonic and stratigraphic elements in the northern Taranaki Basin and eastern Trinidad margins

COMPARISON OF THE TARANAKI BASIN AND EASTERN TRINIDAD CONTINENTAL MARGINS

In Chapter 2, three stages of clinoform development were identified in the Taranaki Basin on the basis of changes in first order clinoform morphologies through time (planar, oblique and sigmoidal). In Chapter 3, I concluded that these stages are the result of changes in accommodation and sediment supply associated with the opening of a graben structure in the early Pliocene and the migration of the Pacific-Australian subduction zone and related uplifting of the Southern Alps in the late Pliocene-Pleistocene. One factor that facilitated clinoform classification in the Taranaki Basin is a considerable period of time (~6 my) that it made possible to record changes in the regional tectonic context. In Trinidad, temporal changes in clinoform morphologies may have been more difficult to grasp because of the shorter period of time of the interval (~120 ky). In fact, most of the clinoforms in the North Structural Domain (NSD) reflect oblique morphologies whereas clinoforms in the South Structural Domain (SSD) are better characterized by sigmoidal morphologies (Chapter 4). The lack of temporal variations in the first order geometry of clinoforms in the eastern Trinidad margin may be the result of its regional tectonic setting (CBTZ) that did not show significant variations during this smaller time period. If comparing both stratigraphic sections, the time interval covered in the Trinidad margin is the equivalent to one single clinoform package studied in the Taranaki Basin, within which morphologies are also similar (Figure 5.1). This comparison would be equivalent to compare 3rd and 4th order cycles, according to sequence stratigraphic nomenclature (Vail et al., 1977).

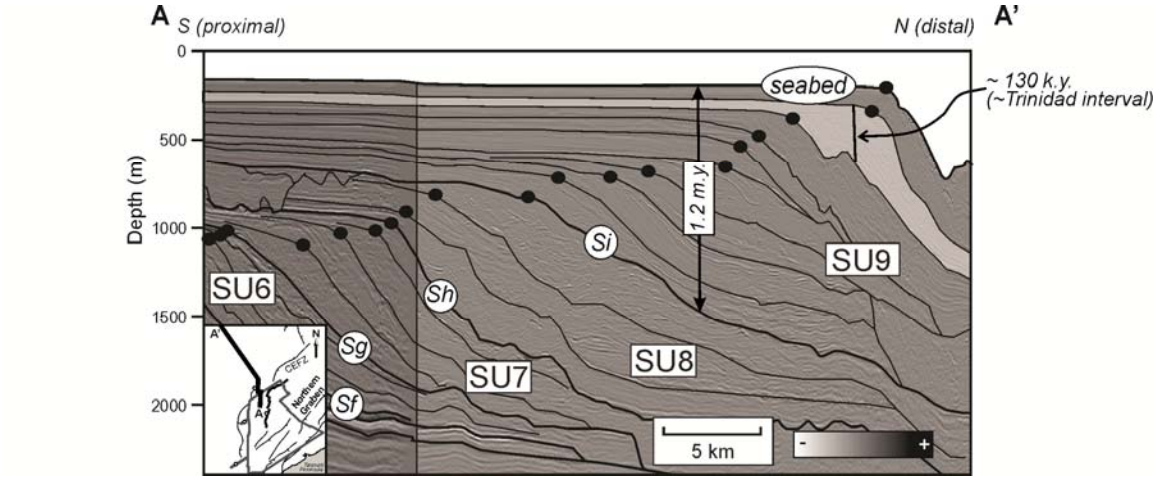

Figure 5.1: Clinoforms of theTaranaki Basin with a comparison of temporal scales between the Taranaki Basin and eastern Trinidad continental margin. Each individual seismic unit in the Taranaki basin is interpreted to have been deposited during the entire interval studied along the Trinidad margin.

More detailed changes in clinoform morphologies are better captured with the study of seismic facies and the application of other classification techniques (e.g., O'Grady et al., 2000; Petter et al., 2013). In the Taranaki Basin, the application of the methodology developed by O'Grady at al. (2000) suggested an important increased of sediment supply in the late Pleistocene (Chapter 2) that was later corroborated by sediment flux estimations using the procedure of Petter et al. (2013; Chapter 3). In the southern portion of the eastern Trinidad margin (TC), both methodologies (O'Grady et al., 2000; Petter et al., 2013) suggest changes in sediment supply in a cyclic manner that is most likely associated with episodes of activation of the Orinoco lobes close to the section. A climatic origin is not likely because this cyclicity is not seen in the northern transect (TA).

In the Taranaki Basin, two dip-oriented seismic transects characterized by different tectonic elements (i.e. a graben associated with Pliocene back-arc rifting) were examined in Chapter 2. Although the presence of the graben did promote increases in

clinoform dimensions and in the distribution of sediment, both transects developed very similar first order morphologies through time (linear to oblique to sigmoidal; Chapter 2) because of a common regional tectonic framework. The seismic transects chosen in Trinidad (TA and TC) are characterized by very different tectonic settings (NSD vs. SSD) that made it possible to develop important changes in clinoform morphologies alongstrike, from oblique morphologies in the north to mainly sigmoidal morphologies in the south. These changes are controlled by differences in specific structural elements and sediment supply rates in each of the structural domains: the NSD is very close and highly influenced by the CBTZ, and associated ridges and troughs, whereas the SSD is mostly controlled by changes in the paleo-Orinoco discharge and the activation of local growth faults (Moscardelli et al., 2012). Parts of the shelf margin in eastern offshore Trinidad, and specifically the NSD (e.g., TA), are characterized by bypass zones and can be classified as erosional shelf margins (Ryan et al., 2009; Moscardelli et al., 2012). This complicates the application of procedures such as Adams and Schlager's (2000) and Petter et al.'s (2013) that use the first order geometry of clinoforms to estimate lithology and sediment supply, respectively. In contrast, some areas in the south (e.g., TC) can be classified as accretionary shelf margins (Ryan et al., 2009; Moscardelli et al., 2012) and the application of these methodologies is easier and more reliable because sediment is deposited and preserved in the shelf and slope positions of the margin.

Role of Paleostructures

In the case of the Taranaki Basin, the opening of a graben structure associated with Pliocene back-arc rifting (Northern Graben) generated an increase in accommodation, recorded by the development of clinoforms characterized by higher foresets (Figure 5.2a). Progradation rates were higher at the initial phases of graben development because of redistribution of sediment as accommodation was generated, but

became smaller as the sediment could not fill the space generated by the structure (graben). In the case of Trinidad, a similar situation took place. The presence of the paleocanyon in the NSD (Figure 4.3) allowed the deposition of higher-relief clinoforms with smaller progradation rates (Figure 5.2d) as a result of the increase in accommodation without a simultaneous increase in sediment supply. In fact, sediment flux is apparently smaller than in the southern transect (Figure 5.2f). However, it is important to consider the lack of clinoform preservation in TA and that part of the sediment was deposited in deeper water positions, which could have led to underestimation of sediment flux using the procedure of Petter et al. (2013). The geometric arrangement of the different structural elements in the SSD also has a significant influence on the architecture of the shelf-margin stratigraphic succession in that area. The SSD is characterized by steeper and shorter clinoform packages having sigmoidal morphologies. These characteristics are associated with the gradual activity of growth faults that were responsible for generating accommodation through hanging wall subsidence (Sydow et al., 2003; Moscardelli et al., 2012) and then stored sediment, especially coarse-grained, within the shelf.

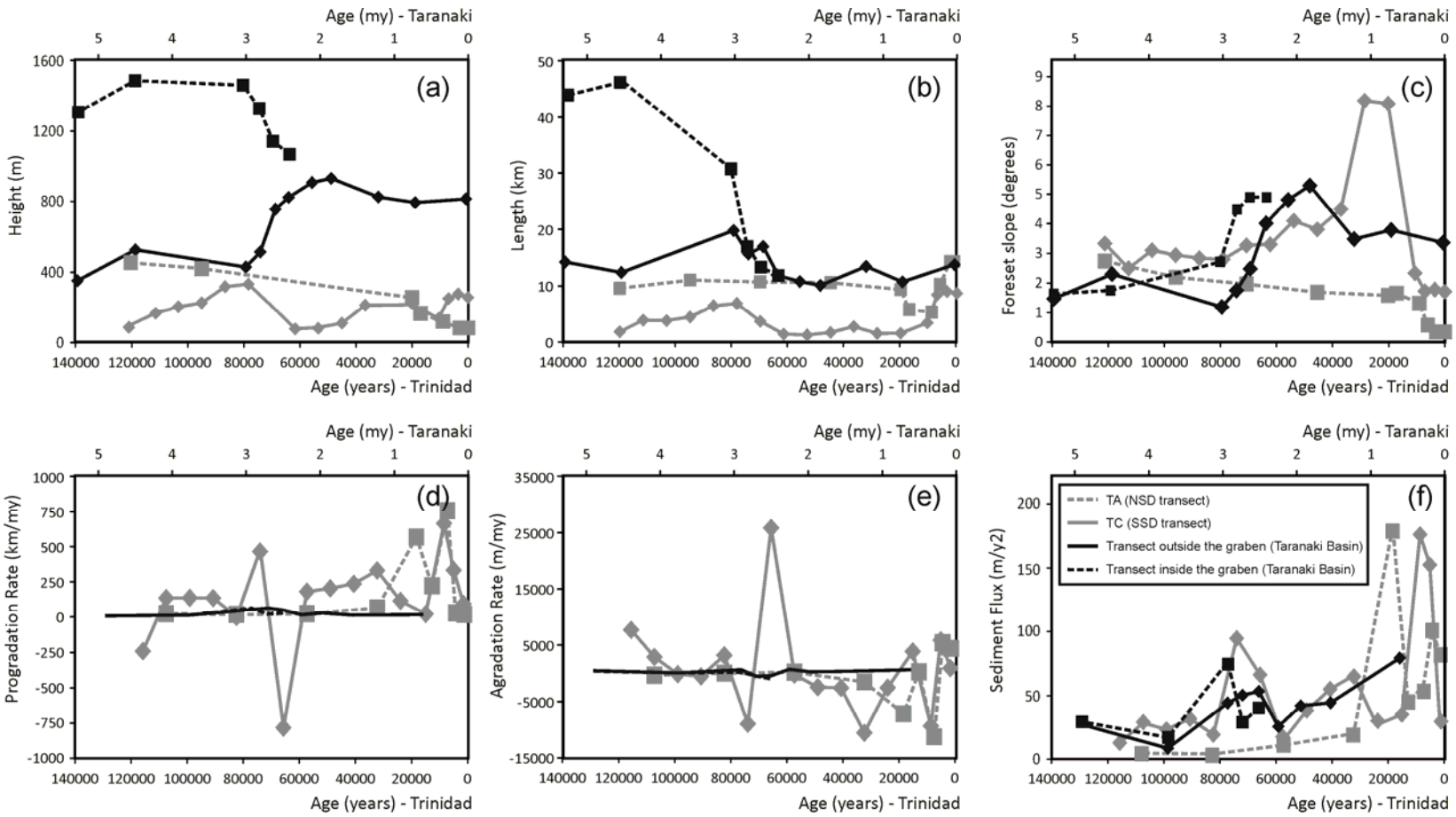

Figure 5.2: Graphs illustrating quantitative relationships of series of morphological parameters through time and their comparison between the eastern Trinidad margin and northern Taranaki Basin. Parameters calculated using measurements of clinoform architectures in seismic transects in the NSD (TA) and in the SSD (TC) include (a) Clinoform heights. (b) Clinoform lengths. (c) Average clinoform foreset inclination values. (d) Progradation rates. (e) Aggradation rates. (f) Sediment flux.

Sediment Flux

Sediment supply played a major role in the Taranaki Basin, especially in the late Pliocene-Pleistocene section (Chapter 3), where high sediment flux sourced by the Southern Alps increased accommodation by means of sediment loading and associated isostatic compensation, and allowed the development of "giant" clinoforms (>700 m). Sediment supply was also fundamental in shaping the architecture of the eastern Trinidad continental margin, and specifically in defining areas of sediment bypass and the time of development of shelf-edge deltas (Chapter 4). Because the Trinidad margin does not have an appropriate age control in the entire section, it is difficult to do a reasonable comparison between sediment flux in the Taranaki and Trinidad margins. However, it can be seen that, in the case of Trinidad, and specifically the SSD, there are three episodes of relatively high sediment flux that might be associated with pulses of activation of the paleo-Orinoco system. The last pulse, which does have age control, is characterized by higher values of sediment flux (up to 175 m^2/y) than those observed in the northern Taranaki Basin (up to 75 m^2/y during the Southern Alps uplifting). This difference can be attributed to two factors. First, the time range used in Trinidad is much smaller than that of the Taranaki Basin. According to Saddler (1981), shorter periods of time will always show higher values of sediment supply due to a higher degree of preservation (Saddler effect). Secondly, high sediment flux in Trinidad indicates the importance of the Orinoco discharge as a source of sediment. In fact, the Orinoco River is categorized as one of the largest rivers in terms of worldwide discharge (Diaz de Gamero, 1996). The Taranaki Basin, on the other hand, is not sourced by one major river, but a series of several small muddy rivers whose discharge was intensified by the Southern Alps uplifting and glacial conditions (Chapter 2).

Figure 5.2f shows the comparison of the values of sediment flux for the northern Taranaki Basin and the eastern Trinidad margin. Except for the youngest section, the Taranaki Basin shows similar values (same order of magnitude), but smaller variations of sediment flux than the Trinidad margin. Higher variations in sediment flux in Trinidad are associated with the different episodes of activation of the Orinoco delta lobes. The much higher values in the youngest interval may be associated with the Saddler effect (Saddler, 1981; Figure 5.2). The highest values of sediment flux in the Taranaki Basin occurred inside the graben structure (Figure 5.2f) when sediment was redistributed inside the graben at the initial phases of opening of the structure.

Indications of Sediment Partitioning

Clinoform trajectories in the Taranaki Basin were used to infer sediment partitioning in the basin, indicating that most sediment moved basinward during the early Pliocene whereas most sediment remained in the shelf in the late Pliocene-Pleistocene (Chapter 2). The presence of the Northern Graben as a localized depocenter also influenced sediment to be stored in this structure. In the eastern Trinidad margin similar features are observed. However, these changes are not observed in the temporal scale, but along strike. Oblique morphologies and flat trajectories in the NSD (Figure 4.3) indicate that an important volume of sediment was likely deposited downdip, in deeper positions of the basin (e.g., mass transport deposits). Underlying structural elements (paleocanyon in the NSD) played a key role in redistributing sediment into deep water positions and the narrowing of the shelf. The SSD, on the other hand, show sigmoidal morphologies (Figure 4.4) that, in conjunction with the generation of accommodation by growth faulting within the shelf, indicate that most sediment was retained on the shelf.

CONCLUSIONS

This study demonstrated that detailed morphological analysis of clinoforms can be an important tool to infer the conditions of sediment transport and deposition in a particular basin and that these observations are valid for different ranges of temporal scales as proven in the Taranaki and eastern Trinidad margins (3^{rd} vs. 4^{th} order systems). Depending on their relative location in the margin, the presence of shelf and upper slope structures can influence sediment movements into deepwater regions or their storage on the shelf. In addition, high sediment flux is a primary control in clinoform morphologies and margin construction. However, it can vary substantially alongstrike (Trinidad case) making it a priority to use a three dimensional approach when evaluating these kind of systems.

CHAPTER 6: INTEGRATION AND IMPLICATIONS OF THIS RESEARCH

INTRODUCTION

Several methodologies have been applied to study the construction of continental margins and sediment delivery to deep water systems. Seismic stratigraphy is one of the most common methods used as a predictive tool, providing information about the distribution of stratal architecture, and their implication in hydrocarbon/reservoir distribution based on seismic data (Vail et al., 1977; Posamentier and Vail, 1988; Van Wagoner et al., 1990). Source to sink approaches are also effective to determine sediment volume distribution and to infer deposition into deeper waters when information of the complete system is provided (Giosan and Bhattacharya, 2005). The analysis of clinoform architectures has also been used to study of continental margin evolution, including estimation of paleo-water depths (e.g., Schlager, 1981; Kominz and Pekar, 2001), estimation of sediment composition (Orton and Reading, 1993; Adams and Schlager, 2000), and sediment partitioning (e.g. analysis of shelf edge trajectories; Johannessen and Steel, 2005; Carvajal and Steel, 2009; Henriksen et al., 2009). This study grouped different methods of clinoform characterization, including quantification of slope morphology (O'Grady et al., 2000; Adams and Schlager, 2000), analysis of shelf edge trajectory, and occurrence of incision to qualitative infer the history of construction of the northern Taranaki Basin margin and potential implication in sediment distribution. The integration with geomorphological analysis using the available 3D dataset allows the interpretation of geological features and depositional environments. In addition, isopach maps allow for establishing relationships between the different stages of margin construction and tectonic elements present in the region. A more quantitative model is proposed through the use of stratigraphic forward modeling techniques such as STRATA.

This methodology provides an alternative to sequence stratigraphic techniques to identify controls other than sea level in clinoform development and the distribution of sands in a specific basin. The advantages of this methodology are that it is based mainly in seismic interpretation and in the detailed description of mainly the shelf edge region. However, its integration with other methodologies such as sequence stratigraphy can lead to a better understanding of the continental margin and avoid misleading conclusions when only one tool is considered.

GENERAL IMPLICATIONS

Results from this study indicate the importance of underlying structures in the development of distinctive clinoform morphologies, location of the shelf edge, and redistribution of sediment within a basin. These results also emphasize the importance of sediment flux on clinoform morphologies. In the Taranaki Basin, sediment flux was key to the development of high relief clinoforms ("Giant" clinoforms) through isostatic compensation. In the eastern Trinidad margin, sediment flux also played an important but different role. Three pulses of high sediment flux associated with the Orinoco river suggest the activation of the system at different times in different areas, and that alongstrike changes can happen in any particular basin where a main river is sourcing the system.

The combination of clinoform morphological analysis, clinoform rollover trajectories analysis, and 3D seismic attribute extraction techniques has great potential in developing qualitative models for the prediction of sand distribution. Therefore, given particular clinoform morphologies, inferences about sand distribution can be made. Figure 6.1 shows a summary of the generalizations that came out of this research. A column represented deepwater seismic facies was not included because of the limited seismic coverage of deepwater positions of the basin, especially towards the northeast.

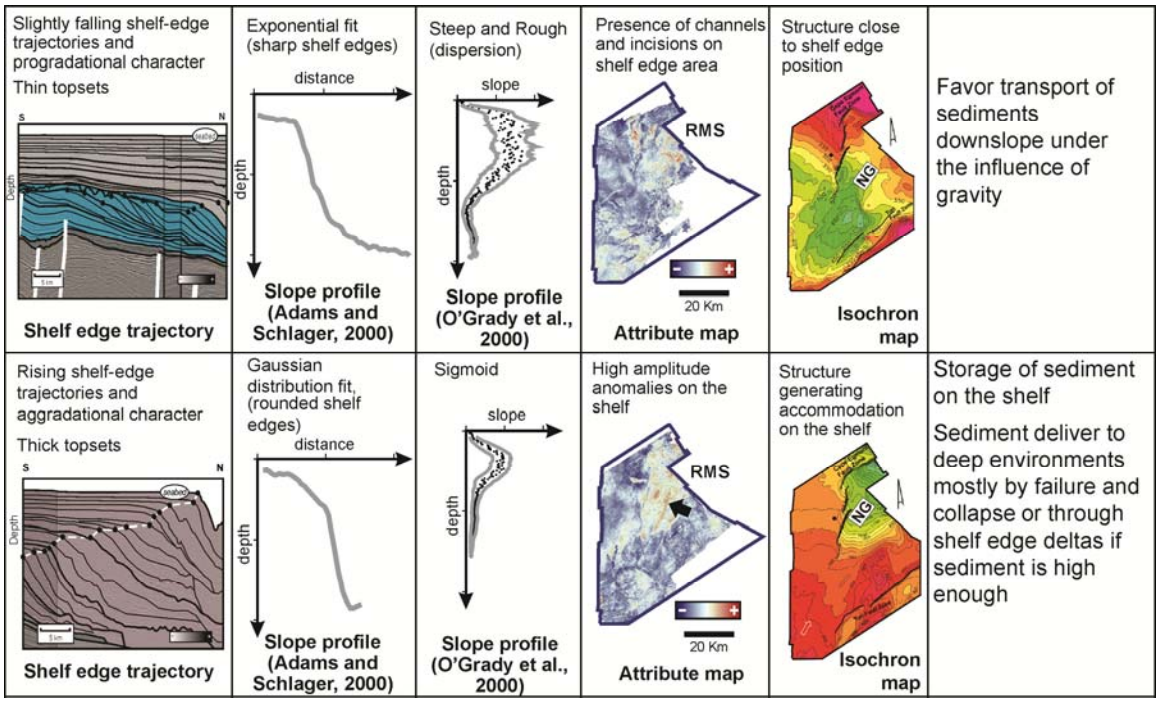

Figure 6.1: Clinoform morphologies that could be potential indicators of deepwater sand delivery.

2D Stratigraphic Forward Modeling and Sediment Distribution

A quantitative model can refine and add predictive power to a conceptual model or show that it is physically impossible. Stratigraphic forward modeling techniques allow us to evaluate the individual effect that sediment supply and generation of accommodation have in margins construction. Different model runs suggest that increases in sediment supply are commonly accompanied by increases in progradation and can play an important role in sediment delivery to deeper water positions in (1) earlier reaching of the shelf edge (even in wide margins; Trinidad Stage 2), and (2) delivery of sediment when accommodation generation is limited (sediment cannot accumulate on the shelf). Without an important contribution of sediment supply it is likely that sediment retreats (Muto and Steel, 2002). Increases in accommodation (simulation of tectonic subsidence) are commonly accompanied by increases in

aggradation and decreases in progradation rates that favor sediment storage on the shelf. If sediment supply is high enough, the resulting clinoforms are usually characterized by progressively steeper clinoforms that can collapse. Modeling techniques also help to determine the conditions needed to develop “giant” clinoforms (>700m) (i.e. high sediment supply and accommodation) and under what specific conditions isostatic compensation can generate enough accommodation.

IMPLICATIONS SPECIFIC TO THE TARANAKI BASIN

This study also allowed a better understanding of the history of the Taranaki Basin. Based on this study, the basin records three types of clinoform morphologies interpreted to be developed during three stages with different conditions of relative sea level, tectonic activity, sediment supply and dominant depositional processes. Stage 1 and 2 clinoforms develop during the lowering of relative sea level. Clinoform morphologies are planar and oblique associated with the abrupt transition between the foresets and bottomsets of these clinoforms. The shelf during Stage 2 is characterized by erosional processes and sediment bypass, suggesting that sediment was delivered to deep-water areas. Stage 3 clinoforms developed during relative sea level rise and highstand periods, and are characterized by slope-confined, erosional features that are not connected with the shelf. The presence of thick topsets and depocenters (graben) on the shelf suggest that most coarse grained sediment was stored on the shelf. This configuration is considered less efficient for sand delivery to the basin floor. Slope collapse and failure was likely the main mechanism of delivery into deep water regions, and muddy deposits are expected.

By comparing three types of clinoforms, I propose a conceptual model which predicts three different styles of slope margin construction in the Taranaki Basin since the Pliocene, with their characteristic depositional internal architectural elements and dominant depositional processes.

Sediment Supply in the Taranaki Basin

Southern Alps uplifting

The southwest migration associated with the advance of the Pacific-Australian plate subduction zone and related uplifting of the Southern Alps in New Zealand's South Island played a key role in the location of sedimentary sources for the Taranaki Basin during the Plio-Pleistocene (Nodder, 1995; King and Thrasher, 1996), and in the deposition of the Giant Foresets Formation. The present mountain ranges of New Zealand emerged only within the last five million years (Dennis, 2009). In fact, the Southern Alps are one of the most rapidly rising mountain ranges in the world (10 mm/yr or more according to Dennis, 2009). On reaching the mountains, moisture-laden air rises, generating heavy rainfall on the west coast of New Zealand, resulting in very rapid rates of weathering and erosion (Tippett and Kamp, 1995; Dennis, 2009). Furthermore, temperate glaciers, such as that on the west side of the New Zealand's South Island, have one of the largest natural sediment yields of any runoff in the world (Milliman and Syvitski, 1992). Modern sedimentation patterns and rates suggest that the west coast of the South Island is presently a major source of sediments deposited on the western North Island shelf via a northeasterly-directed longshore drift sediment transport system (Nodder, 1995). Estimates of the contribution of suspended sediment to the continental shelf by west coast South Island rivers range from 212 x $l0^6$ to 440 x $l0^6$ tonnes/yr (Nodder, 1995), where sediment is derived predominantly from the erosion of the Southern Alps (Adams, 1981). Additional sources of sediment delivered to the Taranaki shelf include deposits from Mount Taranaki and central North Island and the Mesozoic basement rocks of the North Island Axial Ranges (Nodder, 1995). Contributions of suspended sediment to the western continental shelf by North Island rivers is, however,

considerably less than the amounts supplied by South Island fluvial systems (i.e., approximately 9 x $l0^6$ tonnes/yr according to Nodder, 1995).

The southwest migration of the Pacific-Australian plate subduction zone, as well as progressive increase in tectonic uplift and associated Southern Alps relief since ~5 Ma (Tippett and Kamp, 2005) might have triggered a gradual increase in sediment flux from Stage 1 to Stage 3 in the Taranaki Basin. These increases in sediment supply are recorded as changes in clinoform morphologies and reflected in the development of "giant" clinoforms in the basin. Moreover, glacial-interglacial climate changes and mountain glaciations that have occurred in New Zealand since 2.4 Ma may also have contributed to the increase in sedimentation rates during Stage 3 (Tippett and Kamp, 1995).

Action of Waves and Alongshore Currents

One of the implications of the Pleistocene clinoforms (Stage 3) fitting a Gaussian distribution curve is the possibility of strong current action controlling the shelf-edge morphology (Adams & Schlager, 2000). There are several lines of evidence that suggest that current-controlled processes played an important role in the genesis of the Giant Foresets Formation. A section as thick as the Giant Foresets Formation needs high sediment-supply rates to develop; however, New Zealand's North Island during the Plio-Pleistocene was characterized by a lack of large fluvial systems feeding the Taranaki margin. On the other hand, estimates of sedimentation rates on the west coast of the South Island are very high due to the uplifting and erosion of the Southern Alps (Nodder, 1995); therefore a significant percentage of sediments derived from the South Island may have been transported northwards during the Plio-Pleistocene as suspended sediment load or by current-controlled processes. Also, modern oceanographic conditions in the Taranaki Basin favor strong current action, including waves that can reach and affect most of the shelf during major storms (Pratson et al., 2007). A northeasterly-directed

longshore drift sediment-transport system from the South Island's west coast is currently a major source of sediments for the western offshore region of the North Island shelf (Nodder, 1995). This potential modern analogy to the dataset analyzed here suggests that waves and current-controlled processes in general could have played an important role during the deposition of Stage 3 clinoforms, reworking deposits and moving them into deeper, calmer waters where they accumulated. Finally, oceanographic conditions may have been even more favorable for current action during the mid-Pleistocene Climate Transition (~0.9 Ma). There is evidence that this time was marked by a northward migration of the Sub-Tropical Front closer to the North Island (Hayward et al., 2012; see their Fig. 9), the absence of the Cook Strait to deviate currents into the south coast of the North Island, and the presence of major rivers that carried huge loads of sediment to the edge of the continental shelf during the glacial period (Hayward et al., 2012).

RECOMMENDATIONS

The use of this methodology was successfully applied in the eastern Trinidad margin to infer controls on clinoform morphologies in a different margin. It is recommended to apply the methodology in margins with other tectonic regimes (e.g., foreland basin) to generate a more complete database and establish generalizations (e.g., correlations between sand distribution and clinoform trajectory, topset thickness, margin width, and the presence of erosional features in the shelf edge margin).

Because of the lack of information of deepwater facies in the Taranaki Basin, direct correlations of observation and deposition of deepwater sands were not possible. It is suggested to apply this methodology in areas where seismic information can image deepwater fan facies and/or their presence is corroborated by well information.

APPENDIX A: CHRONOSTRATIGRAPHIC FRAMEWORK

Previous chronostratigraphic interpretations based on biostratigraphic data from four wells (Taimana-1, Arawa-1, Witiora-1, and Kanuka-1) located within the study area were available for this study (Crundwell et al., 1992; Hoskins and Raine, 1984; Morgans, 1984; Hansen and Kamp, 2004; Morgans, 2006; Crundwell, 2008). However, some of the well picks that were linked to absolute ages were not compatible with sub-regional seismic correlations because several mismatches were identified during the mapping process. Reports of similar misties have been documented in the past by a variety of other researchers working in this area (e.g., Hansen and Kamp, 2004; Morgans, 2006). This conflict was bypassed by applying a simplified approach in which the use of bioevents was adopted instead of using absolute ages. Bioevents are recognizable where there is a significant change in the composition of fossil assemblages over a relative short period of time (Sageman et al., 1997; Zhang and Barnes, 2004). Bioevents were identified by examining foraminiferal distribution charts from four exploratory wells (Hoskins and Raine, 1984; Crundwell et al., 1992; Morgans, 1984; and Crundwell, 2008). On this revision, I decided to use first downhole appearances (FDHA) of microfossils to define bioevents, because the samples within the Plio–Pleistocene interval came from well cuttings and this practice would avoid misleading interpretations triggered by potential sample contamination (Morgans, 2006). The age of occurrence was determined using the chart of late Miocene–Pleistocene planktonic and benthic foraminiferal events by Crundwell et al. (2004).

Four main bioevents were identified in each well (Table A.1) and correlated across the seismic data (Figure A.1). Bioevent 1 (FDHA Globorotalia sphericomiozea) corresponds to the Pliocene-Miocene boundary (~5.28 Ma) and coincides with surface Sa

(base of SU1) (Figure A.1). Bioevent 2 (FDHA Globorotalia pliozea) coincides with surface Sb (top of SU1) in well Kanuka-1 and is very close to the same surface (Sb) in other well locations. According to Crundwell et al. (2004), Bioevent 2 is equivalent to the 4.48 Ma marker. Bioevent 3 (FDHA Cibicides molestus) presents a good match with surface Sc in all wells except for well Arawa-1 (Figure A.1). Surface Sc (Bioevent 3) defines the top of clinoform package SU2 and its estimated age is 3.0 Ma. In well Arawa-1, the FDHA of Cibicides molestus (Bioevent 3) is reported in a slightly deeper position than the FDHA of Globorotalia pliozea (Bioevent 2). This -18 m depth difference between Bioevents 2 and 3 (see Table A.1) is considered to be a minor mistie that is probably related to the significant reduction in thickness in this location (most likely indicative of erosion and reworking), as well as to the proximity to a fault zone to the northwest that could have caused sampling issues (Figure A.1). Bioevent 4 (2.45 Ma) was interpreted on the basis of the occurrence of a dextral coiling event that affected the Globorotalia crassaformis zone and that was well documented in all wells. Some challenges were encountered when trying to correlate Bioevent 4 from wells Arawa-1 and Taimana-1 to well Kanuka-1 to the northwest (Figure A.1). Wells Arawa-1 and Taimana-1 show the top of the Globorotalia crassaformis zone (dextral coiling) occurring within seismic unit SU4, whereas well Kanuka-1 shows this same marker occurring within seismic unit SU5. This mismatch on the correlation of Bioevent 4 (top dextral Globorotalia crassaformis) was caused by the proximity of the southern wells (Arawa-1, Taimana-1, and Witiora-1) to a sediment bypass zone where increased erosion most likely caused reworking of the fauna and misplacement of FDHAs (Figure A.1). This difficulty was arbitrarily resolved by correlating Bioevent 4 (top dextral Globorotalia crassaformis) with surface Sf (top of clinoform package SU5), becausewell Kanuka-1 is located in an area where sediment bypass did not prevent preservation of the stratigraphic

succession and it is likely that this biostratigraphic event might be "in situ" in this location.

Bioevent number	Bioevent	Estimated Age (according to Crundwell et al. 2004)	Witiora-1	Taimana-1	Arawa-1	Kanuka-1
	Topmost foraminiferal sample	Variable	220m	220 m	665m	550m
5	Plio/Pleistocene	1.8 Ma	Not Available	706 m	670 m	690 m
4	Top Dextral *Globorotalia crassaformis*	2.45Ma	700m	920 m	1015m	1040m
3	FDHA *Cibicides molestus*	3.0Ma	1000m	1180 m	1542m	1630m
2	FDHA *Globorotalia pliozea*	4.48Ma	1060m	1470 m	1524m	1740m
1	FDHA *Globorotalia sphericomiozea*	5.28Ma	1220m	1580 m	1800m	1760m

Table A.1: Bioevents identified in key wells.

In general, the identification of bioevents facilitated the estimation of relative ages within the Pliocene section (2.4–5.3 Ma) and it also helped establish an appropriate framework for key surfaces that were interpreted using seismic data. However, age estimation within the younger stratigraphic succession (<2.4 Ma) was challenging because of the scarcity of biomarkers and the absence of proper sampling. The initial approach was to divide the younger section (<2.4 Ma) by the number of interpreted clinoforms; however, abnormally high rates of aggradation (~2,000 m/my) were obtained for this interval (SU9), thus I decided to discard this approach. Instead, I incorporated the

Pliocene/Pleistocene boundary as reported in previous studies (Morgans, 2006) to constrain age estimations without generating anomalous sedimentation rates. Surface Sh (top seismic unit SU7) appears to be the best approximation for this Pliocene/Pleistocene boundary. Levels of uncertainty for the Pleistocene section increased because no biomarkers were reported for this interval. The only option for the Pleistocene unit was to divide the remaining time by the total number of observed clinoforms so that an estimated age control could be assigned.

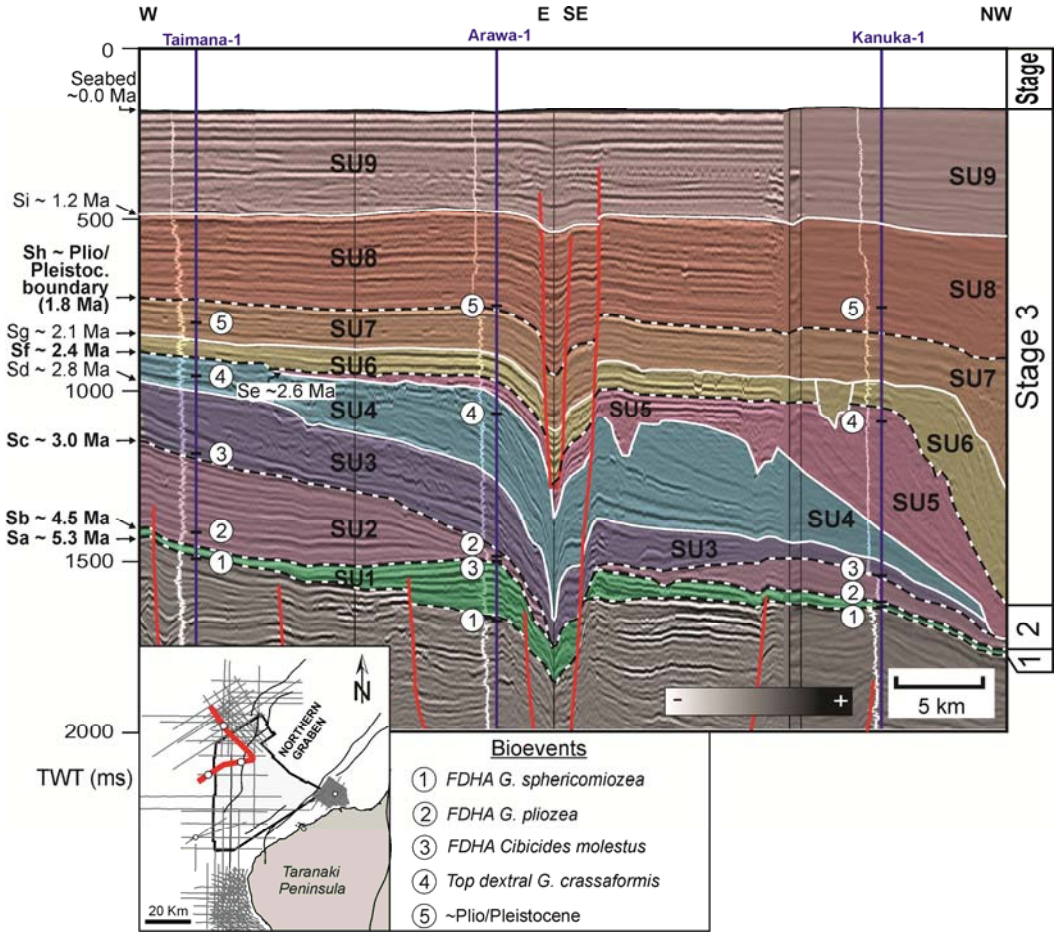

Figure A.1: Composite seismic line connecting wells containing key biostratigraphic information (Taimara-1, Arawa-1, and Kanuka-1). Numbers indicate first biostratigraphic downhole appearances, used to define bioevents (see text for discussion). Dotted lines indicate correlation, calculated using seismic data, of bioevents across study area.

APPENDIX B: REGIONAL PALEOGEOGRAPHIC MAPS

Paleogeographic maps generated by King and Thrasher (1996), Hansen and Kamp (2002) and Baur (2012) were integrated with the northern Taranaki Basin results (this study) to produce paleographic maps of the entire Taranaki Basin. These maps show the approximate migration of both the shoreline and paleoshelf edge through time (Figure B.1 to B.4). Paleodepths were interpreted using biostratigraphic analysis of well of the area (Appendix A). The sedimentary characteristics and the presence and location of different depositional elements (channels, incised valleys, canyons and submarine fans) are inferred using seismic facies analysis and information from wells (i.e. well logs and lithostratigraphy) when present. Location of the shelf, canyons and channels are shown where observed in seismic; however, their extension was inferred where not seismic available. One common element is that the main sediment source is located in the south (Southern Alps; King and Thrasher, 1996; Baur, 2012). This study allowed a more detailed interpretation of the northeastern region of the maps, and they emphasize the importance of paleostructures located in the shelf and slope regions in shaping the shelf edge and in distributing sediment into deep water.

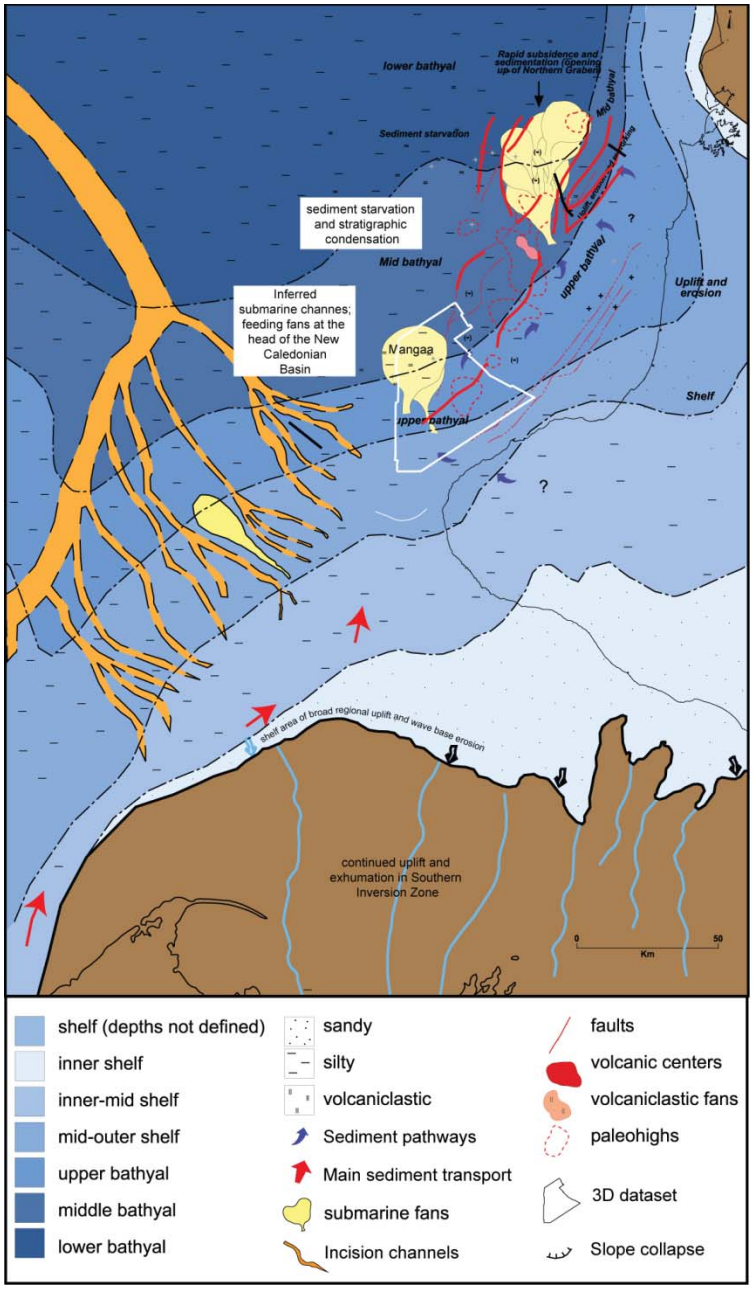

Figure B.1: Paleogeographic interpretation of Taranaki Basin during deposition of Stage 1 (~5.0 Ma). Diversion of gravity flows are deposited in this stage (e.g., Mangaa Formation). The Northern Graben was active in north to the study area, constraining the location of submarine fans. There is a progressive southward migration of extension and volcanism (modified from King and Thraser, 1996; Hansen and Kamp, 2002 and Baur, 2012).

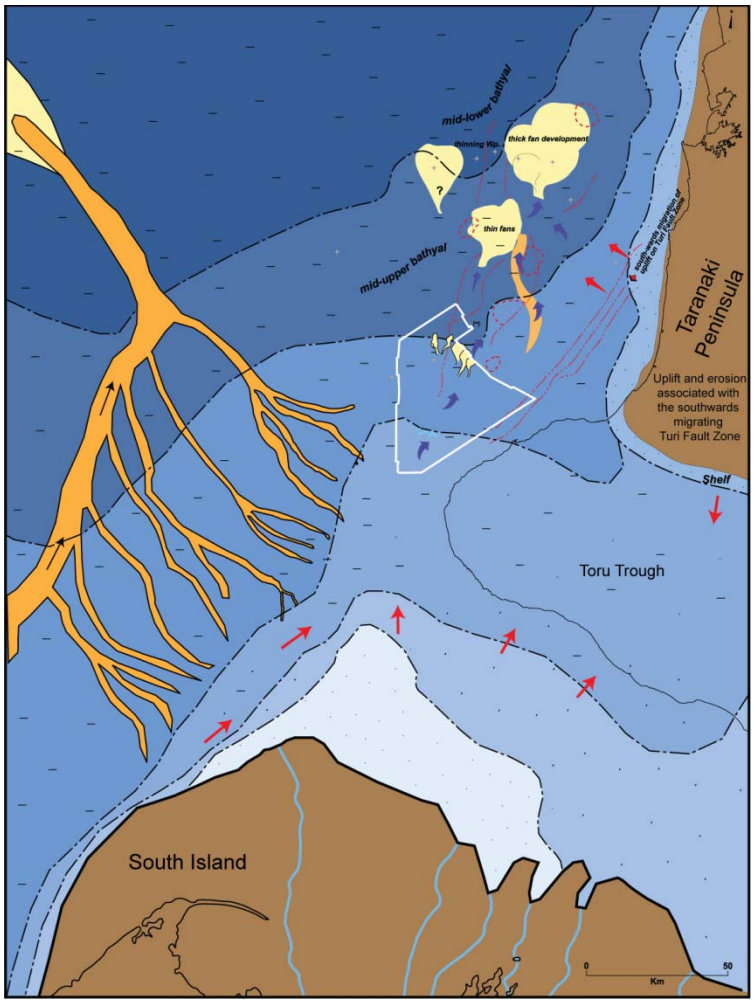

Figure B.2: Paleogeographic interpretation of Taranaki Basin during deposition of Stage 2A (~3.0 Ma). Colors and symbols are according to Figure B.1. This stage is characterized by deposition of gravity flows in the Northern Graben and the subsidence of the Toru Trough towards the east. This structure takes most of the sediment delivered by the Taranaki Peninsula (modified from King and Thraser, 1996; Hansen and Kamp, 2002 and Baur, 2012).

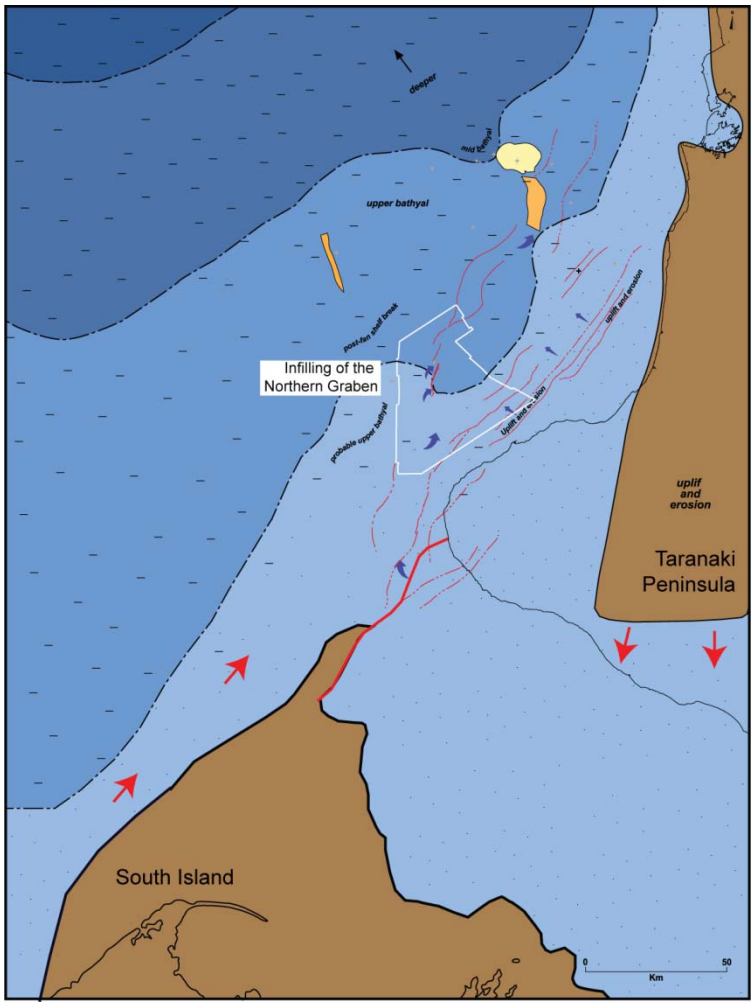

Figure B.3: Paleogeographic interpretation of Taranaki Basin during deposition of Stage 2B (~2.6 Ma). Colors and symbols are according to Figure B.1. Onset of rapid shelf margin progradation is recorded during lowstand conditions. The Northern Graben is filled in the study area and possible deposition of submarine fans is inferred in northern positions, where there is still accommodation associated with the structure. Most sediment is sourced from the South Island, most sediment from the Taranaki Peninsula is transpoted southward (modified from King and Thraser, 1996; Hansen and Kamp, 2002 and Baur, 2012).

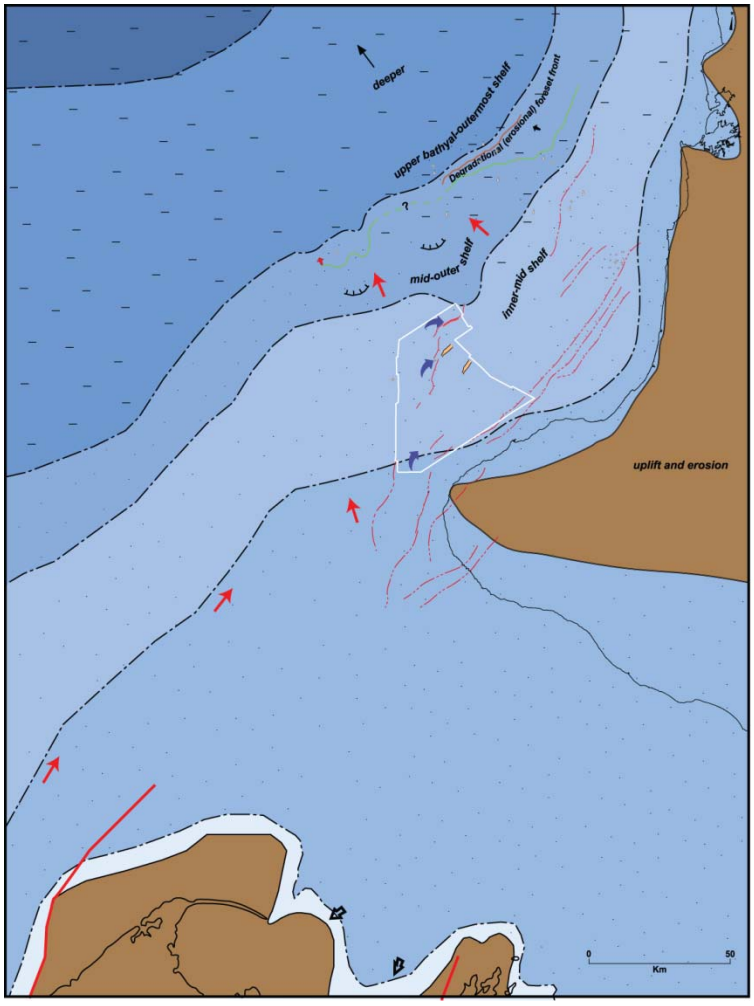

Figure B.4: Paleogeographic interpretation of Taranaki Basin during deposition of Stage 3 (~1.5 Ma). Colors and symbols are according to Figure B.1. A rapid shelf margin progradation is observed when compared with Stage 2. Presence of incisions in the slope are common associated with slope failure and collapse. Reactivation of Northern Graben generates a deposcenter on the shelf that allows deposition along the graben axis (modified from King and Thraser, 1996; Hansen and Kamp, 2002 and Baur, 2012).

APPENDIX C: STRATIGRAPHIC FORWARD MODEL TYPES

GEOMETRIC MODELS

These models do not describe the process itself, but the geometric results of the process associated with the total or partial infill of accommodation (Griffiths, 2001). At the onset of the simulation, geometric models predefine equilibrium profiles of sediment distribution that are then modified by the competing effects of changing sea level, tectonic subsidence or uplift, residual slope, and sediment supply (Jervey, 1988; Reynolds at al. 1991; Pirmez et al., 1998). The simplest predetermined sediment profile is a horizontal plane at sea level that captures only the effects of subsidence in governing stratal geometries (rigid-lid models; Sloss, 1962). Sloss (1962) developed models in a conceptual basis for situations where the relationship between volume of supplied sediment and rate of subsidence varied, demonstrating that variations in sediment supply could generate both regressive and transgressive patterns. Harbaugh and Bonham-Carter (1970) provided a mathematical treatment of Sloss' (1962) conceptual model with the basic premise that mass is conserved in the system. Over the years additional constraints were added (e.g., Pitman, 1978; Jervey, 1988; Ross et al., 1995; Liu et al., 1998; Csato & Kendall, 2002).

Geometric models have been very useful to understand the effects of sea level, sediment supply, and tectonics at the continental margin scale. However, assuming predefined clinoform shapes, these models forfeit formative constraints provided by clinoform geometries (Pirmez et al., 1998). Additionally, they are unable to describe the physical processes that determine small-scale stratal geometries (Jordan and Flemings, 1991; Pirmez et al., 1998; Paola, 2000).

HYDRAULIC MODELS

Hydraulic models (also called process-based models) are derived from the equations of fluid flow (Syvitski et al., 1988; Tezlaff and Harbaugh, 1989). Most of these models are based on solutions of the Navier-Stokes equations describing flow in three dimensions for an isotropic Newtonian fluid (uniform properties in all directions and follows Newton's laws of motion; Tezlaff and Harbaugh; 1989). Sediment transport is a function of the transport capacity of the fluid and effective sediment concentration (Griffiths, 2001).

This type of models have proven to be powerful tools to understand several sedimentary processes and has been successfully applied to simulate specific depositional settings, especially in the reservoir scale, modeling the physical flow processes to a high degree of detail (Syvitski et al., 1988; Tetzlaff, 2005). However, the application of these models is limited because of the necessity to specify a large number of input parameters and they may make computationally intensive to simulate flow and sediment transport in the continental margin scale (Pirmez et al., 1998).

DIFFUSION MODELS

Diffusion-based models (also called topographic-control or potential-gradient models) are derived from the equations of slope-driven motion and conservation of mass (Flemings and Grotzinger, 1996; Paola, 2000). They assume that erosion, transport and deposition occur via linear diffusion, which means that sediment transport is proportional to the topographic slope (Kenyon and Turcotte, 1985; Flemings and Jordan, 1989; Jordan and Flemings, 1991; Flemings and Grotzinger, 1996). These models can successfully reproduce the filling of a basin and the development of a wide range of clinoform architectures, using a few assumptions and simple equations (Jordan and Flemings, 1991; Paola et al., 1992; Flemings and Grotzinger, 1996; Pirmez et al., 1998; Paola, 2000). The

diffusivity or transport coefficient (K) refers to the efficiency with which mass is transported over a given topographic slope (Flemings and Grotzinger, 1996; Kaba, 2004). It presents lower values in the erosional than in the depositional area. One limitation of diffusion-based models is that, although slope-driven processes (e.g., creep, sliding, and slumping; Pirmez et al., 1998) can certainly contribute to sediment distribution, they are not always the main process in the deposition of many clinoform systems (Pirmez et al., 1998).

In these models, the transport of sediment, or flux, is proportional to the slope (Flemings and Grotzinger, 1996). When combined with the assumption of conservation of mass, the result is the diffusion equation:

$$\frac{\partial h}{\partial t} \quad \text{(mass flux)} = K \frac{\partial^2 h}{\partial x^2} \quad (1)$$

h is elevation, *t* is time, *K* is the diffusivity coefficient, x is horizontal position and ($\delta^2 h/\delta x^2$) defines the local change on slope. This equation states that deposition or erosion is proportional to the change in local topographic slope. This equation can produce a broad range of stratal geometries that result from variations in initial and boundary conditions. The disadvantage of the diffusion-based models is that it is a gross approximation of sediment transport behavior, not considering other processes such as currents. This approach has been applied in a wide variety of depositional settings, including fluvial and deltaic environments (Begin et al.,1981; Kenyon and Turcotte, 1985; Paola et al., 1992), evolving foreland basins (Jordan and Flemings, 1991) and marine settings (Kaufman et al.,1991).

These types of models are very useful at larger scales including simulations of stratal geometries in semi-regional seismic sections because they only have a few assumptions and use simple equations. However, they also have some limitations such as

the use of diffusion coefficients, which are parameters hard to define and relate to physical processes. Additionally, diffusion models can only model slope-driven processes (e.g., creep, sliding, and slumping; Pirmez et al., 1998). Areas whose predominant controls are others (e.g., waves and currents) might not be reproduced by these models.

REFERENCES

Adams, E.W., 2001, Subaquatic slope curvature and its relation to sedimentary processes and sediment composition [Ph.D. thesis]: Amsterdam, Vrije Universiteit, 135 p.

Adams, E.W., and W. Schlager, 2000, Basic types of submarine slope curvature. Journal of Sedimentary Research, v. 70, no. 4, p. 814–828.

Allen, P.A., and Allen, J.R., 2005, Basin analysis: Principles and applications: Oxford, Blackwell Scientific Publications, 549 p.

Allis R.G., Funnell, R., and Zhan X., 1998, From basins to mountains and back again: NZ basin evolution since 10 Ma, in Proceedings, 9th International Symposium on Water-Rock Interaction, Taupo, New Zealand, p. 3–7.

Alvarez, T. G., 2008, Tectonic geomorphology of the eastern Trinidad shelf: Implications for influence of structure on reservoir distribution and nature in older basin fill: Master's thesis, University of Texas at Austin, Austin, Texas, 237 p.

Bache, F., Sutherland, R., Stagpoole, V.M., Herzer, R.H., Collot, J., and Rouillard, P., 2012, Stratigraphy of the southern Norfolk Ridge and the Reinga Basin: A record of initiation of Tonga-Kermadec-Northland subduction in the southwest Pacific: Earth and Planetary Science Letters, v. 321–322, p. 41–53.

Bates, R., and Heid, M., 2007, Kanuka-1 well completion report: Crown Minerals, Ministry of Economic Development open-file report PR 3843, 91 p.

Baur, J.R., 2012, Regional seismic attribute analysis and tectono-stratigraphy of offshore South-Western Taranaki Basin, New Zealand [Ph.D. dissertation]: Wellington, Victoria University of Wellington, 373 p.

Baur, J.R., Sutherland, R., and Stern, T., 2013, Anomalous passive subsidence of deep-water sedimentary basins: A prearc basin example, southern New Caledonia Trough and Taranaki Basin, New Zealand: Basin Research, v. 25, p. 1–27.

Begin, S. B., Meyer, D. F., and Schumm, S. A., 1981, Development of longitudinal profiles of alluvial chan nels in response to base-level lowering: Earth Surface Processes and Landforms, v. 6, p. 49–98.

Boyd, R., Ruming, K., Goodwin, I., Sandstrom, M., and Schroder-Adams, C., 2008, Highstand transport of coastal sand to the deep ocean: A case study from Fraser Island, southeast Australia: Geology, v. 36, p. 15–18.

Burgess, P.M., Lammers, H., van Oosterhout, C., and Granjeon D., 2006, Multivariate sequence stratigraphy: Tackling complexity and uncertainty with stratigraphic forward modeling, multiple scenarios, and conditional frequency maps: American Association of Petroleum Geologists Bulletin, v. 90, p. 1–19.

Cardona, P.A., 2009, Depositional history of the Taranaki Basin, New Zealand: Linking sediment accumulation and subsidence rates to tectonic processes [M.Sc. thesis]: The University of Texas at Austin, 106 p.

Carvajal, C., and Steel, R.J., 2009, Shelf-edge architecture and bypass of sand to deepwater: Influence of sediment supply, sea level, and shelf-edge processes: Journal of Sedimentary Research, v. 79, p. 652–672, doi: 10.2110/jsr.2009.059.

Cathro, D.L., Austin, J.A., Jr., and Moss, G.D., 2003, Progradation along a deeply submerged Oligocene-Miocene heterozoan carbonate shelf: How sensitive are clinoforms to sea-level variations?: American Association of Petroleum Geologists Bulletin, v. 87, no. 1, p. 1547–1574.

Crundwell, M.P., 2008, Biostratigraphy and paleoenvironmental study of Kanuka-1 offshore well, Taranaki Basin: (PEP 38488) GNS Science Consultancy Report 2008/21, 64 p.

Crundwell, M.P., Beu, A.G., Morgans, H.E.G., Mildenhall, D.C., and Wilson, G.S., 2004. Chapter 12, Miocene. In Cooper, R.A. (ed.) 2004. The New Zealand Geological Timescale. Institute of Geological and Nuclear Sciences Monograph 22. 284 p.

Crundwell, M.P., Scott, G.H., and Strong, C.P., 1992, Biostratigraphy of Arawa-1 offshore petroleum exploration well, North Taranaki Basin: DSIR GEO Contract Report 1992/18, 49 p.

Csato, I. & Kendall, C.G.St.C., 2002. Modeling of stratigraphic architectural patterns in extensional settings-toward a conceptual model. Computers and Geosciences, 28, 351-356.

Dennis, A., 2009. Mountains: South Island mountains. Te Ara: the Encyclopedia of New Zealand, updated 1-Mar-09 URL: http://www.TeAra.govt.nz/en/mountains/1

Diaz de Gamero, M. L., 1996, The changing course of the Orinoco River during the Neogene: A review: Paleogeography, Paleoclimatology, Paleoecology, v. 123, p. 385-402, doi:10.1016/0031-0182(96)00115-0.

Flemings, P.B., and Grotzinger, J.P., 1996, STRATA: Freeware for analyzing classic stratigraphic problems: GSA Today, v. 6, no. 12, p. 1–7.

Flemings, P.B., and Jordan, T.E., 1989, A synthetic stratigraphic model of foreland basin development: Journal of Geophysical Research, v. 94, p. 3851-3866. Se puede quitar

Garciacaro, E., P. Mann, and A. Escalona, 2011, Regional structure and tectonic history of the obliquely colliding Columbus foreland basin, offshore Trinidad and Venezuela: Marine and Petroleum Geology, v. 28, p. 126–148, doi:10.1016/j.marpetgeo.2009.08.016.

Georgiopoulou, A., Benetti, S., Shannon, P.M., Haughton and McCarron, S., 2011, Gravity flow deposits in the deep rockfall trough, northeast Atlantic, in Yamada, Y., Kawamura, K., Ogawa, Y., Urgeles, R., Mosher, D., Chaytor J., and Strasser M., eds. Submarine mass movements and their consequences: 5th International Symposium, Springer, Netherlands, p. 695–707.

Giba, M., Nicol, A., and Walsh, J.J., 2010, Evolution of faulting and volcanism in a back□arc basin and its implications for subduction processes: Tectonics, v. 29, TC4020, doi:10.1029/2009TC002634.

Giba, M., Walsh, J.J., and Nicol, A., 2012, Segmentation and growth of an obliquely reactivated normal fault: Journal of Structural Geology, v. 39, p. 253–267, doi: 10.1016/j.jsg.2012.01.004.

Giosan, L., and Bhattacharya, J.P., (editors), 2005, River Deltas: Concepts, Models and Examples, SEPM Special Publication, v.83, 502p.

Griffiths, C.M., 2001, Brief review of stratigraphic forward modeling: CSIRO Petroleum, p. 22.

Hansen, R.J., and Kamp, P.J.J., 2002, Evolution of the Giant Foresets Formation, northern Taranaki Basin, New Zealand: New Zealand Petroleum Conference proceedings, p. 419–435.

Hansen, R.J., and Kamp, P.J.J., 2004, Re-evaluation of the late Neogene biostratigraphy of Arawa-1, Ariki-1, Kora-1, and Wainui-1, and integrated seismic and biostratigraphic correlation of 11 wells, northern Taranaki Basin: Wellington, Ministry of Economic Development, Crown Minerals, Petroleum Report PR2938, 39 p.

Haq, B.U., Hardenbol, J., and Vail, P.R., 1987, Chronology of fluctuating sea levels since the Triassic: Science, v. 235, p. 1156–1167.

Hayward, B.W., Sabaa, A.T., Kolodziej, A., Crundwell, M.P., Steph, S., Scott, G.H., Neil, H.L., Bostock, H.C., Carter, L. and Grenfell, H.R., 2012, Planktic Foraminifera-based sea-surface temperature record in the Tasman Sea and history of the Subtropical Front around New Zealand, over the last one million years. Marine Micropaleontology, 82–83, 13–27.

Helland-Hansen, W., and Hampson, G.J., 2009, Trajectory analysis: Concepts and applications: Basin Research, v. 21, p. 454–483.

Henriksen, S., Hampson, G. J., Helland-Hansen, W., Johannessen, E. P. and Steel, R. J., 2009, Shelf edge and shoreline trajectories, a dynamic approach to stratigraphic analysis. Basin Research, 21, 445–453.

Henriksen, S., Helland-Hansen, W. and Bullimore, S., 2011, Relationships between shelf-edge trajectories and sediment dispersal along depositional dip and strike: a different approach to sequence stratigraphy. Basin Research, 23, 3–21.

Holt, W.E., and Stern, T.A., 1991, Sediment loading on the western platform of the New Zealand continent: Implications for the strength of a continental margin: Earth and Planetary Science Letters, v. 107, p. 523–538.

Holt, W.E., and Stern, T.A., 1994, Subduction, platform subsidence, and foreland thrust loading; the late Tertiary development of Taranaki Basin, New Zealand: Tectonics, v. 13, p. 1068–1092.

Hoskins, R.H., and Raine, J.I., 1984, Biostratigraphy of Taimana-1, Lower Hutt, New Zealand Geological Survey: New Zealand Geological Survey report PAL 74, 22 p.

Hubbard, S.M., Fildani, A., Romans, B.W., Covault, J.A., and McHargue, T.R., 2010, High relief clinoform development: insights from outcrop, Magallanes Basin, Chile: Journal of Sedimentary Research, v. 80, p. 357–375.

Hubble, T., Yu, P., Airey, D., Clarke, S., Boyd, R., Keene, J., Exon, N., Gardner, J. and Party, S., 2011, Physical properties and age of continental slope sediments dredged from the eastern Australian continental margin—Implications for timing of slope failure, in Yamada, Y., Kawamura, K., Ogawa, Y., Urgeles, R., Mosher, D., Chaytor J., and Strasser M., eds. Submarine mass movements and their consequences: 5th International Symposium, Springer, Netherlands, p. 43–54.

Jervey, M.T., 1988, Quantitative geological modeling of siliciclastic rock sequences and their seismic expression, in Wilgus, C.K, Hastings, B.S., Ross, C.A., Posamentier, H.W., Van Wagoner, J.C., and Kendall, C.G.St.C., eds., Sea-level changes: An integrated approach: Society of Economic Paleontologists and Mineralogists Special Publication, v. 42, p. 47–69.

Johannessen, E.P., and Steel, R.J., 2005, Shelf-margin clinoforms and prediction of deepwater sands: Basin Research, v. 17, p. 521–550.

Jordan, T.E., and Flemings, P.B., 1991, Large-scale stratigraphic architecture, eustatic variation, and unsteady tectonism: A theoretical evaluation: Journal of Geophysical Research, B, Solid Earth and Planets, v. 96, no. 4, p. 6681–6699.

Kaba, C., 2004, Reconstructing long-term sediment flux from the Brooks Range, Alaska, using shelf edge clinoforms [M.S. thesis]: Cambridge, Massachusetts Institute of Technology, 75 p.

Kaufman, P., Grotzinger, J. P., and McCormick, D. S., 1991, Depth-dependent diffusion algorithm for simulation of sedimentation in shallow marine depositional systems, in Franseen, E. K., et al., eds., Sedimentary modeling: Computer simulations and methods for improved parameter definition: Kansas Geological Survey Bulletin 233, p. 491–508.

Kenyon, P.M., and Turcotte, D.L., 1985, Morphology of a delta prograding by bulk sediment transport: Geological Society of America Bulletin, v. 96, p. 1457–1465.

Kertznus, V., and B. Kneller, 2009, Clinoform quantification for assessing the effects of external forcing on continental margin development: Basin Research, v. 21, p. 738–758.

King, P.R. and Robinson, P.H., 1988, An overview of Taranaki Region geology, New Zealand. Energy Exploration and Exploitation, v. 6, p. 213–232.

King, P.R., and Robinson, P.H., 1988, An overview of Taranaki region geology, New Zealand: New Zealand Oil Exploration Conference (1987: Wairakei): Energy Exploration and Exploitation, v. 6, no. 3, p. 213–232.

King, P.R., and Thrasher, G.P., 1992, Post-Eocene development of the Taranaki Basin, New Zealand: Convergent overprint of a passive margin, in Watkins, J.S., Zhiqiang, F., and McMillen, K.J., eds., Geology and geophysics of continental margins: American Association of Petroleum Geologists Memoir 53, p. 93–118.

King, P.R., and Thrasher, G.P., 1996, Cretaceous-Cenozoic geology and petroleum systems of the Taranaki Basin, New Zealand: Institute of Geological Nuclear Sciences, Monograph 13, 244 p.

Kominz, M.A. and Pekar, S.F., 2001, Oligocene eustasy from two-dimensional sequence stratigraphic backstripping: Geological Society of America Bulletin, v. 113, p. 291–304.

Lisiecki, L.E., and M.E. Raymo, 2005, A Pliocene-Pleistocene stack of 57 globally distributed benthic □18O records. Paleoceanography, 20, PA1003.

Liu, K., Liang, T.C.K., Peterson, L., and Kendall, C.G.St.C., 1998, Computer simulation of the influence of basin physiography on condensed section deposition and maximum flooding surface: Sedimentary Geology, v. 122, p. 181-191.

Maher, J. A., 2007, Architecture and seismic geomorphology of shelf edge deltas along an active tectonic margin, eastern onshore Trinidad: Master's thesis, University of Texas at Austin, Austin, Texas, 144 p.

Martinsen, O.J., and Helland-Hansen, W., 1995, Strike variability of clastic depositional systems: Does it matter for sequence-stratigraphic analysis?: Geology, v. 23, no. 5, p. 432–442.

McKenzie, D.P., 1978, Some remarks on the development of sedimentary basins: Earth and Planetary Science Letters, v. 40, p. 25–32, doi: 10.1016/0012-821X(78)90071-7.

Miall, A.D., 1986, Eustatic sea level changes interpreted from seismic stratigraphy: a critique of the methodology with particular reference to the North Sea Jurassic record: American Association of Petroleum Geologists Bulletin, v. 70, p. 131–137.

Miller, K.G., Kominz, M.A., Browning, J.V., Wright, J.D., Mountain, G.S., Katz, M.E., Sugarman, P.J., Cramer, B.S., Christie-Blick, N., and Pekar, S.F., 2005, The Phanerozoic record of global sea-level change: Science, v. 310, p. 1293–1298.

Milliman, J.D., and Syvitski, J.P.M., 1992, Geomorphic/tectonic control of sediment discharge to the ocean: the importance of small mountainous rivers: The Journal of Geology, v. 100, p. 525–544.

Mitchum, R.M., Jr., Vail, P.R., and Sangree, J.B., 1977, Seismic stratigraphy and global changes of sea levels; Part 6, Stratigraphic interpretation of seismic reflection

patterns in depositional sequences, in Payton, C.E., ed., Seismic stratigraphy—Applications to hydrocarbon exploration: American Association of Petroleum Geologists Memoir 26, p. 117–133.

Mitchum, R.M., J.B. Sangree, P.R. Vail, and W.W. Wornardt, 1993, Recognizing sequences and systems tracts from well logs, seismic data, and biostratigraphy: Examples from the Late Cenozoic of the Gulf of Mexico: AAPG Memoir 58, p. 163–197.

Mitchum, R. and Vail, P., 1977, Seismic stratigraphy and global changes of sea level, part 7: seismic stratigraphic interpretation procedure, in Payton C. E., ed., Seismic Stratigraphy Applications to Hydrocarbon Exploration, American Association of Petroleum Geologists Memoir, v. 26, p. 135–143.

Molnar, P., and P. England, 1990, Late Cenozoic uplift of mountain ranges and global climate change: chicken or egg? Nature, v. 346.

Morgans, H.E.G., 1984, Biostratigraphy of Witiora-1 offshore oil well: Lower Hutt: New Zealand, New Zealand Geological Survey report PAL 80, 33 p.

Morgans, H.E.G., 2006, Foraminiferal biostratigraphy of the early Miocene to Pleistocene sequences in Witiora-1, Taimana-1, Arawa-1 and Okoki-1: GNS Science Report 2006/37, 37 p.

Moscardelli, L., and L. Wood, 2008, New classification system for mass-transport complexes in offshore Trinidad: Basin Research, v. 20, p. 73–98, doi:10.1111/j.1365-2117.2007.00340.x.

Moscardelli, L., L.J.Wood, and D.B. Dunlap, 2012, Shelf-edge deltas along structurally complex margins: a case study from eastern offshore Trinidad: American Association of Petroleum Geologists Bulletin, v. 96, no. 8, 1483–1522.

Moscardelli, L., Wood, L., and Mann, P., 2006, Mass-transport complexes and associated processes in the offshore area of Trinidad and Venezuela: American Association of Petroleum Geologists Bulletin, v. 90, p. 1059-1088, doi:10.1306/02210605052.

Muto, T., and Steel. R.J., 2002, In defense of shelf-edge delta development during falling and lowstand of relative sea level: The Journal of Geology, v. 110, p. 421-436.

Naish, T.R., and Wilson, G.S., 2009, Constraints on the Amplitude of mid-Pliocene (3.6-2.4 Ma) Eustatic sea-level fluctuations from the New Zealand shallow-marine sediment record: Philosophical Transactions of the Royal Society A, v. 367, p. 169–187.

Nicol, A., Mazengarb, C., Chanier, F., Rait, G., Uruski, C., and Wallace, L., 2007, Tectonic evolution of the active Hikurangi subduction margin, New Zealand, since the Oligocene: Tectonics, v. 26, TC4002, doi:10.1029/2006TC002090.

Nodder, S.D., 1995, Late Quaternary transgressive/regressive sequences from Taranaki Continental Shelf, Western New Zealand: Marine Geology, v. 123, no. 3–4, p. 187–214.

O'Grady, D.B., and Syvitski, J.P.M., 2002, Large-scale morphology of arctic continental slopes: The influence of sediment delivery on slope form: Geological Society of London, Special Publications, v. 203, no. 1, p. 11–31.

O'Grady, D.B., J.P.M. Syvitski, L.F. Pratson, and J.F. Sarg, 2000, Categorizing the morphologic variability of siliciclastic passive continental margins. Geology, v. 28, no. 3, p. 207–210.

Orton, G. I. and Reading, H. G., 1993, Variability of deltaic processes in terms of sediment supply, with particular emphasis on gain size: Sedimentology, v. 40, p. 475–512.

Paola, C., 2000, Quantitative models of sedimentary basin filling: Sedimentology, v. 47, p. 121–178.

Paola, C., Heller, P.L., and Angevine, C.L., 1992, The large-scale dynamics of grain-size variation in alluvial basins, 1: Theory: Basin Research, v. 4, no. 2, p. 73–90.

Petter, A.L., Steel, R.J., Mohrig, D., Kim, W., and Carvajal, C., 2013, Estimation of the paleoflux of terrestrial-derived solids across ancient basin margins using the stratigraphic record: Geological Society of America Bulletin, v. 125, no. 3–4, p. 578–593, doi:10.1130/B30603.1.

Pirmez, C., Pratson, L.F., and Steckler, M.S., 1998, Clinoform development by advection-diffusion of suspended sediment; modeling and comparison to natural systems: Journal of Geophysical Research, B, Solid Earth and Planets, v. 103, no. 10, p. 24141–24157.

Pitman, W. C., III, 1978, Relationship between eustacy and stratigraphic sequences of passive margins: Geological Society of America Bulletin, v. 89, p. 1389–1403.

Posamentier, H.W., and Vail, P.R., 1988, Eustatic controls on clastic deposition; II, Sequence and systems tract models, in Wilgus, C.K., Hastings, B.S., Ross, C.A., Posamentier, H.W., Van Wagoner, J.C., and Kendall, C.G.St.C., eds., Sea-level changes: An integrated approach: SEPM Special Publication, v. 42, p. 125–154.

Posamentier, H., 2005, Application of 3D seismic visualization techniques for seismic stratigraphy, seismic geomorphology and depositional systems analysis: examples from fluvial to deep-marine depositional environments, in Dore A.G., and Vining B.A., Petroleum Geology: North-West Europe and Global Perspectives: Geological Society of London, Proceedings of the 6th Petroleum Geology Conference, p. 1565–1576.

Posamentier, H.W. and Kolla, V., 2003, Seismic geomorphology of depositional elements in deep-water settings – An(other) image-heavy paper by the 'Godfather' (and his mate) outlining the application of 3D seismic data to the analysis of deep-water depositional systems: Journal of Sedimentary Research, v. 73, p. 7–388.

Pratson, L.F., Nittrouer, C.A., Wiberg, P.L., Steckler, M.S., Swenson, J.B., Cacchione, D.A., Karson, J.A., Murray, A.B., Wolinsky, M.A., Gerber, T.P., Mullenbach, B.L., Spinelli, G.A., Fulthorpe, C.S., O'grady, D.B., Parker, G., Driscoll, N.W., Burger, R.L., Paola, C., Orange, D.L., Field, M.E., Friedrichs, C.T. and Fedele, J.J., 2007, Seascape evolution on clastic continental shelves and slopes, in Nittrouer, C. A., Austin, J. A., Field, M. E., Kravitz, J. H., Syvitski J. P. M., and Wiberg P. L, Continental Margin Sedimentation: From Sediment Transport to Sequence Stratigraphy: International Association of Sedimentologists, Blackwell Publishing Ltd., Oxford., Special Publication 37, p. 339-380.

Reynolds, D.J., Steckler, M.S., and Coakley, B.J, 1991, The role of the sediment load in sequence stratigraphy: The influence of flexural isostasy and compaction: Journal of Geophysical Research, v. 96, no. B4, p. 6931–6949.

Rich, J.L., 1951, Three critical environments of deposition and criteria for recognition of rocks deposited in each of them: Geological Society of America Bulletin, v. 62, p. 1–20.

Ross, W.C., Watts, D.E., and May, J.A., 1995, Insights from stratigraphic modelling: Mud-limited versus sand-limited depositional systems: American Association of Petroleum Geologists Bulletin, v. 79, p. 231-258.

Ryan, M. C., W. Helland-Hansen, E. P. Johannessen, and R. J. Steel, 2009, Erosional versus accretionary shelfmargins: The influence of margin type on deep-water sedimentation-An example from the Porcupine Basin, offshore western Ireland: Basin Research, v. 21, p. 676–703, doi:10.1111/j.1365-2117.2009.00424.x.

Sadler, P., 1981, Sediment Accumulation Rates and the Completeness of Stratigraphic Sections: The Journal of Geology, v. 89, no. 5, p.569-584, DOI: 10.1086/628623.

Sageman, B.B., Rich, J., Arthur, M.A., Birchfield, G.E., and Dean, W.E., 1997. Evidence for Milankovitch periodicities in Cenomanian–Turonian lithologic and geochemical cycles, Western Interior U.S.: Journal of Sedimentary Research, v. 67, p. 286–301.

Sanchez, C.M., Fulthorpe, C.S. and steel, R.J., 2012, Miocene shelf-edge deltas and their impact on deepwater slope progradation and morphology, Northwest Shelf of Australia: Basin Research, v. 24, p. 683-698.

Schlager, W., 1981, The paradox of drowned reefs and carbonate platforms: Geological Society of America Bulletin, v. 92, p. 197– 211.

Sloss, L. L., 1962, Stratigraphic models in exploration: American Association of Petroleum Geologists Bulletin, v. 46, p. 1050-1057.

Steckler, M.S., Berthelot, F., Lyberis, N., and Le Pichon, X., 1988, Subsidence in the Gulf of Suez: Implications for rifting and plate kinematics: Tectonophysics, v. 153, p. 249–270.

Steel, R.J., and Olsen, T., 2002, Clinoforms, clinoform trajectories and deep water sands, in Armentrout, J.M., and Rosen, N.C., eds., Sequence Stratigraphic Models for Exploration and Production: Evolving Methodology, Emerging Models and Application Histories: Gulf Coast Section SEPM Foundation, 22nd Research Conference, CD, p. 367–380.

Stern T.A., 1990, The application of deep seismic reflection profiling to petroleum exploration; An example from the South Taranaki Basin, in Lyon, G.L., ed., Proceedings, 1989 New Zealand Oil Exploration Conference, Queenstown, New Zealand: p. 42–54.

Stern, T.A., and Davey, F.J., 1990, Deep seismic expression of a foreland basin: Taranaki Basin, New Zealand: Geology, v. 18, p. 979–982.

Stern, T.A., and Holt, W.E., 1994, Platform subsidence behind an active subduction zone: Nature, v. 368, p. 233–236.

Stern, T.A., Quinlan, G.M., and Holt, W.E., 1992, Basin formation behind an active subduction zone: Three-dimensional flexural modelling of Wanganui Basin, New Zealand: Basin Research, v. 4, p. 197–214.

Stern, T.A., Stratford, W.R., and Salmon, M.L., 2006, Subduction evolution and mantle dynamics at a continental margin: Central North Island, New Zealand: Reviews of Geophysics, v. 44, no. 4, RG4002.

Sullivan, S., L. J. Wood, and P. Mann, 2004, Distribution, nature and origin of mobile mud features offshore Trinidad, in P. J. Post, eds., Salt-sediment interactions and hydrocarbon prospectivity: Concepts, applications, and case studies for the 21st century: Gulf Coast Section-SEPM 24th Annual Research Conference, Houston, Texas, December 5–8, p. 840–867.

Syvitski, J.P.M., Smith, J.N., Calabrese, E.A., and Boudreau B.P., 1988, Basin sedimentation and the growth of prograding deltas: Journal of Geophysical Research, v. 93, p. 6895-6908.

Syvitski, J.P.M., A.J. Kettner, I. Overeem, E.W.H. Hutton, M.T. Hannon, G.R. Brakenridge, J. Day, C. Vörösmarty, Y. Saito, L. Giosan, and R.J. Nicholls, 2009, Sinking Deltas due to Human Activities: Nature Geoscience, v. 2, no. 10, p. 681-686. doi: 10.1038/ngeo629.

Sydow, J.C., J. Finneran, A. P. R. Bowman,H.H.N.C. Rosen, R. H. Fillon, and J. B. Anderson, 2003, Stacked shelf-edge reservoirs of the Columbus Basin, Trinidad, West Indies, in H. H. Roberts, N. C. Rosen, R. H. Fillon, and J. B. Anderson, eds., Shelf-margin deltas and linked down slope petroleum systems: Global significance and future exploration potential: Gulf Coast Section–SEPM 23rd Annual Research Conference, Houston, Texas, December 7–10, p. 411–465.

Tetzlaff, D., 2005, Modelling coastal sedimentation through geologic time: Journal of Coastal Research, v. 21, no. 3, p. 610-617.

Tetzlaff, D.M., and Harbaugh, J.W., 1989, Simulating clastic sedimentation: New York, Van Nostrand Rheinold Series on Computer Methods in Geosciences, 202 p.

Tippett, J.M., and Kamp, P.J.J., 1995, Geomorphic evolution of the Southern Alps, New Zealand: Earth Surface Processes and Landforms, v. 20, p. 177–192, doi:10.1002/esp.3290200207.

Vail, P. R., R. M. Mitchum Jr., and S. Thompson, 1977, Seismic stratigraphy and global changes of sea level: Relative changes of sea level from coastal onlap, in C. E. Payton, Seismic stratigraphy: Applications to hydrocarbon exploration: AAPG Memoir 26, p. 63–81.

Van Wagoner, J.C., R.M. Mitchum, K.M. Campion, and V.D. Rahmanian, 1990, Siliciclastic sequence stratigraphy in well logs, cores, and outcrops: Concepts for high-resolution correlation of time and facies: AAPG Methods in Exploration Series 7, 55 p.

Warne, A. G., R. H. Meade, W. A. White, E. H. Guevara, J., Gibeaut, R. C. Smyth, A. Aslan, and T. Tremblay, 2002, Regional controls on geomorphology, hydrology, and ecosystem integrity in the Orinoco delta, Venezuela: Geomorphology, v. 44, p. 273–307, doi:10.1016/S0169-555X(01)00179-9.

Williams, D.F., 1988, Evidence for and against sea-level changes from the stable isotopic record of Cenozoic, in Wilgus, C.K., Hastings, B.S., Kendall, C.G.St.C., Posamentier, H., Ross C.A., and van Wagoner J., Sea-level Changes: an Integrated Approach: Society of Economic Paleontologists and Mineralogists Special Publication 42, p. 30–36.

Wolinsky, M.A., and Pratson, F., 2007, Overpressure and slope stability in prograding clinoforms: Implications for marine morphodynamics: Journal of Geophysical Research, v. 112, F04011.

Wood, L. J., 2000, Chronostratigraphy and tectonostratigraphy of the Columbus Basin, eastern offshore Trinidad: American Association of Petroleum Geologists Bulletin, v. 84, p. 1905–1928.

Xie, X., and Heller, P.L., 2009, Plate tectonics and basin subsidence history: Geological Society of America Bulletin, v. 121, no. 1–2, p. 55–64, doi:10.1130/B26398.1.

Zhu, M., Graham, S., Pang, X. and Mchargue, T., 2010, Characteristics of migrating submarine canyons from the middle Miocene to present: Implication for paleoceanographic circulation, northern South China Sea: Marine and Petroleum Geology, v. 27, p. 307–319.

Vita

Migdalys Beatriz Salazar was born in Maracaibo, Venezuela. She studied Engineering Geophysics at Simon Bolivar University and received her degree of Bachelor of Science in Geophysical Engineering in May of 2001. After some time working as a seismic interpreter in P.D.V.S.A., the national petroleum company of Venezuela, Migdalys went back to college to obtain a Masters Degree at The University of Texas at Austin. Upon completion of this degree, she moved back to Venezuela to continue working in the oil industry. In Fall 2010, Migdalys enrolled in the doctoral program at the University of Texas at Austin. She was advised by Dr. Lorena Moscardelli and Dr. Lesli Wood and pursued her research in the Quantitative Clastics Laboratory at the Bureau of Economic Geology. Migdalys will be employed in May 2014 with ConocoPhillips.

Permanent email: migdasalazar@gmail.com

This dissertation was typed by Migdalys Beatriz Salazar.